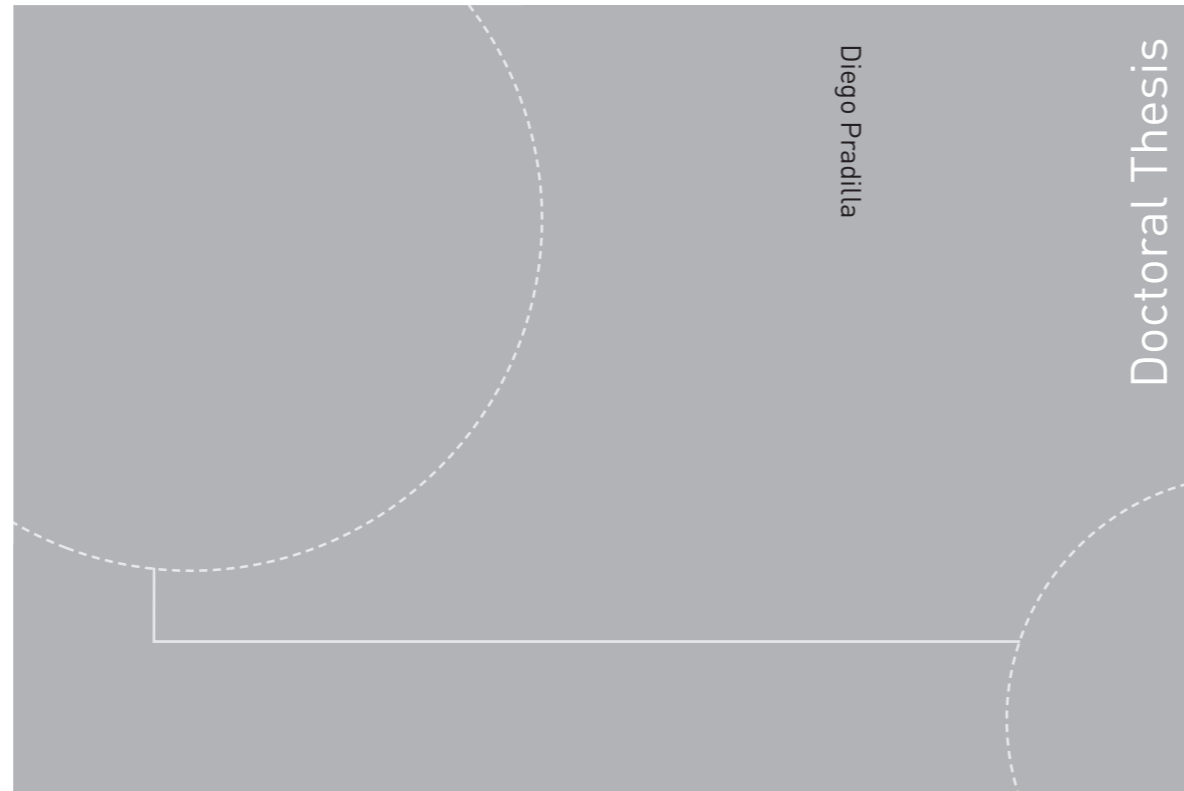


ISBN 978-82-326-1480-6 (printed version)  
ISBN 978-82-326-1481-3 (electronic version)  
ISSN 1503-8181



Doctoral theses at NTNU, 2016:71

Diego Pradilla

**Asphaltenes and Asphaltene model compounds:**

Adsorption, Desorption and Interfacial Rheology.

Doctoral theses at NTNU, 2016:71

**NTNU**  
Norwegian University of  
Science and Technology  
Faculty of Natural  
Sciences and Technology  
Department of Chemical Engineering

 **NTNU**  
Norwegian University of  
Science and Technology

 NTNU

 **NTNU**  
Norwegian University of  
Science and Technology

Diego Pradilla

# **Asphaltenes and Asphaltene model compounds:**

## Adsorption, Desorption and Interfacial Rheology.

Thesis for the degree of Philosophiae Doctor

Trondheim, March 2016

Norwegian University of Science and Technology  
Faculty of Natural  
Sciences and Technology  
Department of Chemical Engineering



Norwegian University of  
Science and Technology

**NTNU**

Norwegian University of Science and Technology

Thesis for the degree of Philosophiae Doctor

Faculty of Natural

Sciences and Technology

Department of Chemical Engineering

© Diego Pradilla

ISBN 978-82-326-1480-6 (printed version)

ISBN 978-82-326-1481-3 (electronic version)

ISSN 1503-8181

Doctoral theses at NTNU, 2016:71



Printed by Skipnes Kommunikasjon as

«C'est un garçon sans importance collective, c'est tout juste un individu»

## Preface

This thesis is submitted to partly fulfil the requirements for the degree of Doctor Philosophiae (Ph.D) at the Norwegian University of Science and Technology (NTNU). This document consists of four publications carried out between 2013 and 2016 under the supervision of Professor Johan Sjöblom and the co-supervision of Dr. Sébastien Simon.

I received my bachelor's degree in Chemical Engineering from Universidad de los Andes (Bogotá, Colombia) in 2009 under the supervision of Dr. Oscar Álvarez working on the rheology of concentrated and highly concentrated water-in-oil emulsions. After the undergraduate studies, I joined The Dow Chemical Company where I worked as an EHS/Process safety engineer. In 2013 I received the title of Master in Chemical Engineering from Universidad de los Andes (Bogotá, Colombia) under the supervision of Dr. Oscar Álvarez working on a multi-scale approach for the manufacturing of emulsions. In August 2013 I was appointed the Ph.D fellowship at the Department of Chemical Engineering (NTNU) and I was affiliated to two projects: **JIP-1** *“To advance fundamental knowledge of the water-oil separation process in order to make it more energy efficient and energy saving”* funded by the Research Council of Norway (NFR), AkzoNobel, BP, Nalco-Champion, Hamworthy, SaudiAramco, Shell, Statoil ASA, ENI, Kemira and Total; and **JIP-Asphaltenes** *“Improved Mechanisms of Asphaltene Deposition, Precipitation and Fouling to Minimize Irregularities in Production and Transport: A Cost Effective and Environmentally Friendly Approach”* funded by the Norwegian Research Council (Petromaks II grant), University of Alberta (Canada), University of Pau (France) and Universidade Federal do Parana (Brazil) AkzoNobel, BP, Canada Natural Resources, Nalco-Champion, Petrobras, Statoil and Total E&P Norge AS.

## Acknowledgements

I would like to thank my supervisor, Professor Johan Sjöblom for accepting me into his group and for his guidance throughout the different stages of this journey. And because not everything was about work, also many thanks for the good times filled with jokes and the finest sarcasm around project dinners and events.

A very special *merci beaucoup* to Dr. Sébastien Simon (1855, fake town, France) for his invaluable input, daily feedback and overwhelming dedication. His willingness to always help no matter what and his impressive brain storage capacity for science, comic books and bad movies, made it easier for me to tackle difficult endeavors.

To May and her “aliens” *tusen takk!* for being there for me since day 0.

And to all the people at Ugelstad Lab, thank you for always allowing good laughs during the daily lunch. Unfortunately, I cannot mention most of the conversation topics here, as they might be considered as a public offense, but it definitely helped me to disconnect from the always hard reality.

Many thanks to Lisbeth B Roel for her constant help and support on everything related to administrative work. They are not kidding when they say that we would need at least 5 persons to replace...half of her.

A mis hermanos Gordo y Duque por estar ahí siempre, en las buenas, en las malas, en las peores y sobretodo, en las mejores. Realmente todo ha sido más llevadero sabiendo que ustedes dos están ahí para apoyarme incondicionalmente y para darme ánimos cada vez que lo he necesitado. Verlos cada semana durante todo este tiempo era más que necesario para poder desconectarme de la cruda realidad.

Y finalmente a mi mamá, porque sin ella sencillamente no estaría alcanzando este logro tan importante. Gracias por responderme siempre ¡sí! a cuanta aventura me ha dado por perseguir y por recordarme siempre lo fundamental en tiempos difíciles.

Any remarks about this book entitled “100 authors against Einstein”?

«Yes. If I were wrong, one would have sufficed»

## **Abstract**

There are numerous problems encountered during extraction, production, transportation and refining of crude oil. Most of these problems are typically oil-specific, meaning that they depend upon the source of the oil, and sometimes they are reservoir-specific, meaning that they depend on the stage of extraction (primary, secondary or enhanced recovery). Nevertheless, a great part of the problems are related to the indigenous surface-active species such as asphaltenes, naphthenates and resins.

The definition of asphaltenes rather than being a single molecule is instead based on a solubility class. This means that they are polydisperse in nature which leads to differences in properties and composition. Asphaltenes are responsible for stabilizing water-in-oil emulsions by forming a mechanically strong gel at the interface that prevents droplet coalescence. Asphaltenes are also known to precipitate and under certain conditions (pressure, temperature, composition) form deposit layers which could lead to plug formation. All this issues generate deficits in flow assurance and evidently, increases in the operational costs.

Two strategies might be implemented to further advance in the understanding of the mechanisms involved in asphaltene adsorption onto various interfaces (liquid-liquid or solid-liquid). (i) Fractionation or (ii) model compounds. The first strategy explores the different sub-fractions that are obtained at different solvent/precipitant ratios using indigenous asphaltenes. The second strategy is to design a molecule, or group of molecules with defined functionalities that mimic the main known asphaltene properties, for instance self-association in solution and interfacial behavior.

In this thesis, the different publications were aimed to study and explore possible solutions to the several problems stated. In the first and second publications, adsorption and desorption aspects of asphaltenes and demulsifiers at the liquid-liquid interface were explored. Furthermore, interactions between asphaltenes and demulsifiers were studied via interfacial tension measurements and interfacial dilatational rheology. The results shed light on the mechanisms involved during chemical demulsification of water-in-crude oil emulsions. In the third publication, rheology and sorption aspects of asphaltene model compounds at the liquid-liquid interface were studied. The main goal of this publication was to establish the interfacial properties inherent to asphaltenes captured by a set of asphaltene model compounds developed at the Ugelstad laboratory. Similarly, in the fourth publication adsorption of

asphaltenes and asphaltene model compounds onto the solid-liquid surface was studied. In this study, the determination of the adsorption enthalpy via microcalorimetry allowed to elucidate the type of bond and the driving force for adsorption onto surfaces of different nature.

With these publications, a complete study at the liquid-liquid interface and the solid-liquid surface was developed for asphaltenes and asphaltene model compounds. This provides a fundamental framework for model systems that can be used to understand the behavior in real applications.



# List of publications

## Paper 1.

Pradilla, Diego., Simon, Sébastien., Sjöblom, Johan.

*Mixed interfaces of asphaltenes and model demulsifiers part I: adsorption and desorption of single components.* Colloids and Surfaces A: Physicochemical and Engineering Aspects **2015**, 466, 45-56.

## Paper 2.

Pradilla, Diego., Simon, Sébastien., Sjöblom, Johan.

*Mixed Interfaces of Asphaltenes and Model Demulsifiers, Part II: Study of Desorption Mechanisms at Liquid/Liquid Interfaces.* Energy & Fuels **2015**, 29 (9), 5507-5518.

## Paper 3.

Pradilla, Diego., Simon, Sébastien., Sjöblom, Johan., Samaniuk, Joseph., Skrzypiec, Marta., Vermant, Jan.

*Sorption and interfacial rheology study of model asphaltene compounds.*  
*Submitted to Langmuir.*

## Paper 4.

Pradilla, Diego., Subramanian, Sreedhar., Simon, Sébastien., Sjöblom, Johan., Beurroies, Isabelle., Denoyel, Renaud.

*A microcalorimetry study on the adsorption of asphaltenes and model asphaltene compounds at the liquid-solid surface.*  
*Submitted to Langmuir.*

The experimental work of the **first** and **second** publications took place at the Ugelstad Laboratory (NTNU) and was performed entirely by me. The manuscripts were read, corrected and approved by all the co-authors listed (Professor Johan Sjöblom and Dr. Sébastien Simon).

The experimental work for the **third** publication was partly carried out in a collaboration work with Dr. Jan Vermant (ETH, Zürich, Switzerland) and his group. All the experiments related to shear interfacial rheology and the use of the SGR model were performed by the members of the ETH group listed as co-authors in the manuscript. All the other experiments were carried out at the Ugelstad Laboratory (NTNU) by me. The manuscript and the submitted version were read, corrected and approved by all the co-authors listed.

The experimental work for the **fourth** publication was partly carried out in a collaboration work with Dr. Renaud Denoyel (Madirel, Marseille, France) and his research group. All people involved are also listed as co-authors in the manuscript. Dr. Denoyel's group carried out all the microcalorimetry experiments. Sreedhar Subramanian (also a co-author of the manuscript, Ugelstad Lab) performed all the QCM-D experiments. The rest of the measurements were performed by me at the Ugelstad Lab.

### **Additional publications**

Pradilla, Diego., Vargas, Watson., Álvarez, Oscar.

*The application of a multi-scale approach to the manufacture of concentrated and highly concentrated emulsions.*

Chemical Engineering Research and Design, **2015**, 95, pp. 162-172.

# Table of Contents

|   |    |
|---|----|
| 1. Introduction.....  | 10 |
| 2. Petroleum.....   | 10 |
| 3. SARA fractionation.....  | 11 |
| 3.1 Maltenes.....   | 12 |
| 3.2 Asphaltenes.....  | 14 |
| 3.2.1 Structure.....  | 14 |
| 3.2.2 Molecular weight.....   | 15 |
| 3.2.3 Chemical composition.....   | 17 |
| 3.2.4 Bulk Properties.....  | 18 |
| 3.2.4.1 Asphaltene self-association.....                                  | 18 |
| 3.2.4.2 Precipitation, flocculation and deposition.....                   | 20 |
| 3.2.5 Surface properties.....   | 22 |
| 3.2.5.1 Adsorption at the liquid-air and liquid-liquid interface.....     | 22 |
| 3.2.5.2 Adsorption at the liquid-solid surface.....                       | 23 |
| 4. Emulsions.....   | 24 |
| 4.1 General aspects.....  | 24 |
| 4.1.1 Formation.....  | 25 |
| 4.1.2 Stabilization.....  | 25 |
| 4.1.3 Destabilization.....  | 28 |
| 4.2 Asphaltene-stabilized emulsions.....                                  | 30 |
| 4.3.1 Rheology of asphaltene interfaces.....                              | 31 |
| 5. Model compounds.....   | 33 |
| 6. Experimental Techniques and Theory.....                                | 37 |
| 6.1. Surface tension (ST) and interfacial tension (IFT) measurements..... | 37 |
| 6.1.1 The Du Noüy ring.....   | 37 |
| 6.1.2 Axisymmetric drop shape analysis (ADSA).....                        | 38 |
| 6.1.2.1 Double coaxial capillary.....                                     | 40 |
| 6.2 Interfacial rheology.....   | 40 |

|  |    |
|--|----|
| 6.2.1 Interfacial dilatational rheology.....                                   | 40 |
| 6.2.2 Interfacial shear rheology and the double wall-ring (DWR) geometry. .... | 42 |
| 6.3 Microcalorimetry .....   | 43 |
| 6.4. Quartz crystal microbalance with dissipation (QCM-D).....                 | 44 |
| 7. Main Results .....  | 46 |
| 7.1 Paper 1 .....  | 46 |
| 7.2 Paper 2 .....  | 49 |
| 7.3 Paper 3 .....  | 54 |
| 7.4 Paper 4 .....  | 59 |
| 8. Concluding remarks .....  | 62 |
| 9. References.....   | 64 |

## 1. Introduction

*«Prescription 8: Pulverize the roots of the ...-tree, ..., and dried river bitumen; pour beer over it, rub it with oil, (and) fasten as poultice»<sup>1</sup>*

*«Prescription 9: Pour strong beer over the resin of...-plant; heat over a fire; put this liquid in river bitumen oil (and) let the (sick) man drink»<sup>1</sup>*

The above two paragraphs are translations from two Sumerian medical tablets inscribed in the third millennium B.C. and constitute “by all odds the oldest pharmacopoeia known to man”<sup>1</sup>. Oil or bitumen (the two words are indistinguishable from the translations) has been known to man since the beginning of civilization itself. Not only as an ingredient for medicine, but also as a fundamental material for construction and lighting<sup>1</sup>.

## 2. Petroleum

Beneath the earth’s surface in geological formations, accumulations of economically valuable hydrocarbons are found. These compounds when refined are used as fuel (energy, industry, heating) and also as raw materials for manufacturing a large assortment of products encountered in the everyday life (plastics, fibers). The term petroleum hence refers to both refined and unrefined elements<sup>2, 3</sup>. Petroleum use is broad, providing more than half of the world’s supply of energy. This situation leads to carbon dioxide buildup (as a natural product of combustion) in the earth’s atmosphere which is a greenhouse gas strongly related to climate change<sup>4</sup>. Until alternative forms of energy become widely available, the motivations for directing efforts towards research for cleaner and more efficient ways of productions are self-evident.

Crude oil is a very complex mixture of different hydrocarbon compounds (paraffins, naphthenes, aromatics) and to a minor extent, non-hydrocarbon constituents (nitrogen, oxygen, sulphur, nickel, vanadium), which probes difficult to map. Table 1 shows the elemental composition range typical of most oils. Keeping in mind that petroleum is a continuum, any boundaries, molecular or physical, will cover a wide range of sub-fractions of varying boiling point and carbon number<sup>2</sup>. The variations among oil fields and reservoirs makes these boundaries inherently arbitrary and thus troublesome to study from a scientific approach. An attempt to deal with this great variation and to devise standard procedures as a

basis for research and laboratory investigations is through fractionation. Evidently, the methods by which these fractions are obtained can also vary. While some of the traditional methods exploit boiling point differences (distillation) others make use of the differences in solubility (solvent treatments), surface activity (adsorption) and chemical reactions (chemical fractionation).

| Element           | Weight percentage |
|-------------------|-------------------|
| Carbon            | 83.0-87.0         |
| Hydrogen          | 10.0-14.0         |
| Nitrogen          | 0.1-2.0           |
| Oxygen            | 0.05-1.5          |
| Sulfur            | 0.05-6.0          |
| Metals (Ni and V) | <1000 ppm         |

**Table 1:** Elemental composition range for most common crude oils. Table reproduced from Speight.<sup>2</sup>

One of the most used methods is the SARA fractionation procedure that splits the oil into four fractions: saturates, aromatics, resins and asphaltenes based on both adsorption and solubility. There is no such thing as “one method fits all” for obtaining the petroleum fractions. Choosing one or a combination of several methods depends on the type of crude oil making fractionation oil-specific<sup>2, 5, 6, 7</sup>. To emphasize the variation and structural complexity of the different constituents of crude oil, Fig. 1 shows the changes in the boiling point with carbon number and molar mass of some of the representative heavy fractions.

### 3. SARA fractionation

SARA (Saturates, Aromatics, Resins, Asphaltenes) fractionation<sup>8</sup> is a process that starts with the removal of asphaltenes from crude oil by precipitation with *n*-alkanes. In this sense, this part separates asphaltenes based on their solubility. The remaining SAR portion (also known as maltenes) is treated via ion-exchange chromatography and adsorption chromatography to separate it into the other three fractions. Different ASTM methods (ASTM D2006, ASTM D2007, ASTM D893, ASTM D3279, ASTM D4124, IP 143) have been proposed to provide a standard way of obtaining asphaltenes. Each method provides asphaltenes with similar characteristics that depend on the asphaltene-resin boundary fixed by the precipitant (i.e. *n*-alkane).

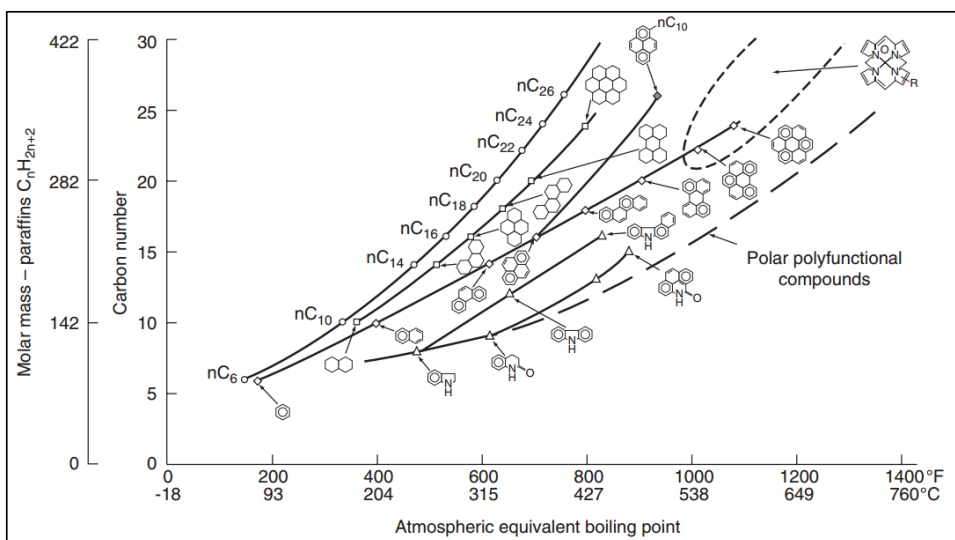


**Figure 1.** Molecular weight and structures of representative heavy fraction of crude oil as a function of their boiling point. Image reproduced from Altgelt and Boduszynski<sup>9</sup>.

If crude oil is mixed with an *n*-alkane (*n*-pentane, *n*-hexane or *n*-heptane), two phases emerge: asphaltenes as precipitate and maltenes as the continuous liquid phase. The type of solvent influences the amounts of the fractions obtained. In fact, it has been shown<sup>2, 10</sup> that the amount of asphaltenes precipitated with *n*-alkanes that have carbon numbers greater than 7 (i.e. *n*-heptane) does not reach a plateau which means that the composition of the asphaltene samples obtained depend on the *n*-alkane used (See Fig. 2). Similarly, the asphaltene yield does not seem to change for volume of precipitant to volume of feedstock ratios greater than 40. It is important to note that all these fractions are solubility classes that are defined within the extent of precipitation and not molecules with well-defined structures.

### 3.1 Maltenes

*Saturates (S)* are normally known as paraffins or paraffin hydrocarbons. They are saturated hydrocarbons that do not have ring structures in their structure and include *n*-paraffins, *iso*-paraffins, cycloparaffins (naphthenes), condensed cycloparaffins and alkyl side chains. This fraction is the lightest and less polar of crude oil. The amount of *n*-paraffins in crude oil varies depending on the source, however, as a reference point, an oil is considered as “paraffinic” if it contains up to 50% of this paraffins. Cycloparaffins (naphthenes) are typically present as cyclopentane and cyclohexane and they could account up to 60% of the total hydrocarbons<sup>2, 11, 12, 13</sup>.

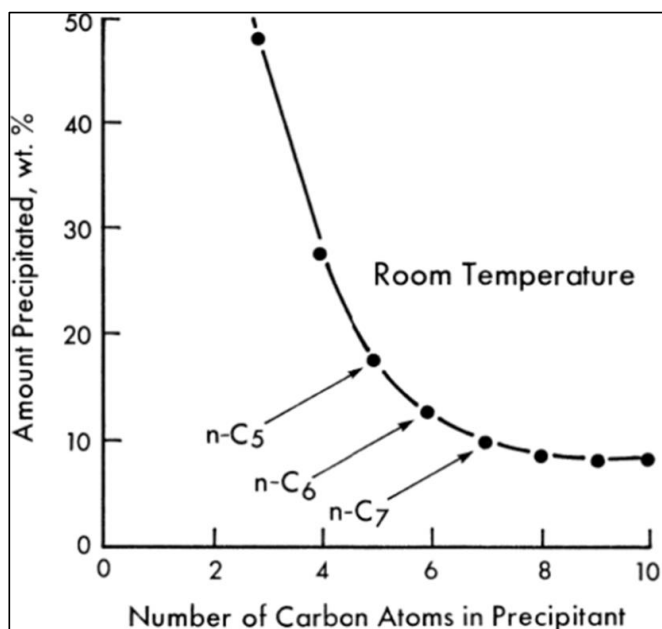


**Figure 2.** Variation of the amount of asphaltenes precipitated with carbon number of the liquid hydrocarbon. Image reproduced from Speight et al.<sup>14</sup>

*Aromatics (A)* are a nonvolatile constituent common to all oils. This solubility class normally contains benzene systems, condensed aromatic systems, aromatic cycloalkyl systems and paraffinic chains on naphthene rings<sup>2, 15</sup>. Due to the fact that oil is a continuum the presence of aromatics transverses all fractions, in fact, resins and asphaltenes contain also aromatic rings in their structure.

*Resins (R)* are the polar fraction of crude oil that contains most of the heteroatoms (N, O, S) and exhibits a higher H/C ratio compared to asphaltenes. Resins are also defined as a solubility class and the boundary between with asphaltenes depends on the type of oil, and the method used for extraction as they might overlap. Resins are soluble in the liquids that precipitate asphaltenes but insoluble in liquid propane and liquid butane. Normally, resins exhibit a lower molecular weight compared to asphaltenes and are key to the stability of petroleum as they are attributed an important role in asphaltene aggregation that holds the colloidal state of oil<sup>2, 16, 17</sup>.



## 3.2 Asphaltenes

*Asphaltenes (A)* are traditionally defined as the most polar fraction of petroleum insoluble in *n*-alkanes (such as *n*-heptane or *n*-hexane) but soluble in aromatic compounds (such as toluene or xylene).<sup>18, 19</sup> Asphaltenes are known to self-associate in model solvents as well as in real crude oil media<sup>20</sup>. When the carbon number of the solvent is decreased (for example from *n*-heptane to *n*-pentane) structures that do not self-assemble are precipitated along with asphaltenes broadening the chemical identity of the latter. The importance of this remark lies in that self-aggregation and interfacial behavior are perhaps key concepts related and interrelated to asphaltenes.

Similar to resins, asphaltenes are considered to be polydisperse in heteroatomic functionality, molecular weight and carbon backbone structure<sup>18</sup>. Asphaltenes are surface active compounds that are largely responsible for several problems during production, transport and refining of crude oil leading to high production costs<sup>21</sup>. Asphaltenes can precipitate and deposit in the reservoirs, wells, pipes and other equipment<sup>22, 23</sup>. They can also stabilize water-in-oil emulsions (W/O) by forming a gel-like continuum<sup>24</sup>, or “skin”<sup>25, 26</sup>, at the oil/water interface that hinders coalescence and retards drainage.<sup>27, 28, 29</sup> It is because of these reasons that they receive special attention and their own chapter in this thesis.

### 3.2.1 Structure

The already mentioned differences in functionalities and molecular weight make it difficult to have a complete overview of asphaltene properties. To attempt a description of a general structure, two models for asphaltenes have been proposed. They are known as the “Archipelago” and “Continental” models. In the former, several aromatic sections are attached to each other via alkyl chains. In the latter, polycyclic aromatic hydrocarbons (PAHs) form a core to which aliphatic chains are attached<sup>30, 31</sup>. Examples of both models are presented in Fig. 3. Even though several structures representative of the Archipelago model have been tested<sup>32</sup>, the evidence strongly suggests the validity of the continental model. The early studies of Groenzin and Mullins<sup>33, 34</sup>, who measured the time-dependent depolarization of asphaltene fluorescence for molecular weight purposes, concluded that the Continental model is at least the dominant molecular structure of different tested asphaltenes. That is, if other structures were to be present simultaneously. Additionally, a recent study<sup>32</sup> in which

several model compounds with an island-type architecture were tested using a single-proton ionization method, also pointed out the dominance of the Continental model.

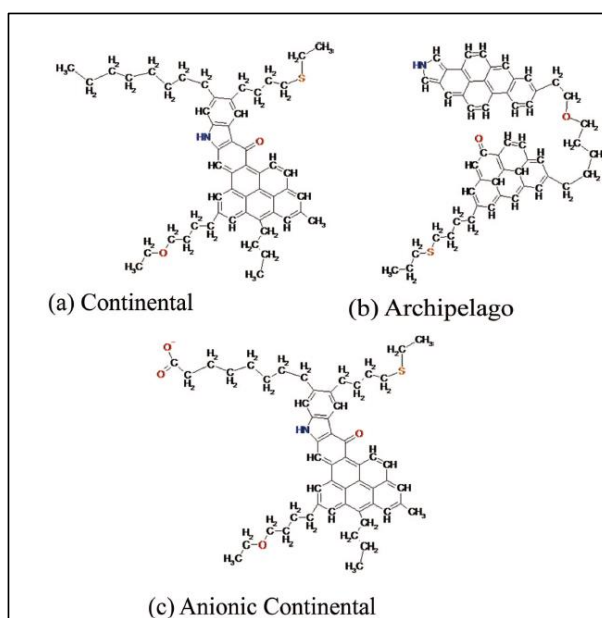


**Figure 3.** Different proposed molecular structures for asphaltenes. Image reproduced from Kuznicki et al.<sup>35</sup>

### 3.2.2 Molecular weight

One of the reasons why asphaltene molecular weight has been a source of disagreement and controversy is that the molecular weight data normally represents an average value of a distribution<sup>18</sup>. Among the several reasons why molecular weight determination is a troublesome endeavor are: (i) Asphaltenes have the tendency to associate in dilute solution in nonpolar solvents (this means that the reported values could be those of the aggregates and not monomers), (ii) asphaltenes exhibit low solubility in some of the liquids used for molecular weight measurements and (iii) asphaltene-resin interactions induce discrepancies in the results (variation of the aggregation level). Traditional methods for determining molecular weight, such as chromatography (pyrolysis/gas chromatography/mass spectrometry and/or high performance liquid chromatography) work very well for light hydrocarbon compounds (saturates, aromatics), but when dealing with the heavier fraction (i.e. asphaltenes and resins) these methods cannot be used<sup>36</sup>. Additionally, different methods report different types of molecular weight: number average  $M_n$ , weight average  $M_w$  or z-average.

Vapor-pressure osmometry (VPO) is based on the thermoelectric effect of the vapor tension decrease of a solution compared with the pure solvent. It yields a number average molecular weight ( $M_n$ ) that is temperature-dependent given that asphaltene association decreases at high values. The values obtained via this technique hence vary according to the experimental setup<sup>36</sup>. Size Exclusion Chromatography (SEC) separates asphaltenes according to their hydrodynamic volume obtained by passing them onto a support bed. It is a relative method that depends upon calibration and yields an average molecular weight ( $M_{SEC}$ ) and its main disadvantage is the adsorption of molecules or aggregates onto the support bed<sup>37</sup>. Small Angle Neutron and X-ray Scattering (SANS and SAXS) have been used because of the possibility of detecting the presence of heterogeneities and because of the possibility of exploring special structures over the nanometer scale. They yield both the weight average molecular weight ( $M_w$ ) and the radii of gyration ( $R_{g,z}$ ). One of the features, disadvantageous to some, is that sometimes the scattering data must be treated with a model which considers the molecules to be, for example, cylinders, discs or spheres yielding different radii of gyration (between 30 and 200 Å) hence different molecular weights<sup>17, 38</sup>. However, model-independent equations such as the Guinier or Zimm have also been used<sup>39</sup>. Finally, Nuclear magnetic resonance (NMR) techniques and pulsed field gradient spin-echo (PFG-<sup>1</sup>H NMR) allow the determination of the self-diffusion coefficient which can be correlated with the aggregation state and hence the molecular weight of the species in solution<sup>40</sup>.

As mentioned before, to determine a true molecular weight, it is imperative to be able to work with very low asphaltene concentrations (i.e. 1 mg/L). To this date, only a few techniques allow such constraint. For example, Mass Spectrometry (MS) is an attractive method for which the ionization protocols must be carefully controlled to avoid molecular fragmentation and differences in the ionization yields. With this technique, values between 600 and 700 Da have been obtained<sup>41</sup>. Time-resolved fluorescence depolarization spectroscopy (FD) is a technique in which an exciting photon is polarized creating a direction for the randomly oriented chromophores that are part of the asphaltene molecules. Emission then takes place after some time that can be correlated to the molecular radius, thus its size<sup>33</sup>.

Despite the wide range of molecular weights for asphaltenes depending on the method used that goes from a few hundred (~500 g/mol) up to several hundredths of thousands (~100000 g/mol)<sup>33</sup> and measurements on highly polar solvents (that tend to prevent association but aggregates are still found) that have placed the molecular weight in ~2000 ±500 g/mol<sup>42</sup>, a

“standard” value of 750 Da is widely used<sup>21</sup> based on the latest (as of 2010) Mass spectrometry and molecular diffusion measurements<sup>43, 44</sup>. As a summary, table 2 shows the average molecular weight for asphaltenes obtained via different techniques.

| Technique                 | Molecular Weight g/mol |
|---------------------------|------------------------|
| Ultracentrifugation       | 300000                 |
| Osmotic pressure          | 80000                  |
| Ultrafiltration           | 80000-140000           |
| Boiling point elevation   | 2500-4000              |
| Freezing point depression | 600-6000               |
| Vapor pressure osmometry  | 1000-8000              |
| Viscosity                 | 900-50000              |
| Light scattering          | 1000-4000              |

**Table 2:** Asphaltene average molecular weight obtained via various techniques. Table reproduced from Speight et al.<sup>45</sup>

### 3.2.3 Chemical composition

An important aspect of the chemical composition of asphaltenes is the size of the polyaromatic hydrocarbons (PAHs) and the functionality of the heteroatoms. The relationship between the number of rings inside the asphaltene core and the solubility/precipitation aspects is as follows: if the molecule has a large number of rings, the solubility in toluene decreases. Analogously, if the number is too low, the precipitation in *n*-heptane increases<sup>46, 47</sup>. Measurements using Scanning Tunneling Microscopy (STM) showed that the main axis of the PAH is ~1nm which corresponds to ~7 fused rings<sup>48</sup>. Measurements on Raman spectra and <sup>13</sup>C NMR reached similar conclusions<sup>49</sup>.

The issue of how the fused rings are arrayed is another matter of discussion. The source of the argument is the resonance structures present in benzene (and other sextet compounds). These structures change when two or more rings are present and thus their optical absorption spectra changes. Pure sextet compounds (benzene, hexabenzocoronene) are stable and the aromatic sextet carbon exhibits blue shifted spectra. Isolated-double-bond carbons on the other hand are less stable and exhibit red-shifted spectra<sup>50, 51, 52, 53, 54</sup>. Most of the evidence points towards the dominance of aromatic-sextet-carbons inside the PAHs which is in agreement with the observations that support the Continental over the Archipelago model. In summary, it can be said that the PAHs have ~7 fused rings in their structure and that the dominant carbons are not isolated-double bonded.

The second relevant aspect regarding chemical composition has to do with the nature and location of heteroatoms such as Nitrogen, Oxygen and Sulfur and to some extent metals such as Nickel and Vanadium that have been shown to impact asphaltene properties. These constituents cannot be properly determined through proton magnetic resonance studies therefore spectroscopic methods are normally used. Some of the methods used to this end are XPS (X-ray Photo-Electron Spectroscopy), EXAFS (Extended X-ray Fine Structure) and XANES (X-ray Absorption Near Edge Spectroscopy)<sup>45</sup>. Oxygen content has been traditionally the less complex heteroatom to detect. However, a large portion of the data is related to oxygen functions present in oxidized material which might not correlate to the content in native material<sup>45</sup>. Despite this, oxygen has been identified in carboxylic, phenolic and ketonic locations and it is less likely to exist in heterocyclic locations<sup>55</sup>. Nitrogen has been shown to be present in heterocyclic structures<sup>21</sup> and largely present in pyrrolic (aromatic) form<sup>56</sup> and some portions in pyridine form. Sulfur occurs in petroleum (and the asphaltene fraction) as benzothiophenes, dibenzothiophenes and naphthenebenzothiophenes<sup>45</sup>. XANES spectroscopy has been used to confirm the presence of thiophene sulfur and sulfide sulfur in asphaltenes<sup>21</sup>.

Metals such as Nickel, Vanadium and iron are present in crude oil. However, it has been shown<sup>57</sup> that most of these metals are concentrated in the asphaltene fraction or in fractions that boil above 540 °C. The occurrence of these metals is typically in complex structures such as petroporphyrins and metallo non-porphyrin compounds<sup>58</sup>. However, whether these porphyrins are part of the asphaltene structure or not is not known.

### **3.2.4 Bulk Properties**

#### **3.2.4.1 Asphaltene self-association**

As seen in the previous section, central to molecular weight determination is asphaltene aggregation. In fact, it has been shown that asphaltenes have the tendency to self-aggregate in hydrocarbon solutions at concentrations as low as 0.1 g/L in toluene<sup>24, 59</sup>. Association of asphaltenes is influenced by their concentration, origin<sup>31</sup>, solvent polarity<sup>18</sup>, temperature, pressure and the presence of resins<sup>60</sup>. The mechanisms that lead to aggregation of asphaltenes in solution have not been yet established. However, there are some aspects that have been identified such as hydrogen bonding, formation of charge-transfer complexes, hydrophobic pockets and  $\pi$ - $\pi$  stacking being the latter the most significant force for dimer formation<sup>61, 62</sup>. Furthermore, asphaltene nanoaggregates, whose formation occurs at high energy binding

sites, have been described as a “hairy tennis ball” with the alkane chains surrounding it and stable against flocculation<sup>59</sup>. It has also been proposed that their shape could be described as cylinders with a high degree of polydispersity<sup>63</sup> or fractal arrangement<sup>64</sup>.

Asphaltene-resin interactions<sup>65, 66</sup> seem to play an important role in asphaltene stability in solution. One reason for this is that resins have intermediate polarity and higher H/C ratio which helps closing the solubility gap between the polar asphaltenes and nonpolar elements in the oil matrix<sup>46, 67, 68</sup>. It appears that the presence of resins induces a decrease of the molar mass of the asphaltene aggregates<sup>24</sup>. Resins attach to the nanoaggregates that are dispersed in the solution as a nano-colloid and when removed, higher molecular weights are observed<sup>18</sup>. Also, desorption of resins from the aggregates leads to asphaltene precipitation<sup>44</sup>. This is evidently tightly linked with the nature of the solvent. For instance, in good solvents (i.e. toluene) swelling of the side chains causes a steric repulsion that consequently causes asphaltenes to repel whereas in poor solvents (i.e. heptane) asphaltenes attract via Van der Waals forces<sup>69</sup>.

One of the most popular models for asphaltene aggregations is the Yen model. It was one of the first multi-scale attempts to provide a realistic relationship between structure and function. The “modified Yen model” or “The Yen-Mullins model” provides a more refined approach because it includes the energy contribution of the different structures at the different scales<sup>20, 21</sup>. The Yen-Mullins model assumes an asphaltene molecule size of approximately 1.5nm with a single moderate-sized PAH ring system and peripheral alkane chains (continental model). These molecules can form nanoaggregates of ~2 nm with aggregation numbers of 6 with a single disordered PAH stack. The nanoaggregates are prone to form clusters (~5 nm) with aggregation numbers of approximately eight. Fig. 4 shows a schematic of the Yen-Mullins model. The concentration at which the nanoaggregates start to be present in solution is known as the critical nanoaggregate concentration (CNAC) and different studies<sup>24, 59, 70</sup> have placed it at ~100 mg/L.

As a summary, some of the generalities and implications from the Yen-Mullins model are: *Asphaltene molecules* follow the continental model as the most predominant architecture with the peripheral alkyl chains providing steric hindrance. Heteroatoms are often found within the asphaltene architecture; the presence of charged species is very low, thus their contribution in terms of energy is virtually non-existent. The PAH is the primary site of interactions. It is polarizable, it exhibits dipole-dipole interactions which are largely responsible for the self-

association behavior and attractive forces are short-range. *Nanoaggregates* are thought to be rather small, containing only a few asphaltene molecules mainly because of the steric hindrance that the side alkyl chains provide once the nanoaggregate is formed; The PAH inside a nanoaggregate are not covalently cross-linked to each other. Hence additional asphaltene molecules will not contribute to increase the size of the nanoaggregate but instead form a new one<sup>20, 46</sup>. *Asphaltene Clusters* are most likely fractal and given that the nanoaggregates are ~2nm, the smallest clusters should be ~6nm. It has been suggested that the strong rheological behavior relationship to temperature is because of the variation in clustering which could be analogous to crystal growth<sup>20</sup>.

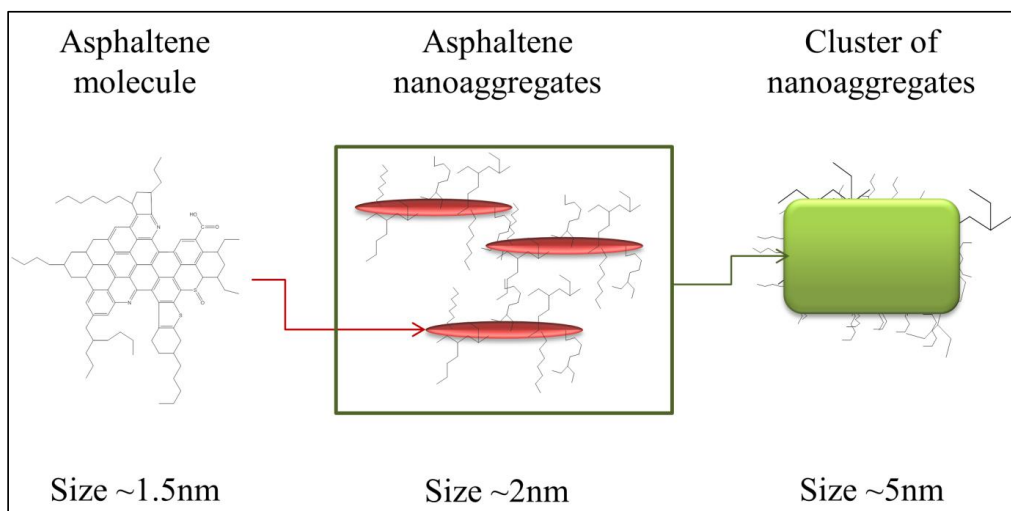


**Figure 4.** The Yen-Mullins model. Asphaltene molecules are assumed to follow the Continental model (predominant asphaltene architecture).

### 3.2.4.2 Precipitation, flocculation and deposition.

One of the main problems in production, separation, transportation and refining of crude oil is precipitation and deposition of heavy organic solids such as asphaltenes. When asphaltene deposits are formed, flow-assurance issues arise and this can significantly affect environmental and economic aspects of the process.<sup>23, 43, 44</sup> Even though precipitation always precedes deposition, it is not a sufficient condition. This means that asphaltenes can remain in the oil, but will not necessarily adhere to any surface. Precipitation of asphaltenes can be attributed to several factors<sup>43, 71</sup>: temperature, solubility and composition (mixing the oil with

miscible and immiscible diluents, carbon dioxide injection), pressure changes (influence of light components), acidification (neutralization of negatively charged asphaltene aggregates) and fouling. In light oils that contain smaller amounts of asphaltenes, precipitation is mainly due to depressurization whereas in heavy oils it is mainly due to the mixing with other fluids such as carbon dioxide or light hydrocarbons.<sup>72</sup>

On the other hand, asphaltene deposition is a more complex process that may lead to equipment plugging (pumps, safety valves), pipeline plugging, well-bore plugging, deactivation of other chemicals and emulsion stabilization among others. Flow shear rate, equipment material and interactions between asphaltenes and the surfaces are some of the keywords of this phenomenon.

When precipitation and deposition occurs, mitigation techniques such as solvent cleaning, mechanical cleaning and inhibitor injection have to be implemented. It is therefore of great importance to be able to reliably predict if and when asphaltene problems will occur, more specifically, when precipitation happens<sup>23, 73</sup>. While some of the studies available in the literature are performed directly on crude oils, a vast number are performed on asphaltene solutions, typically in toluene or xylene which are treated as model systems. The so-called asphaltene phase envelope (APE)<sup>74</sup> presented in Fig. 5 is a diagram typically used to screen for precipitation. This diagram delimits the solubility-stability zone for asphaltenes and includes, in the case of live oils, the bubblepoint border (an area under which asphaltenes may be re-dissolved as the pressure decreases<sup>75</sup>). Asphaltenes tend to be more stable at high pressures and low temperatures<sup>76</sup> and above a certain temperature range, related to the solubility parameter of the gas present (i.e. live oils) asphaltenes transition from stable to unstable<sup>77</sup>. Some of the techniques used for determining the asphaltene precipitation onset include: the gravimetric precipitation method, the acoustic-resonance technique (ART)<sup>78</sup>, near infrared spectroscopy (NIR)<sup>79</sup>, quartz crystal microbalance (QCM-D)<sup>80, 81</sup>, refractive index (RI)<sup>82</sup>, high pressure methods<sup>74</sup>, isothermal calorimetry<sup>83</sup> and electromagnetic viscometry<sup>84</sup>. Similarly, deposition and asphaltene plug formation are studied through capillary flow experiments<sup>72, 85</sup> and Taylor-Couette (TC)<sup>86, 87</sup>.



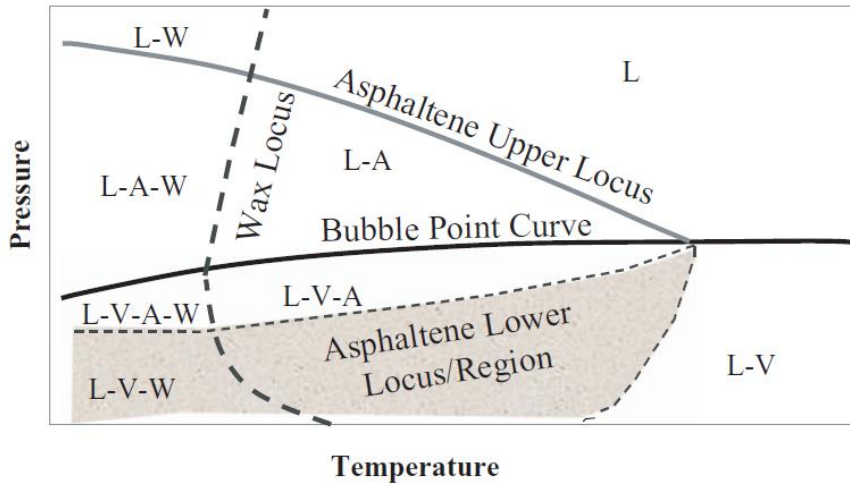


**Figure 5.** Asphaltene phase diagram or APE for unstable reservoir fluids showing the different liquid (L), vapor (V), wax (W) and asphaltene (A) regions. Image reproduced from Hammami et al.<sup>22</sup>

### 3.2.5 Surface properties

Interactions involved in asphaltene aggregation and flocculation are partly responsible for the formation and stabilization of emulsions. Asphaltenes can adsorb at liquid-air, liquid-liquid interfaces and liquid-solid surfaces and each type of interface (surface) plays a key detrimental role in different stages of oil production. For example adsorption at the liquid-liquid interface is of paramount importance when dealing with emulsions and adsorption at the liquid-solid surface is involved in precipitation and deposition.

#### 3.2.5.1 Adsorption at the liquid-air and liquid-liquid interface.

Adsorption at the liquid-air interface normally refers to the formation of foams as an undesired consequence of foam flooding for enhanced oil recovery operations (EOR) or as a result of the liberation of dissolved gas in live-oils in the separators<sup>88, 89</sup>. This broad subject goes beyond the scope of this thesis and for this reason it will not be treated here.

Adsorption at the liquid-liquid interface is strongly related to the formation and stability of emulsions and will be treated in upcoming chapters.

### 3.2.5.2 Adsorption at the liquid-solid surface.

Asphaltene adsorption at the solid-liquid surface has been studied for a wide range of surfaces<sup>90, 91</sup> that include clay/non-clay minerals and metals. Differences in the adsorbed amounts, even within the same surface are not uncommon.

Asphaltene adsorption onto silica and alumina surfaces is a relevant field of study because of the similarities to the naturally occurring rock formations.<sup>92</sup> Different studies have reached similar conclusions in the sense that asphaltene adsorption seems to be dominated by polar interactions between the surface and acidic/basic functionalities present in asphaltene molecules. Polycyclic aromatic hydrocarbons (PAHs) exhibit a higher affinity towards acidified particles which translates to interactions of the type Brønsted and Lewis acidity. In general, adsorption onto silica is higher than onto alumina particles<sup>93, 94, 95, 96, 97, 98</sup>.

Adsorption of asphaltenes onto clay minerals such as kaolinite, illite and montmorillonite, and onto non-clay minerals such as quartz ( $\text{SiO}_2$ ), calcite ( $\text{CaCO}_3$ ), fluorite ( $\text{CaF}_2$ ) and hematite ( $\text{Fe}_2\text{O}_3$ ) has been of particular interest due to their retention capabilities which impacts adsorption and due to their resemblance to reservoir rocks<sup>91, 99, 100, 101</sup>. Generally speaking, adsorption onto minerals tends to be similar or higher than silica and alumina<sup>94, 102</sup>; the adsorption mechanisms seem to be related to the hydration energies of the cations present ( $\text{Mg}^{2+}$ ,  $\text{Ca}^{2+}$ ,  $\text{Na}^+$ ,  $\text{K}^+$ )<sup>103</sup> and interactions between asphaltenes and the polar groups (Si-OH, Al-OH) that are regarded as slightly acidic active sites for adsorption<sup>91, 104</sup>.

Adsorption of asphaltenes onto metal surfaces (stainless steel, iron and aluminum) which have high implications when discussing pipeline plugs and deposits is normally characterized by exhibiting similar to higher adsorbed amounts compared to clay and nonclay minerals<sup>35,36</sup>. The differences in adsorption capacities could be attributed to differences in the morphology of the particles which affect diffusion and asphaltene origin. Additionally, unlike adsorption onto silica and alumina, adsorption onto metal surfaces seems to be driven by electrostatic bonding (provided by elements such as Cr, Ni, Si, C, S and P) coupled with the surface charge of asphaltenes<sup>105, 106</sup>.

## 4. Emulsions

### 4.1 General aspects

Emulsions (i.e. macroemulsions) are a type of colloidal system in which droplets of a liquid are dispersed in a second immiscible liquid. Emulsions are widely used in a variety of industrial applications: cosmetics, food, pharmacy, coatings, oil recovery and the so-called liquid explosives<sup>107, 108</sup>. These products are a non-equilibrium system, which means that they are thermodynamically unstable and consequently two variables must be considered for their formation: energy (which must be incorporated through the emulsification process or any type of shear) and a surfactant that stabilizes the droplets by ensuring repulsive interactions at the interface.

One way of classifying emulsions is by the nature of the dispersed phase. In this sense, they can be considered as water-in-oil (W/O) or oil-in-water (O/W). Here, the terms water and oil are used in a rather simplistic way to denote that the phases can be either hydrophilic or hydrophobic<sup>109</sup>. As an example, Fig. 6 shows the two types of emulsions. They can also be classified according to the microstructure of the continuous phase or the interaction forces between the droplets. Depending on the emulsification process, multiple emulsions can also be formed. For instance, a water-in-oil-in-water emulsion (W/O/W) consists of oil droplets dispersed in a water medium with water droplets inside.<sup>110</sup>

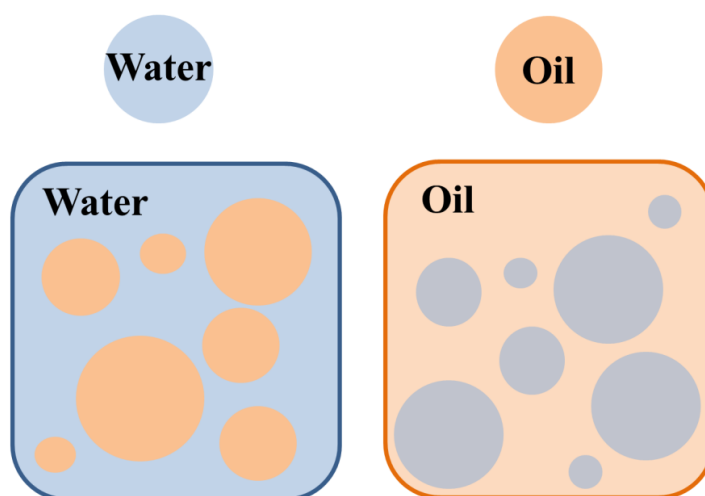


**Figure 6.** Oil-in-water emulsion (left) and water-in-oil emulsion (right). Surfactant not shown.

### 4.1.1 Formation

From an energetic standpoint, the kinetically stable emulsions have a total free energy associated with the formation of droplets ( $\Delta G_f$ ) than can be expressed through the following relationship<sup>111</sup>:

$$\Delta G_f = \gamma A - T\Delta S_f \quad (1)$$

Equation (1) includes the entropic term related to droplet formation ( $\Delta S_f$ ), the total surface area ( $A$ ), the temperature ( $T$ ) and the interfacial tension ( $\gamma$ ). The product  $\gamma A$  tends to be large and in fact, it outweighs the entropic term which means that the total energy is positive. This translates to a non-spontaneous thermodynamic process that requires either an energy input (i.e. emulsification process) or lowering the interfacial tension through a surface active agent or a combination of both. In the latter case, repulsive forces (electrostatic or steric) between the droplets provide a thermodynamic stabilization. Surfactant-stabilized droplets lose their ability to move, thus reducing the probability of collision giving them kinetic stability<sup>112</sup>. Evidently, these systems are not completely efficient in the sense that although some emulsions can be stable for decades, most of them (if not all) undergo through destabilization mechanisms.

To minimize the surface area, droplets tend to retain a spherical shape and so a relationship between the forces that act on the droplets and the interfacial tension can be established. This is known as the Laplace pressure ( $\Delta P$ ) and can be expressed as:

$$\Delta P = \gamma \left( \frac{1}{r_1} + \frac{1}{r_2} \right) \quad (2)$$

In which  $r_i$  are the radii of curvature of the droplet (in a spherical droplet they are equal). If an external force is to disrupt a droplet, it must overcome the Laplace pressure first.

### 4.1.2 Stabilization

The stability of emulsions or any other disperse system is strongly related to phase separation. The mechanisms of emulsion destabilization will be treated in the next section; however the important aspect here is that phase stability is dominated by various types of forces, short- and long-range<sup>113</sup>.

Van der Waals Interaction. Most of attractive forces can be described through this type of interaction. They arise when spontaneous electric and magnetic polarizations happen, thus an

electromagnetic fluctuating field is generated. When measuring these forces, the idea is to detect the variation in the electromagnetic wave energy with the distance between droplets<sup>114</sup>.

Hydrodynamic interactions. When the gap between two approaching droplets is reduced, the liquid between them is drained. These forces arise from viscous dissipation. In the case of emulsions this gap can be considered as a thin planar film and the liquid is drained due to the capillary suction pressure<sup>115</sup>.

Hydration Forces. These are forces of repulsive nature that are due to the dehydration of the polar groups (in a surfactant covered droplet) and a decrease in entropy<sup>115</sup>.

Electrical Double Layer. Emulsions prepared with electrolyte solutions (for example brine) inherently present with electrostatic forces. Naturally, counter-ions are attracted to the surface where as co-ions are repelled<sup>115</sup>. The double layer arises from the fact that the counter-ions try to get closer to the surface/interface, and the co-ions trying to diffuse back to the electrolyte solution. A widely used model to describe this double layer is that of Stern<sup>113</sup> in which part of the charge is within the *Stern layer* and other part is located in the *diffuse layer*. The interaction is governed by the boundary between these two layers, thus the relevant parameter is known as the *Stern Potential*. For relatively low potentials, the linear form of the Poisson-Boltzmann expression is valid<sup>113</sup>.

The discussion of the electrical double layer is necessarily linked to the DLVO theory. Named after its creators (Derjaguin, Landau, Verwey and Overbeek) it was proposed to describe the stability of a colloidal suspension as a competition between the Van der Waals attractive forces and the repulsive forces associated with the electrical double layer. As with any potential energy relationship, attractive forces dominate at very small and very large droplet-droplet distance while the repulsive forces act at moderate distances<sup>116, 117</sup>. Fig. 7 shows a typical DLVO plot. The extent of the magnitudes naturally depends on electrolyte concentration and pH and several scenarios can occur. For example, at long Debye lengths (highly charged surfaces in dilute electrolyte) the long-range repulsion peaks at the *energy barrier* (1-5 nm); the *primary and secondary minima* might be identified in slightly more concentrated electrolyte solutions. In this case, the energy barrier for particles in the proximities of the primary minimum may be too high to overcome, which means that droplets will remain disperse; Flocculation occurs in surfaces of low charge density, which means that

the energy barrier will be lower. When the value is lower than  $W=0$  (Fig. 7), the colloid dispersion is said to be unstable<sup>117</sup>

Hydrophobic Interaction. This type of interaction is a direct consequence of the hydrophobic parts present in an emulsion. In this sense, when hydrogen bonding is not possible (for instance negative charges at the interface), an attractive force emerges at certain spots of the interface. This force can be large and long-range<sup>118</sup>.

Structural forces<sup>116</sup>. These types of interactions come from the steric effects that a dense packed surface yields. In high internal phase emulsions, droplets are very close to one another. When the separation between two surfaces is so small (i.e. comparable to the size of a molecule) an oscillatory density profile is generated. With this profile, net attractive and net repulsive profiles can be studied.

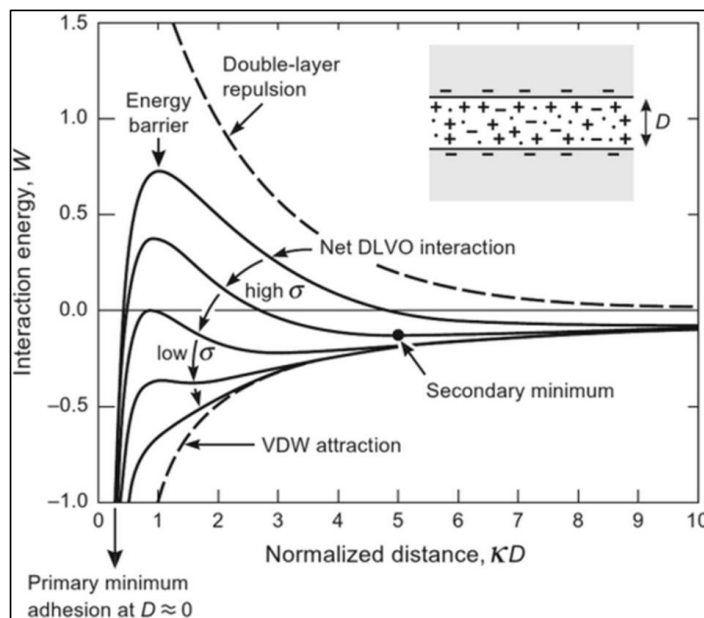


**Figure 7.** Schematic of the typical energy potential with distance in DLVO interactions. The double layer repulsion and Van der Waals attraction (VDW) are also shown. The interaction energy depends on the particle/droplet size or area in the case of planar surfaces. Original image reproduced from Israelachvili<sup>117</sup>

### 4.1.3 Destabilization

The study of the mechanisms that eventually lead to phase separation of emulsions is one of the most relevant aspects of colloidal science. In fact, it is a major field of research of the petroleum industry because emulsified water needs to be removed from the crude oil before refining. Emulsions can break down in different ways. Typically, six mechanisms are identified: creaming, sedimentation, flocculation, Ostwald ripening, phase inversion and coalescence. Emulsions can follow one or multiple mechanisms simultaneously<sup>119</sup>.

Creaming/Sedimentation. Gravity could play a key role in destabilizing emulsions, because of the density difference between the phases of the dispersed system. In W/O emulsions, sedimentation can occur due to the fact that water droplets have a higher density than most of the known oils<sup>120</sup>. The second element relevant to this mechanism is droplet size. Given that Brownian diffusion is exceeded in droplets of 1  $\mu\text{m}$  or more, these two phenomena have a high probability of occurring. The rate of creaming/sedimentation can be calculated using Stoke's law<sup>119</sup>.

$$v_0 = \frac{2 R^2 \Delta \rho g}{9 \eta_0} \quad (3)$$

Where  $R$  is the radius of the falling droplet,  $\rho$  the density difference between the phases,  $g$  the gravity constant and  $\eta_0$  the viscosity of the medium. This expression is valid for diluted emulsions. The creaming/sedimentation rate becomes a complex function of the concentration of the dispersed phase until it becomes zero (above the maximum packing fraction). A way of accelerating the rate of creaming/sedimentation is to use centrifugation; however this may lead to droplet deformation and eventually, to phase separation and flocculation<sup>119</sup>.

Flocculation. The tendency of droplets to aggregate in order to generate a more energetically stable state is known as flocculation. This also happens because the van der Waals attractive energy exceeds the repulsive energy<sup>121</sup>. The important feature of this type of instability is that the droplets keep their individuality, meaning that they do not coalesce. The rate of flocculation can be calculated using the following expression (valid only for dilute emulsions)<sup>119</sup>:

$$\tau = An_0V^2(1 + 2n_0kt) \quad (4)$$

Where  $A$  is an optical constant,  $n_0$  is the number of droplets at a time  $t = 0$ ,  $V$  is the volume of droplets and  $k$  is the constant of flocculation. Flocculation could potentially be addressed by means of light scattering techniques such as spectroscopy or by droplet counting methods. Stabilization of droplets by means of ionic or nonionic surfactants prevents flocculation due to electric double layer interactions and steric impediments.

Ostwald Ripening. It is a phenomenon that depends on the solubility difference between small and big droplets (in a polydisperse system) and the radii of curvature. The principle behind it is mass transfer might. Evidently, this is a thermodynamically-driven process and it is due to diffusion<sup>118, 119</sup>. According to the Lifshitz-Slezov-Wagner (LSW) theory, the rate of Ostwald ripening  $w$  can be calculated using the following expression:

$$\omega = \frac{d}{dt}(r_c^3) = \frac{8DS(\infty)V_m}{9RT} \quad (5)$$

Where  $r_c$  is the critical radius of the droplet,  $D$  is the diffusion coefficient of the dispersed phase in the continuous phase,  $S$  is the solubility of a particle of infinite radius,  $V_m$  is the molar volume of the dispersed phase,  $R$  is the gas constant and  $T$  the temperature. It is important to highlight that this process tends to be very slow compared to other destabilization mechanisms.

Coalescence. Is the mechanism by which two or more droplets merge during contact to form a single daughter droplet. This phenomenon is mainly due to the rupture of the thin film present at the interface. The film ruptures because the liquid that resides between the small gap created by the contacting droplets is drained<sup>122</sup>. Fig. 8 shows a simple schematic depicting two droplets in contact and the motion of the surface active molecules towards the “Barrier Ring”, leaving a surfactant-free area or in other words, film drainage. The generation of a surfactant-free area that leads to coalescence is not as straightforward as shown in Fig. 8. In order for this to happen, the so called Gibbs-Marangoni effect must be overcome. This phenomenon, given that the surfactant is dissolved in the continuous phase, is a self-stabilizing mechanism mainly because when two droplets approach each other and surfactant-free area is being formed, an interfacial tension gradient is created, thus this area will tend to adsorb more surfactant and, consequently, prevent coalescence. This is valid only if the droplets are poorly covered or when there is a non-equilibrium situation<sup>123</sup>. An important concept in coalescence that arises when the interaction between two approaching droplets is relevant enough to form the film is that of the disjoining pressure ( $\Pi$ ). Generally speaking,



positive values of  $\Pi$  represent repulsion between the two surfaces that form the film, and negative values of  $\Pi$  represent an attraction<sup>122</sup>.

How the film actually breaks is another important part of droplet coalescence studies. Different mechanisms have been proposed. First, the *capillary-wave mechanism* states that when the film thickness decreases, the disjoining pressure enhances the amplitude of these waves, eventually causing the surfaces to touch (thus breaking the film after a critical thickness has been reached<sup>124</sup>). Second, the *nucleation of pores* states that in a film with amphiphilic molecules attached to it as monolayers, due to an energy imbalance, a pore is formed and in some cases, the film is broken<sup>114</sup>. Third, the *transport of solute across the film* mechanism is based on heat and mass transfer across the film, which enhances Marangoni instabilities causing forced capillary waves which lead to film break<sup>125</sup>.

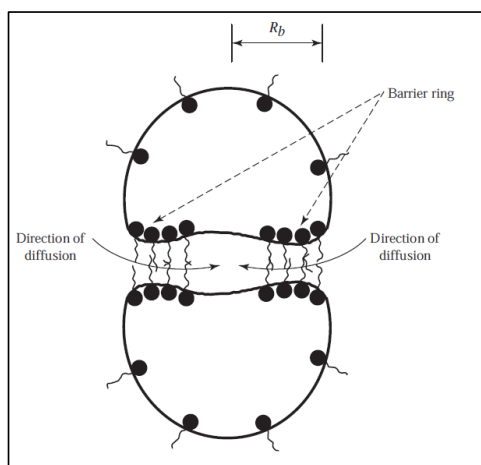


**Figure 8.** Two surfactant-covered droplets in contact. Image reproduced from Giribabu et al.<sup>126</sup>

## 4.2 Asphaltene-stabilized emulsions

Asphaltene adsorption at the liquid-liquid interface is characterized by a rapid initial adsorption with a fast diffusion where the main decrease in the interfacial tension is observed. The time dependence after this step is minor and is attributed to relaxation processes at the interface<sup>25, 127</sup>. The mechanism for emulsion stabilization is attributed to the formation of a mechanically strong film or, “skin”, at the interface that prevents droplets from coalescing. The skin is most likely the result of asphaltene self-association at the liquid-liquid interface and the progressive build-up of a multilayer<sup>128</sup>. In fact, it has been shown<sup>129</sup> that asphaltenes can for instance, stabilize thin organic liquid films at concentrations much lower than

maltenes and bitumen. Similarly, the drainage of such films is much faster for the latter case which also happens to be the case in which the films are much thinner. Additionally, asphaltenes adsorb irreversibly at the oil-water interface<sup>93, 130, 131, 132</sup>. This has been confirmed through interfacial tension measurements and Langmuir films.

Asphaltenes are not considered “classical” surfactants (such as Span 80, Fig. 9) in the sense that they are not precisely amphiphilic molecules. Asphaltenes do not exhibit a critical micelle concentration (CMC), instead, they form nanoaggregates and clusters that are prone to reorganization and relaxation processes<sup>25, 111</sup>. Stability is strongly related to the solvation (aggregation) state of asphaltenes, and it has been shown<sup>29, 133</sup> that when they are close to their precipitation onset (in the presence of *n*-heptane for instance), the emulsions exhibit a maximum in their stability. The pH of the aqueous media influences stability mainly because of the protonation/deprotonation of the –COOH groups and/or action of basic components. Similarly, the presence of electrolytes can contribute to a “salting-out” effect, which makes the molecules less soluble in the aqueous phase<sup>111</sup>.

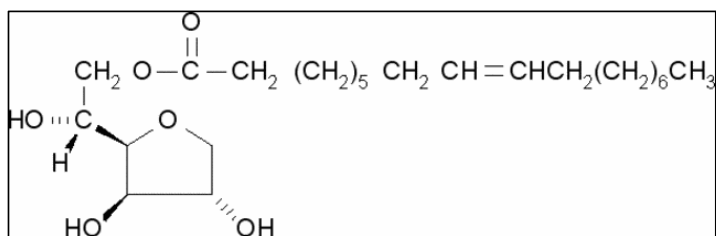


**Figure 9.** Chemical structure of Span 80 (sorbitan monooleate) considered as a “classical” amphiphilic surfactant.

#### 4.3.1 Rheology of asphaltene interfaces

Interfacial rheology is a suitable technique to study and characterize asphaltene interfaces. With these techniques it is possible to obtain shear, dilatational and mix-field flow types which allow elucidating different aspects of asphaltene films. The main difference between shear and dilatational is that in simple shear experiments, flow is induced at a constant area, while in dilation the area of the interface is changed<sup>111</sup>. This might cause adsorption/desorption of material from the interface. In this section, studies using two

different geometries (shear) and studies using the pendant drop technique (dilatational) are highlighted.

Studies on interfacial shear rheology<sup>134, 135</sup> using a biconical geometry showed that asphaltenes form films of high elasticity after several hours of aging. This behavior seems to be more pronounced for asphaltenes with higher heavy metal content, polarity and lower aromaticity<sup>132</sup>. It was also observed that the elastic modulus ( $G'$ ) and adsorption kinetics are enhanced when asphaltene films are formed near the precipitation onset. Furthermore, a concentration threshold range of 2-5 g/L was found for the formation of the mechanically strong film at the oil/water interface after aging. Introduction of resins seemed to cause a rapid reduction in the elasticity of the film.

Samaniuk et al.<sup>136</sup> recently studied asphaltenes at the hexadecane/water interface using a double wall-ring (DWR) geometry<sup>137</sup> confirming the effects of concentration and aging. They concluded that: (i) asphaltene films at the oil/water interface behave as soft-glassy materials; (ii) the crowding of the interface plays a crucial role and, (iii) the concentration/frequency-dependent data is in agreement with a soft-glassy rheology (SGR) model. Using a similar geometry, Harbottle et al.<sup>127</sup> showed that the microstructure of the asphaltene network film at the oil/water interface can be liquid-like or solid-like depending on the initial bulk concentration, aging time of the interface and solvent aromaticity. An important observation made was that the transition states could be related to the shear yield stress (as the film microstructure starts to be dominated by elasticity) which might act as an energy barrier against drop coalescence. In fact, consolidated films around asphaltene droplets do not coalesce after certain aging times. Naturally, Adsorption kinetics plays a key role in the development of the mechanical properties of asphaltene films. It has been shown<sup>138, 139</sup> that asphaltene adsorption is diffusion-controlled at short times with individual molecules, transitioning possibly to a barrier-controlled regime in which larger aggregates are involved.

The literature regarding interfacial dilatational rheological studies (pendant drop technique) of asphaltene films at the liquid-liquid interface is extensive<sup>39, 140, 141, 142, 143, 144</sup>. These studies report a behavior that is somewhat general to asphaltenes. First, the apparent elastic dilatational modulus ( $E'$ ) increases with time. This is an indication of the kinetic build-up of the film, crowding and possible cross-linking of asphaltenes at the interface. Second, a maximum in  $E'$  with concentration is observed, the location will depend on the conditions of

the experiment and asphaltene origin<sup>140, 142, 143, 145</sup>. And third, if the aged interface is contracted, a phenomenon described as crumpling has been observed<sup>142</sup>.

It is imperative to emphasize that in pendant drop experiments, depending on the dominating phenomena, the nature of the measured quantities will vary. For instance, at interfaces largely dominated by interfacial tension, the influence of the exchange with the bulk is dominant (adsorption/desorption dynamics), whereas extra mechanical stresses are essentially negligible; this is often the case for low molecular weight surfactants. At interfaces dominated by extra stresses, as in the case of particle monolayers or asphaltenes that clearly exhibit a skin, the nature of the elastic response is fundamentally different. Hence, when discussing the moduli extracted from dilatational experiments it should be noted that these may not always be true material functions.

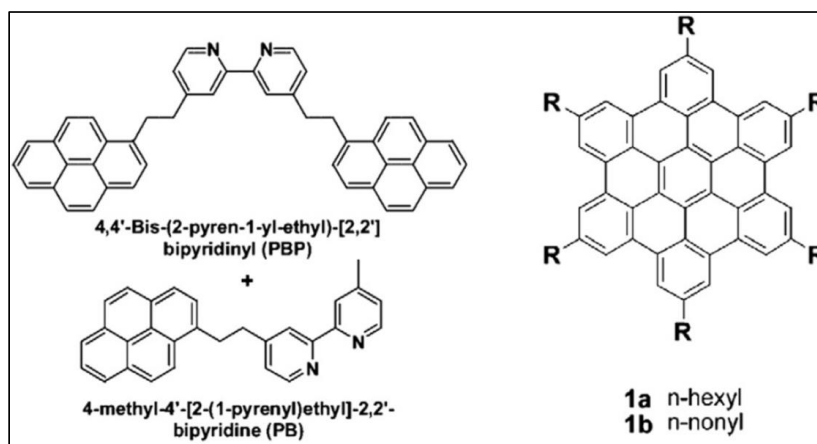
## 5. Model compounds

Sjöblom et al<sup>146</sup>. recognized two possible approaches to tackle the issue of understanding asphaltene properties. One approach is to develop a fractionation plan of the asphaltene content to split it into sub-fractions of different functionalities determined by precipitant/solvent mixtures. The main disadvantage of this approach is that the obtained asphaltene sub-fractions are still polydisperse and heterogeneous, hence accurate determination of the agents responsible for adsorption properties is still troublesome. The second approach is to design a molecule (or a group of molecules) that mimic the main features of asphaltene behavior in terms of self-association and adsorption properties. Substantial work on model compounds has been done following primarily the continental model with few studies based on the Archipelago model.

Different model compounds have been synthesized using different approaches thus it is not uncommon to find different families of these molecules. Here, model compounds based on pyrene, alkylated hexabenzocoronene and perylene are highlighted.

Akbarzadeh et al.<sup>147</sup> studied the self-association properties (aggregation number and stability of aggregates in solution) of a series of derivatives of the four-ring component pyrene. These properties were significantly different than those of the indigenous asphaltenes in similar solutions. More specifically, the model compounds formed, in the best cases, dimers and trimers where asphaltenes are known to have aggregation numbers between 5-7. This lead to

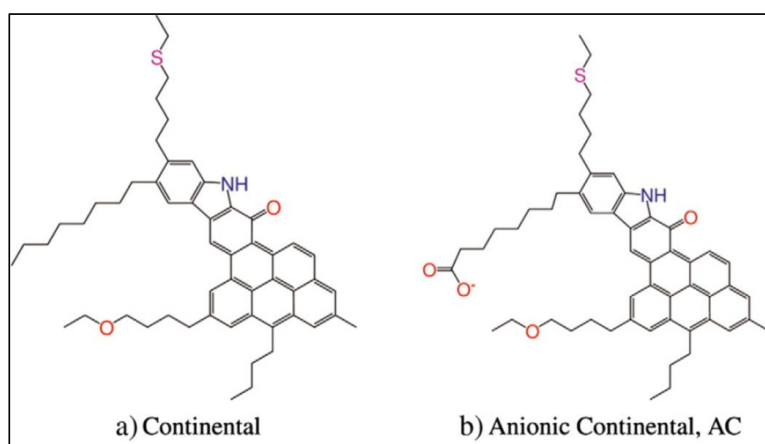
the conclusion that the pyrene-based compounds proposed lack core features that represent real systems. Rakotondradany et al.<sup>148</sup> studied the self-association properties of a model compound based on alkyl hexabenzocoronenes. Their study showed that even at concentrations as high as 15 g/L the model compound tends to form dimers, uncharacteristic of indigenous asphaltenes. The self-association, cracking and coking properties of archipelago pyrene-based model compounds was studied by Tan et al.<sup>149, 150</sup>. The authors found that the compounds self-associate due to  $\pi$ - $\pi$  stacking interactions involving the pyrene rings and the bipyridine spacer and that the model compounds in the presence of heteroatoms exhibited coke yields comparable to hydrocarbon compounds. Fig. 10 shows some of the model compounds used in the previous studies.



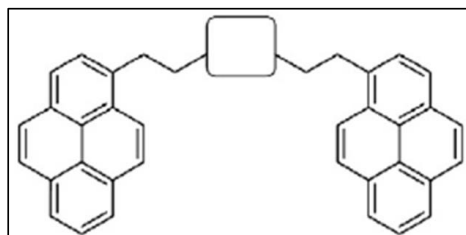
**Figure 10.** Model compounds based on pyrene (left) and hexabenzocoronene (right). Original image reproduced from Sjöblom et al<sup>146</sup>

Molecular dynamic simulations (MDS) performed by S. Bhattacharjee and J. Masliyah<sup>35, 151</sup> using different model compounds (archipelago, continental and anionic continental) showed that, like indigenous asphaltenes, their model compounds tend to self-associate in pure solvents by  $\pi$ - $\pi$  stacking. Similarly, simulations at the oil/water interface showed that aggregates of the model compounds are adsorbed and the acidic functionalities seem to form hydrogen bonds. They found that the stacked polyaromatic rings are perpendicularly oriented to the same interface. Finally, the authors showed that molecules with charged terminal groups are tethered to the toluene-water interface contrary to uncharged compounds. Two continental-based compounds used in MDS studies are shown in Fig. 11 and it can be noted that they have different functionalities.

Three studies<sup>150, 152, 153</sup> of pyrene-based asphaltene model compounds that follow the Archipelago model measured the cracking kinetics and the coke yield. The authors showed that the initial cracked fragments are recombined to form larger structures through a free-radical process. These compounds exhibited higher yields of coke compared to indigenous hydrocarbon compounds. When the biomarker structure 5 $\alpha$ -cholestane was incorporated to the model compounds, cracking kinetics and coke yields improved to value ranges comparable to indigenous components of oil. The basic structure of these model compounds is shown in Fig. 12 in which the blank part in the middle of the molecule is replaced by different components.



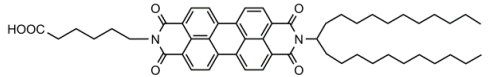
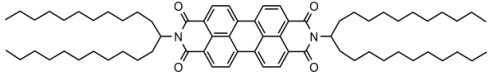
**Figure 11.** Model compounds used for MDS studies. Different functionalities arise by the concentration of heteroatoms. Image partly reproduced from Sjöblom et al<sup>146</sup>.



**Figure 12.** Pyrene-based model compound that follows the Archipelago model. The blank space in the middle of the molecule is replaced by groups of different functionalities. Image partly reproduced from Sjöblom et al<sup>146</sup>.



properties are presented in table 3. C5PeC11 is a molecule with an acidic end group and BisAC11 has aliphatic end groups. The underlying principle of this segregation of functionalities (acidic, basic among others) is the experimentally observed differences of indigenous asphaltenes obtained through various precipitation methods<sup>159</sup>.

| Compound | Molar mass g/mol | Structure  |
|----------|------------------|--|
| C5PeC11  | 827.12           |  |
| BisAC11  | 1035.60          |  |

**Table 3.** General aspects of the model compounds used in this study.

## 6. Experimental Techniques and Theory.

### 6.1. Surface tension (ST) and interfacial tension (IFT) measurements

#### 6.1.1 The Du Noüy ring.

The Du Noüy ring is a known technique used for measurements of the interfacial/surface tension at the liquid-liquid or liquid-air interface. Fig. 14 shows a simple schematic of the ring immersed in two liquids. The cuvette in which the liquids are contained can slowly move up and down and the force ( $F$ ) required for the ring to pass through the liquids (and the interface) is registered by a microbalance attached to the ring as a function of time. The interfacial tension ( $\gamma$ ) is related to the measured force via equation (6) in which ( $r$ ) is the radius of the ring and ( $\beta$ ) is a correction factor<sup>160</sup>.

$$\gamma = \frac{F}{4\pi r} \beta \quad (6)$$

This technique is very versatile and preferred over other techniques mainly because its resolution tends to be very high ( $\pm 0.01$  mN/m) and the fact that the force is being directly measured and not indirectly calculated. With this technique it is also possible to determine the critical micelle concentration (CMC) if the ring set-up is coupled with an accessory that delivers aqueous solution in a controlled way.



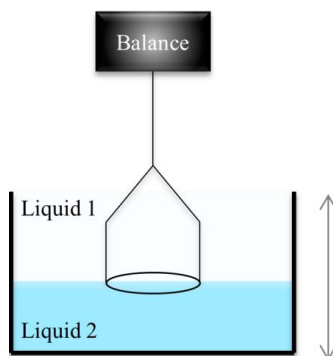


**Figure 14.** The Du Noüy ring. A cuvette filled with two liquids moves in the direction of the arrows. A microbalance registers the force needed for the ring to go through the different phases as a function of time and this force is related to the interfacial tension.

Even though this method is widely used, it has several limitations. (i) surface/interfacial tensions lower than 1 mN/m are not possible to detect; (ii) measurements at short times (< 1 min) are not usually possible, hence kinetics of highly surface active agents that reach equilibrium rather fast are not possible to determine; (iii) every time the ring passes through the surface/interface, the equilibrium state is physically disturbed, which means that a new equilibrium state has to be reached.

### 6.1.2 Axisymmetric drop shape analysis (ADSA).

A Gibbs dividing surface is a zero-thickness mathematical surface that allows a division between the bulk (in which the concentration of a species is rather constant) and a phase boundary (i.e. interface) to which the species has adsorbed and the concentration varies<sup>161</sup>. Such surface is generated in the known pendant-drop and micropipette techniques which allow a measurement of the interfacial (or surface) tension at the liquid-liquid (or liquid-air) interface<sup>162</sup>. In these techniques, when liquid-liquid systems are being studied, a drop of one of the liquids is produced in the second immiscible liquid.<sup>163</sup> The drop can be rapidly analyzed through the use of powerful software coupled with CCD cameras. The technique is commonly known as axisymmetric drop shape analysis (ADSA), and it is widely accepted as a robust and versatile method for measuring the interfacial tension (IFT).<sup>164</sup> The equilibrium surface/interfacial tension data can be described through adsorption isotherms and equations of state. For instance, the well-known isotherms of Henry, Langmuir, Frumkin and

Freundlich have been widely used to describe the adsorption of several surface active compounds onto liquid-air, liquid-liquid interfaces and liquid-solid surfaces.<sup>165, 166</sup>

This technique is an indirect method for determining the surface/interfacial tension of a system. When a drop is created at the tip of a capillary, its contour is recorded. The digital images are then analyzed and fitted to the Young-Laplace equation with an accuracy of  $\pm 0.1 \text{ mN/m}$ . This equation relates the curvature of a liquid drop and the surface/interfacial tension. The built-in software produces a family of theoretical curves by changing the values of the surface/interfacial tension. The curve that yields the best fit to the experimental points represents the measured surface/interfacial tension. For this procedure the densities of the oil and aqueous phase are needed and the volume of the droplet is controlled via constant feedback from the images<sup>164</sup>. A simple schematic of the system is given in Fig. 15.

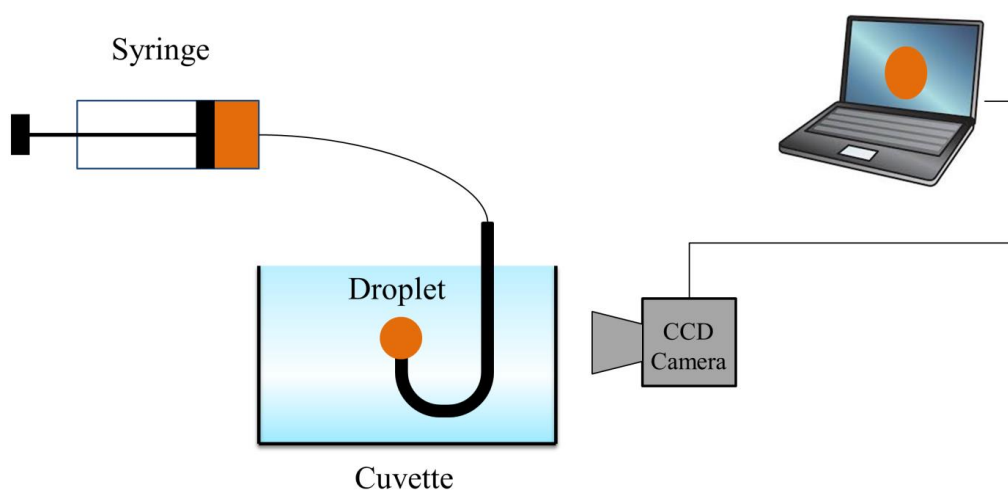


**Figure 15.** Schematic of the ADSA device in which the silhouette of a droplet formed by a syringe/pump system is recorded through a CCD camera for analysis.

Through ADSA it is possible to study: (i) adsorption and desorption kinetics of surface active species, (ii) interfacial dilatational rheology, (iii) time-dependent relaxation processes and (iv) partitioning at various interfaces. Through IFT measurements it is possible to assess the degree of adsorption of chemical species and this can be extrapolated to the effects on emulsions. In the case of asphaltenes at the hydrocarbon-water interface it has been possible to establish that adsorption kinetics is characterized by two regimes: a rapid initial adsorption at short times followed by small changes in the IFT at longer times. Additionally, the absence

of an equilibrium region strongly suggests the presence of important relaxation processes such as reorganization and/or multilayer formation<sup>130, 146</sup>.

If gravity ( $g$ ) is the only force exerted on the droplet, the Young-Laplace equation becomes:

$$\Delta P = (\Delta\rho)gz - \gamma \left( \frac{1}{R_1} + \frac{1}{R_2} \right) \quad (7)$$

In the above equations, ( $R_i$ ) are the radii of curvature of the droplet/bubble, ( $z$ ) represents the distance analogous to the height of a column and ( $\Delta\rho$ ) the density differences between the phases.

One of the main advantages of this technique is that it is possible to determine the interfacial/surface tension at very short times ( $< 5$  s). This allows an analysis of the adsorption kinetics in this range. Other advantages include the easy implementation and the possibility of performing interfacial dilatational rheology measurements.

#### **6.1.2.1 Double coaxial capillary.**

This accessory to the ADSA device originally reported by Ferri et al.<sup>167</sup> and further developed by Kotsmár et al.<sup>168</sup> and Ferri et al.<sup>164</sup> allows the study of convection-enhanced adsorption/desorption kinetics of a liquid-liquid interface. The experimental set-up consists of a pendant (or emerging) drop formed at the end of a primary capillary initially at equilibrium with a bulk concentration of surface active molecules. The interface is then driven away from equilibrium by injecting a surfactant free solution through a secondary syringe/pump system generating a change in the dynamic interfacial tension<sup>164</sup>. The interfacial tension is measured at all stages of this process which means that desorption mechanisms can be followed. A schematic of this system is presented in Fig. 16.

### **6.2 Interfacial rheology**

#### **6.2.1 Interfacial dilatational rheology.**

Axisymmetrical drop shape analysis (ADSA) has been recognized as a reliable method for interfacial rheology measurements<sup>162, 169</sup> besides being an accurate method for interfacial tension experiments. The principle behind interfacial dilatational rheology is that the interfacial tension varies when the area ( $A$ ) of a droplet is changed in an oscillatory manner at a given frequency ( $\omega$ ) from an initial ( $A_0$ ) to a value ( $A_a$ ) following equation (8)<sup>170</sup>.

$$\Delta A = A - A_0 = A_a \sin(\omega t) \quad (8)$$

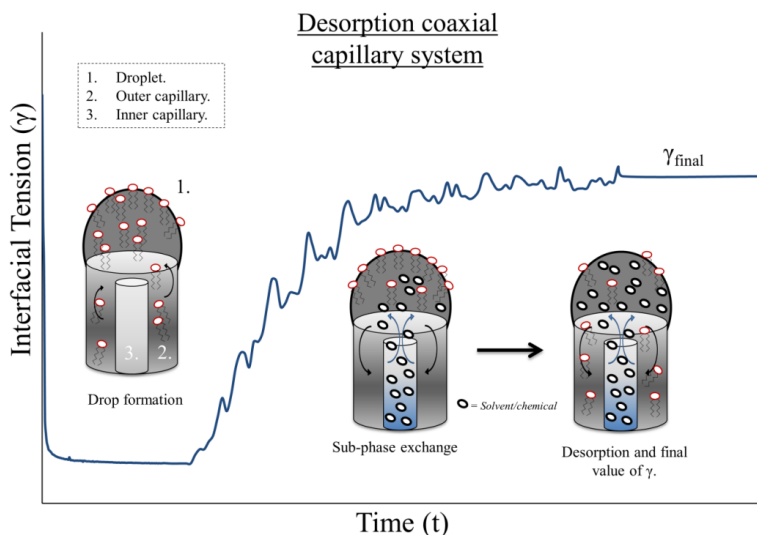


**Figure 16.** Schematic of the coaxial capillary system used for desorption experiments. A droplet (1) of constant volume is formed via an outer capillary (2) and is let to equilibrate for a fixed time. The predetermined volume of solvent or chemical species is pumped via an inner capillary (3) at a given flow rate. The interfacial tension is continuously measured through all steps.

The complex dynamic apparent dilatational modulus ( $E^*$ ) is then typically defined as the Fourier transform ( $\mathcal{F}$ ) of the change in interfacial tension ( $\gamma$ ) relative to the change in interfacial area via equation (9). The complex modulus can also be interpreted by a real and an imaginary part. The real part characterizes the elastic properties of the interfacial layer and the imaginary part characterizes the viscous properties. These parts are referred as to the apparent elastic dilatational modulus  $E'$  and the apparent viscous dilatational modulus  $E''$ .

$$E^*(\omega) = \frac{\mathcal{F}\{\Delta\gamma(t)\}}{\mathcal{F}\{\Delta\ln(A(t))\}} = E'(\omega) + iE''(\omega) \quad (9)$$

Lucassen and van den Tempel<sup>171</sup> proposed a model for the variation of the elastic and viscous dilatational moduli as a function of the concentration ( $c$ ) valid for flat surfaces. The main underlying assumption of this model is that the adsorption is diffusion-controlled. In this model, the elastic and viscous components of the complex modulus depend on the independent contributions of the instantaneous elasticity ( $E_0 = \Gamma(d\gamma/d\Gamma)$ ) and a parameter that accounts for diffusion defined as:  $\Omega = \sqrt{D/2\omega}(dc/d\Gamma)$  in which ( $D$ ) is the diffusion

coefficient. The elastic and dilatational moduli are therefore calculated using equations (10) and (11).

$$E'(\omega) = E_0 \frac{1 + \Omega}{1 + 2\Omega + 2\Omega^2} \quad (10)$$

$$E''(\omega) = E_0 \frac{\Omega}{1 + 2\Omega + 2\Omega^2} \quad (11)$$

### 6.2.2 Interfacial shear rheology and the double wall-ring (DWR) geometry.

There are several devices and measuring probes available to determine the interfacial rheological properties in shear and dilatation mode. In the specific case of shear rheology, a common issue is the correct quantification of the flow profiles at the interface and their interaction with the flow profiles in the bulk<sup>137, 172</sup>. The Boussinesq number (Bo) relates these two flow profiles as the ratio between the surface drag and the subphase drag described in equation (12)<sup>137</sup>.

$$Bo = \frac{\eta_s(V_1/L_1)P_1}{\eta(V/L_s)A_s} = \frac{\eta_s}{\eta G} \quad (12)$$

In this equation,  $\eta_s$  is the surface shear viscosity in steady shear flow,  $\eta$  is the average bulk viscosity,  $V$  is the characteristic velocity,  $L_1$  and  $L_s$  are characteristic length scales,  $P_1$  is the contact perimeter between the probe and the interface and  $A_s$  is the contact area between the geometry and the subphase. The term  $\frac{A_s L_1}{L_s P_1} = G$  is defined as a characteristic length and depends on the dimensions of the geometry. The Bo number can be transformed to incorporate non-Newtonian and viscoelastic interfaces. The double wall-ring (DWR) geometry is a device that minimizes the value of  $G$  hence maximizing the Bo number for a given  $\eta_s/\eta$  ratio. This leads to higher sensitivity in oscillatory and rotational measurements. Furthermore, the DWR can be coupled with a Langmuir trough and, in this way, the determination of the rheological properties of an interface at different surface coverage is possible<sup>137, 172</sup>.

The DWR + trough setup (Fig. 17) consists of a Pt/Ir ring + Teflon cup accessory placed on a Langmuir trough and connected to a stress-controlled rheometer. The cup and the ring have openings along their surfaces to ensure a uniform measuring interface inside and outside the DWR. The main advantage of this system is that two kinds of measurement can be performed at the liquid/air or liquid/liquid interface: steady-state shear flow and oscillatory flow. In this

way, surface pressure isotherms, interfacial shear rheology and monolayer or multilayer microstructure can be systematically studied.

For the Langmuir trough part of this setup, it can be said that a Langmuir layer refers to a monolayer of molecules adsorbed at a given interface. Langmuir and Langmuir-Blodgett (LB) film techniques are suitable for studying such films because of (i) the presence of a large interfacial area in which monolayers can be formed hence conformations can be inferred, (ii) the monitoring of the interfacial pressure ( $\pi$ -A isotherms) during compression/expansion of the interfacial film, (iii) the possibility to transfer such films onto a solid substrate to study its topographical features and (iv) the possibility to add any type of molecules onto the film to study interactions between already adsorbed species<sup>173, 174, 175, 176</sup>.

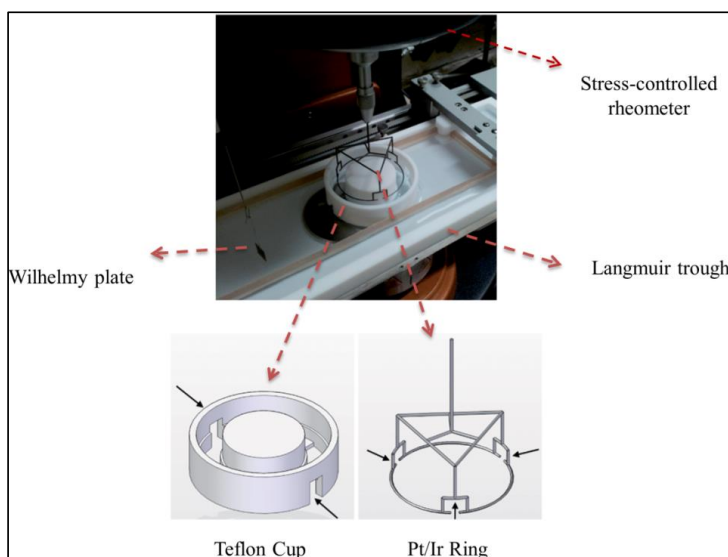


**Figure 17.** Double wall-ring (DWR) + Langmuir trough system adapted to a stress-controlled rheometer. The openings in the Teflon cup and the ring (black arrows) allow a uniform interface inside and outside the system. Image taken from Hermans and Vermant<sup>172</sup>.

### 6.3 Microcalorimetry

Adsorption of a solute from a solution is a physical phenomenon that is normally accompanied by a heat effect<sup>177</sup>. If the main features of the surface are known, microcalorimetry is a suitable method to follow the adsorption process because the adsorption

enthalpy depends on the nature and density of the adsorbing sites, the conformations of the adsorbed molecule(s) and the interactions among adsorbed species (also known as lateral interactions).<sup>178, 179</sup> Fig. 18 shows a typical setup for titration calorimetry experiments. A suspension of the adsorbent is stirred inside a calorimetric cell. Once thermal equilibrium has been attained, the stock solution of the species of interest is introduced step-by-step into the cell and the heat registered through the use of thermopiles. The calorimetric peak (i.e. experimental point) is then treated to separate the heat of adsorption from the heat of dilution (blank experiment).

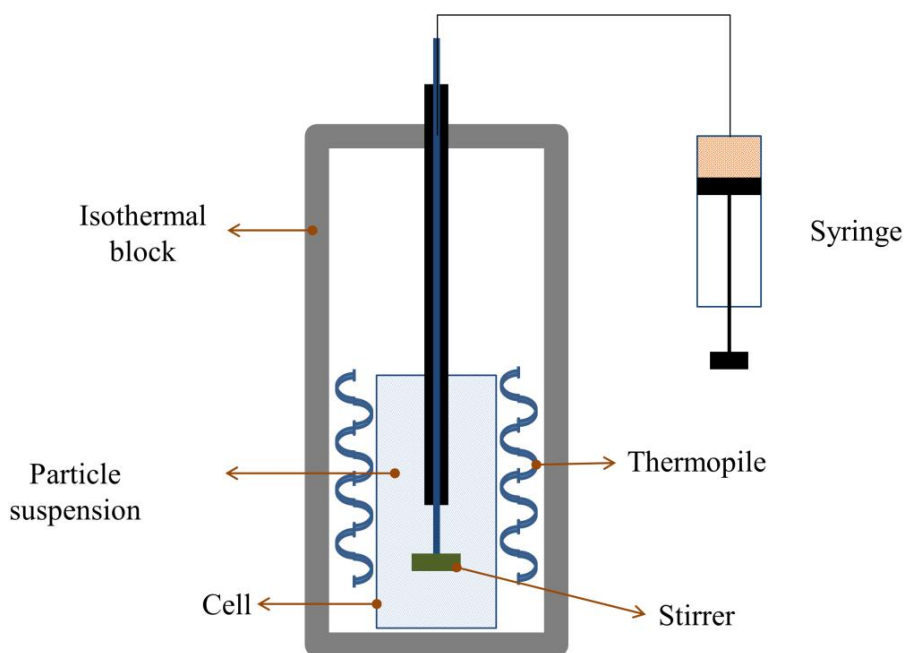


**Figure 18.** Experimental setup of a titration calorimeter. A syringe that contains the stock solution of the species of interest is injected to the measuring cell that contains a suspension of the adsorbate. The system is continuously stirred and the heat measure via the thermopiles.

#### 6.4. Quartz crystal microbalance with dissipation (QCM-D)

QCM-D operates based on the property of piezoelectricity. The piezoelectric quartz coated-crystal is located between the two metal electrodes. By applying an AC voltage across the electrodes, the crystal is excited to oscillate. The frequency of oscillation depends on the mass adsorbed onto the surface of the crystal. The relationship between the change in

frequency ( $\Delta f$ ) due to the mass adsorbed ( $\Delta m$ ) was established by Sauerbrey<sup>180</sup> through equation (13):

$$\Delta m = -\frac{\rho_q t_q}{f_o n} \Delta f = -\frac{\rho_q v_q}{2f_o^2 n} \Delta f = -\frac{C}{n} \Delta f \quad (13)$$

Where  $\rho_q$  and  $t_q$  are the mass density and thickness of the crystal respectively,  $v_q$  is the shear wave velocity in quartz,  $f_o$  is the fundamental frequency of crystal and  $n$  is the overtone number and C is a constant. The Sauerbrey equation is valid only when the mass adsorbed is evenly distributed on the surface,  $\Delta m$  is smaller than the mass of the crystal and the adsorbed mass is rigidly attached to the surface<sup>180</sup>.

The change in dissipation due to adsorption is given by equation (14)<sup>181</sup>:

$$D = \frac{E_{dissipated}}{2\pi E_{stored}} \quad (14)$$

Where D is the dissipation factor,  $E_{dissipated}$  is the energy dissipated during one period of oscillation and  $E_{stored}$  is the energy stored in the oscillating system. In the case of formation of viscoelastic films on the surface, the Sauerbrey relationship equation (13) is no longer valid.



## 7. Main Results

### 7.1 Paper 1

#### *Mixed interfaces of asphaltenes and model demulsifiers part I: adsorption and desorption of single components*

In this article, aspects related to competitive adsorption and desorption dynamics between a model molecular demulsifier (Brij®-93) and asphaltenes at the liquid-liquid interface are studied.

First, the Langmuir and Frumkin isotherms were successfully used to describe the interfacial tension data allowing the determination of the equilibrium adsorption parameters of asphaltenes and Brij®-93. Table 7.1.1 shows the equilibrium constants ( $K_L$ -  $K_F$ ) and the maximum adsorbed amount ( $\Gamma_\infty$ ) for both species using both isotherms. In general both equations of state (EoS) can be used; however care should be taken because of the assumptions behind each model. For example, the Langmuir EoS assumes that there is no interaction among adsorbed species which seems to occur given the non-zero value of the parameter ( $A$ ) when using the Frumkin EoS. Based on the K-values it was concluded that the model molecular demulsifier is more surface active than indigenous asphaltenes.

| <b>Asphaltenes</b> | <b>Technique</b> | $K_L$ - $K_F$ [ $m^3/mol$ ] | $\Gamma_\infty$ [ $mol/m^2$ ] | $A$  |
|--------------------|------------------|-----------------------------|-------------------------------|------|
| <i>Langmuir</i>    | ADSA             | 228                         | $9.54 \times 10^{-7}$         | 0    |
|                    | Du Noüy          | 106                         | $9.32 \times 10^{-7}$         | 0    |
| <i>Frumkin</i>     | ADSA             | 97                          | $9.56 \times 10^{-7}$         | 1    |
|                    | Du Noüy          | 161                         | $7.85 \times 10^{-7}$         | 1    |
| <b>Brij® 93</b>    |                  |                             |                               |      |
| <i>Langmuir</i>    | ADSA             | 834                         | $1.06 \times 10^{-6}$         | 0    |
|                    | Du Noüy          | 300                         | $1.27 \times 10^{-6}$         | 0    |
| <i>Frumkin</i>     | ADSA             | 620                         | $1.19 \times 10^{-6}$         | -0.4 |
|                    | Du Noüy          | 748                         | $1.19 \times 10^{-6}$         | -0.2 |

**Table 7.1.1.** Equilibrium parameters of asphaltenes and Brij-93 using the Langmuir and Frumkin isotherms.

The values reported in table 7.1.1 are in agreement with the fact that asphaltenes have been shown to self-associate in solution; hence interactions at the interface are expected. This would be represented by the non-zero value of the parameter  $A$ <sup>159, 182</sup>. On the other hand, the

negative values for the interaction parameter A could indicate the presence of repulsive forces acting at the interface<sup>183</sup>.

Second, desorption of single compounds from the xylene/water interface was followed through the use of a double coaxial capillary system. Fig. 7.1.1 is a mixed plot showing the influence of the total volume exchanged, solvent flow rate and adsorption time on desorption of asphaltenes induced by xylene. It was found that asphaltenes are irreversibly adsorbed (~2% amount desorbed assuming that a Langmuir-based model is valid) at the oil/water interface even at low surface coverage and low adsorption times, which confirms the strong interactions present. These findings are in agreement to what has traditionally been reported for asphaltenes. It has been suggested that the irreversible nature of asphaltene adsorption is closely related to the formation of the mechanically strong film which happens to be a consequence of the initial fast adsorption of bulk aggregates followed by multilayer formation of asphaltenic stacks<sup>25, 155, 184</sup>.

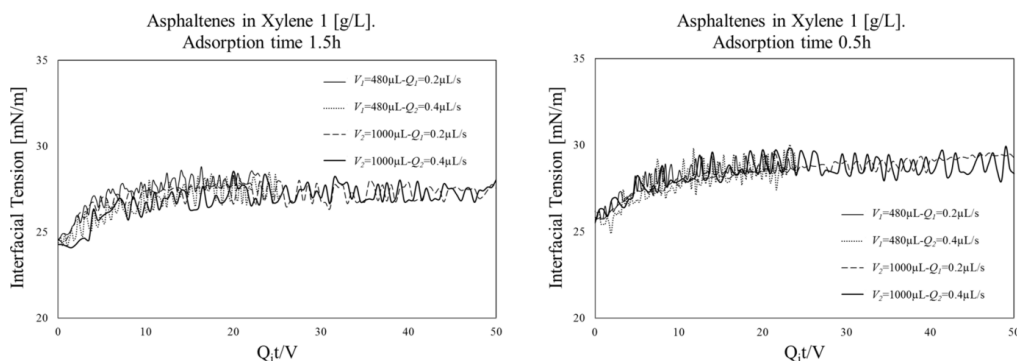


**Figure 7.1.1.** Asphaltene desorption from the xylene/water interface at different experimental conditions.

It was also found that desorption is independent of the solvent flow rate and the total volume exchanged. Similarly, Fig. 7.1.2 shows a similar plot of desorption of asphaltenes by xylene. In this plot, the effect of the initial asphaltene concentration is only seen at values ranging from 1 to 6 g/L. At low concentrations (0.1 g/L), the amount desorbed is lower. These experiments were performed to evaluate the effect of initial bulk concentration which is related to asphaltene aggregation and hence to sorption aspects. It has been recently pointed out<sup>129</sup> that emulsion stability is not solely driven by a reduction of the interfacial tension. There are other mechanisms present such as complex network formation enhanced by  $\pi$ - $\pi$  stacking and H-bonding that influence sorption dynamics and through these experiments it was possible to have a glance of those ideas.

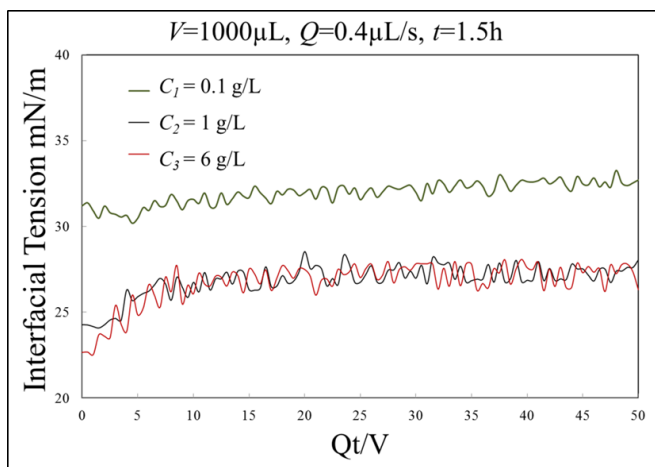


**Figure 7.1.2.** Asphaltene desorption from the xylene/water interface at different initial concentrations.

Finally, Fig. 7.1.3 shows a plot of desorption of Brij-93 by xylene at different initial concentrations. Experimental conditions are also shown. The results show that the model demulsifier Brij®-93 is partly desorbed (~20%) from the xylene/water interface and that the effect of the initial concentration is negligible at low values (10 ppm) whereas at high values (100-500 ppm) the degree of desorption is similar. This could be attributed to the distribution of ethyl oxide (EO) groups in the polydisperse sample or to the polydispersity of the aggregates adsorbed which have different adsorption energies. It has been shown<sup>39, 185</sup> that larger aggregates could freeze at the interface which means that only the smaller aggregates are able to desorb. The results here would be in agreement with that statement.

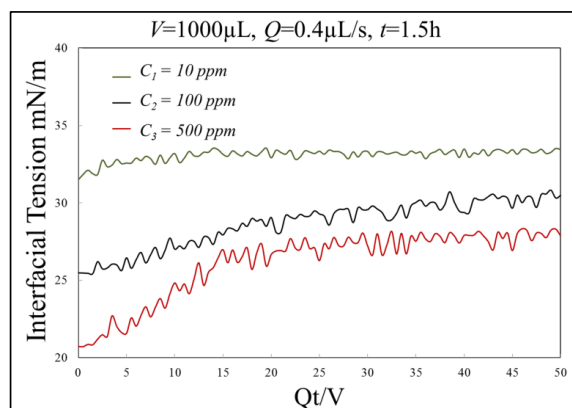


**Figure 7.1.3.** Brij-93 desorption from the xylene/water interface.

## 7.2 Paper 2

### *Mixed Interfaces of Asphaltenes and Model Demulsifiers, Part II: Study of Desorption Mechanisms at Liquid/Liquid Interfaces*

The findings of **paper 1** were extended in this study to include a second demulsifier of different chemical structure and properties and to assess the mechanisms involved during desorption induced by demulsifiers.

The composition of mixed interfaces of asphaltenes and two demulsifiers (Brij®-93 and Pluronic® PE8100) was studied. The difference between these two demulsifiers lies in their chemical structure. Brij®-93 is a low molecular weight (357 g/mol) molecule whereas Pluronic® PE8100 is a high molecular weight (2800 g/mol) polydisperse block co-polymer. Desorption of asphaltenes by demulsifiers, and vice versa, was determined.

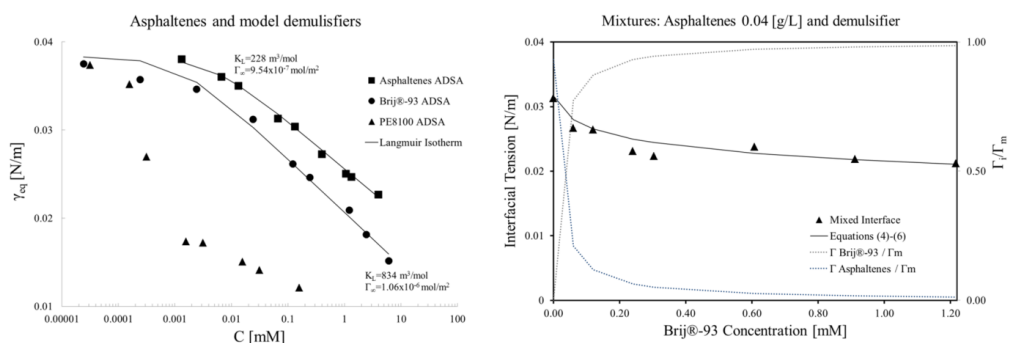


**Figure 7.2.1.** (left) adsorption isotherms and Langmuir fit for asphaltenes, Brij-93 and PE8100. (right) composition of a mixed interface and fit to a Langmuir-based model.

First, the composition of a mixed interface (asphaltenes and demulsifiers) through the use of the Langmuir equation of state (EoS) was determined. Fig. 7.2.1 shows both results. It can be seen that the Langmuir isotherm correctly describes the adsorption IFT data for asphaltenes and the model molecular demulsifier Brij-93. Even though the assumptions behind the Langmuir EoS are not necessarily met, this approach has been shown to be useful when giving a semi-quantitative description of adsorption at equilibrium of complex systems such as polymers<sup>186</sup>. However, this is not the case for the model polymeric demulsifier PE8100. The sharp decrease of the interfacial tension in a narrow concentration range is indicative of high surface activity. This has been reported<sup>187, 188</sup> for different diblock and triblock PEO-PPO(-PEO) copolymers and the behavior is attributed to the fast initial adsorption followed

by relaxation, reorganization and multiple phase transitions at the interface. The results in figure 7.2.1 seem to indicate similar behavior.

In the case of competitive adsorption between asphaltenes and Brij®-93 (Fig. 7.2.1 right) it can be seen the interface at equilibrium is dominated by the model demulsifier Brij-93, even at low concentrations. This is consistent with the higher surface activity of the demulsifier compared to asphaltenes. The model based on the Langmuir EoS describes the data well. In fact this model has also been previously used to describe competitive adsorption of unfolding proteins<sup>189</sup>. The relevance of these results lies in the fact that when asphaltenes and a demulsifier are co-adsorbed, the formation of a mechanical strong film is hindered.

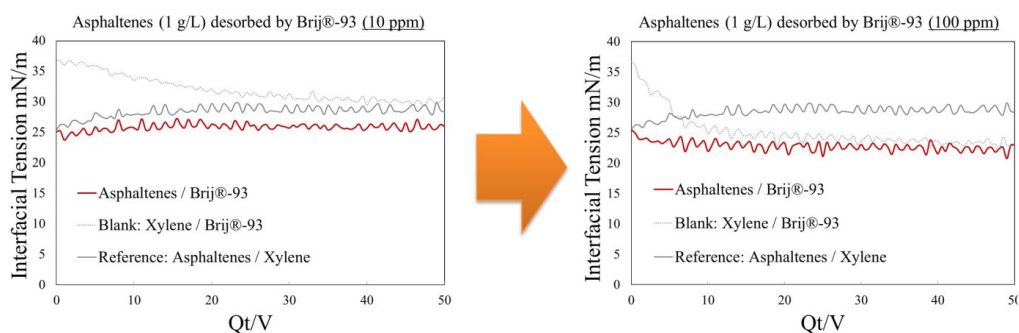


**Figure 7.2.2.** Desorption of asphaltenes by Brij-93. Effect of increasing the concentration of demulsifier.

Second, an experimental set-up that aims to understand chemical demulsification of water-in-crude oil emulsions during the production stages was used (coaxial capillary). Desorption of already adsorbed asphaltenes at the liquid-liquid interface by the action of two demulsifiers (Brij®-93 and Pluronic® PE8100) was assessed. Fig. 7.2.2 shows the effect of desorption of asphaltenes by Brij-93 from a low (10ppm) to a high concentration (100ppm) and Fig. 7.2.3 shows similar plots for desorption of asphaltenes by a second demulsifier, namely Pluronic PE8100. It was found that desorption is always initiated by interactions between demulsifiers and asphaltenes. It is followed by the plausible formation of complex-like structures to finally end in the replacement, by displacement from the interface, of asphaltenes by demulsifiers. It is clear from these plots that the polymeric demulsifier Pluronic® PE8100, given its higher surface activity, displays a more pronounced behavior. This means that the displacement/replacement mechanisms are faster and require lower concentration. The formation of complex-structures is still speculative. However given the chemical characteristics of both demulsifiers (especially the polymeric one) it seems plausible that

these are the kind of interactions involved. This would also be in agreement with Yen-Mullins model in which the alkyl chains that stick out of the asphaltene nanoaggregates would interact with the polymeric chains of the demulsifier<sup>20, 30</sup>.

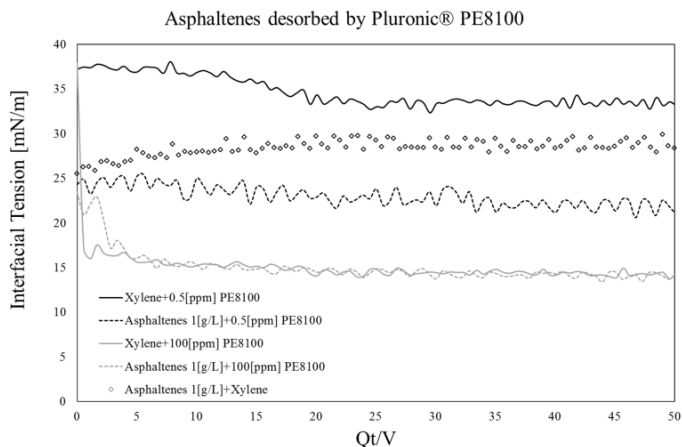


**Figure 7.2.3.** Desorption of asphaltenes by Pluronic® PE8100. Effect of increasing the concentration of demulsifier.

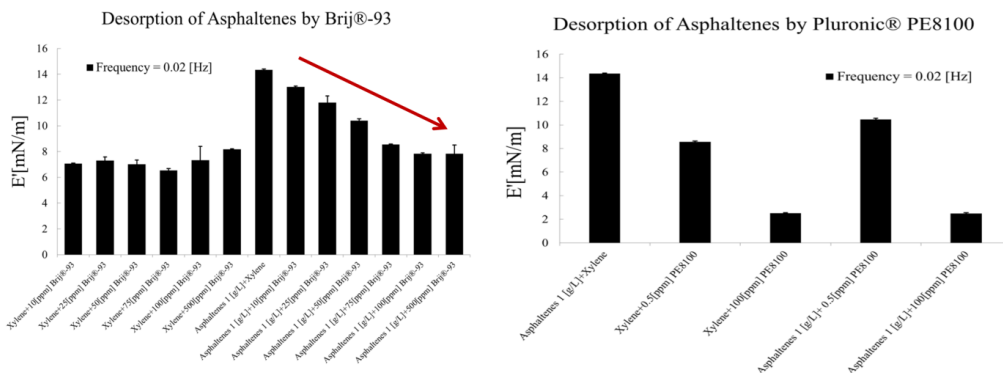


**Figure 7.2.4.** Changes in the elastic dilatational modulus after desorption of asphaltenes by Brij®-93 (left) and Pluronic® PE8100 (right).

Similarly, Fig. 7.2.4 shows the effect of the two demulsifiers on the elastic dilatational modulus. The modulus was measured after the desorption experiments to assess the composition of the interface. As it can be seen, Brij®-93 at intermediate concentrations of demulsifier (10-100 ppm) the interface exhibits a mixed composition and at high concentration (500 ppm) the interface seems to be fully replaced. A similar observation is made for the polymeric demulsifier Pluronic® PE8100 but in this case the replacement is

sharper. At an intermediate concentration of 100 ppm the interface is dominated by the demulsifier showing once more its high efficiency. These results show the progressive replacement and effect of two different demulsifiers in an asphaltene covered interface. These results, coupled with the results available in the literature that deal with Langmuir films<sup>27, 140</sup> give a broad picture of the mechanisms involved in sorption at the liquid-liquid interface.

Finally, a set of similar experiments was performed to assess the ability of asphaltenes to desorb both demulsifiers. Fig. 7.2.5 shows the desorption experiments and it can be seen that in the case of Brij®-93 at low concentration (100 ppm), asphaltenes at 1 g/L can desorb the demulsifier. At high concentrations (2500 ppm) the effect of asphaltenes is the same as the effect observed in pure solvent (xylene) meaning that the same degree of desorption is achieved. Analogously, in the case of Pluronic® PE8100 it can be seen that at low concentrations (0.5 ppm) asphaltenes are able to fully replace the interface whereas at high concentrations (100 ppm) the interface remains dominated by the demulsifier. The mechanisms of replacement/displacement are speculated to be similar as in the previous cases. This means that asphaltene aggregates are able, in some cases, to entrap parts of the demulsifiers and occupy their adsorption sites. In the cases where this is not possible, it seems that the long-entangled polymeric chains do not allow the asphaltene aggregates to access the interface.

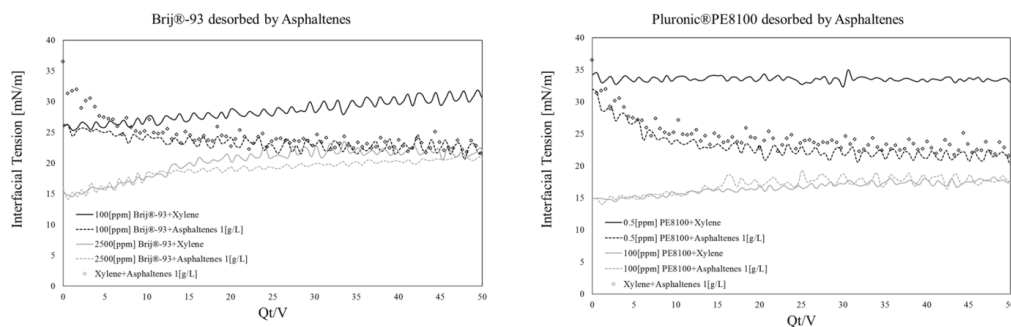


**Figure 7.2.5.** Desorption of by Brij-93 (left) and Pluronic® PE8100 (right) by asphaltenes at 1g/L. Effect of increasing the concentration of demulsifier.

These results are rather unique in the sense that it is not typical to test the desorbing capabilities of asphaltenes. Re-emulsification and demulsifier overdosing are two minor issues that can occur and so understanding the mechanisms involved is relevant. Unlike competitive adsorption, it seems that under certain conditions asphaltenes are able to occupy sites at the interface even though they are less surface active than the demulsifiers. A

summary of the main results is presented in table 7.2.1 and the main features of desorption by demulsifiers and asphaltenes are shown.

| Asphaltene Desorption         |   |  | Demulsifier Desorption        |   |   |
|-------------------------------|---|--|-------------------------------|---|---|
| demulsifier/<br>concentration | $\gamma_{\text{Asphaltene}}^{\text{vs}} \gamma_{\text{Demulsifier}}^{\text{vs}}$<br>(30 min) <sup>b</sup> | conclusions  | demulsifier/<br>concentration | $\gamma_{\text{Asphaltene}}^{\text{vs}} \gamma_{\text{Demulsifier}}^{\text{vs}}$<br>(30 min) <sup>b</sup> | conclusions   |
| <b>Brij-93</b>                |   |  | <b>Brij-93</b>                |   |   |
| 10 ppm                        | >   | interactions; partial desorption of asphaltenes              | 100 ppm                       | ≈   | asphaltene desorb demulsifier; no interactions visible        |
| 100 ppm                       | ≈   | interactions; almost complete replacement                    | 2500 ppm                      | >   | desorption or interactions                                    |
| 2500 ppm                      | <   | no interactions visible; complete replacement by demulsifier | <b>PE8100</b>                 |   |   |
| <b>PE8100</b>                 |   |  | 0.5 ppm                       | <   | asphaltene desorb demulsifier; no interactions visible        |
| 0.5 ppm                       | >   | strong interactions and synergy; no desorption of asphaltene | 100 ppm                       | >   | asphaltene do not desorb demulsifier; no interactions visible |
| 100 ppm                       | <   | no interactions visible; complete replacement by demulsifier |                               |   |   |

**Table 7.2.1.** Summary of the main results regarding the mechanisms of desorption of asphaltene by two demulsifiers and vice-versa.



### 7.3 Paper 3

#### *Sorption and interfacial rheology study of model asphaltene compounds.*

Papers 1 and 2 shed light on the adsorption/desorption mechanisms that take place at the liquid-liquid interface. In this paper, the study is extended to include the determination of the sorption (adsorption/desorption) and rheological (shear and dilatational) properties of the acidic asphaltene model compound C5PeC11 at the liquid-liquid and liquid-air interface. Subsequent comparison to the properties of indigenous asphaltenes is provided to evaluate which features can be captured with a molecule of defined chemical structure.

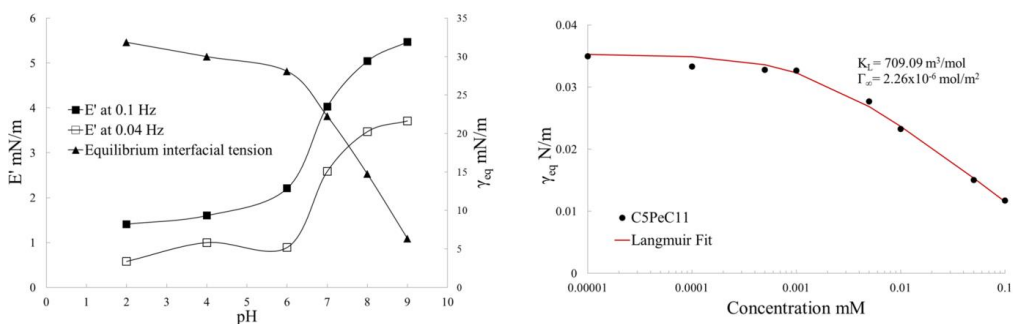


**Figure 7.3.1.** Evolution of the equilibrium interfacial tension as a function of the pH (left) and concentration (right). The evolution of the apparent elastic dilatational modulus as a function of the pH (left) is also shown.

First, Fig. 7.3.1 shows the evolution of the equilibrium interfacial tension of the asphaltene model compound C5PeC11 as a function of the pH and the concentration respectively. These findings are similar to the pH-dependent surface activity observed in hexane-precipitated ( $C_6$ -) asphaltenes. The equilibrium parameters are similar to those reported in paper 1 and 2 and the results show that C5PeC11 is more surface active than asphaltenes.

Second, interfacial dilatational rheology on C5PeC11 shown in Fig. 7.3.1 shows that the interfacial activity at the liquid-liquid interface is more pronounced when the  $-\text{COOH}$  groups are ionized (high pH), something observed in  $C_6$ -asphaltenes. C5PeC11 does not seem to form a mechanically robust film at the liquid-liquid interface. However the interface can be said to be mostly elastic based on Fig. 7.3.2. This does not mean extra stresses are absent, but it indicates that the response to dilatational deformations is dominated by interfacial tension and its variations. Fig. 7.3.2 also shows the fits of the apparent elasticity using the Lucassen-Van den Temple (LvdT) model for C5PeC11. The evolution of the moduli is well described

quantitatively, especially close to the maxima, which are well predicted, and the decrease of the moduli at higher bulk concentrations. A similar trend for  $E'$  has been reported for  $C_6$ -asphaltenes. However, the implementation of the LvdT model has been unsuccessful most likely due to the intermolecular interactions at the interface and the evident dominance of extra stresses in the asphaltene interface (skin)<sup>190</sup>. Unlike indigenous asphaltenes, adsorption of C5PeC11 seems to be reversible and no skin (or crumpling) was observed.

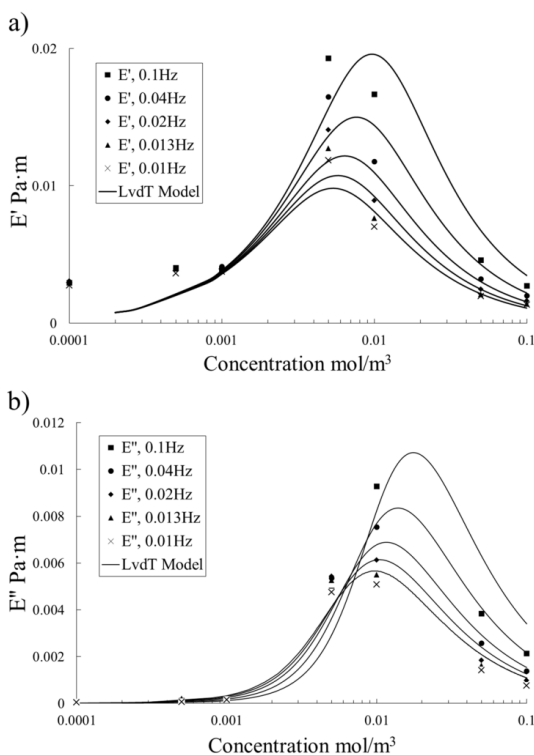


**Figure 7.3.2.** Fit of the apparent elastic and loss dilatational moduli using the LvdT model.

Third, desorption of C5PeC11 from the oil/water interface was evaluated. Figure 7.3.3 shows the desorption curves induced by three different species: solvent (toluene), a mixture of heptane and toluene (HepTol) and the model compound BisAC11 (which only has aliphatic functionalities). Desorption by toluene, although reversible, is slower than for non-interacting molecules. In fact, the desorption experiments seem to indicate the presence of interactions ( $\pi$ - $\pi$  stacking, H-bond) at the interface. Desorption by HepTol at a concentration near the precipitation onset did not present any change suggesting that the irreversibility of asphaltene adsorption is not related to solubility. Similarly, the model compound BisAC11 has no influence on desorption of C5PeC11 at the liquid-liquid interface.

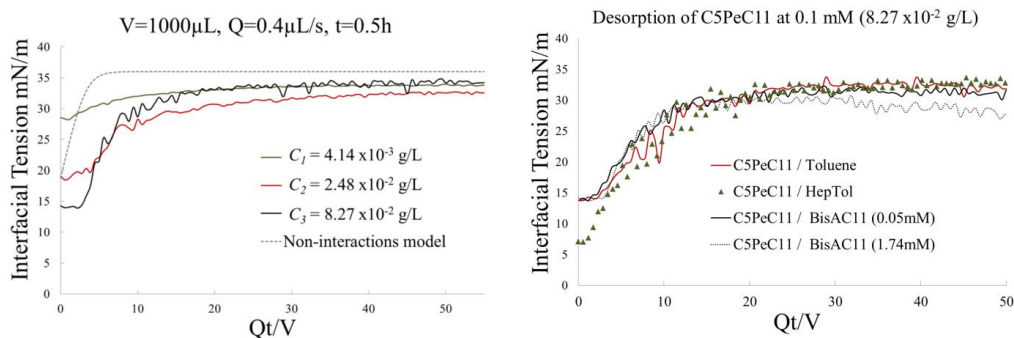


**Figure 7.3.3.** Desorption of C5PeC11 as a function of the characteristic time induced by: pure solvent (left), HepTol and BisAC11 (right).

Finally, extra stresses at the liquid-liquid and liquid-air interface were probed through interfacial shear rheology. Fig. 7.3.4 shows a series of compression-expansion curves the liquid-air interface that suggests molecular rearrangements at monolayer coverage, irreversible aggregate formation and the formation of multilayers. Fig. 7.3.5 shows the evolution of the elastic and loss moduli for C5PeC11 at the liquid-air interface as a function of the strain and frequency. The results are indicative of a material with elastic, fragile microstructure suggesting a strongly interacting insoluble system. These aspects are similar to what has been reported for indigenous asphaltenes using similar techniques.

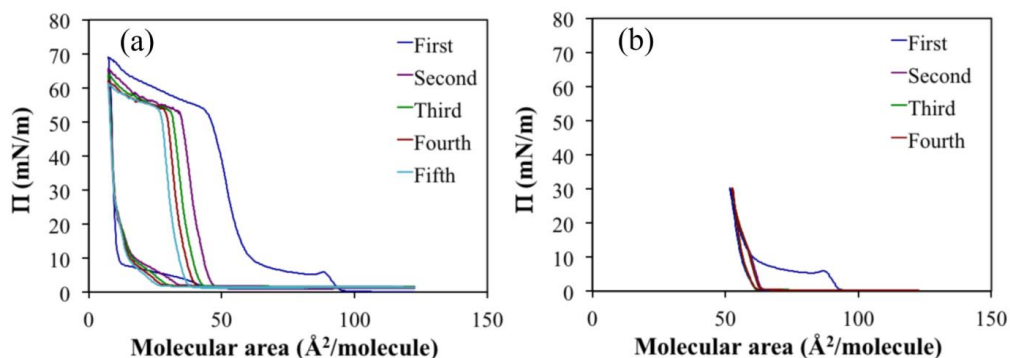


**Figure 7.3.4.** Compression-expansion curves for C5PeC11 at the liquid-air interface. (a) evidence of aggregation when large surface pressures are achieved, and (b) complete reversibility when surface pressure is kept below 30 mN/m.

The case for the liquid-liquid interface is presented in Fig. 7.3.6 and Fig. 7.3.7. A similar non-thermodynamic local maximum was observed suggesting tilting of the molecules at the interface and the presence of fragile structures is also observed. The frequency dependence in Fig. 7.3.7 reveals a viscoelastic structure with a broad range of relaxation time. This

rheological behavior is characteristic of a soft-glassy material, where rearrangement under flow of a densely packed internal structure takes place with a broad range of characteristic times. A soft-glassy rheology (SGR) model was used to describe this behavior and it was observed that C5PeC11 required higher surface pressures to achieve similar values of the effective noise temperature reported for asphaltenes. This means that indigenous asphaltenes form a more crowded interface. The parallel case of indigenous asphaltenes has been reported<sup>136</sup> and it was also concluded that: asphaltene films at the oil/water interface behave as soft-glassy materials and that the SGR models correlates well with the data. This is a very important remark because it means that asphaltene model compounds are able to capture these features. The compression-expansion curves at the oil/water interface at different pH values presented in Fig. 7.3.8 show that the interfacial activity of C5PeC11 is also pH-dependent and the arrangements at the interface vary. This behavior is also similar to that of asphaltenes in which changes in the conformations have been observed.

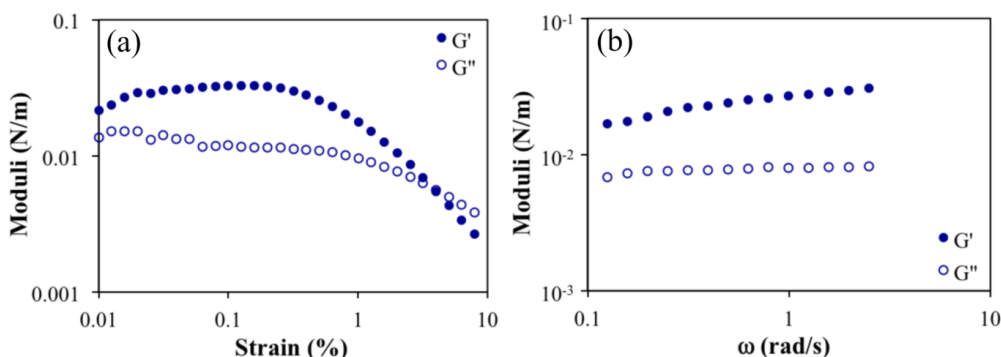


**Figure 7.3.5.** Elastic and loss moduli for C5PeC11 at the liquid-air interface as a function of strain (left) and frequency (right).

Important fundamental differences between shear and dilatational rheology were also stated. While through shear rheology true material functions can be established, dilatational rheology yields an apparent elasticity. This is because extra stresses that arise from interfaces not dominated entirely by surface tension are not detected in the latter. Asphaltenes form a mechanically robust film at the oil/water interface that consequently produces extra stresses that do not influence the interfacial tension but do influence the elasticity. The limitations of dilatational rheology and the apparent elasticity has also been previously acknowledged<sup>191</sup> and so with both results at hand it is possible to have a broad picture of how the system behaves under different conditions.

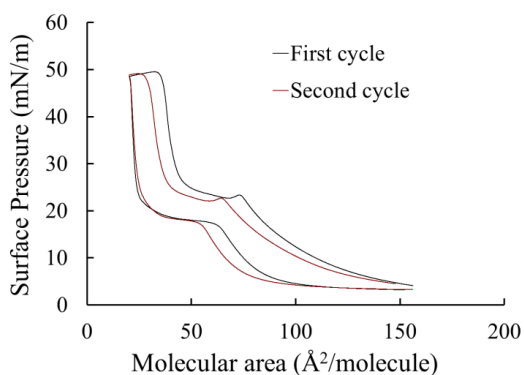


**Figure 7.3.6.** Compression-expansion curves from C5PeC11 at a decane/water interface.

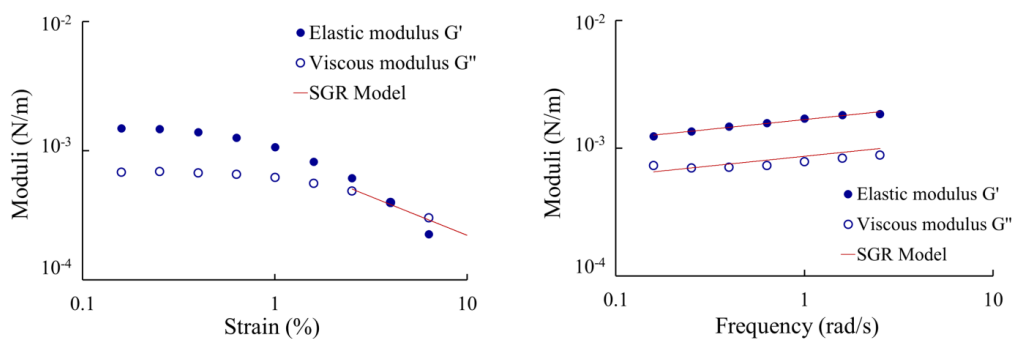


**Figure 7.3.7.** Dynamic moduli of C5PeC11 at an decane/water interface as a function of (a) strain, and as a function of (b) frequency.

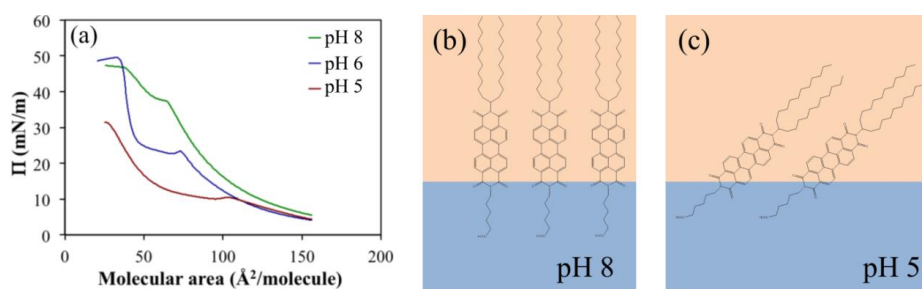


**Figure 7.3.8.** Compression curves for C5PeC11 at a decane/water interface showing the different arrangements depending on the pH.

## 7.4 Paper 4

### *A microcalorimetry study on the adsorption of asphaltenes and model asphaltene compounds at the liquid-solid surface.*

Having studied asphaltene adsorption/desorption mechanisms at the liquid-liquid interface in **paper 1** and **paper 2** and film properties in **paper 3**, in this paper the adsorption study is extended to the liquid-solid surface. The adsorption isotherms of C5PeC11 and indigenous asphaltenes are determined onto three different surfaces. This is followed by the determination of the differential adsorption enthalpy  $\Delta H_{ads}$  through microcalorimetry experiments. This enthalpy of adsorption is characterized by the parameter  $\Delta H_z$  (the enthalpy at zero coverage). Finally, the influence of H-bonds and polar interactions for adsorption is assessed via the comparison of adsorption of esterified and non-esterified by QCM-D experiments.

First, Fig. 7.4.1 shows the adsorption isotherms of C5PeC11 and C<sub>6</sub>-asphaltenes onto three different surfaces: silica, calcite and stainless steel. These isotherms were determined via the depletion method (DM). Results show that adsorption between the two species presents some similarities. They both present a plateau and the adsorption affinity ranking is similar: stainless steel > calcite > silica. However, it is clear from these plots that C5PeC11 exhibits a higher total adsorbed amount in all cases. This is attributed to the single functionality of the model compound compared to the polydisperse response of indigenous asphaltenes. Overall, the values obtained for C<sub>6</sub>-asphaltenes are consistent with typical values found in the literature. Indeed the values obtained for silica vary between 1.81 mg/m<sup>2</sup> and 3.78 mg/m<sup>2</sup>, the values for calcite are ca. 3.4 mg/m<sup>2</sup> and the values for stainless steel which are generally higher are ca. 9 mg/m<sup>2</sup>.<sup>91, 105</sup>

Second, Fig. 7.4.2 shows the differential adsorption enthalpy for C5PeC11 and C<sub>6</sub>-asphaltenes for the same surfaces as a function of the concentration. The adsorption enthalpy for C5PeC11 tends to decrease slightly with concentration suggesting the presence of rearrangements and/or differences in the active sites of the surface (some sites might be more energetic than others) at the liquid-solid surface. On the other hand in the case of asphaltenes the adsorption enthalpy tends to increase with concentration, this is indicative of lateral interactions and aggregation at the interface. The parameter  $\Delta H_z$  (the enthalpy at zero coverage) obtained from a linear regression model was used to establish the type and the

driving force of adsorption onto the liquid-solid surface. Adsorption of C5PeC11 onto silica is shown to be driven primarily by H-bonds ( $\Delta H_z = -34.9 \text{ kJ/mol}$ ) unlike adsorption onto calcite where polar Van der Waals and acidic/basic interactions are thought to be predominant ( $\Delta H_z = -23.5 \text{ kJ/mol}$ ). Interactions between C5PeC11 and stainless steel are found to be weak ( $\Delta H_z = -7.7 \text{ kJ/mol}$ ) and definitely not a result of H-bonding. To the best of our knowledge this is the first time such approach (microcalorimetry) to determine the type of interactions in asphaltenes is used.

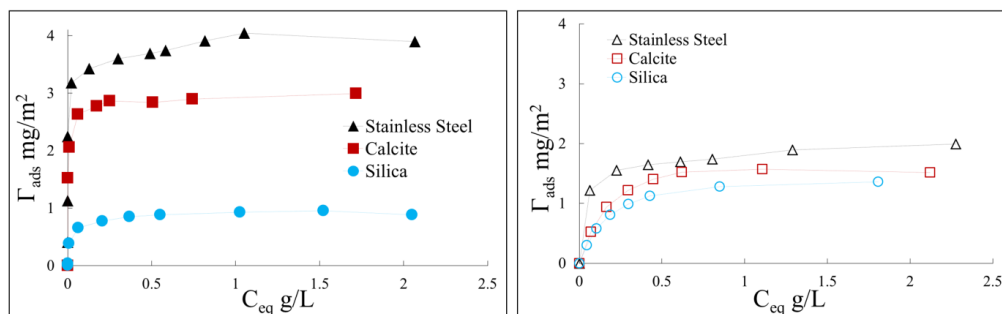


**Figure 7.4.1.** Adsorption isotherms obtained via de depletion method for C5PeC11 (left) and C6-asphaltenes (right) onto three surfaces: silica, calcite and stainless steel.

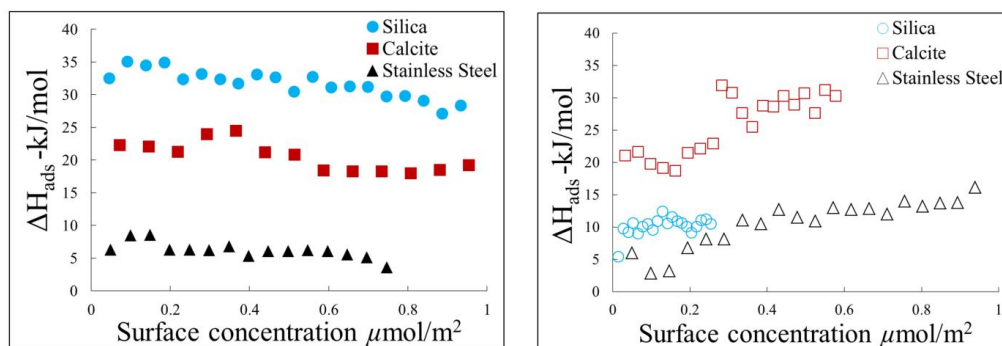


**Figure 7.4.2.** Differential adsorption enthalpy obtained via calorimetry experiments for C5PeC11 (left) and C6-asphaltenes (right) onto three surfaces: silica, calcite and stainless steel.

Finally, the influence of  $-\text{COOH}$  groups on adsorption at the liquid-solid surface was assessed. An esterification protocol was implemented to methylate the acidic groups in indigenous asphaltenes and determine the adsorption isotherms via the depletion method and QCM-D experiments. Fig. 7.4.3 shows isotherms obtained via DM and QCM-D experiments

for both the esterified and non-esterified asphaltenes. This plot strongly suggests that adsorption of indigenous asphaltenes at the liquid-solid surface is not dominated by the influence of acidic functionalities contrary to C5PeC11 for silica and possibly calcite surfaces.

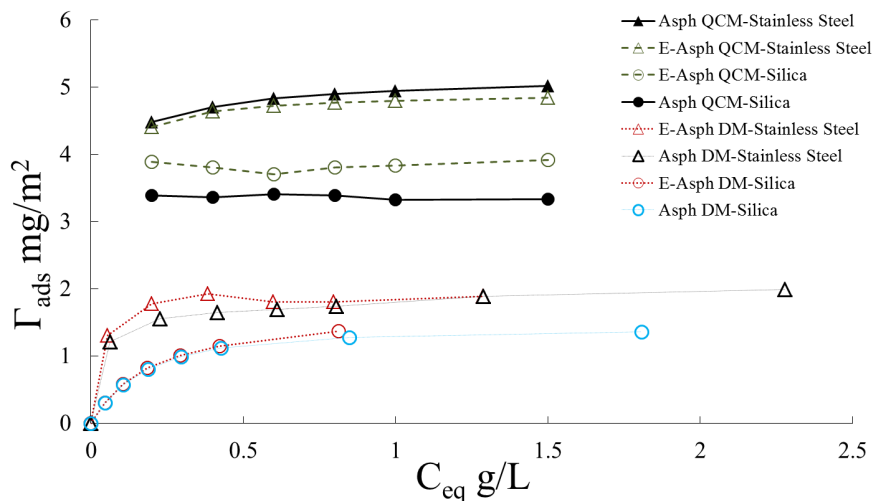


**Figure 7.4.3.** Asphaltene (Asph) and esterified-asphaltene (E-Asph) isotherms conducted via the depletion method (DM) and quartz crystal microbalance (QCM) experiments onto two surfaces: stainless steel (open triangles) and silica (open circles).



## 8. Concluding remarks

In this thesis, sorption aspects of different species of interest in the petroleum industry especially in flow assurance were systematically studied at various interfaces. The species selected for this work are directly related to the different stages involved in crude oil production. Asphaltenes are responsible for several problems; Asphaltene model compounds provide an alternative viable way of capturing the main features in terms of interfacial properties associated with asphaltenes; and chemical demulsifiers play an essential role in water separation to meet quality standards. Analogously, the interfaces studied in this work are also directly related to the different phenomena that occur. Liquid-liquid interfaces are encountered during flooding operations and crude oil emulsions; Solid-liquid interfaces not only occur naturally inside the reservoirs but are also present at all stages of production; and Liquid-air interfaces are typically used to postulate adsorption mechanisms and the arrangement of chemical species.

The study of asphaltenes and demulsifiers was the main goal of **paper 1** and **paper 2**. In **paper 1**, adsorption/desorption of single compounds was systematically studied using a coaxial capillary accessory to the ADSA device. In this paper, it was established that asphaltenes are almost irreversibly adsorbed at the xylene/water interface and that a low molecular weight demulsifier (Brij 93) is partly reversibly adsorbed at the same interface. These findings were extended in **paper 2** to include a second type of demulsifier (PE8100, polymeric and high molecular weight). Additionally, convection-enhanced desorption was induced to establish the mechanisms by which demulsifiers typically found in the oil production industry act to replace/displace asphaltenes from the oil/water interface. These mechanisms were also corroborated by interfacial dilatational measurements that showed the same trend.

In **paper 3**, sorption and rheological properties (shear and dilatational) of asphaltene model compounds at the liquid/liquid and liquid/air interface were studied. It was shown that the model compound C5PeC11 which has an acidic functionality is reversibly adsorbed at the toluene/water interface and that its desorption is slower than for non-interacting species suggesting the presence of interactions. It was also shown that C5PeC11 forms a viscoelastic film with fragile structures prone to rearrangements at the liquid-liquid and liquid-air interface. Similarities between indigenous asphaltenes and the model compound were

established by using a soft-glassy rheology (SGR). Finally, important fundamental differences between dilatational and shear rheology were assessed.

In **paper 4**, results from **paper 3** were extended to study adsorption of indigenous asphaltenes and model compounds (C5PeC11) at the solid-liquid surface. In this case, asphaltene model compounds as well as indigenous asphaltenes were used to establish the type of adsorption present on solid surfaces of different nature. Microcalorimetry experiments allowed determining the driving force for adsorption onto three different types of surfaces: silica, calcite and stainless steel. These surfaces are present in different stages of oil production and therefore treated as representative. It was shown that adsorption of C5PeC11 onto silica is driven primarily by H-bonds and adsorption onto calcite seems to be driven by polar Van der Waals and acidic/basic interactions. Adsorption onto stainless steel is definitely not driven by polar interactions given that the adsorption enthalpy is very low. Additionally, it was shown the negligible influence of acidic asphaltenes in adsorption at the liquid-solid surface as shown by adsorption measurements of esterified asphaltenes.

Thinking about future work there are several areas in which the results of this thesis can be extended. For instance, it would be relevant to continue the investigation of the relationship between chemical structure and properties of asphaltene model compounds. The main goal would be that the most relevant properties, depending on the application, could be captured by this family of molecules. In this sense, developing model compounds that form a mechanically robust film at the liquid-liquid interface would be interesting. A second aspect would be to transition between a model system (asphaltene solutions in toluene) to real systems (crude oil) in the desorption experiments with the coaxial capillary accessory. This would give a better understanding in a real situation. Finally, the DWR geometry could be further exploited by including mixed interfaces. In this way, a more complete picture of interactions between demulsifiers and asphaltenes / asphaltene model compounds would be possible and relevant to compare.

## 9. References

1. Noah Kramer, S. *The Sumerians: Their History, Culture and Character*; The University of Chicago Press: London, 1963.
2. Speight, J. G. Exploration, Recovery, and Transportation. In *The Chemistry and Technology of Petroleum*, Fourth Edition ed.; CRC Press. Taylor and Francis group, LLC: Boca Raton, 2007.
3. Lyons, W. *Petroleum & Natural Gas Engineering* [Online]; Gulf Publishing Company: Houston, 1996.
4. Le Treut, H., R. Somerville, U. Cubasch, Y. Ding, C. Mauritzen, A. Mokssit, T. Peterson and M. Prather. 2007: Historical Overview of Climate Change. In *Climate Change 2007: The Physical Science Basis. Contribution of Working Group I to the Fourth Assessment Report of the Intergovernmental Panel on Climate Change [Solomon, S., D. Qin, M. Manning, Z. Chen, M. Marquis, K.B. Averyt, M. Tignor and H.L. Miller (eds.)]*. United Kingdom and New York, NY, USA.
5. Aske, N.; Kallevik, H.; Sjöblom, J. Determination of saturate, aromatic, resin, and asphaltenic (SARA) components in crude oils by means of infrared and near-infrared spectroscopy. *Energy and Fuels* **2001**, *15* (5), 1304-1312.
6. Yarranton, H. W.; Masliyah, J. H. Molar mass distribution and solubility modeling of asphaltenes. *AIChE Journal* **1996**, *42* (12), 3533-3543.
7. Yang, F.; Tchoukov, P.; Pensini, E.; Dabros, T.; Czarnecki, J.; Masliyah, J.; Xu, Z. Asphaltene subfractions responsible for stabilizing water-in-crude oil emulsions. Part 1: Interfacial behaviors. *Energy and Fuels* **2014**, *28* (11), 6897-6904.
8. Jewell, D. M.; Albaugh, E. W.; Davis, B. E.; Ruberto, R. G. Integration of Chromatographic and Spectroscopic Techniques for the Characterization of Residual Oils. *Industrial & Engineering Chemistry Fundamentals* **1974**, *13* (3), 278-282.
9. Altgelt, K. H. *Composition and Analysis of Heavy Petroleum Fractions*; Taylor & Francis 1993.
10. Yan, J.; Plancher, H.; Morrow, N. R. Wettability Changes Induced by Adsorption of Asphaltenes. *SPE-37232-PA* **1997**.
11. Musser, B. J.; Kilpatrick, P. K. Molecular Characterization of Wax Isolated from a Variety of Crude Oils. *Energy & Fuels* **1998**, *12* (4), 715-725.
12. Coto, B.; Coutinho, J. A. P.; Martos, C.; Robustillo, M. D.; Espada, J. J.; Peña, J. L. Assessment and Improvement of n-Paraffin Distribution Obtained by HTGC To Predict Accurately Crude Oil Cold Properties. *Energy & Fuels* **2011**, *25* (3), 1153-1160.
13. Coto, B.; Martos, C.; Espada, J. J.; Robustillo, M. D.; Merino-García, D.; Peña, J. L. Study of New Methods To Obtain the n-Paraffin Distribution of Crude Oils and Its Application to Flow Assurance. *Energy & Fuels* **2011**, *25* (2), 487-492.
14. Speight, J. G. Chapter 8: Fractional Composition. In *The chemistry and technology of petroleum*, 4th Edition ed ed.; CRC Press. Taylor & Francis group: Boca Ratón, FL, 2007, pp 205-238.
15. Hummer, H. Fuel Science and Technology Handbook (Chemical Industries Series/41). Herausgeg. von J. G. Speight. Marcel Dekker. Inc., New York 1990. XII, 1193 S., zahlr. Abb. u. Tab., geb. . *Chemie Ingenieur Technik* **1990**, *62* (10), 856-856.
16. Andersen, S. I.; Speight, J. G. Petroleum resins: Separation, Character and Role in Petroleum. *Petroleum Science and Technology* **2001**, *19* (1-2), 1-34.
17. Sheu, E. Y. Petroleum Asphaltene Properties, Characterization, and Issues. *Energy & Fuels* **2002**, *16* (1), 74-82.

18. Speight, J. G. Chapter 11: Asphaltene Constituents. In *The chemistry and technology of petroleum*, 4th Edition ed.; CRC Press. Taylor & Francis group. : Boca Ratón, FL. , 2007, pp 315-344.
19. Sjöblom, J.; Aske, N.; Auflem, I. H.; Brandal, Ø.; Havre, T. E.; Sæther, Ø.; Westvik, A.; Johnsen, E. E.; Kallevik, H. Our current understanding of water-in-crude oil emulsions. Recent characterization techniques and high pressure performance. *Advances in Colloid and Interface Science* **2003**, 100-102 (SUPPL.), 399-473.
20. Mullins, O. C. The Modified Yen Model. *Energy & Fuels* **2010**, 24 (4), 2179-2207.
21. Mullins, O. C. The Asphaltenes. *Annual Review of Analytical Chemistry* **2011**, 4 (1), 393-418.
22. Hammami, A., Ratulowski, John. Chapter 23. Precipitation and Deposition of Asphaltenes in Production Systems: A Flow Assurance Overview. In *Asphaltenes, Heavy Oils, and Petroleomics*, Mullins, O. C., Sheu, E., Hammani, A., Marshall, A., Ed.; Springer, LLC, 2007.
23. Buckley, J. S. Asphaltene Deposition. *Energy & Fuels* **2012**, 26 (7), 4086-4090.
24. Simon, S.; Jestin, J.; Palermo, T.; Barré, L. Relation between Solution and Interfacial Properties of Asphaltene Aggregates. *Energy & Fuels* **2008**, 23 (1), 306-313.
25. Jeribi, M.; Almir-Assad, B.; Langevin, D.; Hénaut, I.; Argillier, J. F. Adsorption kinetics of asphaltenes at liquid interfaces. *Journal of Colloid and Interface Science* **2002**, 256 (2), 268-272.
26. Hannisdal, A.; Orr, R.; Sjöblom, J. Viscoelastic properties of crude oil components at oil-water interfaces. 1. The effect of dilution. *Journal of Dispersion Science and Technology* **2007**, 28 (1), 81-93.
27. Pensini, E., Harbottle, D., Yang, F., Tchoukov, P., Li, Z., Kailey, I., Behles, J., Masliyah, J., Xu, Z. Demulsification Mechanism of Asphaltene-Stabilized Water-in-Oil Emulsions by a Polymeric Ethylene Oxide–Propylene Oxide Demulsifier. *Energy & Fuels* **2014**.
28. Zhang, L. Y.; Xu, Z.; Masliyah, J. H. Langmuir and Langmuir-Blodgett films of mixed asphaltene and a demulsifier. *Langmuir* **2003**, 19 (23), 9730-9741.
29. McLean, J. D.; Kilpatrick, P. K. Effects of Asphaltene Solvency on Stability of Water-in-Crude-Oil Emulsions. *Journal of Colloid and Interface Science* **1997**, 189 (2), 242-253.
30. Yen, T. F.; Erdman, J. G.; Pollack, S. S. Investigation of the Structure of Petroleum Asphaltenes by X-Ray Diffraction. *Analytical Chemistry* **1961**, 33 (11), 1587-1594.
31. Espinat, D. Application of Light, X-ray and Neutron diffusion Techniques to the study of colloidal systems. *Rev. Inst. Fr. Pet* **1991**, 45, 775-820.
32. Sabbah, H.; Morrow, A. L.; Pomerantz, A. E.; Zare, R. N. Evidence for island structures as the dominant architecture of asphaltenes. *Energy and Fuels* **2011**, 25 (4), 1597-1604.
33. Groenzin, H.; Mullins, O. C. Asphaltene Molecular Size and Structure. *The Journal of Physical Chemistry A* **1999**, 103 (50), 11237-11245.
34. Groenzin, H.; Mullins, O. C.; Eser, S.; Mathews, J.; Yang, M.-G.; Jones, D. Molecular Size of Asphaltene Solubility Fractions. *Energy & Fuels* **2003**, 17 (2), 498-503.
35. Kuznicki, T.; Masliyah, J. H.; Bhattacharjee, S. Molecular Dynamics Study of Model Molecules Resembling Asphaltene-Like Structures in Aqueous Organic Solvent Systems. *Energy & Fuels* **2008**, 22 (4), 2379-2389.
36. Merdrignac, I., Espinat, D. Physicochemical Characterization of Petroleum Fractions: the State of the Art. *Oil & Gas Science and Technology – Rev. IFP* **2007**, 62 (1), 7-32.

37. Merdrignac, I.; Truchy, C.; Robert, E.; Guibard, I.; Kressmann, S. Size Exclusion Chromatography: Characterization of Heavy Petroleum Residues. Application to Resid Desulfurization Process. *Petroleum Science and Technology* **2004**, *22* (7-8), 1003-1022.
38. Espinat, D.; Fenistein, D.; Barré, L.; Frot, D.; Briolant, Y. Effects of Temperature and Pressure on Asphaltene Agglomeration in Toluene. A Light, X-ray, and Neutron Scattering Investigation. *Energy & Fuels* **2004**, *18* (5), 1243-1249.
39. Bouriat, P.; El Kerri, N.; Graciaa, A.; Lachaise, J. Properties of a Two-Dimensional Asphaltene Network at the Water–Cyclohexane Interface Deduced from Dynamic Tensiometry. *Langmuir* **2004**, *20* (18), 7459-7464.
40. Evdokimov, I. N.; Eliseev, N. Y.; Akhmetov, B. R. Initial stages of asphaltene aggregation in dilute crude oil solutions: studies of viscosity and NMR relaxation. *Fuel* **2003**, *82* (7), 817-823.
41. Tanaka, R.; Sato, S.; Takanohashi, T.; Hunt, J. E.; Winans, R. E. Analysis of the Molecular Weight Distribution of Petroleum Asphaltenes Using Laser Desorption-Mass Spectrometry. *Energy & Fuels* **2004**, *18* (5), 1405-1413.
42. Sheu, E. Y.; De Tar, M. M.; Storm, D. A.; DeCanio, S. J. Aggregation and kinetics of asphaltenes in organic solvents. *Fuel* **1992**, *71* (3), 299-302.
43. Kokal, S. L.; Sayegh, S. G. Asphaltenes: The Cholesterol Of Petroleum. Society of Petroleum Engineers.
44. Akbarzadeh, K., Hammami, A., Kharrat, A., Zhang, D., Allenson, S., Creek, J., Kabir, S., Jamaluddin, A., Marshall, A., Rodgers, R., Mullins, O., Solbakken, T. Asphaltenes: Problematic but rich in potential. *Oilfield Review* **2007**, 22-43.
45. Speight, J. G., Wernick, D., Gould, K., Overfield, R., Rao, B., Savage, D. Molecular Weight and Association of Asphaltenes: a Critical Review. *Oil & Gas Science and Technology - Rev. IFP* **1985**, *40* (1), 51-61.
46. Mullins, O. C.; Betancourt, S. S.; Cribbs, M. E.; Dubost, F. X.; Creek, J. L.; Andrews, A. B.; Venkataramanan, L. The colloidal structure of crude oil and the structure of oil reservoirs. *Energy and Fuels* **2007**, *21* (5), 2785-2794.
47. Ralston, C. Y.; Mitra-Kirtley, S.; Mullins, O. C. Small Population of One to Three Fused-Aromatic Ring Moieties in Asphaltenes. *Energy & Fuels* **1996**, *10* (3), 623-630.
48. Zajac, G., Sethi, N., Joseph, J. Molecular imaging of petroleum asphaltenes by scanning-tunneling-microscopy - verification of structure from C-13 and proton nuclear-magnetic-resonance data *Scanning microscopy* **1994**, *8* (3), 463-470.
49. Bouhadda, Y.; Fergoug, T.; Sheu, E. Y.; Bendedouch, D.; Krallafa, A.; Bormann, D.; Boubguira, A. Second order Raman spectra of Algerian Hassi-Messaoud asphaltene. *Fuel* **2008**, *87* (15–16), 3481-3482.
50. Ruiz-Morales, Y. HOMO–LUMO Gap as an Index of Molecular Size and Structure for Polycyclic Aromatic Hydrocarbons (PAHs) and Asphaltenes: A Theoretical Study. *The Journal of Physical Chemistry A* **2002**, *106* (46), 11283-11308.
51. Ruiz-Morales, Y. The Agreement between Clar Structures and Nucleus-Independent Chemical Shift Values in Pericondensed Benzenoid Polycyclic Aromatic Hydrocarbons: An Application of the Y-Rule. *The Journal of Physical Chemistry A* **2004**, *108* (49), 10873-10896.
52. Oña-Ruales, J. O.; Ruiz-Morales, Y. The Predictive Power of the Annellation Theory: The Case of the C<sub>32</sub>H<sub>16</sub> Benzenoid Polycyclic Aromatic Hydrocarbons. *The Journal of Physical Chemistry A* **2014**, *118* (28), 5212-5227.
53. Ruiz-Morales, Y.; Mullins, O. C. Measured and Simulated Electronic Absorption and Emission Spectra of Asphaltenes. *Energy & Fuels* **2009**, *23* (3), 1169-1177.

54. Ruiz-Morales, Y.; Mullins, O. C. Singlet–Triplet and Triplet–Triplet Transitions of Asphaltene PAHs by Molecular Orbital Calculations. *Energy & Fuels* **2013**, *27* (9), 5017-5028.
55. Ritchie, R. G. S.; Roche, R. S.; Steedman, W. Pyrolysis of Athabasca tar sands: analysis of the condensable products from asphaltene. *Fuel* **1979**, *58* (7), 523-530.
56. Mitra-Kirtley, S.; Mullins, O. C.; Van Elp, J.; George, S. J.; Chen, J.; Cramer, S. P. Determination of the nitrogen chemical structures in petroleum asphaltenes using XANES spectroscopy. *Journal of the American Chemical Society* **1993**, *115* (1), 252-258.
57. Reynolds, J. G.; Jones, E. L.; Bennett, J. A.; Biggs, W. R. Characterization of nickel and vanadium compounds in tar sand bitumen by UV-vis spectroscopy and size exclusion chromatography coupled with element specific detection *Fuel Science and Technology International* **1989**, *7* (5-6), 625-642.
58. Reynolds, J. G. B., W.R. ; Fetzer, J.C. ; Gallegos, E.J. ; Fish, R.H. ; Komlenic, J.J. ; Wines, B.K. . In *Molecular characterization of vanadyl and nickel non-porphyrin compounds in heavy crude petroleum and residua*, International symposium on characterization of heavy crude oils and petroleum residues, Lyon, 1984; Technip, É., Ed.
59. Andreatta, G.; Goncalves, C. C.; Buffin, G.; Bostrom, N.; Quintella, C. M.; Arteaga-Larios, F.; Pérez, E.; Mullins, O. C. Nanoaggregates and Structure–Function Relations in Asphaltenes. *Energy & Fuels* **2005**, *19* (4), 1282-1289.
60. Spiecker, P. M.; Gawrys, K. L.; Trail, C. B.; Kilpatrick, P. K. Effects of petroleum resins on asphaltene aggregation and water-in-oil emulsion formation. *Colloids and Surfaces A: Physicochemical and Engineering Aspects* **2003**, *220* (1–3), 9-27.
61. Murgich, J. Intermolecular forces in aggregates of asphaltenes and resins. *Petroleum Science and Technology* **2002**, *20* (9-10), 983-997.
62. Sedghi, M.; Goual, L.; Welch, W.; Kubelka, J. Effect of Asphaltene Structure on Association and Aggregation Using Molecular Dynamics. *The Journal of Physical Chemistry B* **2013**, *117* (18), 5765-5776.
63. Gawrys, K. L.; Blankenship, G. A.; Kilpatrick, P. K. Solvent Entrainment in and Flocculation of Asphaltenic Aggregates Probed by Small-Angle Neutron Scattering. *Langmuir* **2006**, *22* (10), 4487-4497.
64. Fenistein, D.; Barré, L.; Broseta, D.; Espinat, D.; Livet, A.; Roux, J.-N.; Scarsella, M. Viscosimetric and Neutron Scattering Study of Asphaltene Aggregates in Mixed Toluene/Heptane Solvents. *Langmuir* **1998**, *14* (5), 1013-1020.
65. Moschopedis, S. E.; Speight, J. G. Investigation of hydrogen bonding by oxygen functions in Athabasca bitumen. *Fuel* **1976**, *55* (3), 187-192.
66. Koots, J. A.; Speight, J. G. Relation of petroleum resins to asphaltenes. *Fuel* **1975**, *54* (3), 179-184.
67. Mostowfi, F.; Indo, K.; Mullins, O. C.; McFarlane, R. Asphaltene nanoaggregates studied by centrifugation. *Energy and Fuels* **2009**, *23* (3), 1194-1200.
68. Czarnecki, J.; Tchoukov, P.; Dabros, T. Possible role of asphaltenes in the stabilization of water-in-crude oil emulsions. *Energy and Fuels* **2012**, *26* (9), 5782-5786.
69. Wang, S.; Liu, J.; Zhang, L.; Masliyah, J.; Xu, Z. Interaction Forces between Asphaltene Surfaces in Organic Solvents. *Langmuir* **2010**, *26* (1), 183-190.
70. Goncalves, S.; Castillo, J.; Fernández, A.; Hung, J. Absorbance and fluorescence spectroscopy on the aggregation behavior of asphaltene–toluene solutions. *Fuel* **2004**, *83* (13), 1823-1828.
71. Hoepfner, M. P.; Limsakoune, V.; Chuenmeechao, V.; Maqbool, T.; Fogler, H. S. A Fundamental Study of Asphaltene Deposition. *Energy & Fuels* **2013**, *27* (2), 725-735.
72. Broseta, D.; Robin, M.; Savvidis, T.; Fejean, C.; Durandau, M.; Zhou, H. Detection of Asphaltene Deposition by Capillary Flow Measurements. Society of Petroleum Engineers.

73. Wang, J.; Buckley, J. S.; Creek, J. L. Asphaltene Deposition on Metallic Surfaces. *Journal of Dispersion Science and Technology* **2004**, *25* (3), 287-298.
74. Buenrostro-Gonzalez, E.; Lira-Galeana, C.; Gil-Villegas, A.; Wu, J. Asphaltene precipitation in crude oils: Theory and experiments. *AIChE Journal* **2004**, *50* (10), 2552-2570.
75. Marcano, F.; Antonieta Ranaudo, M.; Chirinos, J.; Castillo, J.; Daridon, J. L.; Carrier, H. Study of Asphaltenes Aggregation in Toluene/n-Heptane/CO<sub>2</sub> Mixtures under High-Pressure Conditions. *Energy & Fuels* **2013**, *27* (8), 4598-4603.
76. Verdier, S.; Carrier, H.; Andersen, S. I.; Daridon, J.-L. Study of Pressure and Temperature Effects on Asphaltene Stability in Presence of CO<sub>2</sub>. *Energy & Fuels* **2006**, *20* (4), 1584-1590.
77. Gonzalez, D. L.; Vargas, F. M.; Hirasaki, G. J.; Chapman, W. G. Modeling Study of CO<sub>2</sub>-Induced Asphaltene Precipitation. *Energy & Fuels* **2008**, *22* (2), 757-762.
78. Jamaluddin, A. K. M.; Creek, J.; Kabir, C. S.; McFadden, J. D.; Cruz, D.; Manakalathil, J.; Joshi, N.; Ross, B. Laboratory Techniques to Measure Thermodynamic Asphaltene Instability.
79. Karan, K.; Hammami, A.; Flannery, M.; Artur Stankiewicz, B. Evaluation of Asphaltene Instability and a Chemical Control During Production of Live Oils. *Petroleum Science and Technology* **2003**, *21* (3-4), 629-645.
80. Tavakkoli, M.; Panuganti, S. R.; Vargas, F. M.; Taghikhani, V.; Pishvaie, M. R.; Chapman, W. G. Asphaltene Deposition in Different Depositing Environments: Part 1. Model Oil. *Energy & Fuels* **2014**, *28* (3), 1617-1628.
81. Tavakkoli, M.; Panuganti, S. R.; Taghikhani, V.; Pishvaie, M. R.; Chapman, W. G. Asphaltene Deposition in Different Depositing Environments: Part 2. Real Oil. *Energy & Fuels* **2014**, *28* (6), 3594-3603.
82. Buckley, J. S. Predicting the Onset of Asphaltene Precipitation from Refractive Index Measurements. *Energy & Fuels* **1999**, *13* (2), 328-332.
83. Verdier, S.; Plantier, F.; Bessières, D.; Andersen, S. I.; Stenby, E. H.; Carrier, H. Study of Asphaltene Precipitation by Calorimetry. *Energy & Fuels* **2007**, *21* (6), 3583-3587.
84. Mendoza de la Cruz, J. L.; Cedillo-Ramírez, J. C.; Aguirre-Gutiérrez, A. d. J.; García-Sánchez, F.; Aquino-Olivos, M. A. Incompatibility Determination of Crude Oil Blends from Experimental Viscosity and Density Data. *Energy & Fuels* **2015**, *29* (2), 480-487.
85. Boek, E. S.; Ladva, H. K.; Crawshaw, J. P.; Padding, J. T. Deposition of Colloidal Asphaltene in Capillary Flow: Experiments and Mesoscopic Simulation†. *Energy & Fuels* **2008**, *22* (2), 805-813.
86. Akbarzadeh, K.; Dhillon, A.; Svrcek, W. Y.; Yarranton, H. W. Methodology for the characterization and modeling of asphaltene precipitation from heavy oils diluted with n-alkanes. *Energy and Fuels* **2004**, *18* (5), 1434-1441.
87. Zougari, M.; Jacobs, S.; Ratulowski, J.; Hammami, A.; Broze, G.; Flannery, M.; Stankiewicz, A.; Karan, K. Novel Organic Solids Deposition and Control Device for Live-Oils: Design and Applications. *Energy & Fuels* **2006**, *20* (4), 1656-1663.
88. Sheng, J. J.; Maini, B. B.; Hayes, R. E.; Tortike, W. S. Experimental Study of Foamy Oil Stability.
89. Mannhardt, K. Core Flood Evaluation of Solvent Compositional And Wettability Effects On Hydrocarbon Solvent Foam Performance.
90. Zahabi, A.; Gray, M. R.; Czarnecki, J.; Dabros, T. Flocculation of Silica Particles from a Model Oil Solution: Effect of Adsorbed Asphaltenes. *Energy & Fuels* **2010**, *24* (6), 3616-3623.
91. Adams, J. J. Asphaltene adsorption, a literature review. *Energy and Fuels* **2014**, *28* (5), 2831-2856.

92. Turgman-Cohen, S.; Fischer, D. A.; Kilpatrick, P. K.; Genzer, J. Asphaltene Adsorption onto Self-Assembled Monolayers of Alkyltrichlorosilanes of Varying Chain Length. *ACS Applied Materials & Interfaces* **2009**, *1* (6), 1347-1357.
93. Turgman-Cohen, S.; Smith, M. B.; Fischer, D. A.; Kilpatrick, P. K.; Genzer, J. Asphaltene Adsorption onto Self-Assembled Monolayers of Mixed Aromatic and Aliphatic Trichlorosilanes. *Langmuir* **2009**, *25* (11), 6260-6269.
94. Dudášová, D.; Simon, S.; Hemmingsen, P. V.; Sjöblom, J. Study of asphaltenes adsorption onto different minerals and clays: Part 1. Experimental adsorption with UV depletion detection. *Colloids and Surfaces A: Physicochemical and Engineering Aspects* **2008**, *317* (1-3), 1-9.
95. Fritschy, G.; Papirer, E. Interactions between a bitumen, its components and model fillers. *Fuel* **1978**, *57* (11), 701-704.
96. Tayakout, M.; Ferreira, C.; Espinat, D.; Arribas Picon, S.; Sorbier, L.; Guillaume, D.; Guibard, I. Diffusion of asphaltene molecules through the pore structure of hydroconversion catalysts. *Chemical Engineering Science* **2010**, *65* (5), 1571-1583.
97. Nassar, N. N.; Hassan, A.; Pereira-Almao, P. Effect of surface acidity and basicity of aluminas on asphaltene adsorption and oxidation. *Journal of Colloid and Interface Science* **2011**, *360* (1), 233-238.
98. Araújo, R. S.; Azevedo, D. C. S.; Cavalcante Jr, C. L.; Jiménez-López, A.; Rodríguez-Castellón, E. Adsorption of polycyclic aromatic hydrocarbons (PAHs) from isooctane solutions by mesoporous molecular sieves: Influence of the surface acidity. *Microporous and Mesoporous Materials* **2008**, *108* (1-3), 213-222.
99. Jada, A.; Debih, H. Hydrophobation of Clay Particles by Asphaltenes Adsorption. *Composite Interfaces* **2009**, *16* (2-3), 219-235.
100. Perneszi, T.; Patzkó, Á.; Berkesi, O.; Dékány, I. Asphaltene adsorption on clays and crude oil reservoir rocks. *Colloids and Surfaces A: Physicochemical and Engineering Aspects* **1998**, *137* (1-3), 373-384.
101. Cosultchi, A.; Cordova, I.; Valenzuela, M. A.; Acosta, D. R.; Bosch, P.; Lara, V. H. Adsorption of Crude Oil on Na<sup>+</sup>-Montmorillonite. *Energy & Fuels* **2005**, *19* (4), 1417-1424.
102. Dudášová, D.; Silset, A.; Sjöblom, J. Quartz Crystal Microbalance Monitoring of Asphaltene Adsorption/Deposition. *Journal of Dispersion Science and Technology* **2008**, *29* (1), 139-146.
103. Clementz, D. Interaction of Petroleum Heavy ends with Montmorillonite. *Clays and Clay Minerals* **1976**, *24*, 312-319.
104. Tombácz, E.; Szekeres, M. Surface charge heterogeneity of kaolinite in aqueous suspension in comparison with montmorillonite. *Applied Clay Science* **2006**, *34* (1-4), 105-124.
105. Alboudwarej, H.; Pole, D.; Svrcek, W. Y.; Yarranton, H. W. Adsorption of Asphaltenes on Metals. *Industrial & Engineering Chemistry Research* **2005**, *44* (15), 5585-5592.
106. Kokal, S.; Tang, T.; Schramm, L.; Sayegh, S. Electrokinetic and adsorption properties of asphaltenes. *Colloids and Surfaces A: Physicochemical and Engineering Aspects* **1995**, *94* (2-3), 253-265.
107. Dimitrova, T., Leal-Calderon, F. . Bulk elasticity of concentrated protein-stabilized emulsions. *Langmuir* **2001**, *17*, 3235-3244.
108. Pal, R. Rheology of high internal phase ratio emulsions. *Food Hydrocolloids* **2006**, *20*, 997-1005.
109. Leal-Calderon, F., Schmitt, V., Bibette, J. *Emulsion Science: Basic Principles.* ; Springer: New York, 2007.
110. Binks, B. *Modern Aspects of Emulsion Science*; Royal Society of Chemistry 1998.



111. Sjöblom, J., Stenius, Per., Simon Sébastien and Grimes, Brian. Emulsion Stabilization. In *Encyclopedia of Colloid and Interface Science*, Tadros, T., Ed.; Springer: Berlin, 2013; Vol. 1-A-M, pp 415-454.
112. Danov K, K., P., Ivanov, I. . Dynamic Processes in Surfactant-stabilized Emulsions. In *Encyclopedic Handbook of Emulsion Technology*, J, S., Ed.; Marcel Dekker: New York, 2001.
113. Dukhin S, S., J., Saether, O. An Experimental and Theoretical Approach to the Dynamic Behavior of Emulsions. In *Emulsions and Emulsion Stability*, 2nd ed.; Sjöblom, J., Ed.; CRC Press. Taylor and Francis Group: Boca Raton, FL, 2006.
114. Derjaguin BV, C., N. V., Muller, V. M. *Surface Forces*; Springer US: New York, 1987.
115. Claesson, P., Blomberg, E., Poptoshev, E. Surface Forces and Emulsion Stability. In *Encyclopedic Handbook of Emulsion Technology*, Sjoblom, J., Ed.; Marcel Dekker Inc: New York, 2001.
116. Holmberg, K.; Jönsson, B.; Kronberg, B.; Lindman, B. *Surfactants and Polymers in Aqueous Solution*; Wiley2002.
117. Israelachvili, J. *Intermolecular and surface forces*; third ed.; Elsevier: San Diego; Oxford, 2011.
118. Claesson, P. M.; Christenson, H. K. Very long range attractive forces between uncharged hydrocarbon and fluorocarbon surfaces in water. *Journal of Physical Chemistry* **1988**, *92* (6), 1650-1655.
119. Tadros, T. Application of rheology for assessment and prediction of the long-term physical stability of emulsions. *Advances in Colloid and Interface Science* **2004**, *108-109*, 227-258.
120. Dobias, B.; Qiu, X.; von Rybinski, W. *Solid - Liquid Dispersions*; Taylor & Francis1999.
121. Verwey, E. J. W.; Overbeek, J. T. G. *Theory of the Stability of Lyophobic Colloids*; Dover Publications1999.
122. Danov, K., Kralchevsky, P., Ivanov, I. Dynamic Processes in Surfactant-stabilized Emulsions. In *Encyclopedic Handbook of Emulsion Technology*, Sjoblom, J., Ed.; Marcel Dekker: New York, 2001.
123. Walstra, P. Principles of emulsion formation. *Chemical Engineering Science* **1993**, *48* (2), 333-349.
124. de Vries, A. J. Foam stability: Part V. Mechanism of film rupture. *Recueil des Travaux Chimiques des Pays-Bas* **1958**, *77* (5), 441-461.
125. Ivanov, I. B.; Chakarova, S. K.; Dimitrova, B. I. Instability of emulsion liquid films induced by the transfer of acetic acid. *Colloids and Surfaces* **1987**, *22* (2), 301-309.
126. Giribabu, K.; Ghosh, P. Adsorption of nonionic surfactants at fluid-fluid interfaces: Importance in the coalescence of bubbles and drops. *Chemical Engineering Science* **2007**, *62* (11), 3057-3067.
127. Harbottle, D.; Chen, Q.; Moorthy, K.; Wang, L.; Xu, S.; Liu, Q.; Sjoblom, J.; Xu, Z. Problematic Stabilizing Films in Petroleum Emulsions: Shear Rheological Response of Viscoelastic Asphaltene Films and the Effect on Drop Coalescence. *Langmuir* **2014**, *30* (23), 6730-6738.
128. Verruto, V. J.; Le, R. K.; Kilpatrick, P. K. Adsorption and Molecular Rearrangement of Amphoteric Species at Oil–Water Interfaces. *The Journal of Physical Chemistry B* **2009**, *113* (42), 13788-13799.
129. Tchoukov, P.; Yang, F.; Xu, Z.; Dabros, T.; Czarnecki, J.; Sjöblom, J. Role of Asphaltenes in Stabilizing Thin Liquid Emulsion Films. *Langmuir* **2014**, *30* (11), 3024-3033.

130. Freer, E. M.; Radke, C. J. Relaxation of asphaltenes at the toluene/water interface: diffusion exchange and surface rearrangement. *The Journal of Adhesion* **2004**, *80* (6), 481-496.
131. Freer, E. M.; Svitova, T.; Radke, C. J. The role of interfacial rheology in reservoir mixed wettability. *Journal of Petroleum Science and Engineering* **2003**, *39* (1-2), 137-158.
132. Spiecker, P. M.; Kilpatrick, P. K. Interfacial Rheology of Petroleum Asphaltenes at the Oil–Water Interface. *Langmuir* **2004**, *20* (10), 4022-4032.
133. McLean, J. D.; Kilpatrick, P. K. Effects of Asphaltene Aggregation in Model Heptane–Toluene Mixtures on Stability of Water-in-Oil Emulsions. *Journal of Colloid and Interface Science* **1997**, *196* (1), 23-34.
134. Fan, Y.; Simon, S.; Sjöblom, J. Interfacial shear rheology of asphaltenes at oil–water interface and its relation to emulsion stability: Influence of concentration, solvent aromaticity and nonionic surfactant. *Colloids and Surfaces A: Physicochemical and Engineering Aspects* **2010**, *366* (1–3), 120-128.
135. Spiecker, P. M.; Kilpatrick, P. K. Interfacial rheology of petroleum asphaltenes at the oil-water interface. *Langmuir* **2004**, *20* (10), 4022-4032.
136. Samaniuk, J. R.; Hermans, E.; Verwijlen, T.; Pauchard, V.; Vermant, J. Soft-Glassy Rheology of Asphaltenes at Liquid Interfaces. *Journal of Dispersion Science and Technology* **2015**, *36* (10), 1444-1451.
137. Vandebriel, S.; Franck, A.; Fuller, G. G.; Moldenaers, P.; Vermant, J. A double wall-ring geometry for interfacial shear rheometry. *Rheologica Acta* **2010**, *49* (2), 131-144.
138. Natarajan, A.; Kuznicki, N.; Harbottle, D.; Masliyah, J.; Zeng, H.; Xu, Z. Understanding Mechanisms of Asphaltene Adsorption from Organic Solvent on Mica. *Langmuir* **2014**, *30* (31), 9370-9377.
139. Rane, J. P.; Harbottle, D.; Pauchard, V.; Couzis, A.; Banerjee, S. Adsorption kinetics of asphaltenes at the oil-water interface and nanoaggregation in the bulk. *Langmuir* **2012**, *28* (26), 9986-9995.
140. Yarranton, H. W.; Sztukowski, D. M.; Urrutia, P. Effect of interfacial rheology on model emulsion coalescence: I. Interfacial rheology. *Journal of Colloid and Interface Science* **2007**, *310* (1), 246-252.
141. Yarranton, H. W.; Urrutia, P.; Sztukowski, D. M. Effect of interfacial rheology on model emulsion coalescence: II. Emulsion coalescence. *Journal of Colloid and Interface Science* **2007**, *310* (1), 253-259.
142. Alvarez, G.; Poteau, S.; Argillier, J. F.; Langevin, D.; Salager, J. L. Heavy oil-water interfacial properties and emulsion stability: Influence of dilution. *Energy and Fuels* **2009**, *23* (1), 294-299.
143. Sztukowski, D. M.; Yarranton, H. W. Rheology of asphaltene-toluene/water interfaces. *Langmuir* **2005**, *21* (25), 11651-11658.
144. Nenningsland, A. L.; Simon, S.; Sjöblom, J. Influence of Interfacial Rheological Properties on Stability of Asphaltene-Stabilized Emulsions. *Journal of Dispersion Science and Technology* **2014**, *35* (2), 231-243.
145. Nenningsland, A. L.; Simon, S.; Sjöblom, J. Surface properties of basic components extracted from petroleum crude oil. *Energy and Fuels* **2010**, *24* (12), 6501-6505.
146. Sjöblom, J.; Simon, S.; Xu, Z. Model molecules mimicking asphaltenes. *Advances in Colloid and Interface Science* **2015**, *218*, 1-16.
147. Akbarzadeh, K.; Bressler, D. C.; Wang, J.; Gawrys, K. L.; Gray, M. R.; Kilpatrick, P. K.; Yarranton, H. W. Association Behavior of Pyrene Compounds as Models for Asphaltenes. *Energy & Fuels* **2005**, *19* (4), 1268-1271.

148. Rakotondradany, F.; Fenniri, H.; Rahimi, P.; Gawrys, K. L.; Kilpatrick, P. K.; Gray, M. R. Hexabenzocoronene Model Compounds for Asphaltene Fractions: Synthesis & Characterization. *Energy & Fuels* **2006**, *20* (6), 2439-2447.
149. Tan, X.; Fenniri, H.; Gray, M. R. Pyrene Derivatives of 2,2'-Bipyridine as Models for Asphaltenes: Synthesis, Characterization, and Supramolecular Organization. *Energy & Fuels* **2008**, *22* (2), 715-720.
150. Alshareef, A. H.; Scherer, A.; Tan, X.; Azyat, K.; Stryker, J. M.; Tykwinski, R. R.; Gray, M. R. Effect of Chemical Structure on the Cracking and Coking of Archipelago Model Compounds Representative of Asphaltenes. *Energy & Fuels* **2012**, *26* (3), 1828-1843.
151. Kuznicki, T.; Masliyah, J. H.; Bhattacharjee, S. Aggregation and Partitioning of Model Asphaltenes at Toluene–Water Interfaces: Molecular Dynamics Simulations. *Energy & Fuels* **2009**, *23* (10), 5027-5035.
152. Alshareef, A. H.; Scherer, A.; Stryker, J. M.; Tykwinski, R. R.; Gray, M. R. Thermal Cracking of Substituted Cholestane–Benzoquinoline Asphaltene Model Compounds. *Energy & Fuels* **2012**, *26* (6), 3592-3603.
153. Alshareef, A. H.; Scherer, A.; Tan, X.; Azyat, K.; Stryker, J. M.; Tykwinski, R. R.; Gray, M. R. Formation of Archipelago Structures during Thermal Cracking Implicates a Chemical Mechanism for the Formation of Petroleum Asphaltenes. *Energy & Fuels* **2011**, *25* (5), 2130-2136.
154. Nordgård, E. L.; Sørland, G.; Sjöblom, J. Behavior of asphaltene model compounds at W/O interfaces. *Langmuir* **2010**, *26* (4), 2352-2360.
155. Nordgård, E. L.; Landsem, E.; Sjöblom, J. Langmuir Films of Asphaltene Model Compounds and Their Fluorescent Properties. *Langmuir* **2008**, *24* (16), 8742-8751.
156. Nordgård, E. L.; Sjöblom, J. Model compounds for asphaltenes and C80 isoprenoid tetraacids. Part I: Synthesis and interfacial activities. *Journal of Dispersion Science and Technology* **2008**, *29* (8), 1114-1122.
157. Nenningsland, A. L.; Gao, B.; Simon, S.; Sjöblom, J. Comparative study of stabilizing agents for water-in-oil emulsions. *Energy and Fuels* **2011**, *25* (12), 5746-5754.
158. Bi, J.; Yang, F.; Harbottle, D.; Pensini, E.; Tchoukov, P.; Simon, S.; Sjöblom, J.; Dabros, T.; Czarnecki, J.; Liu, Q.; Xu, Z. Interfacial Layer Properties of a Polyaromatic Compound and its Role in Stabilizing Water-in-Oil Emulsions. *Langmuir* **2015**, *31* (38), 10382-10391.
159. Fossen, M.; Kallevik, H.; Knudsen, K. D.; Sjöblom, J. Asphaltenes precipitated by a two-step precipitation procedure. 1. Interfacial tension and solvent properties. *Energy and Fuels* **2007**, *21* (2), 1030-1037.
160. Du Noüy, P. L. An Interfacial Tensiometer for Universal Use. *The Journal of General Physiology* **1925**, *7* (5), 625-633.
161. Gibbs, J. W. *The Collected Works of John Willard Gibbs, Ph.D., LL.D.*; Longmans, Green and Co. 1928; Vol. 1: Thermodynamics.
162. Yeung, A.; Dabros, T.; Masliyah, J.; Czarnecki, J. Micropipette: a new technique in emulsion research. *Colloids and Surfaces A: Physicochemical and Engineering Aspects* **2000**, *174* (1-2), 169-181.
163. Svitova, T. F.; Wetherbee, M. J.; Radke, C. J. Dynamics of surfactant sorption at the air/water interface: Continuous-flow tensiometry. *Journal of Colloid and Interface Science* **2003**, *261* (1), 170-179.
164. Ferri, J. K.; Gorevski, N.; Kotsmar, C.; Leser, M. E.; Miller, R. Desorption kinetics of surfactants at fluid interfaces by novel coaxial capillary pendant drop experiments. *Colloids and Surfaces A: Physicochemical and Engineering Aspects* **2008**, *319* (1-3), 13-20.
165. Hsu, C. T.; Chang, C. H.; Lin, S. Y. Comments on the adsorption isotherm and determination of adsorption kinetics. *Langmuir* **1997**, *13* (23), 6204-6206.

166. Eastoe, J.; Dalton, J. S. Dynamic surface tension and adsorption mechanisms of surfactants at the air-water interface. *Advances in Colloid and Interface Science* **2000**, *85* (2), 103-144.
167. Ferri, J. K.; Miller, R.; Makievski, A. V. Equilibrium and dynamics of PEO/PPO/PEO penetration into DPPC monolayers. *Colloids and Surfaces A: Physicochemical and Engineering Aspects* **2005**, *261* (1-3), 39-48.
168. Kotsmár, C.; Grigoriev, D. O.; Makievski, A. V.; Ferri, J. K.; Krägel, J.; Miller, R.; Möhwald, H. Drop profile analysis tensiometry with drop bulk exchange to study the sequential and simultaneous adsorption of a mixed  $\beta$ -casein/ C12DMPO system. *Colloid and Polymer Science* **2008**, *286* (8-9), 1071-1077.
169. Ravera, F.; Loglio, G.; Kovalchuk, V. I. Interfacial dilational rheology by oscillating bubble/drop methods. *Current Opinion in Colloid & Interface Science* **2010**, *15* (4), 217-228.
170. Derkach, S. R.; Krägel, J.; Miller, R. Methods of measuring rheological properties of interfacial layers (Experimental methods of 2D rheology). *Colloid Journal* **2009**, *71* (1), 1-17.
171. Lucassen, J.; Van Den Tempel, M. Dynamic measurements of dilational properties of a liquid interface. *Chemical Engineering Science* **1972**, *27* (6), 1283-1291.
172. Hermans, E.; Vermant, J. Interfacial shear rheology of DPPC under physiologically relevant conditions. *Soft Matter* **2014**, *10* (1), 175-186.
173. Chandra, M. S.; Xu, Z.; Masliyah, J. H. Interfacial Films Adsorbed from Bitumen in Toluene Solution at a Toluene–Water Interface: A Langmuir and Langmuir–Blodgett Film Approach. *Energy & Fuels* **2008**, *22* (3), 1784-1791.
174. Zhang, L. Y.; Breen, P.; Xu, Z.; Masliyah, J. H. Asphaltene Films at a Toluene/Water Interface. *Energy & Fuels* **2007**, *21* (1), 274-285.
175. Solovyev, A.; Zhang, L. Y.; Xu, Z.; Masliyah, J. H. Langmuir Films of Bitumen at Oil/Water Interfaces. *Energy & Fuels* **2006**, *20* (4), 1572-1578.
176. Zhang, L. Y.; Lopetinsky, R.; Xu, Z.; Masliyah, J. H. Asphaltene Monolayers at a Toluene/Water Interface. *Energy & Fuels* **2005**, *19* (4), 1330-1336.
177. Denoyel, R. In situ methods for studying adsorbed phases at the solid-liquid interface: Microcalorimetry and ellipsometry. *Comptes Rendus - Geoscience* **2002**, *334* (9), 689-702.
178. Alipour Tabrizy, V.; Denoyel, R.; Hamouda, A. A. Characterization of wettability alteration of calcite, quartz and kaolinite: Surface energy analysis. *Colloids and Surfaces A: Physicochemical and Engineering Aspects* **2011**, *384* (1-3), 98-108.
179. Denoyel, R. Microcalorimetry and ellipsometry in surfactant adsorption studies. *Colloids and Surfaces A: Physicochemical and Engineering Aspects* **2002**, *205* (1-2), 61-71.
180. Sauerbrey, G. Verwendung von Schwingquarzen zur Wägung dünner Schichten und zur Mikrowägung. *Z. Physik* **1959**, *155* (2), 206-222.
181. Rodahl, M.; Höök, F.; Krozer, A.; Brzezinski, P.; Kasemo, B. Quartz crystal microbalance setup for frequency and Q-factor measurements in gaseous and liquid environments. *Review of Scientific Instruments* **1995**, *66*, 3924-3930.
182. Simon, S.; Jestin, J.; Palermo, T.; Barre, L. Relation between solution and interfacial properties of asphaltene aggregates. *Energy and Fuels* **2009**, *23* (1), 306-313.
183. Chang, C. H.; Franses, E. I. Adsorption dynamics of surfactants at the air/water interface: a critical review of mathematical models, data, and mechanisms. *Colloids and Surfaces A: Physicochemical and Engineering Aspects* **1995**, *100* (C), 1-45.
184. Ese, M. H.; Galet, L.; Clause, D.; Sjöblom, J. Properties of langmuir surface and interfacial films built up by asphaltenes and resins: Influence of chemical demulsifiers. *Journal of Colloid and Interface Science* **1999**, *220* (2), 293-301.
185. Anton, N.; Vandamme, T. F.; Bouriat, P. Dilatational rheology of a gel point network formed by nonionic soluble surfactants at the oil-water interface. *Soft Matter* **2013**, *9* (4), 1310-1318.

186. Simon, S.; Picton, L.; Le Cerf, D.; Muller, G. Adsorption of amphiphilic polysaccharides onto polystyrene latex particles. *Polymer* **2005**, *46* (11), 3700-3707.
187. Georgiev, G. A.; Gurov, R.; Jordanova, A.; Vassilieff, C. S.; Lanchev, Z. Properties of alkyl-phosphatidylcholine monolayers in the presence of surface-active three-block copolymers. *Colloids and Surfaces B: Biointerfaces* **2010**, *80* (1), 40-44.
188. Hädicke, A.; Blume, A. Interactions of Pluronic block copolymers with lipid monolayers studied by epi-fluorescence microscopy and by adsorption experiments. *Journal of Colloid and Interface Science* **2013**, *407* (0), 327-338.
189. Hunter, J. R.; Carbonell, R. G.; Kilpatrick, P. K. Coadsorption and exchange of lysozyme/ $\beta$ -casein mixtures at the air/water interface. *Journal of Colloid and Interface Science* **1991**, *143* (1), 37-53.
190. Nenningsland, A. L.; Simon, S.; Sjöblom, J. Influence of Interfacial Rheological Properties on Stability of Asphaltene-Stabilized Emulsions. *Journal of Dispersion Science and Technology* **2013**, *35* (2), 231-243.
191. Reichert, M. D.; Alvarez, N. J.; Brooks, C. F.; Grillet, A. M.; Mondy, L. A.; Anna, S. L.; Walker, L. M. The importance of experimental design on measurement of dynamic interfacial tension and interfacial rheology in diffusion-limited surfactant systems. *Colloids and Surfaces A: Physicochemical and Engineering Aspects* **2015**, *467*, 135-142.

*Mixed interfaces of asphaltenes and model demulsifiers part I:  
adsorption and desorption of single components.*





Contents lists available at ScienceDirect

# Colloids and Surfaces A: Physicochemical and Engineering Aspects

journal homepage: [www.elsevier.com/locate/colsurfa](http://www.elsevier.com/locate/colsurfa)

## Mixed interfaces of asphaltenes and model demulsifiers part I: Adsorption and desorption of single components



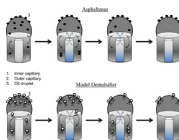
Diego Pradilla\*, Sébastien Simon, Johan Sjöblom

Ugelstad Laboratory, Department of Chemical Engineering, Norwegian University of Science and Technology (NTNU), NO-7491 Trondheim, Norway

### HIGHLIGHTS

- Asphaltenes and Brij®-93 follow Langmuir and Frumkin-type isotherms at liquid–liquid interface.
- Asphaltenes are irreversibly adsorbed at the liquid–liquid interface.
- Brij®-93 is partly desorbed when flushed with pure solvent.

### GRAPHICAL ABSTRACT



### ARTICLE INFO

#### Article history:

Received 16 July 2014

Received in revised form 27 October 2014

Accepted 29 October 2014

Available online 4 November 2014

#### Keywords:

Adsorption

Desorption

Chemical demulsification

Emulsion stability

Brij®-93

### ABSTRACT

This article is the first in a series of two aiming to understand the competitive adsorption and desorption dynamics of asphaltenes and a model demulsifier (Brij®-93) at the liquid–liquid interface to broaden the knowledge of the stability of crude-oil emulsions. In this article, the properties of single components are studied. First, the Langmuir and Frumkin isotherms were successfully used to describe the interfacial tension data allowing the determination of the equilibrium adsorption parameters of asphaltenes and Brij®-93. Second, desorption of single compounds (from pure xylene, the adsorption medium) was followed through the use of a double coaxial capillary system. It was found that asphaltenes are irreversibly adsorbed (~2% amount desorbed) at the oil/water interface even at low surface coverage and adsorption times which confirm the strong interactions present. It was also found that desorption is independent of the pure solvent flow condition and the total volume exchanged. Third, results show that the model demulsifier Brij®-93 is partly desorbed (~20%) from the oil/water interface. This could be attributed to the distribution of ethyl oxide (EO) groups in the polydisperse sample or to the polydispersity of the aggregates adsorbed which have different adsorption energies. This work provides the fundamental framework for the second part of the series in which adsorption and desorption dynamics of a mixed interface composed of asphaltenes and Brij®-93 will be studied.

© 2014 Elsevier B.V. All rights reserved.

### 1. Introduction

Petroleum extraction is undoubtedly linked to water co-production. Water is present at several stages of the production process and one of the main issues in terms of transportation from the reservoirs to the cracking plants is the formation of emulsions. That is, the stabilization of water-in-oil (W/O) emulsions by

crude oil indigenous surfactants such as asphaltenes, resins and naphthenates [1,2]. Asphaltenes are defined as the fraction of petroleum insoluble in *n*-alkane but soluble in toluene (aromatic solvents). Therefore they are not a single chemical compound, but instead a solubility class composed of molecules with different molecular weights and functionalities [3–5]. Asphaltenes are largely responsible for the formation of organic deposits and due to their surface active nature, also responsible for wettability changes of mineral surfaces in the reservoirs [6,7]. It has also been reported that Naphthenic acids [8] are surface active under certain conditions related mainly to pH and that they can influence

\* Corresponding author. Tel.: +47 942 41 988; fax: +47 735 94 080.

E-mail addresses: [diego.c.p.ragua@ntnu.no](mailto:diego.c.p.ragua@ntnu.no), [diegocp6@hotmail.com](mailto:diegocp6@hotmail.com) (D. Pradilla).



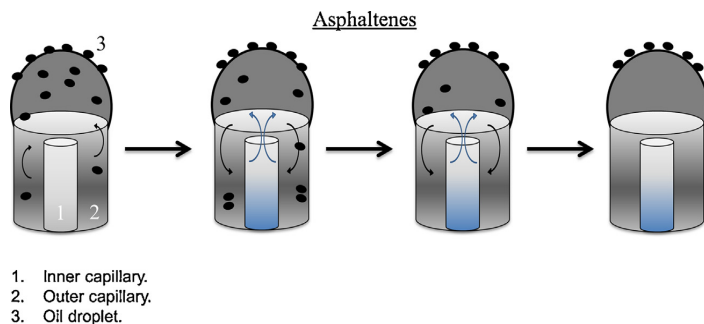


**Fig. 1.** Coaxial double capillary system showing the desorption process of a surface active molecule that exhibits partly reversible adsorption after the injection of a predetermined volume of pure solvent.

in the stability of emulsions, even if the main mechanisms of emulsion stabilization are attributed to the asphaltenes. The main mechanism of asphaltene-stabilized emulsions is the formation of a rigid and mechanically strong film around the water droplets which prevents them from coalescing [9]. Evidently, stable W/O emulsions are undesired in the oil industry due to high transportation costs, energy demands, corrosion of pipe lines flow assurance issues due to the viscosity increase and subsequent problems in the refining stages. Typical market demands are in the order of 0.5% BSW by volume (bottom, solids, water), which means that efficient and effective methods for removing the water are imperative [10].

Demulsification is the process of breaking emulsions to separate the water from the rest of the crude oil. There are several methods for the separation of water, among them gravitational, centrifugal and electro-coalescence methods. Chemical demulsification refers to the addition of certain chemicals, typically in the order of 1 up to 1000 ppm to promote phase separation by reducing the interfacial tension, thus making it possible for the demulsifiers to mix with the indigenous surfactants (asphaltenes) at the interface [2]. The chemicals (i.e. Demulsifiers) should exhibit both high diffusion rates, so they can quickly go to the interface and interact or compete with the emulsifiers already present [11]; and they should be able to affect the rigid skin that surrounds the water droplets. They can act on the protecting film by changing the elasticity or interfacial viscosity, they can form a film giving rise to an oil-in-water (O/W) emulsion, they can operate as a wetting agent and most of these results being consequences of their interaction with the asphaltene network [12]. The composition of commercially available demulsifiers is broad [11]. Starting with simple organic solvents that dissolve the indigenous surfactants such as benzene, acetone and short-chain alcohols and going up to the category of nonionic surfactants that are known to act as efficient demulsifiers. Members of the latter group include fatty esters, fatty amides, alkyl phenol ethers and polyoxopropylene glycol ethers (PEO-PPO block co-polymers), only to mention some.

Adsorption and desorption kinetics of surface active chemicals can be investigated through dynamic tensiometry, that is, the measurement of the dynamic surface/interfacial tension. When liquid–liquid systems are being studied, a drop of one of the liquids is produced in the second immiscible liquid [13]. This drop can be either pendant or emerging depending on the type of system that is to be studied; it can be either an oil droplet or a water droplet. These drops can nowadays be rapidly analyzed through the use of powerful software coupled with CCD cameras. The technique is commonly known as axisymmetric drop shape analysis (ADSA), and it is widely accepted as a robust and versatile method for measuring the interfacial tension (IFT) [14]. The equilibrium surface/interfacial tension data can be described through adsorption isotherms and equations

of state. For instance, the well-known isotherms of Henry, Langmuir, Frumkin and Freundlich have been widely used to describe the adsorption of several surface active compounds onto liquid–air, liquid–liquid and liquid–solid interfaces [15,16].

Several experimental protocols based on the ADSA technique have been proposed to study desorption kinetics or multilayer formation [17–19]. They are of particular interest, mainly because of the ability to follow the interfacial tension as a function of time when the surface active molecules are being desorbed from the interface (see Figs. 1 and 2). The novel coaxial capillary apparatus reported by Ferri et al. [20] and further developed by Kotsmár et al. [21] and Ferri et al. [14] allows the study of convection-enhanced adsorption/desorption kinetics of a liquid–liquid interface. The experimental design consists of a pendant (or emerging) drop formed at the end of a capillary initially at equilibrium with a bulk concentration of surface active molecules. The interface is then driven away from equilibrium by injecting a surfactant free solution (i.e. solvent), thus generating a change in the dynamic interfacial tension [14]. Several factors such as reorganization, multilayer formation, unfolding (proteins), conformations and more importantly the reversibility of adsorption at the interface can also be addressed through this novel method coupled with other studies available in the literature.

This work will elucidate new insight on the coalescence process by studying the interactions present in a mixed interface between asphaltenes and a model demulsifier. This will enhance the understanding of emulsion stability at a molecular level. This is the first part of a series of two publications in which the adsorption and desorption aspects of asphaltenes and Brij®-93 are investigated using a system based on ADSA. First, an analysis on adsorption of single compounds onto liquid–liquid interfaces is performed to obtain equilibrium parameters. Second, using a coaxial capillary system, desorption from a pure solvent is performed to follow the kinetics of the same components (i.e. asphaltenes and a demulsifier). And finally, adsorption isotherms and equations of state are used to describe the IFT versus time data, making it possible to establish the composition at the interface, the percentage of desorption and possible destabilization mechanisms.

## 2. Experimental

### 2.1. Asphaltenes

Asphaltenes were extracted by precipitation with *n*-hexane from a chemical-free heavy crude oil of the Norwegian continental shelf. Basic analysis of the crude oil is given in Table 1. To extract the asphaltenes, the crude oil was first heated at a temperature of 60 °C. It was subsequently shaken to ensure homogeneity of the

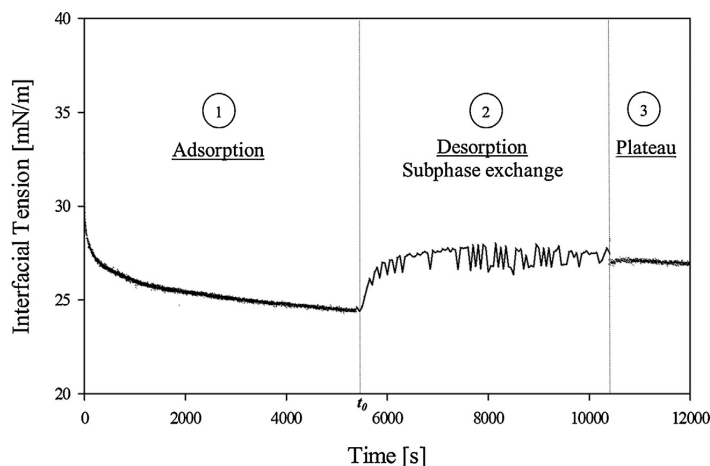


**Fig. 2.** Evolution of the interfacial tension as a function of time during the adsorption/desorption experiments of asphaltene solutions in xylene. Stage 1 corresponds to the adsorption and equilibration step of the surface active molecules. At a time  $t_0$  the injection of pure solvent starts, thus stage 2 represents the desorption step. Finally, during stage 3 the pre-determined volume is fully exchanged and a plateau value for the IFT is reached. The experimental conditions for this experiment are: flow rate  $Q_2 = 0.4 \mu\text{L/s}$ , total volume exchanged  $V_2 = 1000 \mu\text{L}$ , adsorption time  $t_3 = 1.5 \text{ h}$  and initial bulk concentration  $C_2 = 1 \text{ g/L}$ .

**Table 1**

Characteristics of the heavy crude oil sample used in this work for asphaltene extraction. (\*): Determined by Karl-Fisher titration. (\*\*): The SARA composition determination method by HPLC is described by Hannisdal et al. [48].

| Density @ 15 °C | TAN (mg g <sup>-1</sup> ) | Water content (wt.%) (*) | SARA analysis (**) |                  |               |                                      |
|-----------------|---------------------------|--------------------------|--------------------|------------------|---------------|--------------------------------------|
|                 |                           |                          | Saturates (wt.%)   | Aromatics (wt.%) | Resins (wt.%) | Asphaltenes, hexane insoluble (wt.%) |
| 0.939           | 2.15                      | 0.11                     | 37                 | 44               | 16            | 2.5                                  |

sample. Second, the crude oil was mixed with the *n*-hexane at a weight/volume ratio of 1:40 (w/v). Third, the mixture was stirred for at least 24 h to ensure precipitation. Fourth, the asphaltene fraction was recovered using a 0.45  $\mu\text{m}$  HVLP (Millipore) membrane filter washing with additional amounts of *n*-hexane. Finally, the recovered asphaltenes were put into a nitrogen atmosphere degasser and dried for 48 h. The asphaltenes were weighted every 12 h until the mass was constant to ensure complete evaporation of *n*-hexane. The elemental composition of asphaltenes after extraction is given in Table 2. An average molecular weight of 750 g/mol was used for all the calculations according to Buch et al. [22] and Groenzin et al. [23] who established this value as an adequate average for *n*-heptane precipitated asphaltenes. *n*-hexane precipitated asphaltenes are not expected to deviate from this range.

## 2.2. Demulsifier

The model demulsifier selected for this work was a polyethylene glycol oleyl ether, commercially known and available as Brij® 93 provided by Sigma-Aldrich. It has an approximate average number molecular weight of 357 g/mol and a hydrophilic–lipophilic balance (HLB) of 4. The chemical was used as provided. Bottle tests confirmed that this chemical actively separates water from asphaltene stabilized emulsions.

**Table 2**

Elemental composition of asphaltenes recovered from the heavy crude oil used in this work.

|             | wt.% C | wt.% H | wt.% N | wt.% O | wt.% S | C/H atomic ratio |
|-------------|--------|--------|--------|--------|--------|------------------|
| Asphaltenes | 86.1   | 8.28   | 1.29   | 1.97   | 2.10   | 0.867            |

## 2.3. Water phase

The water phase was a buffer solution of pH 7 prepared with ultra-pure water (resistivity of 18.2  $\Omega$ ) and 0.1 M  $\text{KH}_2\text{PO}_4$  adjusted with 0.1 M NaOH solutions.

## 2.4. Solvents

Asphaltene and demulsifier solutions were prepared using xylene AnalaR NORMAPUR® provided by VWR-Norway. The *n*-hexane used for precipitation was HiPerSolv CHROMANORM® for HPLC quality also provided by VWR-Norway. Both solvents were used as received.

## 2.5. Tensiometry

A commercially available pendant drop tensiometer (PAT 1 m, SINTERFACE Technologies, Berlin, Germany) was used for all the experiments. It calculates the surface/interfacial tension of a surfactant-covered drop by recording the silhouette onto a CCD camera. The digital images are then analyzed and fitted to the Young-Laplace equation with an accuracy of  $\pm 0.1 \text{ mN/m}$ . This equation relates the curvature of a liquid drop and the surface/interfacial tension. The built-in software produces a family of theoretical curves by changing the values of the surface/interfacial tension. The curve that yields the best fit to the experimental points represents the measured surface/interfacial tension. For this procedure the densities of the oil and aqueous phase are needed. A custom-made accessory for the apparatus consisting of two concentric capillary tubes (an inner capillary and an outer capillary) was used for the desorption experiments. Specific details of the technique are described elsewhere [14].

Experiments were also performed using a KSV Sigma 70 (KSV instruments-Finland) tensiometer equipped with a Du Nouy ring at 22 °C. The system was tested prior to each experiment by measuring pure water obtaining an average value within  $72.8 \pm 1$  mN/m. Unless otherwise specified, all experiments were run by duplicates. Good reproducibility was observed.

### 3. Theory

#### 3.1. Adsorption

The main consideration when discussing IFT data is the application of an appropriate isotherm. The ultimate goal of the adsorption isotherm is to relate the bulk concentration and the composition at the interface. The Gibbs equation provides a model based on thermodynamics. The equation is as follows [16]:

$$\Gamma = -\frac{1}{nRT} \cdot \frac{d\gamma}{d \ln(c)} \quad (1)$$

Here  $\Gamma$  is the equilibrium surface excess,  $n$  is a constant that is equal to 1 for nonionic surfactants,  $R$  is the gas constant,  $T$  the temperature,  $\gamma$  the surface/interfacial tension and  $c$  the concentration in the bulk. The  $\Gamma$  vs.  $c$  curve can be obtained by fitting an adequate adsorption isotherm [16,24].

The most commonly and widely used non-linear adsorption isotherm is that of Langmuir. It is a two parameter equation which assumes that there are no interactions between the adsorbed species and that the molecules are adsorbed as a monolayer. The typical form of the Langmuir isotherm is,

$$\Gamma = \Gamma_{\infty} \left( \frac{K_L c}{1 + K_L c} \right) \quad (2)$$

where  $\Gamma_{\infty}$  is the surface excess at saturation and  $K_L$  is known as the adsorption constant. These two parameters are adjustable. The analogous equation of state is known as the Szyszkowski equation, as reported by Chang and Franses [16],

$$\pi = nRT\Gamma_{\infty} \ln(1 + K_L c) \quad (3)$$

In which  $\pi$  is the surface pressure or the difference in IFT between a clean interface, for instance that of a pure solvent and the value when the surface active agents have been adsorbed.

The Frumkin isotherm accounts interactions between the solute and the solvent and also interactions that can occur at a non-ideal lattice. This is a three parameter equation, in which the third parameter accounts for those interactions. The Frumkin adsorption isotherm and the corresponding equation of state are,

$$c = \frac{1}{K_F} \cdot \frac{\Gamma}{\Gamma_{\infty} - \Gamma} \exp \left[ -A \frac{\Gamma}{\Gamma_{\infty}} \right] \quad (4)$$

$$\pi = nRT\Gamma_{\infty} \ln \left( 1 - \frac{\Gamma}{\Gamma_{\infty}} \right) - \frac{nRTA}{2} \Gamma_{\infty} \left( \frac{\Gamma}{\Gamma_{\infty}} \right)^2 \quad (5)$$

Here,  $K_F$  is the adsorption constant and  $A$  is the interaction parameter. When the interactions are negligible (i.e.  $A=0$ ), the Frumkin isotherm reduces to the Langmuir equation.

#### 3.2. Desorption

When the equilibrium of an interface in a pendant drop experiment is disturbed by the subphase exchange, that is the injection of pure solvent, the adsorbed molecules tend to desorb. This is a convection driven process that generates a change in the concentration at the interface. Therefore, it is necessary to use an equation that accurately describes this process [14]. Sivitova et al. [13] modeled the concentration change using an analogy based on the internal-age distribution of a solute inside a continuously stirred mixed

reactor (CSTR) [25]. In a perfectly mixed CSTR, the concentration of molecules in a portion of fluid leaving the reactor is exactly the same as the concentration at any point inside the reactor. Therefore, if pure solvent is being injected, the concentration decays according to [13]:

$$C = C_0 \exp \left( \frac{Q_i t}{V_i} \right) \quad (6)$$

where  $V_i$  is the initial concentration in the bulk,  $\gamma_0$  is the pre-determined total volume to be exchanged and  $Q_i$  is the solvent flow rate. This means that Equation (6) coupled with equation (3) describe the evolution of the interfacial tension as a function of time while the surface active molecules are being desorbed from the interface if the adsorption is of Langmuir type. Therefore, in this work the term  $Q_i$  will be used to describe the volumetric flow rate of the exchange, that is, the rate at which the fluid is being pumped from the inner capillary as explained later in section 4.2. Furthermore, the term  $Q_i$ , which is analogous to the residence time distribution in a CSTR, also serves as a characteristic dimensionless time used for normalization. This approach has been shown to work [13,14] for several systems under the assumption that the surface active molecules exhibit complete reversible adsorption and when the desorption is faster than the evolution of the concentration inside the droplet. Evidently, deviations from this model could be attributed to a non-Langmuir type of adsorption or irreversible adsorption.

#### 3.3. Adsorption kinetics

The well-known Ward-Tordai equation is widely used to model adsorption kinetics limited only by diffusion of surfactants towards an interface. It allows the calculation of diffusion coefficients based on the interfacial tension data. As the IFT decays, this model accounts for how the molecules are being diffused and subsequently adsorbed onto the interface. There are two main mechanisms included into this model. First, at short times and with a fresh interface the monomers will adsorb directly, thus it is assumed that every molecule arrives at an empty site. Second, with the molecules present at the oil–water interface, back diffusion takes place, this means that the molecules that arrive at an already occupied site will return to the bulk [16].

The equation in its usual form cannot be solved, therefore asymptotic solutions have been proposed [26]. When the short-time approximation is used, the measured interfacial tension will be close to that of the pure solvent; hence it can be assumed that the solution is dilute. When this happens, the Henry isotherm can be applied and the diffusion coefficient can be obtained from the following equation [16],

$$\gamma_{t \rightarrow 0} = \gamma_0 - 2nRTc_0 \sqrt{\frac{Dt}{\pi}} \quad (7.a)$$

In this equation,  $D$  is the diffusion coefficient of the adsorbing molecule,  $\gamma_0$  is the interfacial tension of pure solvent and  $c_0$  is the concentration in the bulk.

When the long-time approximation is used, the subsurface concentration will approach that of the bulk. The asymptotic solution is as follows:

$$\gamma_{t \rightarrow \infty} = \gamma_{eq} + \frac{nRT\Gamma_{eq}^2}{c} \sqrt{\frac{\pi}{4Dt}} \quad (7.b)$$

In this equation,  $\Gamma_{eq}$  is the equilibrium surface excess of surfactant,  $\gamma_0$  the equilibrium interfacial tension and  $c$  the concentration of surfactant in the bulk.

**Table 3**

Diffusion coefficient for asphaltene and Brij®-93 solutions in xylene using the short-time approximation (ST) and the long-term approximation (LT) of the ward-Tordai equation.

| System                     | Concentration (m-mol/L) | $D$ (m <sup>2</sup> /s) |
|----------------------------|-------------------------|-------------------------|
| Asphaltenes in Xylene (ST) | $2.94 \times 10^{-3}$   | $1.49 \times 10^{-12}$  |
|                            | $1.47 \times 10^{-2}$   | $5.99 \times 10^{-14}$  |
|                            | $2.94 \times 10^{-2}$   | $9.37 \times 10^{-14}$  |
|                            | $1.47 \times 10^{-1}$   | $9.59 \times 10^{-15}$  |
|                            | $2.94 \times 10^{-1}$   | $9.37 \times 10^{-16}$  |
|                            | $7.37 \times 10^{-1}$   | $3.83 \times 10^{-16}$  |
|                            | 1.47                    | $5.39 \times 10^{-17}$  |
|                            | 2.94                    | $1.34 \times 10^{-17}$  |
|                            | 7.37                    | $2.15 \times 10^{-18}$  |
|                            | Brij®-93 in xylene (ST) | $2.42 \times 10^{-3}$   |
| Brij®-93 in xylene (LT)    | $2.43 \times 10^{-4}$   | $4.68 \times 10^{-12}$  |
|                            | $2.43 \times 10^{-3}$   | $6.09 \times 10^{-12}$  |
|                            | $2.43 \times 10^{-2}$   | $2.33 \times 10^{-13}$  |
|                            | $1.21 \times 10^{-1}$   | $8.75 \times 10^{-14}$  |
|                            | $2.43 \times 10^{-1}$   | $2.53 \times 10^{-14}$  |
|                            | 1.21                    | $2.35 \times 10^{-15}$  |
|                            | 1.21                    | $2.35 \times 10^{-15}$  |

## 4. Results and discussion

### 4.1. Dynamic and static adsorption of single components

#### 4.1.1. Kinetic aspects of single compounds

Table 3 summarizes the values of the diffusion coefficient calculated using equation (7.a) for asphaltenes and Brij®-93 solutions in xylene. As expected, asphaltenes show a very low diffusion coefficient ( $D \sim 10^{-12}$  to  $10^{-18}$  m<sup>2</sup>/s) which suggests that the mechanism of adsorption is not diffusion-controlled. In this case, the decrease in the IFT is not explained through the diffusion of molecules to the interface, but instead it is possible that an adsorption barrier is present. Evidently the self-aggregation of asphaltenes in the bulk [3] and stacking contribute to this finding. The method proposed by Chaverot et al. [27] could have been used to analyze the data. However, their method was developed to study a bitumen-water system in which the concentration of the surface active species, namely asphaltenes and naphthenic acids, was unknown. Additionally, this method assumed a diffusion-controlled type of adsorption, even at short times when the interface is nearly empty. In the system used for this work, the concentration of asphaltenes is known and from the calculated diffusion coefficients at short-times it can be concluded that the adsorption is not diffusion-controlled. Furthermore, this method is not applicable to the asphaltene system studied.

Several authors [10,28,29] have proposed phenomenological equations to fit the asphaltene IFT. Under the assumption that asphaltenes are not adsorbed as single molecules but instead as larger aggregates, Jerebi et al. [29], attempted a description of the interfacial tension data of asphaltene solutions in toluene using a model initially proposed to describe protein adsorption. With this model, they conclude that asphaltenes diffuse very fast and that the changes in IFT are due to reorganization at the interface. Asphaltene adsorption onto liquid–liquid interfaces was studied by Fossen et al. [28]. In their publication, a four-parameter bi-exponential model was proposed to describe the IFT vs. time data. The parameters account for rate at which the IFT decays in two parts: fast decrease at short times and slow decay at longer times. This is due to differences in the relaxation processes at the interface which could be a consequence of slow/fast diffusion, adsorption barriers, reorganization of the asphaltene network and partitioning. Similarly, the competitive adsorption of demulsifiers at the crude oil/water interface was studied by Fan et al. [10]. Using the same model, the description of the different mechanisms that are present at the interface depends on the functionality of the surface active agents.

**Table 4**

Langmuir and Frumkin equilibrium adsorption constants for asphaltene and Brij®93 solutions in xylene using two techniques: ASDA and Du Nouy ring.

| Asphaltenes     | Technique | $K_L, K_F$<br>(m <sup>3</sup> /mol) | $\Gamma_\infty$ (mol/m <sup>2</sup> ) | A    |
|-----------------|-----------|-------------------------------------|---------------------------------------|------|
| Eq. (2) and (3) | ASDA      | 228                                 | $9.54 \times 10^{-7}$                 | 0    |
|                 | Du Nouy   | 106                                 | $9.32 \times 10^{-7}$                 | 0    |
| Eq. (4) and (5) | ASDA      | 97                                  | $9.56 \times 10^{-7}$                 | 1    |
|                 | Du Nouy   | 161                                 | $7.85 \times 10^{-7}$                 | 1    |
| Brij® 93        |           |                                     |                                       |      |
| Eq. (2) and (3) | ASDA      | 834                                 | $1.06 \times 10^{-6}$                 | 0    |
|                 | Du Nouy   | 300                                 | $1.27 \times 10^{-6}$                 | 0    |
| Eq. (4) and (5) | ASDA      | 620                                 | $1.19 \times 10^{-6}$                 | -0.4 |
|                 | Du Nouy   | 748                                 | $1.19 \times 10^{-6}$                 | -0.2 |

More recently, Rane et al. [30] proposed a mechanism of asphaltene adsorption at short times based on kinetics and later, Pauchard et al. [31] extended this concept to long-term adsorption by considering a transition between diffusion-controlled adsorption at short times to a nondiffusion-controlled kinetics (adsorption barrier) at longer times. At short times only the monomers and not the nanoaggregates (the authors report a critical nanoaggregation concentration – CNAC – of 200 ppm) are adsorbed creating a monolayer. Later, steric hindrance effects slow down the adsorption. In all cases, the Langmuir adsorption isotherm adequately describes the IFT data. As the results presented in Table 3 suggest, asphaltenes do not follow a diffusion-controlled adsorption.

The diffusion coefficient calculated for Brij®-93 (Table 3) using equation (7.a) seems to be somewhat low to consider it as indicative of a diffusion-controlled process. However, molecules with similar molecular weight report [16] values for the diffusion coefficient of  $\sim 10^{-10}$  m<sup>2</sup>/s which could be comparable. It was not possible to determine the diffusion coefficient for a broader Brij®-93 concentration range due to the failure of the assumptions of the model. A small increase in the concentration causes a rapid IFT drop, hence the assumption of a dilute solution fails, and a small decrease in the concentration did not provide a viable IFT drop. Table 3 also shows the values for the diffusion coefficient calculated using the long-time approximation, equation (7.b). The values are between  $D \sim 10^{-12}$  and  $10^{-15}$  m<sup>2</sup>/s which leads to the conclusion that the adsorption process of Brij®-93 is no longer diffusion-controlled at long times.

#### 4.1.2. Equilibrium aspects of single compounds

To start with, a set of adsorption experiments were performed to determine the equilibrium parameters and the composition at the interface using the Langmuir and Frumkin isotherms represented by Equations (2–5) for asphaltene and demulsifier solutions in xylene. The demulsifier was carefully chosen based on unique criteria developed in this study. While the effectiveness of breaking W/O emulsions of the so-called *pluronic* demulsifiers, which are normally, block or triblock co-polymers of poly ethylene oxide (PEO), poly propylene oxide (PPO) is unquestionable [32–34], their study is somewhat troublesome given the multiple phase transitions, polymer unfolding, reorganization and multilayer accommodation at the interface. This leads to a type of adsorption that cannot be described by the typical adsorption isotherms (i.e. Langmuir, Frumkin, and Freundlich).

Fig. 3 shows a plot of the equilibrium IFT as a function of the bulk concentration for asphaltene solutions in xylene and the demulsifier Brij® 93 solutions in xylene, measured with two techniques: ASDA and Du Nouy ring. The equilibrium values were obtained after letting the system adsorb for 8 h and 3 h, respectively. At this point the change in the IFT values was less than 0.5 mN/m. Also in this figure, the solid lines represent the best fit to equations (2) and (3). Table 4 summarizes the equilibrium parameters using

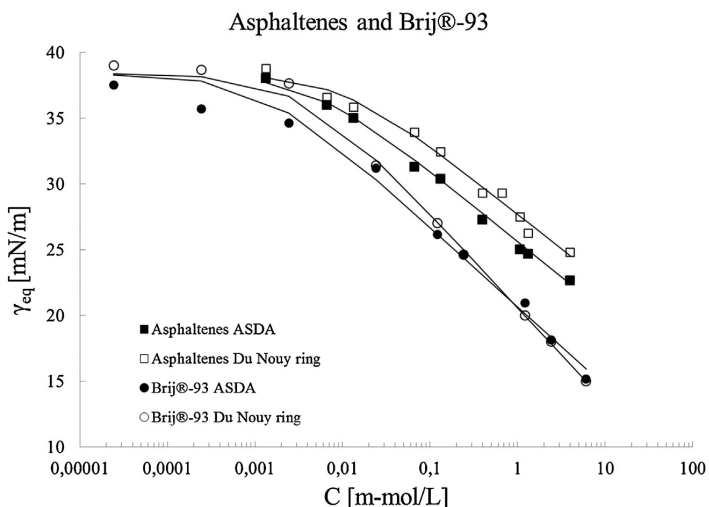


**Fig. 3.** Equilibrium interfacial tension ( $\gamma_{eq}$ ) as a function of bulk concentration for asphaltene and Brij®-93 solutions in xylene. The IFT was measured using two available techniques: ASDA and Du Nouy ring. The solid line represents the best fit to equations (2) and (3).

the Langmuir and the Frumkin Isotherm. Both techniques and both models yield reasonable results. The equilibrium parameters are similar, within the same order of magnitude and comparable. The positive value in the parameter  $A$  of the Frumkin isotherm fit for the asphaltene solutions is an indication of small attractive forces acting on the interface. This agrees with the fact that asphaltenes self-associate in solution [6,28]. On the other hand, for the demulsifier solutions, it can be concluded that both techniques yield similar results. The negative interaction parameter  $A$  obtained when using the Frumkin isotherm could be an indication of repulsive forces acting on the interface [24]. In general, the Langmuir isotherm gives good results for the system studied and it is clear that a mixed interface between these two compounds would yield strong interactions.

#### 4.2. Dynamics of desorption for single components

This section covers a set of desorption experiments using the coaxial capillary system described in the experimental section. The desorption dynamics of Asphaltene and Brij® 93 solutions in xylene was followed by measuring the IFT as a function of time. It is important to note that all the figures presented in this section correspond to average results of at least two parallels.

Fig. 1 depicts a schematic of a system that exhibits partial desorption and can be used as a reference. First, an oil droplet (i.e. Asphaltene/demulsifier solutions in xylene) is formed using the outer capillary and allowed to equilibrate for a certain period of time inside a cuvette (25 mL) that contains the water phase. At this point, this is essentially an adsorption experiment and equilibrium parameters can be calculated. Second, at a time  $t_0$  the droplet subphase is exchanged by injection of pure solvent (i.e. Xylene) through the inner capillary at a volumetric flow rate  $Q_i$ . The interfacial area (droplet volume = 20  $\mu$ L) is kept constant via feedback control, thus withdrawal of liquid is simultaneously performed using the outer capillary. During this stage, desorption of surface active molecules may occur; hence an increase of the interfacial tension is expected. Ideally, the IFT value will increase until that of the pure solvent, if the surface active molecules exhibit reversible desorption. Third, when the predetermined total volume  $V_i$  has been exchanged, pumping from the inner capillary stops and the

IFT reaches a plateau value. All experiments were done at 22 °C. Fig. 2 shows the evolution of the interfacial tension as a function of time during the three steps just described for a given asphaltene solution in xylene. It is important to highlight the fact that the IFT is being continuously monitored during all steps of the experiment.

Experimental data from the desorption stage (see Fig. 2) were treated differently in order to avoid handling a large number of points. For this part, a smoothing procedure based on the running average method was performed over a period of 2 s on the software SigmaPlot v. 12.0. The method ensures that no vital information is lost, thus the resulting curve is a true representation of the experimental data points. Scattering of the data points is inherently linked to volume control during the injection of the solvent.

The accessory was first tested with a known system that exhibits complete reversible adsorption to ensure the validity of the results. Following the experimental conditions reported by Svitova et al. [13], Cetyltrimethylammonium bromide (CTAB) solutions in ultra-pure water were prepared and the surface tension was measured as a function of time on the liquid–air surface. The data was then fitted using equations (3) and (6) using the equilibrium parameters taken from the same reference. The results are shown in Fig. 4 (a) and as it can be observed, the model adequately describes the desorption process of this surfactant. The authors report an equilibrium surface tension value of  $\sim 36$  mN/m after an equilibration time of  $\sim 10$  min which is similar to the values shown in Fig. 4(a). Also, the complete reversibility of CTAB is confirmed due to the fact that after the exchange of the subphase, the surface tension recorded is that of the pure solvent ( $\sim 72$  mN/m). A similar test was done to evaluate the reversibility of adsorption onto the oil/water interface. Fig. 4(b) shows that Equations (3) and (6) adequately describe desorption of CTAB from the xylene/ultra-pure water interface. Even though the surface tension and the interfacial tension are not correlated, in this case both systems showed complete reversible desorption, thus corroborating that the coaxial system can be used as a method to follow adsorption and desorption dynamics at both the air/water and oil/water interface.

Both experiments in Fig. 4 also show that the droplet formed is homogeneous in the sense that there is perfect mixing of the surface active molecules throughout the desorption stage inside

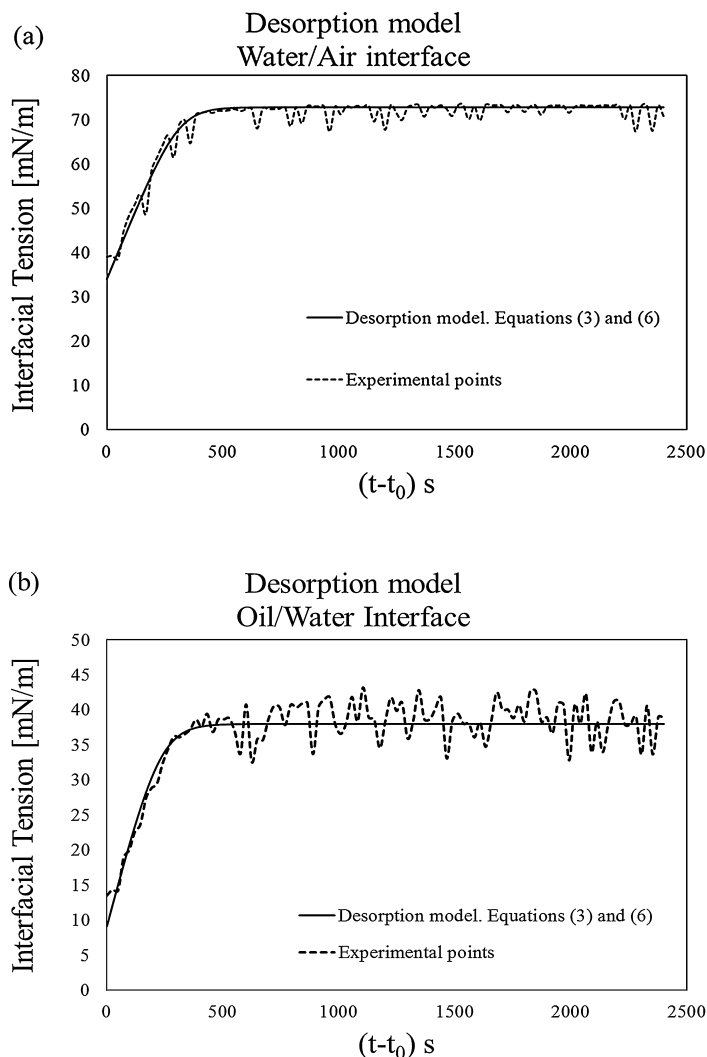


**Fig. 4.** Surface/interfacial tension of cetyltrimethylammonium bromide (CTAB) solutions in ultra-pure water as a function of time measured at the (a) air/water interface and (b) oil/water interface. The solid line represents the prediction of the desorption model (Equations 3 and 6).

the droplet. The same situation can be assumed for an emerging drop.

#### 4.2.1. Asphaltenes

This section is dedicated to the analysis of the dynamics of desorption of asphaltenes. Fig. 5 shows a plot of the interfacial tension as a function of the dimensionless characteristic time for asphaltene solutions in xylene with an initial bulk concentration of 1 g/L. The time lapse covered by this plot starts with the injection of pure solvent and finishes when the predetermined total volume ( $V_t$ ) has been exchanged at a given flow rate ( $Q_t$ ). The initial equilibration adsorption time ( $t_i$ ) was 1.5 h and the volume of the droplet ( $V_D$ ) was kept constant throughout all the experiments at 20  $\mu\text{L}$ . Two conditions for the flow rate ( $Q_1 = 0.2 \mu\text{L/s}$ ,  $Q_2 = 0.4 \mu\text{L/s}$ ) and the total volume exchanged ( $V_1 = 480 \mu\text{L}$ ,  $V_2 = 1000 \mu\text{L}$ ) were tested. The same final interfacial tension value was reached at the end of the experiment, suggesting that there is a similar final composition

at the interface. Thus, from Fig. 5 it can be concluded that these two variables have no apparent effect on asphaltene desorption (same master curve). It is important to highlight the fact that the value  $V_t \gg 100 V_D$  ensures that a plateau on the IFT is reached and thus no further desorption is possible. When the equilibration adsorption time is reduced to 0.5 h, a similar master curve is obtained. This is shown in Fig. 6 for the same system under the same conditions. These experiments ensure that the condition of perfect mixing, while the subphase is being exchanged, remains valid. Hence the measured values of the interfacial tension are a direct consequence of a desorption process instead of a simple effect of dilution. The results are in agreement with a previous analysis [14].

Fig. 5 and Fig. 6 also show that asphaltenes are irreversibly adsorbed at the oil/water interface. The difference between the value of the surface coverage calculated at the beginning and the end of the subphase exchange is less than 2%. The values were calculated by assuming that the equilibrium adsorption

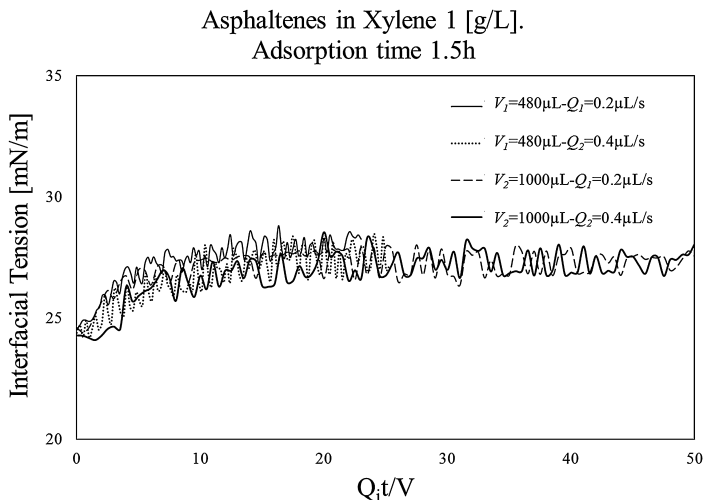


**Fig. 5.** Influence of the flow rate ( $Q_1 = 0.2 \mu\text{L/s}$ ,  $Q_2 = 0.4 \mu\text{L/s}$ ) and the total volume exchanged ( $V_1 = 480 \mu\text{L}$ ,  $V_2 = 1000 \mu\text{L}$ ) on the interfacial tension for asphaltene solutions in xylene at a fixed adsorption time (1.5 h) and initial bulk concentration (1 g/L).

parameters, namely the surface coverage and the adsorption constant, remain valid throughout the desorption stage. A 2% of amount desorbed corresponds to a  $\sim 3 \text{ mN/m}$  total change in the interfacial tension which is an indication of the mechanically strong film that the asphaltene network forms. It has been suggested [29] that the formation of the so-called skin around the water droplets could be a consequence of the adsorption of bulk aggregates (fast process) made of asphaltenic stacks that promote multilayer formation (slow process). Furthermore, direct observations on the skin and compression/expansion experiments show that the rigid film remains unchanged which could be due to the irreversibility of the asphaltene adsorption [35]. The results presented in Figs. 5 and 6 are a strong evidence of these different mechanisms involved in asphaltene adsorption and desorption. The novelty of these results

lies in the fact that throughout IFT measurements, it is possible to corroborate many of the hypotheses suggested to explain the mechanisms of asphaltene-film formation.

The effect of the adsorption time was also studied to determine if the irreversibility of the adsorption is a consequence of any sub-process taking place at long time-scales. Fig. 7 shows a plot of the variation of the IFT as the adsorption time ( $t_i$ ) is varied from 10 min to 3 h. The initial concentration of asphaltenes in the bulk is 1 g/L and desorption was followed at a flow rate of  $Q_2 = 0.4 \mu\text{L/s}$ , total volume exchanged  $V_2 = 100 \mu\text{L}$  and a droplet volume  $V_D = 20 \mu\text{L}$ . The experimental conditions were chosen so that asphaltene desorption is independent of both the flow rate and the total volume exchanged (Figs. 5 and 6). Also, the values are chosen based on practical limitations to ensure drop stability. It

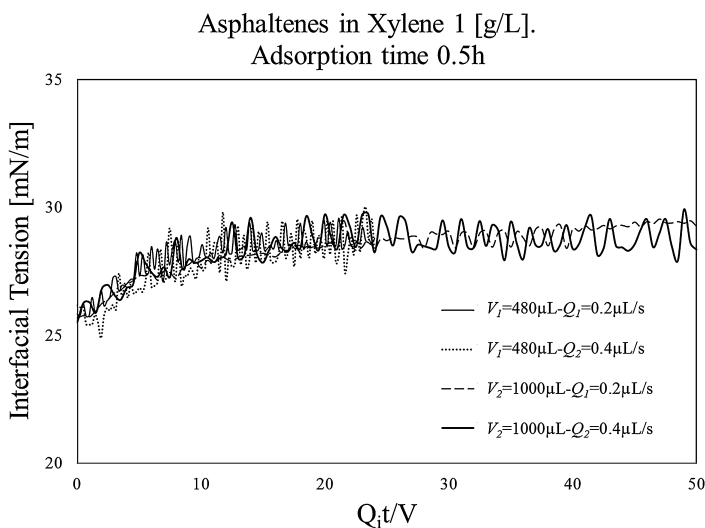


**Fig. 6.** Influence of the flow rate ( $Q_1 = 0.2 \mu\text{L/s}$ ,  $Q_2 = 0.4 \mu\text{L/s}$ ) and the total volume exchanged ( $V_1 = 480 \mu\text{L}$ ,  $V_2 = 1000 \mu\text{L}$ ) on the interfacial tension for asphaltene solutions in xylene at a fixed adsorption time (0.5 h) and initial bulk concentration (1 g/L).

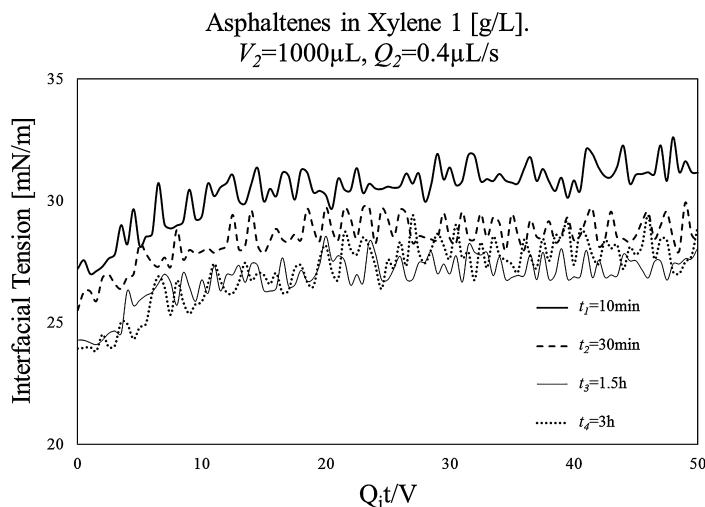


**Fig. 7.** Influence of the adsorption time ( $t_1 = 10$  min,  $t_2 = 30$  min,  $t_3 = 1.5$  h,  $t_4 = 3$  h) on the interfacial tension for asphaltene solutions in xylene at a fixed flow rate ( $Q_2 = 0.4 \mu\text{L/s}$ ), fixed total volume exchanged ( $V_2 = 1000 \mu\text{L}$ ) and fixed initial bulk concentration (1 g/L).

can be observed that asphaltene desorption is also independent of the initial adsorption time under these conditions. The percentage desorbed calculated for all adsorption times corresponds again to  $\sim 2\%$  indicating irreversibility. This suggests that the mechanically strong film is formed even at low timescales. Further reduction of the IFT could be attributed to multilayer formation, reorganization and aggregate formation at the interface [36].

The effect of bulk concentration on desorption dynamics of asphaltenes was also evaluated. Fig. 8 shows a plot of the variation in IFT during desorption of asphaltene solutions with different initial bulk concentrations ( $C_i$ ). The other experimental conditions are similar, as shown before ( $Q_2 = 0.4 \mu\text{L/s}$ ,  $V_2 = 100 \mu\text{L}$ ,  $t_3 = 1.5$  h). Once again, the total amount desorbed corresponds to  $\sim 2\%$  validating the previous results indicating that asphaltenes are irreversibly adsorbed at the oil/water interface. In this case, this is also true even for low concentrations (0.1 g/L) suggesting the fast formation of the rigid skin at the interface and packing effects [37].

While asphaltene aggregation is still a current object of study [38,39] it is clear that it influences the different mechanisms of adsorption, hence desorption. As recently pointed out by Tchoukov et al. [40], regardless of the fact that asphaltenes might not be the most interfacially active fraction of crude oil, which means that emulsion stability is not driven by the reduction in IFT solely, the complex network formed, the aromatic  $\pi$ - $\pi$  stacking, the hydrogen bonding, etc. [41], definitely affect the dynamics of adsorption and desorption. Furthermore, these interactions combined with multilayer formation create a mechanically strong film which must be thinned in order to break up W/O emulsions. The critical thickness of this film (which has a Bingham plastic nature) is thus a key parameter for emulsion stability [40]. Results from Langmuir trough experiments coupled with atomic force microscopy (AFM) images performed on asphaltenes at the toluene/water interface show similar results [42]. First, a monolayer is formed at the interface. This monolayer is strongly attached to the water phase and cannot be removed even after several wash-outs with pure solvent. Secondly, subsequent deposition of aggregates generates a multilayer 3D conformation that is anchored to the first layer [42]. Recently, Molecular Dynamics Simulations (MD) made on asphaltene model compounds (perylene-based molecules) showed the variations in nanoaggregation and structure of nanoaggregates in

bulk depending on the functionality of the end-groups [43,44]. This is attributed to the importance of the  $\pi$ - $\pi$  stacking and interactions between the solvent and the molecules.

The results presented in Figs. 5–8 indicate that the negligible amount of asphaltenes desorbed are weakly bounded to the asphaltene aggregates that are part of the 3D network, compared to the portion of asphaltenes that remain irreversibly adsorbed at the oil/water interface, possibly as a monolayer. Implications of these results point out to the necessity of a different emulsion breaking strategies that involve different types of surface active molecules (i.e. demulsifiers) which can strongly interact with the portion of asphaltenes that form the rigid skin at the interface. For example, it has been shown [45] that under some circumstances some of the so-called yellow chemicals can perform significantly better when directly injected into the Dense-packed layer instead of the crude-oil emulsion.

#### 4.2.2. Demulsifier: Brij® 93

The final section of this article is dedicated to the desorption dynamics of the model demulsifier chosen for this work, namely Brij® 93. Fig. 9 shows a plot of the interfacial tension as a function of the characteristic time during desorption for demulsifier solutions in xylene at different initial bulk concentrations ( $C_i$ ) representative of the concentrations used in chemical demulsification in the petroleum industry. The experimental conditions are similar to those reported in the previous section ( $Q_2 = 0.4 \mu\text{L/s}$ ,  $V_2 = 100 \mu\text{L}$ ,  $t_3 = 1.5$  h). Once again, the values of the IFT reported correspond to the stage of the experiment at which the subphase is being exchanged.

First, there is an increase in the IFT with time. This result was expected due to the nature of the model demulsifier. As the concentration increases from 10 ppm to 500 ppm, the decrease in the IFT becomes more relevant. As mentioned before, typical chemical demulsification strategies consider the addition of chemicals in the order of 1–1000 ppm, which is sufficient to strongly interact with the irreversibly adsorbed asphaltenes and other indigenous surfactants that might be present. Secondly, it can be observed that the IFT increase is significantly higher than the asphaltenes. Calculation of the percentage of Brij®93 desorbed after the subphase exchange yields approximately 20% (except for



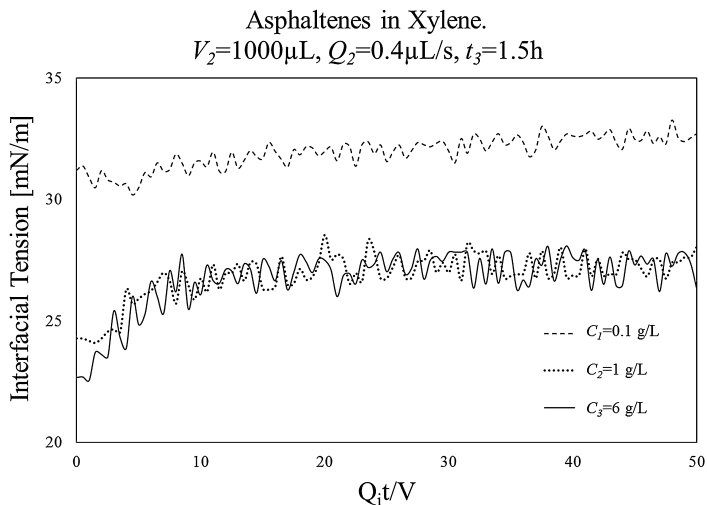


**Fig. 8.** Influence of the initial bulk concentration ( $C_1 = 0.1$  g/L,  $C_2 = 1$  g/L,  $C_3 = 6$  g/L) on the interfacial tension for asphaltene solutions in xylene at a fixed flow rate ( $Q_2 = 0.4$   $\mu\text{L/s}$ ), fixed total volume exchanged ( $V_2 = 1000$   $\mu\text{L}$ ) and fixed adsorption time ( $t_3 = 1.5$  h).

low concentrations  $-2.421 \times 10^{-3}$  m-mol/L) which also indicates that a portion of the demulsifier molecules stay at the interface.

One plausible explanation of this behavior is related to the chemistry of the demulsifier. Brij®93 is a polydisperse Ethoxylated fatty alcohol which suggests that depending on the length of the ethyl oxide (EO) chain after polymerization, the adsorption process will exhibit some differences. It is possible that the portion of the demulsifier being desorbed corresponds to the part of the molecular weight distribution with longer EO chains which are more hydrophilic than the smaller more hydrophobic counterparts. This also suggests that it is possible to have a multilayer arrangement at the interface and reorganization effects.

A second plausible explanation of this phenomenon is related to the adsorption energy. As pointed out by Bouriat et al. [46] and Anton et al. [47] a two-dimensional network of polydisperse

aggregates that behaves as a gel near its gelation point exhibits different mechanisms for adsorption. The cluster connectivity changes depending on which aggregates are being adsorbed/desorbed. This means that larger aggregates could “freeze” once adsorbed, and only the smaller aggregates are able to desorb, mainly due to the lower adsorption energy needed. This also serves as an explanation of the differences in the relaxation times. The authors also showed that this could also be true for asphaltenes, although the analysis is to be performed through dilatational rheological measurements.

Generally speaking, it is clear from the results presented in the previous sections that the chemistry, adsorption and desorption aspects of the single compounds used in this work, namely asphaltenes and a model available demulsifier, are to some extent complex. This leads to two important topics. First, a study of a mixed interface between the two compounds is necessary to give

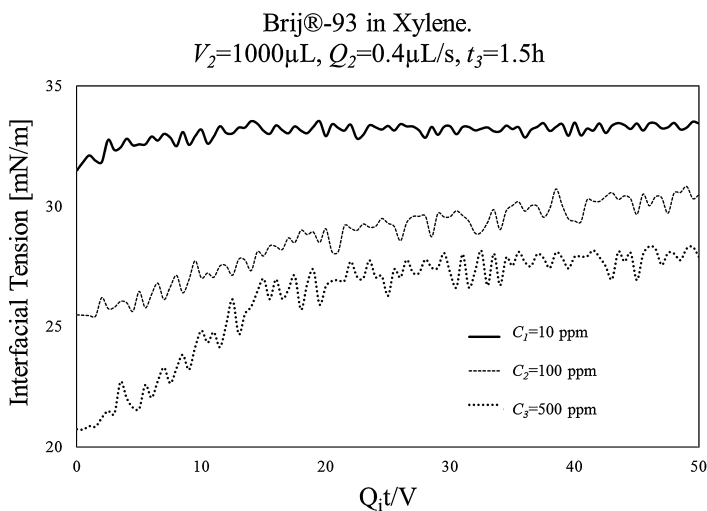


**Fig. 9.** Influence of the initial bulk concentration:  $C_1 = 10$  ppm ( $2.428 \times 10^{-2}$  m-mol/L),  $C_2 = 100$  ppm ( $2.428 \times 10^{-1}$  m-mol/L),  $C_3 = 500$  ppm (1.214 m-mol/L), on the interfacial tension for Brij®-93 solutions in xylene at a fixed flow rate ( $Q_2 = 0.4$   $\mu\text{L/s}$ ), fixed total volume exchanged ( $V_2 = 1000$   $\mu\text{L}$ ) and fixed adsorption time ( $t_3 = 1.5$  h).

a broader insight on the possible interactions among them, thus expanding the understanding of the mechanisms present in chemical demulsification. Second, IFT studies on desorption dynamics and desorption kinetics are presented as a novel methodology for the measurement of adsorption reversibility. As acknowledged by Ferri et al. [14], the broad applicability of this framework in different research fields is given by the possibility of having a vast concentration range, which could not be accomplished by normal techniques.

## 5. Conclusions

Study of static and dynamic adsorption/desorption of single components is highly relevant to the understanding of mixed interfaces as a first step. Possible interactions, reorganization effects, multilayer formation, reversibility of adsorption among other issues can be elucidated. Throughout this work, the complete characterization in terms of equilibrium and dynamic adsorption and desorption has been presented for two single compounds, namely asphaltenes and a model demulsifier Brij®-93. It was shown that the kinetics of asphaltenes is low ( $D \sim 10^{-12}$  to  $10^{-18}$  m<sup>2</sup>/s) suggesting that the process is not diffusion-controlled as expected. On the other hand, kinetics of a model demulsifier show that the process could possibly be diffusion-controlled ( $D \sim 10^{-11}$  m<sup>2</sup>/s) at short-times which is in agreement with surfactants of similar molecular weight [16]. At longer times, it was shown that the model demulsifier does not adsorb via a diffusion-controlled mechanism given the low values calculated ( $D \sim 10^{-12}$  to  $10^{-15}$  m<sup>2</sup>/s). It has also been shown that the Langmuir and Frumkin isotherm are good models to describe the adsorption process of these compounds.

A novel coaxial capillary pendant drop apparatus [14,18,20] made it possible to follow desorption dynamics of the same single compounds through interfacial tension measurements. It was shown that after the injection of pure solvent, the total change in the interfacial tension values for asphaltenes was approximately 3 mN/m which corresponds to a total desorption of ~2%. This suggests that asphaltenes are irreversibly adsorbed at the oil/water interface which has also been reported previously [40,42]. One plausible mechanism that explains this behavior proposes an asphaltene monolayer that quickly adsorbs onto the interface followed by aggregate deposition. The entire complex is responsible for the formation of the mechanically strong film. On the other hand, a surfactant that acts as a model demulsifying agent shows partly reversible adsorption onto the oil/water interface. Results show a total desorption of ~20%. Due to the polydisperse nature of the ethoxylated surfactant, it is possible that the long EO chains, which are more hydrophilic than the shorter counterpart, do not remain at the interface while desorption takes place. Another possibility arises due to the polydispersity of the adsorbed aggregates in the 2D network. Larger clusters get "stuck" to the interface due to the higher energy requirements, while the smaller aggregates are able to desorb more easily.

The results provide a new insight on the overall knowledge of coalescence and break up of emulsions through interfacial tension measurements. It has been recognized [40] that lowering the interfacial tension is not sufficient to promote flocculation and coalescence, thus the study of desorption dynamics is presented as an additional methodology to obtain valuable information vital for chemical demulsification strategies relevant for the petroleum industry.

## Acknowledgements

The authors gratefully acknowledge financial support for this work from the Research Council of Norway (NFR) and the industrial

consortium JIP-1 (Joint Industrial Project): AkzoNobel, BP, Nalco-Champion, Hamworthy, SaudiAramco, Shell, Statoil ASA, ENI, and Total.

## References

- [1] J. Sjöblom, G. Øye, W. Glomm, A. Hannisdal, M. Knag, Ø. Brandal, M. Ese, P. Hemmingsen, Modern characterization techniques for crude oils, their emulsions and functionalized surfaces, in: J. Sjöblom (ed.), *Emulsions and Emulsion Stability*, second ed., CRC Press, Boca Raton, 2006, pp. 415–476.
- [2] D. Daniel-David, A. Le Folloc, I. Pezron, et al., Destabilisation of water-in-crude oil emulsions by silicone copolymer demulsifiers, *Oil Gas Sci. Technol.* 63 (2008) 165–173.
- [3] J. Sjöblom, N. Aske, I.H. Auflem, et al., Our current understanding of water-in-crude oil emulsions. Recent characterization techniques and high pressure performance, *Adv. Colloid Interface Sci.* 100–102 (2003) 399–473.
- [4] N. Aske, H. Kallevik, J. Sjöblom, Determination of saturate, aromatic, resin, and asphaltenic (SARA) components in crude oils by means of infrared and near-infrared spectroscopy, *Energy Fuels* 15 (2001) 1304–1312.
- [5] N. Aske, H. Kallevik, J. Sjöblom, Water-in-crude oil emulsion stability studied by critical electric field measurements. Correlation to physico-chemical parameters and near-infrared spectroscopy, *J. Petrol. Sci. Eng.* 36 (2002) 1–17.
- [6] S. Simon, J. Jestin, T. Palermo, L. Barre, Relation between solution and interfacial properties of asphaltene aggregates, *Energy Fuels* 23 (2009) 306–313.
- [7] J. Jestin, S. Simon, L. Zupancic, L. Barré, A small angle neutron scattering study of the adsorbed asphaltene layer in water-in-hydrocarbon emulsions: structural description related to stability, *Langmuir* 23 (2007) 10471–10478.
- [8] S. Simon, E. Nordgård, P. Bruheim, J. Sjöblom, Determination of C80 tetracid content in calcium naphthenate deposits, *J. Chromatogr. A* 1200 (2008) 136–143.
- [9] L.Y. Zhang, Z. Xu, J.H. Masliyah, Langmuir and Langmuir-Blodgett films of mixed asphaltene and a demulsifier, *Langmuir* 19 (2003) 9730–9741.
- [10] Y. Fan, S. Simon, J. Sjöblom, Chemical destabilization of crude oil emulsions: effect of nonionic surfactants as emulsion inhibitors, *Energy Fuels* 23 (2009) 4575–4583.
- [11] C.W. Angle, Chemical demulsification of stable crude oil and bitumen emulsions in petroleum recovery—a review, in: J. Sjöblom (Ed.), *Encyclopedic Handbook of Emulsion Technology*, Marcel Dekker, New York, 2001, pp. 541–594.
- [12] J. Sjöblom, H. Söderlund, S. Lindblad, E.J. Johansen, I.M. Skjærvø, Water-in-crude oil emulsions from the Norwegian continental shelf, *Colloid Polym. Sci.* 268 (1990) 389–398.
- [13] T.F. Svitova, M.J. Wetherbee, C.J. Radke, Dynamics of surfactant sorption at the air/water interface: continuous-flow tensiometry, *J. Colloid Interface Sci.* 261 (2003) 170–179.
- [14] J.K. Ferri, N. Gorevski, C. Kotsmar, M.E. Leser, R. Miller, Desorption kinetics of surfactants at fluid interfaces by novel coaxial capillary pendant drop experiments, *Colloids Surf. A: Physicochem. Eng. Aspects* 319 (2008) 13–20.
- [15] C.T. Hsu, C.H. Chang, S.Y. Lin, Comments on the adsorption isotherm and determination of adsorption kinetics, *Langmuir* 13 (1997) 6204–6206.
- [16] J. Eastoe, J.S. Dalton, Dynamic surface tension and adsorption mechanisms of surfactants at the air-water interface, *Adv. Colloid Interface Sci.* 85 (2000) 103–144.
- [17] V.B. Fainerman, V.I. Kovalchuk, E.H. Lucassen-Reynders, et al., Surface-pressure isotherms of monolayers formed by microsize and nanosize particles, *Langmuir* 22 (2006) 1701–1705.
- [18] V.B. Fainerman, R. Miller, J.K. Ferri, H. Watzke, M.E. Leser, M. Michel, Reversibility and irreversibility of adsorption of surfactants and proteins at liquid interfaces, *Adv. Colloid Interface Sci.* 12 (2006) 3–126, 163–71.
- [19] J.K. Ferri, W.F. Dong, R. Miller, Ultrathin free-standing polyelectrolyte nanocomposites: a novel method for preparation and characterization of assembly dynamics, *J. Phys. Chem. B* 109 (2005) 14764–14768.
- [20] J.K. Ferri, R. Miller, A.V. Makievski, Equilibrium and dynamics of PEO/PPO/PEO penetration into DPPC monolayers, *Colloids Surf. A: Physicochem. Eng. Aspects* 261 (2005) 39–48.
- [21] C. Kotsmár, D.O. Grigoriev, A.V. Makievski, et al., Drop profile analysis tensiometry with drop bulk exchange to study the sequential and simultaneous adsorption of a mixed  $\beta$ -casein/C12DMPO system, *Colloid Polym. Sci.* 286 (2008) 1071–1077.
- [22] L. Buch, H. Groenzin, E. Buenostro-Gonzalez, S.I. Andersen, C. Lira-Galeana, O.C. Mullins, Molecular size of asphaltene fractions obtained from residuum hydrotreatment, *Fuel* 82 (2003) 1075–1084.
- [23] H. Groenzin, O.C. Mullins, Asphaltene molecular size and structure, *J. Phys. Chem. A* 103 (1999) 11237–11245.
- [24] C.H. Chang, E.I. Franses, Adsorption dynamics of surfactants at the air/water interface: a critical review of mathematical models, data, and mechanisms, *Colloids Surf. A: Physicochem. Eng. Aspects* 100 (1995) 1–45.
- [25] H.S. Fogler, *Elements of Chemical Reaction Engineering*, second ed., Prentice-Hall, New Jersey, 1992, pp. 708–731.
- [26] V.B. Fainerman, A.V. Makievski, R. Miller, The analysis of dynamic surface tension of sodium alkyl sulphate solutions, based on asymptotic equations of adsorption kinetic theory, *Colloids Surf. A: Physicochem. Eng. Aspects* 87 (1994) 61–75.

- [27] P. Chaverot, A. Cagna, S. Glita, F. Rondelez, Interfacial tension of bitumen–water interfaces. Part 1: Influence of endogenous surfactants at acidic pH, *Energy Fuels* 22 (2008) 790–798.
- [28] M. Fossen, H. Kallevik, K.D. Knudsen, J. Sjöblom, Asphaltenes precipitated by a two-step precipitation procedure. 1. Interfacial tension and solvent properties, *Energy Fuels* 21 (2007) 1030–1037.
- [29] M. Jeribi, B. Almir-Assad, D. Langevin, I. Hénaut, J.F. Argillier, Adsorption kinetics of asphaltenes at liquid interfaces, *J. Colloid Interface Sci.* 256 (2002) 268–272.
- [30] J.P. Rane, D. Harbottle, V. Pauchard, A. Couzis, S. Banerjee, Adsorption kinetics of asphaltenes at the oil–water interface and nanoaggregation in the bulk, *Langmuir* 28 (2012) 9986–9995.
- [31] V. Pauchard, J.P. Rane, S. Zarkar, A. Couzis, S. Banerjee, Long-term adsorption kinetics of asphaltenes at the oil–water interface: a random sequential adsorption perspective, *Langmuir* (2014).
- [32] M.G. Muñoz, F. Monroy, F. Ortega, R.G. Rubio, D. Langevin, Monolayers of symmetric triblock copolymers at the air–water interface. 1. Equilibrium properties, *Langmuir* 16 (2000) 1083–1093.
- [33] M.G. Muñoz, F. Monroy, F. Ortega, R.G. Rubio, D. Langevin, Monolayers of symmetric triblock copolymers at the air–water interface 2. Adsorption kinetics, *Langmuir* 16 (2000) 1094–1101.
- [34] J. Diuje, X. Yang, I.J. Fjellanger, J. Sjöblom, E. Pelizzetti, Chemical destabilization of crude oil based emulsions and asphaltene stabilized emulsions, *Colloid Polym. Sci.* 279 (2001) 232–239.
- [35] M.H. Ese, L. Galet, D. Clause, J. Sjöblom, Properties of langmuir surface and interfacial films built up by asphaltenes and resins: influence of chemical demulsifiers, *J. Colloid Interface Sci.* 220 (1999) 293–301.
- [36] E.L. Nordgård, E. Landsem, J. Sjöblom, Langmuir films of asphaltene model compounds and their fluorescent properties, *Langmuir* 24 (2008) 8742–8751.
- [37] Y. Fan, S. Simon, J. Sjöblom, Influence of nonionic surfactants on the surface and interfacial film properties of asphaltenes investigated by Langmuir balance and Brewster angle microscopy, *Langmuir* 26 (2010) 10497–10505.
- [38] M. Agrawala, H.W. Yarranton, An asphaltene association model analogous to linear polymerization, *Ind. Eng. Chem. Res.* 40 (2001) 4664–4672.
- [39] S. Wang, J. Liu, L. Zhang, J. Masliyah, Z. Xu, Interaction forces between asphaltene surfaces in organic solvents, *Langmuir* 26 (2010) 183–190.
- [40] P. Tchoukov, F. Yang, Z. Xu, T. Dabros, J. Czarnecki, J. Sjöblom, Role of asphaltenes in stabilizing thin liquid emulsion films, *Langmuir* 30 (2014) 3024–3033.
- [41] M.R. Gray, R.R. Tykewinski, J.M. Stryker, X. Tan, Supramolecular assembly model for aggregation of petroleum asphaltenes, *Energy Fuels* 25 (2011) 3125–3134.
- [42] L.Y. Zhang, P. Breen, Z. Xu, J.H. Masliyah, Asphaltene films at a toluene/water interface, *Energy Fuels* 21 (2007) 274–285.
- [43] R.B. Teklebrhan, L. Ge, S. Bhattacharjee, Z. Xu, J. Sjöblom, Probing structure–nanoaggregation relations of polyaromatic surfactants: a molecular dynamics simulation and dynamic light scattering study, *J. Phys. Chem. B* 116 (2012) 5907–5918.
- [44] R.B. Teklebrhan, L. Ge, S. Bhattacharjee, Z. Xu, J. Sjöblom, Initial partition and aggregation of uncharged polyaromatic molecules at the oil–water interface: a molecular dynamics simulation study, *J. Phys. Chem. B* 118 (2014) 1040–1051.
- [45] A. Barrabino, S. Keleşoğlu, G. Sørland, S. Simon, J. Sjöblom, Enhanced Sedimentation and Coalescence by New Generation of Yellow Chemicals of Petroleum Crude Oil Emulsions, (in preparation), 2014.
- [46] P. Bouriat, N. El Kerri, A. Graciaa, J. Lachaise, Properties of a two-dimensional asphaltene network at the water–cyclohexane interface deduced from dynamic tensiometry, *Langmuir* 20 (2004) 7459–7464.
- [47] N. Anton, T.F. Vandamme, P. Bouriat, Dilatational rheology of a gel point network formed by nonionic soluble surfactants at the oil–water interface, *Soft Matter* 9 (2013) 1310–1318.
- [48] A. Hannisdal, P.V. Hemmingsen, J. Sjöblom, Group-type analysis of heavy crude oils using vibrational spectroscopy in combination with multivariate analysis, *Ind. Eng. Chem. Res.* 44 (2005) 1349–1357.

*Mixed Interfaces of Asphaltenes and Model Demulsifiers, Part II: Study of Desorption Mechanisms at Liquid/Liquid Interfaces.*



# Mixed Interfaces of Asphaltenes and Model Demulsifiers, Part II: Study of Desorption Mechanisms at Liquid/Liquid Interfaces

Diego Pradilla,\* Sébastien Simon, and Johan Sjöblom

Ugelstad Laboratory, Department of Chemical Engineering, Norwegian University of Science and Technology (NTNU), NO-7491 Trondheim, Norway

## Supporting Information

**ABSTRACT:** This article is the continuation of a preceding paper (Part I) in which the adsorption and desorption of asphaltenes from the oil/water interface by pure solvent and model demulsifiers was studied. In this second part, the composition of mixed interfaces of asphaltenes and two demulsifiers (Brij-93 and Pluronic PE8100) was studied. Desorption of asphaltenes by demulsifiers, and vice versa, was determined. First, the composition of a mixed interface (asphaltenes and demulsifiers) through the use of the Langmuir equation of state (EoS) was determined. Second, an experimental setup that mimics, to some extent, the chemical demulsification of water-in-crude oil emulsions during the production stages was used. Desorption of already-adsorbed asphaltenes at the liquid/liquid interface by the action of two demulsifiers was assessed. It was found that desorption is always initiated by interactions between demulsifiers and asphaltenes. It is followed by the plausible formation of complex-like structures to finally end in the replacement, by displacement from the interface, of asphaltenes by demulsifiers. Third, the assessment of Brij-93 and PE8100 desorption from the oil/water interface by the action of asphaltenes was also carried out. It was found that asphaltenes can desorb PE8100 at low surface coverage.

## 1. INTRODUCTION

The formation of stable water-in-oil (W/O) emulsions during petroleum extraction is undoubtedly unavoidable.<sup>1,2</sup> Transport, refining, and production costs are deeply affected by the formation of such systems.<sup>3</sup> The action of indigenous surfactants such as asphaltenes, resins, and naphthenates hinder coalescence by forming a mechanically strong film, by retarding film drainage or by producing steric repulsion.<sup>4,5</sup> However, the main mechanisms of emulsion stabilization are attributed mainly to asphaltenes, because of their ability to form a gel-like continuum at the oil/water interface.<sup>6</sup> Asphaltenes are typically defined as the solubility class of crude oil that is insoluble in *n*-alkanes (*n*-pentane, *n*-hexane) but soluble in aromatic compounds (xylene, toluene).<sup>7,8</sup> Because of this very broad definition, asphaltenes can exhibit different properties, functionalities, and molecular weights that are dependent primarily on the type of crude oil.<sup>9,10</sup> However, many bulk properties and interfacial behavior have been shown to have a certain degree of uniformity.<sup>11</sup>

Chemical demulsification refers to the process of breaking up emulsions to separate the water from the crude oil using a class of surface active agents, known as demulsifiers that promote coalescence and film drainage.<sup>12</sup> It has been recognized as the most efficient method for water separation.<sup>13</sup> Because of their high surface active nature, these chemicals are typically added in a concentration range of 1–1000 ppm.<sup>14</sup> Once the demulsifiers have been incorporated into the naturally formed crude oil emulsion, they quickly go to the oil/water interface and affect the stability of water droplets. Different mechanisms for emulsion stability can be stated: for instance, demulsifiers can change the elasticity or the interfacial viscosity of the surrounding skin resulting in a displacement/replacement of the indigenous surfactants (i.e., asphaltene network).<sup>15,16</sup> The

formation of asphaltene–demulsifier complexes, because of chemical similarities and suppression of interfacial tension gradients (Marangoni effects), are also plausible phenomena.<sup>17</sup>

A widely recognized, accepted, and versatile method for measuring the dynamic interfacial tension (IFT) of various interfaces is commonly known as axisymmetric drop shape analysis (ADSA).<sup>18–20</sup> In this technique, a liquid droplet or an air bubble is formed at the end of a capillary. Then, a CCD camera continuously records the shape generating a set of images that are later analyzed to resolve the Young–Laplace equation yielding the best fit for the IFT. This method allows the accurate study of sorption kinetics (i.e., adsorption and desorption) of surface active agents at the liquid/liquid or liquid/air interface. The main advantages are first, the possibility of obtaining IFT data at very short times. Second, the constant feedback between the software and the CCD camera allows the accurate control of the volume of the droplet/bubble, hence making it possible to perform interfacial rheology measurements. Third, it is possible to follow the IFT while surface active species are being adsorbed/desorbed maintaining the drop/bubble volume constant.<sup>21–23</sup>

A novel coaxial capillary apparatus developed by Ferri et al.<sup>22</sup> allows monitoring the interfacial tension as a function of time while surfactants are being desorbed from the liquid/liquid interface. Furthermore, with this device, it is also possible to study convection-enhanced sorption kinetics. For example, adsorbed species at equilibrium are driven away from it by injecting a surfactant-free solution (i.e., pure solvent). Hence, changes in the IFT can be related to factors such as irreversible

Received: March 2, 2015

Revised: August 7, 2015

Published: August 13, 2015

adsorption, reorganization, complex formation, and unfolding (proteins) phenomena.<sup>24–27</sup> Such device was successfully validated and used to follow the desorption of a nonionic surfactant (Triton X-100) and a series of *n*-alkyl dimethyl phosphine oxide surfactants by Ferri et al.<sup>18</sup> Similarly, Kotsmar et al.<sup>23</sup> followed the desorption kinetics of a surfactant–protein complex ( $C_{12}$ -dimethyl phosphine oxide and  $\beta$ -casein) concluding that displacement by the formation of complex-like structures was the main cause of desorption.

Interfacial dilatational rheology is of high significance in colloidal systems, because of the possibility of studying changes in the interfacial tension as a consequence of surface relaxation processes or diffusion.<sup>28,29</sup> On the other hand, other studies<sup>30,31</sup> showed that there is no reorganization or cross-linking at the interface and that asphaltenes are adsorbed as monomers instead of nanoaggregates. This was concluded after fitting adsorption data to an equation of state (Langmuir EoS) which yielded an adsorbed amount that would only be possible if a flat-on adsorption of asphaltene monomers occurred. Moreover, it was shown that interfacial tension is only dependent on surface coverage. Interfacial dilatational rheology has also been used to link interfacial activity and the mechanical behavior of different colloidal systems such as emulsions.<sup>32–34</sup> This is subsequently linked to the mechanisms of emulsion stability, and, hence, to the demulsifier performance.<sup>5</sup> The determination of dilatational elastic and viscous moduli presents an effective way for comparing the changes in the elasticity of the surrounding film in an asphaltene-covered water droplet once desorption has occurred.<sup>35,36</sup>

In the first part of this work,<sup>27</sup> the competitive adsorption and desorption of asphaltenes and a model molecular demulsifier (Brij-93) was studied at the liquid/liquid interface. Through the use of the coaxial capillary apparatus, it was observed that asphaltenes are almost irreversibly adsorbed at the oil/water interface after subphase exchange experiments with pure solvent (the changes in the measured IFT were  $\sim 2$  mN/m). This is a known phenomenon that has been previously reported in the literature.<sup>37–40</sup> Desorption was found to be independent of both the flow rate and the total amount of solvent exchanged (for volumes more than 50 times greater than the volume of the droplet) yielding  $\sim 2\%$  of asphaltenes desorbed under the conditions studied. Similarly, it was found that the model molecular demulsifier is partly desorbed ( $\sim 20\%$ ) from the oil/water interface. It is important to note that these values were obtained assuming that the Langmuir EoS linking the adsorbed amount with the interfacial tension are still valid after desorption. A similar approach on a partly irreversible system was used by Svitova et al.<sup>21</sup> to establish the degree of desorption. However, it must be mentioned that if asphaltenes adsorb as multilayers, the asphaltene monomer and/or part of the aggregate that is not in direct contact with the liquid–liquid interface or boundary and therefore adsorbed as second, third or *n*th layer, would have little to no influence on the interfacial tension values; hence, their adsorption would not be detected.<sup>40,41</sup>

The main goal of this article is to study, through interfacial tension measurements and dilatational interfacial rheology, desorption of asphaltenes and demulsifiers from the liquid/liquid interface. Desorption of species from the oil/water interface is convection-induced through the use of a coaxial capillary system based on ADSA. The experimental setup in which the  $C_6$ -asphaltenes (*n*-hexane precipitated) are allowed to adsorb first followed by injection of the demulsifier (Brij-93

or Pluronic PE8100) mimics, to some extent, the operational conditions in which chemical demulsification is employed in some stages of crude oil production in which the crude oil emulsions are already formed. At these stages, the added demulsifiers must adsorb at the interface, which is already populated with indigenous crude oil components such as asphaltenes, and displace them to break the film and promote coalescence. Finally, desorption of model demulsifiers by asphaltenes is investigated to establish their desorbing capabilities.

## 2. MATERIALS AND METHODS

**2.1. Asphaltenes.**  $C_6$ -asphaltenes were extracted with *n*-hexane from a solvent/chemical-free heavy crude oil of the Norwegian continental shelf. The extraction proceeded as follows: first, the crude oil was heated to 60 °C for 24 h. After this, the oil was shaken several times before use, to ensure homogeneity of the samples. The crude oil then was diluted in *n*-hexane at a 1:40 weight/volume ratio. Finally, the mixture was stirred for 24 h and the asphaltene fraction was recovered using a 0.45  $\mu\text{m}$  HVLP (Millipore) membrane filter washing with excess *n*-hexane. Finally, the recovered asphaltenes were put into a nitrogen atmosphere degasser and dried for 48 h. This time was enough to ensure that the solvent was fully evaporated; therefore, the weight of the samples did not change. Buch et al.<sup>42</sup> and Groenzin et al.<sup>9,10</sup> established an average molecular weight range for  $C_5$ -asphaltenes (*n*-pentane precipitated) of 500–1000 g/mol. Because of the high degree of polydispersity in this solubility class,<sup>43–45</sup> an average value of 750 g/mol was used for this study, given that the behavior and the molecular weight of  $C_6$ -asphaltenes is not expected to deviate significantly from that of  $C_5$ -asphaltenes.<sup>32</sup> Basic analysis of the crude oil used in this study and the elemental composition of the extracted asphaltenes is given in the first part of this study.<sup>27</sup>

**2.2. Model Demulsifiers.** Two demulsifiers were used in this study. The first one is a low-molecular-weight polyethylene glycol ether, commercially known as Brij 93 provided by Sigma–Aldrich,  $M_w \approx 357$  g/mol (HLB 4). The second one is a high-molecular-weight polyoxyethylene–polyoxypropylene–polyoxyethylene (PEO–PPO–PEO) block copolymer, commercially available as Pluronic PE8100 provided by BASF,  $M_w \approx 2750$  g/mol (HLB 2). Both demulsifiers were used as received. Bottle tests were performed to ensure that the chemicals are able to separate asphaltene-stabilized emulsions.

**2.3. Water Phase.** The water phase was a buffer solution of pH 7 prepared with ultrapure water (resistivity of 18.2  $\text{M}\Omega\text{ cm}$ ) and 0.1 M  $\text{KH}_2\text{PO}_4$  adjusted with 0.1 M NaOH solutions.

**2.4. Solvents.** Asphaltene and demulsifier solutions were prepared using xylene AnalaR NORMAPUR, provided by VWR–Norway. The *n*-hexane used for precipitation was HiPerSolv CHROMANORM for HPLC quality, which was also provided by VWR–Norway. Both solvents were used as received.

**2.5. Interfacial Tension Measurements.** A commercially available pendant drop tensiometer (PAT 1m, SINTERFACE Technologies, Berlin, Germany) was used for all the experiments. It determines the surface/interfacial tension of a surfactant-covered liquid droplet (or air bubble) by recording the silhouette onto a CCD camera. The digital images are then analyzed and fitted to the Young–Laplace equation with an accuracy of  $\pm 0.1$  mN/m. This equation relates the curvature of a liquid drop and the surface/interfacial tension. The built-in software produces a family of theoretical curves by changing the values of the surface/interfacial tension. The curve that yields the best fit to the experimental points represents the measured surface/interfacial tension. For this procedure, only the densities of the oil and aqueous phase are needed. A custom-made accessory for the apparatus consisting of two concentric capillary tubes (an inner capillary and an outer capillary) was used for the desorption experiments. Specific details of the technique are described elsewhere;<sup>18,22,27</sup> however, a simple schematic is presented in Figure A1 of the Supporting Information.

### 3. THEORETICAL CONSIDERATIONS

**3.1. Adsorption: Equilibrium Aspects.** The well-known Gibbs equation provides a model based on thermodynamic aspects of surfactant adsorption. It relates the composition at the given interface to the change in interfacial/surface tension caused by changes in bulk concentration. The interfacial tension can be measured through different techniques. The equation is<sup>46</sup>

$$\Gamma = -\frac{1}{nRT} \frac{d\gamma}{d \ln(c)} \quad (1)$$

Here,  $\Gamma$  is the equilibrium surface excess,  $n$  is a constant that is equal to 1 for nonionic surfactants,  $R$  is the universal gas constant,  $T$  the temperature at which the experiments are carried out,  $\gamma$  the surface/interfacial tension, and  $c$  the bulk concentration.

Another adsorption isotherm used is that of Langmuir eq 2.<sup>46,47</sup> It is a nonlinear equation that can be used to relate the concentration in the bulk to the composition of an interface with adsorbed species. It is also useful to assess the surface activity of a chemical compound, provided that two main assumptions are met: first, the adsorption sites are energetically equivalent; second, there are no interactions between adsorbed molecules. Even though the assumptions are not usually entirely valid, the use of this isotherm provides an adequate notion of the behavior of surfactants. In the following equation,  $\Gamma_\infty$  is the surface excess at the saturation point and  $K_L$  is known as the adsorption equilibrium constant.

$$\Gamma = \Gamma_\infty \left( \frac{K_L c}{1 + K_L c} \right) \quad (2)$$

The analogous explicit equation of state used along eq 2 to solve for the two equilibrium parameters is known as the Szyzkowski equation, as reported by Chang and Franses:<sup>47</sup>

$$\pi = nRT\Gamma_\infty \ln(1 + K_L c) \quad (3)$$

Here,  $\pi$  is the difference in interfacial/surface tension between a freshly formed interface/surface and the value at a given concentration of surface active species.

Based on the Langmuir adsorption isotherm, Chang and Franses<sup>47</sup> presented a set of equations that involved binary surfactant mixtures. Equations 4–6 carry the same assumptions of the Langmuir isotherm itself. However, once again, this simple description is sufficient to assess the behavior of a mixed interface and detect possible signs of interactions.

$$\Gamma_A = \Gamma_m \frac{K_{L,A} c_A}{1 + K_{L,A} c_A + K_{L,B} c_B} \quad (4)$$

$$\Gamma_B = \Gamma_m \frac{K_{L,B} c_B}{1 + K_{L,A} c_A + K_{L,B} c_B} \quad (5)$$

$$\pi = -RT\Gamma_m \ln \left( 1 - \frac{\Gamma_A}{\Gamma_m} - \frac{\Gamma_B}{\Gamma_m} \right) \quad (6)$$

In eqs 4–6,  $\Gamma_A$  and  $\Gamma_B$  are the surface excess concentrations of the two surfactants and  $\Gamma_m$  the surface excess of the mixture. With these equations, it is possible to solve the system with three equilibrium parameters, namely, the individual surface excess  $\Gamma_i$  and the two adsorption constants  $K_{L,i}$ .

**3.2. Interfacial Dilatational Rheology.** Besides being a method to accurately obtain IFT measurements, ADSA has also been recognized as a reliable tool for measuring interfacial rheology.<sup>28,48</sup> When harmonic oscillations compress and expand the interfacial layer, relaxation processes start to take place; hence, the interfacial tension starts to vary accordingly. Depending on the oscillation frequency applied ( $\omega$ ), the droplet's area ( $A$ ) will change from an initial value,  $A_0$ , to an amplitude value,  $A_a$ , according to<sup>49,50</sup>

$$\Delta A = A - A_0 = A_a \sin(\omega t) \quad (7)$$

Hence, the complex dynamic dilatational modulus can be defined as the change in the interfacial tension, relative to the change in interfacial area:

$$E^*(\omega) = E'(\omega) + E''(\omega) = \frac{d\gamma^*(t)}{d \ln A^*(t)} \quad (8)$$

In eq 8, the real part characterizes the elastic properties of the interfacial layer and the imaginary part characterizes the viscous properties. The parts are referred to as the elastic dilatational modulus ( $E'$ ) and the viscous dilatational modulus ( $E''$ ).

### 4. RESULTS AND DISCUSSION

In this section, aspects concerning sorption of asphaltenes and model demulsifiers at the oil/water interface are presented. Competitive adsorption aspects of this system are presented first. The second and third parts involve the desorption of surfactants from the liquid/liquid interface followed by a coaxial capillary system based on ASDA. Desorption of asphaltenes by two model demulsifiers is first presented and, then, desorption of the model demulsifiers by asphaltenes. With this framework, it is possible to elucidate new aspects of asphaltene desorption and the performance of typical demulsifiers used in the petroleum industry.

**4.1. Adsorption of Single Compounds.** The interfacial tension at equilibrium as a function of the bulk concentration for C<sub>6</sub>-asphaltenes, the model molecular demulsifier Brij-93 and the model polymeric demulsifier PE8100 solutions in xylene is presented in Figure 1. The IFT was measured via ADSA and

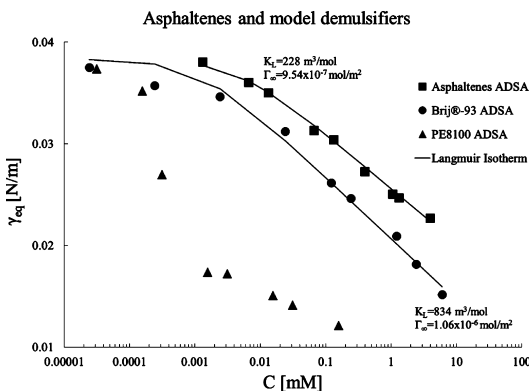


**Figure 1.** Equilibrium interfacial tension ( $\gamma_{eq}$ ) as a function of the bulk concentration for three components in xylene: asphaltenes, Brij-93, and Pluronic PE8100. Experimental points measured using ADSA. Solid lines represent the best fits to eqs 2 and 3. Equilibrium parameters are also shown.



the system was allowed to equilibrate for 8 h in the case of asphaltenes, and 3 h in the case of the model demulsifiers. At this point, the changes in IFT were  $<0.5$  mN/m. The solid lines represent the fit to the Langmuir EoS (eq 2). It is noteworthy to mention that some of the assumptions of these equations do not apply to the studied system, especially since the asphaltene–demulsifier system shows almost irreversible behavior.<sup>27,37,38</sup> However, it has been previously shown<sup>51</sup> that the Langmuir equation is valid even for complex systems such as polymers. It can be seen that the Langmuir isotherm correctly describes the adsorption IFT data for asphaltenes and the model molecular demulsifier Brij-93 (equilibrium parameters are also shown). However, this is not the case for the model polymeric demulsifier PE8100. There is a sharp decrease of the interfacial tension in a narrow concentration range, showing the high surface active nature of the polymeric surfactant. Surface pressure<sup>52,53</sup> and interfacial tension measurements<sup>54,55</sup> on different diblock and triblock PEO–PPO(–PEO) copolymers have reported a similar behavior, which is evidently not Langmuir-type. This has been attributed to the fast initial adsorption, followed by reorganization and relaxation processes at long times, as well as multiple phase transitions and multilayer accommodation at the interface. Models and equations of state that describe this behavior can be found elsewhere.<sup>56,57</sup>

Based on the work of Pauchard et al.<sup>20,31</sup> and that of Rane et al.,<sup>19,30</sup> one could argue that this is not the case. In their studies with the pendant drop technique and the Langmuir isotherm (EoS or eqs 2 and 3), the authors conclude that there is no reorganization of asphaltenes at the oil/water interface. Furthermore, they conclude that no relaxation occurs at the interface, mainly because asphaltenes adsorb as monomers, following a two-dimensional (2D) random close packing of polydisperse disk-type adsorption (or flat-on adsorption). Care should be taken when using the Langmuir isotherm, mainly because of the assumptions behind it. For example, the Langmuir isotherm is valid for systems that are reversibly adsorbed and asphaltene adsorption is not reversible. Therefore, the arguments related to long-time relaxation and changes in conformations at the interface stated before seem more plausible. In addition, the Langmuir isotherm only allows adsorption of a monolayer and rules out the possibility of multilayer formation, which is also not the case in asphaltene adsorption. Based on the same reasoning, the Langmuir isotherm is not valid when fitting desorption data of irreversibly adsorbed species. In summary, what can be stated from Figure 1 is that the surface activity of the chemical species can be ranked as follows: Pluronic PE8100 > Brij-93 > C<sub>6</sub>-asphaltenes.

**4.2. Competitive Adsorption.** In this section, a small set of experiments are presented to show the behavior of the interfacial tension when both surface active species (asphaltene and demulsifier) are present at the same time, thus emulating competitive adsorption, to some extent. Figure 2 shows a plot of the equilibrium interfacial tension as a function of demulsifier (Brij-93) concentration for asphaltene solutions in xylene at 0.04 g/L. The solid line represents the prediction of the IFT by the mixture model (eqs 4–6), and the dotted lines are the dimensionless composition at the interface ( $\Gamma_i/\Gamma_m$ ). Figures A2-1 and A2-2 of the Supporting Information show similar plots for higher concentrations of asphaltenes. From Figure 2, it can be seen that the competitive adsorption model based on the Langmuir EoS, correctly predicts the behavior of the interfacial tension for the mixtures in a broad concentration

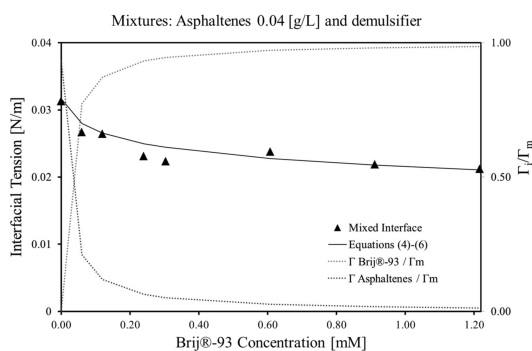


**Figure 2.** Equilibrium interfacial tension for a mixed interface between asphaltenes at 0.04 g/L and Brij-93. The solid line is the prediction of eqs 4–6, and the dotted lines the dimensionless composition at the interface.

range for both components. This is partly due to the similar values of  $\Gamma_{i,A}$  which comply with the main assumption of the model:  $\Gamma_{i,A} = \Gamma_{i,B} = \Gamma_m$ . Despite the fact that this model does not allow to infer about how the surface active materials are adsorbed (i.e., segregation or complete mixing), it is possible to conclude that the interface, at equilibrium, is dominated by the model demulsifier Brij-93, even at low concentration (0.1 mM or 0.04 g/L of Brij-93, compared to 0.04 g/L of asphaltenes). This is consistent with the higher surface activity of Brij-93. This model has also been previously used on a system of proteins, which are known to unfold and exhibit relaxation after adsorption.<sup>58</sup>

Even though the formation of a mechanically strong asphaltene film has been postulated as the main mechanism for water-in-crude oil emulsion stability,<sup>7,13,15,59,60</sup> in this case, such a formation would be difficult. If both surface active compounds (i.e., asphaltene and demulsifiers) are present in the oil phase at the moment of the formation of a fresh interface, the one that has a higher surface activity will adsorb first, ending up with an unrealistic situation. This is the main reason why desorption experiments that mimic chemical demulsification strategies are of significant importance. These experiments will yield information about how different molecules interact with the already-formed asphaltene network to disrupt the film.

**4.3. Desorption of Asphaltene from the Oil/Water Interface.** This section covers the study of desorption of C<sub>6</sub>-asphaltene from the liquid/liquid interface by means of two model demulsifiers. The word “model” is used here only to emphasize that the chemical structure of the substance is known. This is not the case for commercial demulsifiers in which blends are normally used. Brij-93 is a low-molecular-weight amphiphilic molecule, whereas PE8100 is a high-molecular-weight polymeric demulsifier that resembles those used in the petroleum industry.<sup>5,13</sup> Both are oil-soluble (low HLB). A set of desorption experiments were performed using the double coaxial capillary accessory previously described. Details on how the interfacial tension is followed, as a function of time, and the subsequent volume exchange are described in the first part of this work.<sup>27</sup> Essentially, with this accessory to the ADSA device, an oil droplet (i.e., asphaltene/xylene droplet) is formed at the tip of an outer capillary with a pump. The droplet is allowed to equilibrate for a fixed period of

time ( $t_0 = 30$  min) inside a cuvette (25 mL) that contains the aqueous solution (pH 7 buffer). The choice of this particular value of the equilibration time is due to several reasons. It has been shown<sup>37,61</sup> that asphaltenes do not reach a true equilibrium even after  $\sim 10$  h, because of rearrangements in the interfacial asphaltene layer. Consequently, and strictly speaking, measurements at equilibrium would not be possible. In addition, it was shown in the first part of this article<sup>27</sup> that asphaltene adsorption is, for the most part, almost irreversible after 30 min and the degree of desorption (based on the final values of the IFT) is constant, even after 1.5 h.

After the fixed equilibration time, the convection-driven subphase exchange inside the well-mixed droplet begins. Demulsifier solution is injected through an inner capillary using a second pump at a given volumetric flow rate ( $Q = 0.4 \mu\text{L/s}$ ). During this stage, the droplet volume is kept constant at  $20 \mu\text{L}$  through simultaneous withdrawal from the outer capillary using the first pump. Once the total predetermined volume ( $V = 1000 \mu\text{L}$ ) has been exchanged, pumping/withdrawal stops and the IFT reaches a plateau value. This process takes exactly 2500 s:

$$\frac{V}{Q} = \frac{1000 \mu\text{L}}{0.4 \mu\text{L/s}} = 2500 \text{ s}$$

It is important to note that the interfacial tension is continuously measured during all stages of the experiments and that experiments were performed at  $22^\circ\text{C}$  by duplicate. All the plots of the upcoming sections correspond to the average of the duplicates and only the IFT-time lapse that corresponds to the desorption stage is shown (2500 s). That is, from  $t_0$  until the time at which  $V$  has been exchanged. The dimensionless term  $Qt/V$  is used in these plots as a characteristic time, because, as noted by Ferri et al.,<sup>18,22</sup> it gives a correct description of how the well-mixed droplet is influenced by the convection-enhanced subphase exchange. Figure A1 of the Supporting Information shows a schematic of this process; more details of the coaxial system can be found in the first part of this study.<sup>27</sup>

Finally, to avoid handling large amounts of experimental points, this part of the data was smoothened with SigmaPlot Version 12.0 (Systat Software, Inc.) using a running average method over a period of 2 s ensuring that no vital information was lost. This means that the resulting curves presented are a true representation of the experimental points.

**4.3.1. Desorption Driven by Brij-93.** Figures 3 and 4 show plots of the interfacial tension as a function of the dimensionless characteristic time ( $Qt/V$ ) for desorption of asphaltenes by Brij-93 (solutions in xylene). The concentration range goes from 10 ppm to 100 ppm for Brij-93 and asphaltenes concentration remains at 1 g/L. In these plots, there are three curves, corresponding to a reference experiment (light gray line), a blank experiment (black solid line), and the exchange experiment (dashed line). The labels of the curves are to be interpreted as follows: the first species in the name is the one that was allowed to adsorb for 30 min at the given concentration. The second species, present after the plus sign (+), corresponds to the compound that was injected (exchanged) via the secondary pump at the given concentration. Plots of intermediate and higher concentrations are shown in the Supporting Information (Figures A3–A6).

In Figure 3, which corresponds to low concentration of demulsifier (10 ppm), it can be seen that, for the blank experiments, Brij-93 adsorbs relatively slowly to the interface as

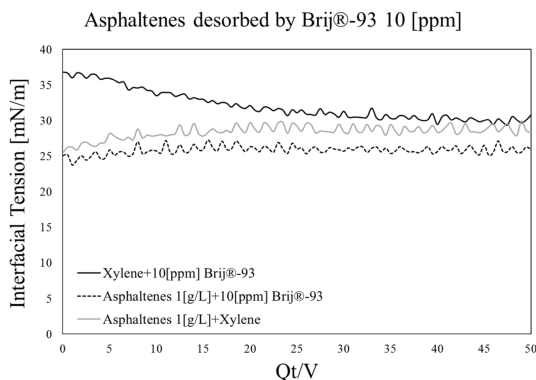


**Figure 3.** Interfacial tension as a function of the dimensionless characteristic time for desorption ( $Qt/V$ ) of asphaltenes at 1 g/L by Brij-93 (solutions in xylene) at 10 ppm. The experimental conditions for the experiments were as follows: exchange flow rate,  $Q = 0.4 \mu\text{L/s}$ ; total predetermined volume,  $V = 1000 \mu\text{L}$ .

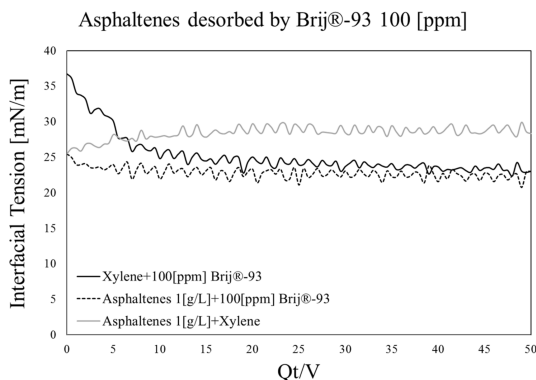


**Figure 4.** Interfacial tension as a function of the dimensionless characteristic time for desorption ( $Qt/V$ ) of asphaltenes at 1 g/L by Brij-93 (solutions in xylene) at 100 ppm. The experimental conditions for the experiments were as follows: exchange flow rate,  $Q = 0.4 \mu\text{L/s}$ ; total predetermined volume,  $V = 1000 \mu\text{L}$ .

the exchange progresses until the equilibrium value is reached ( $\gamma \approx 31 \text{ mN/m}$ ). This part is in agreement to the equilibrium single-compound adsorption (Section 4.1).

Second, the desorption of asphaltenes by xylene (light gray line), as reported in a previous work,<sup>27</sup> is very low. The IFT increases from  $\sim 25$  to  $\sim 27 \text{ mN/m}$ , which strongly suggests the almost irreversible nature of adsorption of asphaltenes, which is consistent with the literature.

Third, when asphaltenes at a fixed concentration start to be desorbed (dashed line), it is possible to see that the interfacial tension has a tendency to plateau. The final value, once the pumping/withdrawal stops ( $Qt/V = 50$ ), is  $\sim 27 \text{ mN/m}$ . The value is lower than the reference experiment ( $\sim 30 \text{ mN/m}$ ) and the single-compound adsorption of Brij-93 ( $\sim 31 \text{ mN/m}$ ). This suggests the presence of a mixed interface and a certain degree of interaction between the model molecular demulsifier and the asphaltene network. This also suggests that this particular demulsifier at this concentration is not enough to displace/replace the asphaltenes from the liquid/liquid interface;

therefore, a low degree of coalescence would be expected in real systems (i.e., crude oil emulsions).

At this point, it is important to mention that the increase of the IFT after desorption of all experiments must be treated cautiously, because of the physical limits between the Gibbs surface and the multilayers formed. As mentioned previously, the reported values on IFT during desorption correspond to the desorption of the first adsorbed layer, that is, to the species directly adsorbed onto the interface. The subsequent layers, if present, will most likely not influence the IFT in the same way, thus their desorption might not cause a change in the measured IFT. However, when discussing interfacial dilatational rheology, multilayer formation seems to be largely responsible for film stability and elasticity.

As the concentration of demulsifier increases (Figure 4), interactions between adsorbed asphaltenes and Brij-93 molecules are clearly visible at short desorption times. This is because the interfacial tension of the asphaltenes–Brij-93 system is lower than the asphaltenes–xylene and xylene–Brij-93 systems. The behavior just described could be attributed to the formation of complexes that are more surface active than the compounds alone. These complex-like structures could be the result of interactions between the alkyl chains that stick out of the asphaltene nanoaggregates (in agreement with the Yen–Mullins model<sup>62,63</sup>) and clusters with the active spots of the demulsifier molecule. Interactions between functional groups from both species could also enhance this behavior. At longer times, the interfacial tension value corresponding to adsorption of Brij-93 as a single compound reaches a similar value to that of the asphaltenes–Brij-93 system. This indicates that the interface is entirely composed of Brij-93 and all the asphaltenes have been removed. It is important to mention that reaching similar values of IFT could be purely coincidental and other conclusions could be drawn. For instance, as previously shown by Hunter et al.,<sup>58</sup> each species might occupy a different available site at the interface. This means that both adsorbing compounds could contribute to the reduction (and final value) of the interfacial tension. However, as it will be seen, interfacial dilatational rheology results show unambiguously that this is not the case.

In Figure 4, which corresponds to a demulsifier concentration of 100 ppm, after ~70% of the predetermined volume has been exchanged or at  $Qt/V = 35$ , the interfacial tension of the mixed interface is the same as that of single Brij-93. The effect is even clearer when the concentration goes up to 500 ppm. Figure A6 shows that even when a low portion of the predetermined volume has been exchanged ( $Qt/V \approx 10$ ), the liquid/liquid interface is dominated by the model molecular demulsifier. The curves corresponding to the blank experiments and desorption of asphaltenes overlap, suggesting that the composition at the interface is the same. Because of the fast desorption of asphaltenes at high concentration of Brij-93, it is troublesome to determine the presence of interactions at the interface.

The evolution of the elasticity of the oil/water interface and the mechanically strong film of asphaltenes was determined through interfacial dilatational rheology measurements after the predetermined volume ( $V = 1000 \mu\text{L}$ ) was exchanged at the fixed flow rate ( $0.4 \mu\text{L/s}$ ) (that is, after 2500 s). Figure 5 shows the values of the elastic dilatational modulus,  $E'$  [mN/m], for the desorption experiments just described. These experiments were carried out automatically after the predetermined volume was exchanged (that is, after 2500 s). In addition, a plateau in

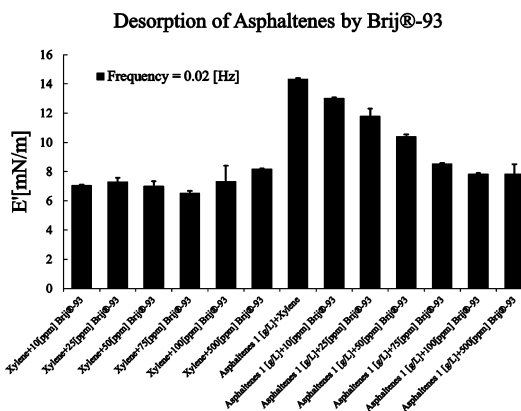


**Figure 5.** Elastic dilatational modulus taken at 0.02 Hz for asphaltenes at 1 g/L desorbed by Brij-93 (solutions in xylene) from 10 ppm to 500 ppm. The modulus was measured after the predetermined volume (1000  $\mu\text{L}$ ) was exchanged (that is, automatically after 2500 s). Blank experiments labeled as “Xylene + ...” are also shown.

the IFT was observed. A frequency sweep from 0.01 Hz to 0.1 Hz was performed with an amplitude of 15%. The values reported correspond to the average at 0.02 Hz. This particular value for the frequency was chosen based on the same trends observed for the other frequencies. From this figure, one can first note the presence of the strong film that was formed after the equilibration time. The highest value of the plot ( $\sim 14.3$  mN/m), which corresponds to the desorption of asphaltenes by pure solvent (xylene), coupled with the fact that asphaltenes are almost irreversibly adsorbed at the interface,<sup>27</sup> corroborate the high elasticity of such a film.

Second, comparing the blank experiments (solid black lines) to the desorption of asphaltenes by the demulsifier (dashed black lines), the formation of a mixed interface between asphaltenes and Brij-93 can be seen. From 10 ppm to 100 ppm of Brij-93, the elastic modulus exhibits a monotonic decrease until similar values are reached. These values are intermediate between those obtained by desorption of single components, which suggests the presence of both components at the interface.

From 100 ppm of demulsifier, the values of the blank experiments compared to the mixed system are exactly the same ( $\sim 8$  mN/m); therefore, it can be concluded that the interface is composed of Brij-93 only and the asphaltene film is no longer present.

Figures 3–5 (and Figures A3–A6) show results that can explain the removal of asphaltenes from the interface. Indeed, it was seen in a previous study<sup>27</sup> that asphaltenes are almost irreversibly adsorbed at the liquid/liquid interface, which is in agreement with the literature. The results of this study show that the displacement of asphaltenes from the oil/water interface starts with interactions between them and Brij-93 that, as a consequence, have the formation of structures that are more surface active than the components by themselves. This process is followed by desorption of asphaltenes and the subsequent adsorption of Brij-93. Complete desorption of asphaltenes is reached when a 100 ppm solution of Brij-93 is injected. At lower concentrations, a mixed interface is systematically obtained at the end of the exchange experiments. This concentration corresponds to an interfacial tension value

of  $\sim 24$  mN/m, which, compared to the interfacial tension value of asphaltenes at 1 g/L ( $\sim 25$  mN/m), is slightly lower. Evidently, this means that, at these concentrations, Brij-93 is more surface active than the asphaltenes.

The novelty of these results is 2-fold. First, a complete study of the oil/water interface through a Gibbs film that, compared to the studies performed on Langmuir films,<sup>5,35,36</sup> results in a more reliable description. Second, the approach of a simultaneous analysis of convection-induced desorption and interfacial rheology, which are the foundation for emulsion stability and coalescence aspects. These aspects are all in agreement to each other. Furthermore, based on Figures 3–5, customized dosage of demulsifier based on the characteristic desorption time ( $Qt/V$ ) could be proposed for in-field operations. Depending on the desorption capability and performance of a given demulsifier, an adequate demulsification strategy can be conceived.

**4.3.2. Desorption Driven by Pluronic PE8100.** In this section, similar desorption and interfacial rheology experiments were performed using a high-molecular-weight demulsifier (namely, PE8100). These types of polymeric demulsifiers are commonly used in the oil industry, because of their high surface activity and high performance at low concentrations. Based on the isotherm presented in Figure 1, the competitive sorption of this type of molecule is expected to be different from that of Brij-93. These polymers have different anchor points (three blocks), besides having some degree of polydispersity, which reflects onto the possible interactions with other molecules (short or long chains with different functional groups).

Figure 6 shows a plot of the interfacial tension as a function of the dimensionless characteristic time of desorption ( $Qt/V$ )

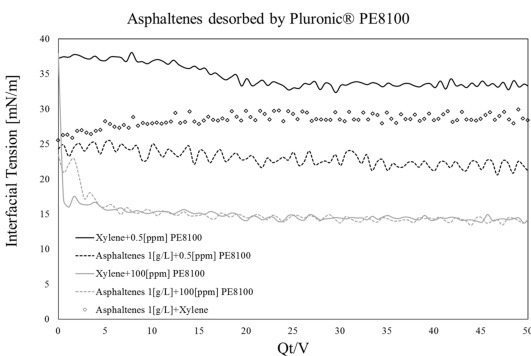


**Figure 6.** Desorption of asphaltenes at 1 g/L by means of PE8100 (dashed lines). Blank experiments (solid lines), as well as the reference experiments (empty symbols), are also shown.

for asphaltene solutions in xylene at 1 g/L by the polymeric demulsifier PE8100. Only desorption (after 30 min of equilibration time) carried out by subphase volume exchange is shown. In this case, two conditions for demulsifier concentration were used (that is, 0.5 ppm and 100 ppm). These concentrations were chosen based on bottle tests. As a reference, desorption of asphaltenes by pure solvent (empty symbols) is also shown.

The first aspect noteworthy of Figure 6 is the analysis at a low concentration of demulsifier. The curve corresponding to the blank experiment (solid black line) shows a slow adsorption at low-to-intermediate times ( $Qt/V \approx 30$ ), followed by a

plateau value ( $\gamma \approx 34$  mN/m). When asphaltenes are desorbed by PE8100 at 0.5 ppm, the final plateau value is  $\gamma \approx 23$  mN/m. This value is significantly lower than the reference value ( $\gamma \approx 30$  mN/m), which is an indication of the strong interactions between the demulsifier and asphaltenes at the interface. Furthermore, negligible desorption of asphaltenes is observed. This could be explained through the formation of complex-like asphaltenes–PE8100 structures, in which the large polymeric molecules anchor to the asphaltene aggregates, with some of the free PEO chains penetrating the asphaltene film.

The second important aspect of Figure 6 is related to the high concentration of demulsifier. It is clear from this figure that, at 100 ppm of PE8100, the oil/water interface is dominated entirely by the polymeric demulsifier. This polymer rapidly replaces the adsorbed asphaltenes and reaches a plateau value at very short times ( $Qt/V < 10$ ). The fact that the curves at high concentration of PE8100 overlap so rapidly is a clear indication of the effectiveness in penetrating the asphaltene film and replacing the interface of this particular demulsifier. This effect was not observed with the previous demulsifier even at higher concentration. The interfacial tension at equilibrium ( $\gamma \approx 15$  mN/m) value is attained after very short times. The sharp decrease of the IFT (low amount exchanged) is an indication of the high surface activity of PE8100. This was also observed in the single-component isotherm presented in Figure 1.

Interfacial dilatational rheology results for the pluronic system show results similar to those of Brij-93. Figure 7 is a

#### Desorption of Asphaltenes by Pluronic® PE8100

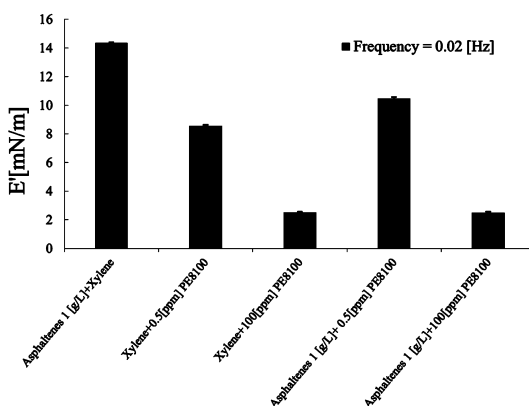


**Figure 7.** Elastic dilatational modulus at 0.02 Hz for the same experiments presented in Figure 6. The modulus was measured after the predetermined volume (1000  $\mu$ L) was exchanged (that is, automatically after 2500 s).

plot of the elastic dilatational modulus at 0.02 Hz for the same experiments presented in Figure 6, measured after the predetermined volume exchange (that is, automatically after 2500 s). The small synergy observed with the IFT is also shown here. At low concentrations of demulsifier, there is an increase of  $\sim 2$  mN/m between the blank experiments and the desorption of asphaltenes, which indicates that the mixed interface exhibits a small increase in the elasticity. However, it is clear that, at high concentrations of demulsifier, the elasticity of the interface is significantly reduced ( $E' \approx 2.3$  mN/m) and is dominated by the demulsifier. Once again, through elasticity

measurements, it is possible to visualize the high efficiency of this particular demulsifier to soften the interfacial film.

In this section, desorption and interfacial dilatational rheology aspects of asphaltenes at the oil/water interface were elucidated. Two chemically different demulsifiers were used to assess their performance. This provides fundamental knowledge for chemical demulsification strategies and coalescence studies. These two demulsifiers showed different behavior, mainly because of the differences in their surface activity. In addition, the difference in molecular weight plays an important role. In one hand, the low-molecular-weight demulsifier, Brij-93, adsorbs slowly to the interface and the possible complexation mechanisms seem to require longer times. However, at the flow rate and total volume exchange conditions tested, this demulsifier effectively desorbs asphaltenes from the liquid/liquid interface. On the other hand, the high-molecular-weight demulsifier (PE8100) shows a similar but sharper behavior. This means that less time and less amount of this demulsifier are needed to achieve similar degrees of desorption. The mechanisms of replacement seem to be similar between the two model demulsifiers. It is clear that, at short times, interactions between demulsifiers and asphaltenes are visible for all the conditions tested, except at 100 ppm of Pluronic PE8100. However, this point represents the fastest separation achieved in this article. The interactions result in a surface activity that is higher, compared to single-component analysis. These interactions and mechanisms are perhaps the key to understanding the process of desorption and replacement of almost-irreversibly adsorbed asphaltenes by model demulsifiers. Weakening and softening of the interfacial film was also made evident, which means that the two demulsifiers are effective in desorbing the almost-irreversibly adsorbed asphaltenes.

The next step is to assess the ability of the asphaltene (asphaltene nanoaggregates and clusters) to desorb the model demulsifiers. Generally speaking, surfactants do not have a tendency to form mechanically strong films at the interface; therefore, the stabilization mechanisms are related to interfacial tension gradients and steric hindrance, and are partially related to irreversible adsorption. Similarly, chemical demulsifiers exhibit these properties as well; therefore, it is of significant relevance to evaluate the performance of asphaltenes under desorbing conditions. In the following section, these topics are discussed.

**4.4. Desorption of Model Demulsifiers from the Oil/Water Interface.** This section covers desorption experiments performed on model demulsifier-covered droplets. The experimental conditions are similar to those of the previous sections, except that, in this case, asphaltene solutions are being pumped via the inner capillary. The Brij-93/PE8100 droplet is allowed to equilibrate for  $t_0 = 30$  min inside a cuvette (25 mL) that contains the aqueous pH 7 buffer solution. After this time, asphaltene solution is injected through an inner capillary using a second pump at a given volumetric flow rate ( $Q = 0.4 \mu\text{L/s}$ ). During this stage, the droplet volume was kept constant at 20  $\mu\text{L}$  through simultaneous withdrawal from the outer capillary using the first pump. Once the total predetermined volume ( $V = 1000 \mu\text{L}$ ) has been exchanged, pumping/withdrawal stops and the IFT reaches a plateau value.

#### 4.4.1. Desorption of Brij-93 from the Oil/Water Interface.

Figure 8 shows a plot of the interfacial tension as a function of the dimensionless desorption characteristic time for Brij-93 solutions at two different concentrations, namely, 100 and 2500

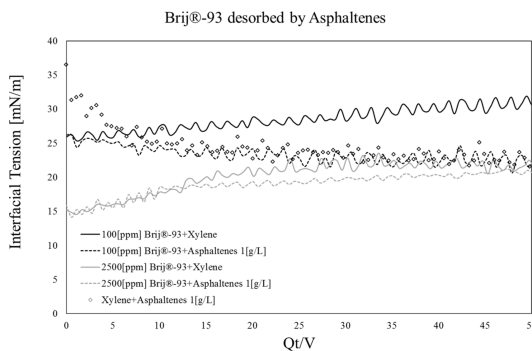


**Figure 8.** Interfacial tension as a function of the dimensionless characteristic time for desorption ( $Qt/V$ ) of Brij-93 by asphaltenes (solutions in xylene) at 1 g/L. The solid lines are the blank experiments, the dashed lines are the desorption experiments, and the empty symbols represent the reference experiment. Experimental conditions for the experiments: exchange flow rate,  $Q = 0.4 \mu\text{L/s}$ ; total predetermined volume,  $V = 1000 \mu\text{L}$ .

ppm. The latter concentration was chosen to accurately compare two demulsifiers that generate similar values in interfacial tension reduction (i.e., down to  $\sim 15$  mN/m). Desorption is done by asphaltenes at 1 g/L. As a reference (empty symbols), exchange of xylene and asphaltenes is also shown.

First, it is important to note that, as observed in the first part of this work,<sup>27</sup> Brij-93 shows partial desorption from the liquid/liquid interface (solid black line). Second, comparing the blank curve (solid black line) and the desorption curve (dashed black line), it is clear that asphaltenes can effectively desorb this model demulsifier at low concentrations. Furthermore, the asphaltenes are subsequently adsorbed at the interface. This can be seen at the region where the reference (empty symbols) overlaps and collapses at low times ( $Qt/V > 10$ ). This also means that, after the exchange, there is an asphaltene-dominated interface. No signs of interaction or synergy are observed between the adsorbed species.

At high concentrations of demulsifier, Brij-93 exhibits a similar degree of desorption by pure solvent (solid light gray curve). However, when asphaltenes are injected (dashed light gray curve), it can be seen that they are not able to provide the same level of desorption. Actually, there seems to be a small synergy effect, given that the latter curve is always below the former.

Interfacial dilatational rheology results, presented in Figure A7 in the Supporting Information, show a similar trend. At low concentrations of demulsifier, the elastic modulus reaches the same value as that of the reference experiment. Similarly, the small synergy effect is also present at high concentrations of demulsifier, given that the elastic modulus reaches a lower value, compared to the reference.

The desorbing performance of asphaltenes was tested in this section. This issue is of significance to the oil industry during chemical demulsification, mainly because of the possibility of re-emulsification or inverse effects caused by demulsifier overdosing.<sup>12</sup>

**4.4.2. Desorption of Pluronic PE8100 from the Oil/Water Interface.** Finally, Figure 9, and Figure A8 in the Supporting Information, show the interfacial tension and interfacial

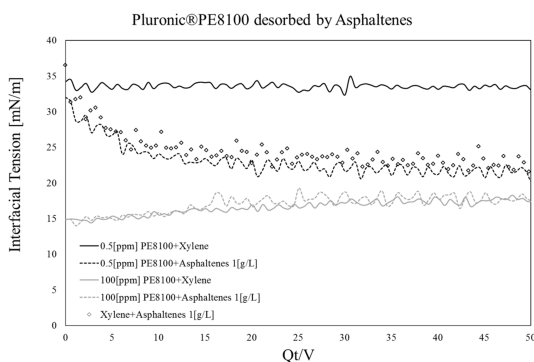


**Figure 9.** Interfacial tension, as a function of the dimensionless characteristic time for desorption ( $Qt/V$ ) of PE8100 by asphaltenes (solutions in xylene) at 1 g/L. The solid lines are the blank experiments, the dashed lines are the desorption experiments, and the empty symbols represent the reference experiment. Experimental conditions for the experiments: exchange flow rate,  $Q = 0.4 \mu\text{L/s}$ ; total predetermined volume,  $V = 1000 \mu\text{L}$ .

dilatational rheology after desorption of the model polymeric demulsifier PE8100 by asphaltenes at 1 g/L. The trends in desorption at low and high concentration are similar to those presented in the previous section. However, it is important to note the differences in the concentration range for the demulsifiers. In this case, 0.5–100 ppm of PE8100 was enough to obtain a similar behavior, whereas in the previous case, up to 2500 ppm was needed.

In this case, at low concentrations of demulsifier (black lines), the oil/water interface exhibits complete replacement by asphaltenes. Asphaltenes are not able to desorb the polymeric demulsifier at high concentration (light gray lines), because, as seen in Figure 9, these two curves overlap at all times. The elastic modulus shows a similar trend, which is in agreement with the IFT results.

Two different demulsifiers were tested under convection-enhanced desorption by asphaltenes. These demulsifiers are chemically and structurally different. Asphaltenes at 1 g/L have the ability to desorb model demulsifiers from the liquid/liquid interface at low concentration. This replacement occurs with no visible interactions between the compounds. When the reverse condition is considered, that is, desorption of asphaltenes by model demulsifiers, the opposite is true. At high concentrations of demulsifier, when the interfacial tension values after 30 min of equilibration time reach  $\sim 15 \text{ mN/m}$ , significant differences are observed between Brij-93 and PE8100. While Brij-93 is partly desorbed by asphaltenes (Figure 8), in the case of the polymeric demulsifier, it seems that the interface remains unaffected by them. Although desorption is present, it is not caused by the action of asphaltenes and no interactions between these two compounds are observable. It is important to highlight the fact that these effects are not only attributed to the suppression of the interfacial tension gradient but also to the large molecular weight difference. Table 1 summarizes the main conclusions of this work comparing the interfacial tension values before desorption experiments.

## 5. CONCLUSIONS

In this work, competitive adsorption and desorption aspects of mixed interfaces were studied. A model system—namely,  $C_6$ -

**Table 1. Summary of the Main Results of This Work Comparing Surface Activity<sup>a</sup>**

| Asphaltene Desorption         |   |   |
|-------------------------------|---|---|
| demulsifier/<br>concentration | $\gamma_{\text{Demulsifier}}$ VS<br>$\gamma_{\text{Asphaltene}}$<br>(30 min) <sup>b</sup> | conclusions   |
| Brij-93                       |   |   |
| 10 ppm                        | >   | interactions; partial desorption of asphaltenes               |
| 100 ppm                       | $\approx$   | interactions; almost complete replacement                     |
| 2500 ppm                      | <   | no interactions visible; complete replacement by demulsifier  |
| PE8100                        |   |   |
| 0.5 ppm                       | >   | strong interactions and synergy; no desorption of asphaltene  |
| 100 ppm                       | <   | no interactions visible; complete replacement by demulsifier  |
| Demulsifier Desorption        |   |   |
| demulsifier/<br>concentration | $\gamma_{\text{Asphaltene}}$ VS<br>$\gamma_{\text{Demulsifier}}$<br>(30 min) <sup>b</sup> | conclusions   |
| Brij-93                       |   |   |
| 100 ppm                       | $\approx$   | asphaltene desorb demulsifier; no interactions visible        |
| 2500 ppm                      | >   | desorption or interactions                                    |
| PE8100                        |   |   |
| 0.5 ppm                       | <   | asphaltene desorb demulsifier; no interactions visible        |
| 100 ppm                       | >   | asphaltene do not desorb demulsifier; no interactions visible |

<sup>a</sup>The upper part of the table corresponds to the desorption of asphaltene by two different demulsifiers from the oil/water interface. The lower part of the table corresponds to the desorption of two demulsifiers by asphaltene. <sup>b</sup>Comparison between the interfacial tension of asphaltene and the demulsifier used in this work after 30 min of equilibration time. Desorption experiments were performed after this time.

asphaltene and two chemically and structurally different demulsifiers—were chosen to emulate the behavior of the oil/water interface when chemical demulsification processes occur during crude oil production. At these stages, water-in-crude oil emulsions are already formed. Furthermore, interfacial dilatational rheology was used to couple these results with features related to the elasticity of the film formed at the liquid/liquid interface. Asphaltene desorption has been traditionally studied at the solid/air or liquid/air interfaces through Langmuir trough, Langmuir–Blodgett films (LB), Brewster angle microscopy (BAM),<sup>4,13,15,64–66</sup> and quartz crystal microbalance technique.<sup>4,67,68</sup> In this work, a study at the liquid/liquid interface is proposed. This approach provides a framework that allows further understanding of the different phenomena that occur when demulsifiers interact with indigenous crude oil surfactants during water separation.

A first semiquantitative approach on the surface activity of the two different demulsifiers—namely, Brij-93 and Pluronic PE8100—was observed in Figure 1. The affinity ranking was as follows: Pluronic PE8100 > Brij-93 >  $C_6$ -asphaltene. Using a noninteraction model based on the Langmuir EoS (eqs 4–6), it was observed that the model demulsifier Brij-93 has a tendency to dominate the oil/water interface. The effect of PE8100 is more evident as lower concentrations are needed.

In the second part of this work, the desorption of asphaltene from the oil/water interface by means of two model

demulsifiers was studied. Interfacial tension measurements, coupled with interfacial dilatational rheology measurements, showed that there is a degree of interaction between Brij-93 and the asphaltenes at the oil/water interface prior to replacement, depending on the demulsifier concentration. Similarly, when a polymeric demulsifier (namely, Pluronic PE8100) was used, sharper behavior was observed. This means that the replacement of asphaltenes takes place at lower concentrations and it occurs more rapidly. However, the mechanism seems to be similar to that observed when using the molecular model demulsifier Brij-93. This behavior is attributed not only to the high differences in surface activity of the demulsifiers (Figure 1) but also to the differences in chemical structure and molecular weight. In both cases, formation of complex-like structures seems to be the most plausible mechanism prior to desorption. These complex-like structures could be enhanced by the alkyl chains that stick out of the asphaltene nanoaggregates and clusters, according to the Yen–Mullins model.<sup>62,63</sup> Interactions between functional groups from both species could also promote this phenomenon.

Analogously, in the final part of this article, desorption of the two model demulsifiers by means of asphaltenes was studied. Results showed that asphaltenes can effectively desorb both demulsifiers at low concentration (with some interactions present) but not at high concentrations, especially in the case of the polymeric demulsifier PE8100. This is not only attributed to the interfacial tension gradient but also to the poor ability of asphaltene aggregates to reach the liquid/liquid interface and form complexes.

## ■ ASSOCIATED CONTENT

### ● Supporting Information

The Supporting Information is available free of charge on the ACS Publications website at DOI: 10.1021/acs.energyfuels.Sb01302.

Tabular summary of the main results of this work comparing surface activity (PDF)

Schematic of the coaxial capillary system used for the desorption experiments (Figure A1), equilibrium interfacial tension for a mixed interface between asphaltenes and Brij-93 (Figure A2), interfacial tension as a function of the dimensionless characteristic time for desorption of asphaltenes by Brij-93 (solutions in xylene) at various concentrations (Figures A3–A6), elastic dilatational modulus at 0.02 Hz for the same experiments presented in Figures 8 and 9 (Figures A7 and A8, respectively) (PDF)

## ■ AUTHOR INFORMATION

### Corresponding Author

\*E-mail: diego.c.p.ragua@ntnu.no. Tel.: +47 942 41 988. Fax: +47 735 94 080.

### Notes

The authors declare no competing financial interest.

## ■ ACKNOWLEDGMENTS

The authors gratefully acknowledge financial support for this work from the Research Council of Norway (NFR) and the industrial consortium JIP-1 (Joint Industrial Project): Akzo-Nobel, BP, Nalco-Champion, ENI, Hamworthy, Saudi Aramco, Shell, Statoil ASA, and Total.

## ■ REFERENCES

- (1) Sjöblom, J.; Øye, G.; Glomm, W.; Hannisdal, A.; Knag, M.; Brandal, Ø.; Ese, M.; Hemmingsen, P.; Havre, T. E.; Oschmann, H.-J.; Kallevik, H. Modern characterization techniques for crude oils, their emulsions, and functionalized surfaces. In *Emulsions and Emulsion Stability*, Second Edition; Sjöblom, J., Ed.; CRC Press: Boca Raton, FL, 2006; pp 415–476.
- (2) Speight, J. G. Exploration, Recovery, and Transportation. In *The Chemistry and Technology of Petroleum*, Fourth Edition; CRC Press, and Taylor and Francis Group, LLC: Boca Raton, FL, 2007; pp 99–141.
- (3) Jestin, J.; Simon, S.; Zupancic, L.; Barré, L. A Small Angle Neutron Scattering Study of the Adsorbed Asphaltene Layer in Water-in-Hydrocarbon Emulsions: Structural Description Related to Stability. *Langmuir* **2007**, *23*, 10471–10478.
- (4) Zhang, L. Y.; Xu, Z.; Masliyah, J. H. Langmuir and Langmuir-Blodgett films of mixed asphaltene and a demulsifier. *Langmuir* **2003**, *19*, 9730–9741.
- (5) Pensini, E.; Harbottle, D.; Yang, F.; Tchoukov, P.; Li, Z.; Kailey, L.; Behles, J.; Masliyah, J.; Xu, Z. Demulsification Mechanism of Asphaltene-Stabilized Water-in-Oil Emulsions by a Polymeric Ethylene Oxide–Propylene Oxide Demulsifier. *Energy Fuels* **2014**, *28*, 6760.
- (6) Simon, S.; Jestin, J.; Palermo, T.; Barré, L. Relation between Solution and Interfacial Properties of Asphaltene Aggregates. *Energy Fuels* **2009**, *23*, 306–313.
- (7) Sjöblom, J.; Aske, N.; Auflem, I. H.; Brandal, Ø.; Havre, T. E.; Sæther, O.; Westvik, A.; Johnsen, E. E.; Kallevik, H.; et al. Our current understanding of water-in-crude oil emulsions. Recent characterization techniques and high pressure performance. *Adv. Colloid Interface Sci.* **2003**, *100–102*, 399–473.
- (8) Agrawala, M.; Yarranton, H. W. An asphaltene association model analogous to linear polymerization. *Ind. Eng. Chem. Res.* **2001**, *40*, 4664–4672.
- (9) Groenzin, H.; Mullins, O. C. Asphaltene Molecular Size and Structure. *J. Phys. Chem. A* **1999**, *103*, 11237–11245.
- (10) Groenzin, H.; Mullins, O. C.; Eser, S.; Mathews, J.; Yang, M.-G.; Jones, D. Molecular Size of Asphaltene Solubility Fractions. *Energy Fuels* **2003**, *17*, 498–503.
- (11) Calemma, V.; Iwanski, P.; Nali, M.; Scotti, R.; Montanari, L. Structural Characterization of Asphaltenes of Different Origins. *Energy Fuels* **1995**, *9*, 225–230.
- (12) Angle, C. W. Chemical Demulsification of Stable Crude Oil and Bitumen Emulsions in Petroleum Recovery—A Review. In *Encyclopedic Handbook of Emulsion Technology*; Sjöblom, J., Ed.; Marcel Dekker: New York, 2001; pp 541–594.
- (13) Hou, J.; Feng, X.; Masliyah, J.; Xu, Z. Understanding Interfacial Behavior of Ethylcellulose at the Water–Diluted Bitumen Interface. *Energy Fuels* **2012**, *26*, 1740–1745.
- (14) Djuve, J.; Yang, X.; Fjellanger, I. J.; Sjöblom, J.; Pelizzetti, E. Chemical destabilization of crude oil based emulsions and asphaltene stabilized emulsions. *Colloid Polym. Sci.* **2001**, *279*, 232–239.
- (15) Ese, M. H.; Galet, L.; Clausse, D.; Sjöblom, J. Properties of langmuir surface and interfacial films built up by asphaltenes and resins: Influence of chemical demulsifiers. *J. Colloid Interface Sci.* **1999**, *220*, 293–301.
- (16) Fan, Y.; Simon, S.; Sjöblom, J. Interfacial shear rheology of asphaltenes at oil–water interface and its relation to emulsion stability: Influence of concentration, solvent aromaticity and nonionic surfactant. *Colloids Surf, A* **2010**, *366*, 120–128.
- (17) Kim, Y. H.; Wasan, D. T. Effect of Demulsifier Partitioning on the Destabilization of Water-in-Oil Emulsions. *Ind. Eng. Chem. Res.* **1996**, *35*, 1141–1149.
- (18) Ferri, J. K.; Gorevski, N.; Kotsmar, C.; Leser, M. E.; Miller, R. Desorption kinetics of surfactants at fluid interfaces by novel coaxial capillary pendant drop experiments. *Colloids Surf, A* **2008**, *319*, 13–20.
- (19) Rane, J. P.; Harbottle, D.; Pauchard, V.; Couzis, A.; Banerjee, S. Adsorption kinetics of asphaltenes at the oil–water interface and nanoaggregation in the bulk. *Langmuir* **2012**, *28*, 9986–9995.

- (20) Pauchard, V.; Rane, J. P.; Banerjee, S. Asphaltene-laden interfaces form soft glassy layers in contraction experiments: A mechanism for coalescence blocking. *Langmuir* **2014**, *30*, 12795–12803.
- (21) Svitova, T. F.; Wetherbee, M. J.; Radke, C. J. Dynamics of surfactant sorption at the air/water interface: Continuous-flow tensiometry. *J. Colloid Interface Sci.* **2003**, *261*, 170–179.
- (22) Ferri, J. K.; Miller, R.; Makievski, A. V. Equilibrium and dynamics of PEO/PPO/PEO penetration into DPPC monolayers. *Colloids Surf., A* **2005**, *261*, 39–48.
- (23) Kotsmár, C.; Grigoriev, D. O.; Makievski, A. V.; et al. Drop profile analysis tensiometry with drop bulk exchange to study the sequential and simultaneous adsorption of a mixed  $\beta$ -casein/ $C_{12}$ DMPO system. *Colloid Polym. Sci.* **2008**, *286*, 1071–1077.
- (24) Fainerman, V. B.; Kovalchuk, V. I.; Lucassen-Reynders, E. H.; et al. Surface-pressure isotherms of monolayers formed by microsize and nanosize particles. *Langmuir* **2006**, *22*, 1701–1705.
- (25) Fainerman, V. B.; Makievski, A. V.; Miller, R. The analysis of dynamic surface tension of sodium alkyl sulphate solutions, based on asymptotic equations of adsorption kinetic theory. *Colloids Surf., A* **1994**, *87*, 61–75.
- (26) Fainerman, V. B.; Miller, R.; Ferri, J. K.; Watzke, H.; Leser, M. E.; Michel, M. Reversibility and irreversibility of adsorption of surfactants and proteins at liquid interfaces. *Adv. Colloid Interface Sci.* **2006**, *123–126*, 163–171.
- (27) Pradilla, D.; Simon, S.; Sjöblom, J. Mixed interfaces of asphaltenes and model demulsifiers, Part I: Adsorption and desorption of single components. *Colloids Surf., A* **2015**, *466*, 45–56.
- (28) Ravera, F.; Loglio, G.; Kovalchuk, V. I. Interfacial dilational rheology by oscillating bubble/drop methods. *Curr. Opin. Colloid Interface Sci.* **2010**, *15*, 217–228.
- (29) Turgman-Cohen, S.; Fischer, D. A.; Kilpatrick, P. K.; Genzer, J. Asphaltene Adsorption onto Self-Assembled Monolayers of Alkyltrichlorosilanes of Varying Chain Length. *ACS Appl. Mater. Interfaces* **2009**, *1*, 1347–1357.
- (30) Rane, J. P.; Pauchard, V.; Couzis, A.; Banerjee, S. Interfacial rheology of asphaltenes at oil–water interfaces and interpretation of the equation of state. *Langmuir* **2013**, *29*, 4750–4759.
- (31) Pauchard, V.; Rane, J. P.; Zarkar, S.; Couzis, A.; Banerjee, S. Long-term adsorption kinetics of asphaltenes at the oil-water interface: A random sequential adsorption perspective. *Langmuir* **2014**, *30*, 8381–8390.
- (32) Nenningsland, A. L.; Simon, S.; Sjöblom, J. Influence of Interfacial Rheological Properties on Stability of Asphaltene-Stabilized Emulsions. *J. Dispersion Sci. Technol.* **2014**, *35*, 231–243.
- (33) Erni, P. Deformation modes of complex fluid interfaces. *Soft Matter* **2011**, *7*, 7586–7600.
- (34) Angle, C. W.; Hua, Y. Dilational Interfacial Rheology for Increasingly Deasphalted Bitumens and  $n$ - $C_{12}$  Asphaltenes in Toluene/ $\text{NaHCO}_3$  Solution. *Energy Fuels* **2012**, *26*, 6228–6239.
- (35) Yarranton, H. W.; Sztukowski, D. M.; Urrutia, P. Effect of interfacial rheology on model emulsion coalescence: I. Interfacial rheology. *J. Colloid Interface Sci.* **2007**, *310*, 246–252.
- (36) Yarranton, H. W.; Urrutia, P.; Sztukowski, D. M. Effect of interfacial rheology on model emulsion coalescence: II. Emulsion coalescence. *J. Colloid Interface Sci.* **2007**, *310*, 253–259.
- (37) Freer, E. M.; Radke, C. J. Relaxation of Asphaltenes at the Toluene/Water Interface: Diffusion Exchange and Surface Rearrangement. *J. Adhes.* **2004**, *80*, 481–496.
- (38) Freer, E. M.; Svitova, T.; Radke, C. J. The role of interfacial rheology in reservoir mixed wettability. *J. Pet. Sci. Eng.* **2003**, *39*, 137–158.
- (39) Turgman-Cohen, S.; Smith, M. B.; Fischer, D. A.; Kilpatrick, P. K.; Genzer, J. Asphaltene Adsorption onto Self-Assembled Monolayers of Mixed Aromatic and Aliphatic Trichlorosilanes. *Langmuir* **2009**, *25*, 6260–6269.
- (40) Spiecker, P. M.; Kilpatrick, P. K. Interfacial Rheology of Petroleum Asphaltenes at the Oil–Water Interface. *Langmuir* **2004**, *20*, 4022–4032.
- (41) Verruto, V. J.; Kilpatrick, P. Water-in-Model Oil Emulsions Studied by Small-Angle Neutron Scattering: Interfacial Film Thickness and Composition. *Langmuir* **2008**, *24*, 12807–12822.
- (42) Buch, L.; Groenzin, H.; Buenrostro-Gonzalez, E.; Andersen, S. L.; Lira-Galeana, C.; Mullins, O. C. Molecular size of asphaltene fractions obtained from residuum hydrotreatment. *Fuel* **2003**, *82*, 1075–1084.
- (43) Mullins, O. C. The Asphaltenes. *Annu. Rev. Anal. Chem.* **2011**, *4*, 393–418.
- (44) Mostowfi, F.; Indo, K.; Mullins, O. C.; McFarlane, R. Asphaltene nanoaggregates studied by centrifugation. *Energy Fuels* **2009**, *23*, 1194–1200.
- (45) Speight, J. G. Asphaltene Constituents. In *The Chemistry and Technology of Petroleum*, 4th Edition; CRC Press, and Taylor & Francis Group: Boca Raton, FL; 2007: Chapter 11, pp 315–344.
- (46) Eastoe, J.; Dalton, J. S. Dynamic surface tension and adsorption mechanisms of surfactants at the air–water interface. *Adv. Colloid Interface Sci.* **2000**, *85*, 103–144.
- (47) Chang, C. H.; Franses, E. I. Adsorption dynamics of surfactants at the air/water interface: A critical review of mathematical models, data, and mechanisms. *Colloids Surf., A* **1995**, *100*, 1–45.
- (48) Yeung, A.; Dabros, T.; Masliyah, J.; Czarneci, J. Micropipette: A new technique in emulsion research. *Colloids Surf., A* **2000**, *174*, 169–181.
- (49) Tambe, D. E.; Sharma, M. M. Factors Controlling the Stability of Colloid-Stabilized Emulsions: III. Measurement of the Rheological Properties of Colloid-Laden Interfaces. *J. Colloid Interface Sci.* **1995**, *171*, 456–462.
- (50) Derkach, S. R.; Krägel, J.; Miller, R. Methods of measuring rheological properties of interfacial layers (Experimental methods of 2D rheology). *Colloid J.* **2009**, *71*, 1–17.
- (51) Simon, S.; Picton, L.; Le Cerf, D.; Muller, G. Adsorption of amphiphilic polysaccharides onto polystyrene latex particles. *Polymer* **2005**, *46*, 3700–3707.
- (52) Georgiev, G. A.; Gurov, R.; Jordanova, A.; Vassiliev, C. S.; Lalchev, Z. Properties of alkyl-phosphatidylcholine monolayers in the presence of surface-active three-block copolymers. *Colloids Surf., B* **2010**, *80*, 40–44.
- (53) Hädicke, A.; Blume, A. Interactions of Pluronic block copolymers with lipid monolayers studied by epi-fluorescence microscopy and by adsorption experiments. *J. Colloid Interface Sci.* **2013**, *407*, 327–338.
- (54) Blomqvist, B. R.; Wårnheim, T.; Claesson, P. M. Surface Rheology of PEO–PPO–PEO Triblock Copolymers at the Air–Water Interface: Comparison of Spread and Adsorbed Layers. *Langmuir* **2005**, *21*, 6373–6384.
- (55) Torcello-Gómez, A.; Maldonado-Valderrama, J.; Jódar-Reyes, A. B.; Foster, T. J. Interactions between Pluronics (F127 and F68) and Bile Salts (NaTDC) in the Aqueous Phase and the Interface of Oil-in-Water Emulsions. *Langmuir* **2013**, *29*, 2520–2529.
- (56) Muñoz, M. G.; Monroy, F.; Ortega, F.; Rubio, R. G.; Langevin, D. Monolayers of symmetric triblock copolymers at the air-water interface. 1. Equilibrium properties. *Langmuir* **2000**, *16*, 1083–1093.
- (57) Muñoz, M. G.; Monroy, F.; Ortega, F.; Rubio, R. G.; Langevin, D. Monolayers of symmetric triblock copolymers at the air–water interface. 2. Adsorption kinetics. *Langmuir* **2000**, *16*, 1094–101.
- (58) Hunter, J. R.; Carbonell, R. G.; Kilpatrick, P. K. Coadsorption and exchange of lysozyme/ $\beta$ -casein mixtures at the air/water interface. *J. Colloid Interface Sci.* **1991**, *143*, 37–53.
- (59) Fan, Y.; Simon, S.; Sjöblom, J. Chemical destabilization of crude oil emulsions: Effect of nonionic surfactants as emulsion inhibitors. *Energy Fuels* **2009**, *23*, 4575–4583.
- (60) Harbottle, D.; Chen, Q.; Moorthy, K.; et al. Problematic Stabilizing Films in Petroleum Emulsions: Shear Rheological Response of Viscoelastic Asphaltene Films and the Effect on Drop Coalescence. *Langmuir* **2014**, *30*, 6730–6738.
- (61) Verruto, V. J.; Le, R. K.; Kilpatrick, P. K. Adsorption and Molecular Rearrangement of Amphoteric Species at Oil–Water Interfaces. *J. Phys. Chem. B* **2009**, *113*, 13788–13799.



- (62) Yen, T. F.; Erdman, J. G.; Pollack, S. S. Investigation of the Structure of Petroleum Asphaltenes by X-ray Diffraction. *Anal. Chem.* **1961**, *33*, 1587–1594.
- (63) Mullins, O. C. The Modified Yen Model. *Energy Fuels* **2010**, *24*, 2179–2207.
- (64) Le Follotec, A.; Pezron, I.; Noik, C.; Dalmazzone, C.; Metlas-Komunjer, L. Triblock copolymers as destabilizers of water-in-crude oil emulsions. *Colloids Surf., A* **2010**, *365*, 162–170.
- (65) Fan, Y.; Simon, S.; Sjöblom, J. Influence of Nonionic Surfactants on the Surface and Interfacial Film Properties of Asphaltenes Investigated by Langmuir Balance and Brewster Angle Microscopy. *Langmuir* **2010**, *26*, 10497–10505.
- (66) Hua, Y.; Angle, C. W. Brewster Angle Microscopy of Langmuir Films of Athabasca Bitumens, *n*-C<sub>5</sub> Asphaltenes, and SAGD Bitumen during Pressure–Area Hysteresis. *Langmuir* **2013**, *29*, 244–263.
- (67) Goual, L.; Horváth-Szabó, G.; Masliyah, J. H.; Xu, Z. Adsorption of Bituminous Components at Oil/Water Interfaces Investigated by Quartz Crystal Microbalance: Implications to the Stability of Water-in-Oil Emulsions. *Langmuir* **2005**, *21*, 8278–8289.
- (68) Rudrake, A.; Karan, K.; Horton, J. H. A combined QCM and XPS investigation of asphaltene adsorption on metal surfaces. *J. Colloid Interface Sci.* **2009**, *332*, 22–31.

*Sorption and interfacial rheology study of model asphaltene compounds.*



# Sorption and interfacial rheology study of model asphaltene compounds.

*Diego Pradilla\**<sup>1</sup>, *Sébastien Simon*<sup>1</sup>, *Johan Sjöblom*<sup>1</sup>

<sup>1</sup>Ugelstad Laboratory, Department of Chemical Engineering, Norwegian University of Science and Technology (NTNU), NO-7491 Trondheim, Norway.

*Joseph Samaniuk*<sup>2</sup>, *Marta Skrzypiec*<sup>3</sup>, *Jan Vermant*<sup>2</sup>

<sup>2</sup> Soft Materials Laboratory, Department of Materials, ETH Zürich, Vladimir-Prelog-Weg 5, 8093 Zürich, Switzerland

<sup>3</sup>Institute of Chemical Technology and Engineering, Poznan University of Technology, Berdychowo 4, 60-965 Poznan, Poland

\*Corresponding Author

E-mail: [diego.c.p.ragua@ntnu.no](mailto:diego.c.p.ragua@ntnu.no)

Phone: +47 735 94 080

Notes

The authors declare no competing financial interest.

**KEYWORDS:** Dilatational rheology, shear rheology, desorption, asphaltene model compounds.

## Abstract

In this article, the sorption and rheological properties of an acidic polyaromatic asphaltene model compound (C5PeC11) are determined. The results show that C5PeC11 exhibits the type of pH-dependent surface activity and interfacial shear rheology observed in C<sub>6</sub>-asphaltenes with a decrease in the interfacial tension concomitant to the elastic modulus when the pH increases. Surface pressure-area ( $\Pi$ -A) isotherms show evidence of aggregation behavior and  $\pi$ - $\pi$  stacking at both the air/water and oil/water interfaces. Similarly, interactions between adsorbed C5PeC11 compounds are evidenced through desorption experiments at the water/oil interface. Indeed adsorption is reversible contrary to indigenous asphaltenes, but desorption is slower than for non-interacting species. Shear and dilatational rheology show that C5PeC11 forms a predominantly elastic film both at the liquid/air and the liquid/liquid interface. Furthermore, a soft glassy rheology model (SGR) fits the data obtained at the liquid/liquid interface. It is shown that the effective noise temperature determined from the SGR model for C5PeC11 is higher than for indigenous asphaltenes measured under similar conditions. Finally, from a colloidal and rheological standpoint, the results highlight the importance of adequately addressing the distinction between the material functions and true elasticity extracted from a shear measurement and the apparent elasticity measured in dilatational-pendant drop set-ups.

## 1. Introduction

Asphaltenes are commonly defined as the fraction of petroleum insoluble in *n*-alkanes (such as heptane or hexane) but soluble in aromatic compounds (such as toluene or xylene)<sup>1</sup>. These surface active polar compounds are largely responsible for problems during production, transport and refining of crude oil resulting in higher production costs<sup>2</sup>. For example, asphaltenes can precipitate and deposit in the reservoirs, wells, pipes and other equipment<sup>3, 4, 5</sup>. They can also stabilize water-in-oil emulsions<sup>6</sup> (W/O) by forming a solid-like interface, or “skin”<sup>7, 8</sup>, at the oil/water interface that hinders coalescence and retards film drainage<sup>9, 10, 11</sup>. This “skin” is due to interfacial asphaltene-crowding<sup>12</sup> enhanced by self-association at the liquid-liquid interface and even the build-up of multilayers<sup>13</sup>. The properties of this interfacial film need to be understood and characterized and interfacial rheology is an adequate tool to fulfill such goal.

Shear, dilatational, and mix-field flow types can be obtained in interfacial rheological techniques. In simple shear experiments, flow is induced at a constant area, while in dilation

the area of the interface is changed. Studies on interfacial shear rheology<sup>14, 15</sup> using a biconical geometry showed that asphaltenes form films of high elasticity after several hours of aging. Furthermore, a concentration threshold range of 2-5 g/L was found for the formation of the mechanically strong film at the oil/water interface after aging. Samaniuk et al.<sup>12</sup> recently studied asphaltenes at the hexadecane/water interface using a double wall-ring (DWR) geometry confirming the effects of concentration and aging. They also concluded that: (i) asphaltene films at the oil/water interface behave as soft-glassy materials, (ii) the crowding of the interface plays a crucial role and, (iii) the concentration/frequency-dependent data is in agreement with a soft-glassy rheology (SGR) model. Using a similar geometry, Harbottle et al.<sup>16</sup> showed that the microstructure of the asphaltene network film at the oil/water interface can be liquid-like or solid-like depending on the initial bulk concentration, aging time of the interface and solvent aromaticity. The transition states could be related to the shear yield stress which might act as an energy barrier against drop coalescence.

The literature regarding interfacial dilatational rheological studies of asphaltene films at the liquid-liquid interface is extensive<sup>17, 18, 19, 20, 21, 22</sup>. It is imperative to emphasize that in such experiments, depending on the dominating phenomena, the nature of the measured quantities will vary. For instance, at interfaces largely dominated by interfacial tension, the influence of the exchange with the bulk is dominant (adsorption/desorption dynamics), whereas extra mechanical stresses are essentially negligible; this is often the case for low molecular weight surfactants. At interfaces dominated by extra stresses, as in the case of particle monolayers or asphaltenes that clearly exhibit a skin, the nature of the elastic response is fundamentally different. Hence, when discussing the moduli extracted from dilatational experiments it should be noted that these may not always be true material functions.

Literature studies report a behavior that is somewhat general to asphaltenes. First, the apparent elastic dilatational modulus ( $E'$ ) increases with time and concentration. This is an indication of the kinetic build-up of the film, crowding and possible cross-linking of asphaltenes at the interface. Second, a maximum in  $E'$  with concentration is observed, the location will depend on the conditions of the experiment and asphaltene origin<sup>18, 20, 21, 22</sup>. And third, if the aged interface is contracted, a phenomenon described as crumpling was observed<sup>20</sup>.

The exchange of surfactant between the bulk and the interface and its effects on the apparent elastic dilatational modulus are typically described using the Lucassen van den Tempel

(LvdT) approach<sup>23</sup> which assumes that the adsorption at the interface is diffusion-controlled and reversible. The application of the LvdT model to asphaltenes has, however, been less successful. Two explanations have been so far put forward: first, asphaltenes adsorb irreversibly to oil/water interfaces and give rise to an extra mechanical stress at the interface<sup>12</sup>. Second, the diffusion coefficient tends to be low and to vary with concentration<sup>18</sup>.

From the broad definition of asphaltenes as a solubility class, and therefore polydisperse, it follows that they are heterogeneous in chemical composition. The different functionalities, molecular weights, and molecular architectures make it challenging to obtain a complete understanding of their properties. Sjöblom et al<sup>24</sup>. indicated two main strategies that can be used to tackle this issue: fractionation of the complete asphaltene content into sub-fractions of reduced complexity (but still polydisperse<sup>25, 26</sup> and different among reservoirs<sup>27</sup>) or synthesis of model molecules of defined chemical structure that mimic the average chemical structure of indigenous asphaltenes..

The latter strategy has received special attention during the last ten years as a fundamental approach to understand the physical behavior of indigenous asphaltenes in terms of aggregation, adsorption, desorption and other interfacial properties by establishing similarities and differences through various experiments and simulations. The “Archipelago” and “Continental” models for asphaltenes have been traditionally used to attempt a description of a general structure for asphaltenes. In the former, several aromatic sections are attached to each other via alkyl chains. In the latter, polycyclic aromatic hydrocarbons (PAHs) form a core to which aliphatic chains are attached<sup>28, 29</sup>. The work of Groenzin and Mullins<sup>30, 31, 32</sup> shows strong evidence that points towards the validity of the continental over the archipelago model for asphaltenes.

Numerous works on model compounds have been presented following primarily the continental model with little studies based on the Archipelago model. A recent review<sup>24</sup> on the up-to-date literature highlighted a number of these studies. Akbarzadeh et al.<sup>33</sup> studied the self-association properties (aggregation number and stability of aggregates in solution) of a series of derivatives of the four-ring component, pyrene. These properties were significantly different than those of the indigenous asphaltenes in similar solutions concluding that the pyrene-based compounds proposed lack core features that represent real systems. Rakotondradany et al.<sup>34</sup> studied the self-association properties of a model compound based on alkyl hexabenzocoronenes. Their study showed that even at concentrations as high as 15 g/L

the model compound tends to form dimers, uncharacteristic of indigenous asphaltenes. Tan et al studied the self-association, cracking and coking properties of archipelago pyrene-based model compounds<sup>35, 36</sup>. The authors found that the compounds self-associate due to  $\pi$ - $\pi$  stacking interactions involving the pyrene rings and the bypyridine spacer and that the model compounds in the presence of heteroatoms exhibited coke yields comparable to hydrocarbon compounds. Molecular dynamic simulations (MDS) performed by S. Bhattacharjee and J. Masliyah<sup>37, 38</sup> using different model compounds (archipelago, continental and anionic continental) showed that molecules with charged terminal groups are tethered to the toluene-water interface whereas uncharged compounds do not. Additionally, they found that the stacked polyaromatic rings are perpendicularly inclined to the same interface.

The research by Sjöblom and coworkers<sup>39, 40</sup> on model compounds consisting of a polyaromatic core (perylene-based) with a fixed hydrophobic part in one side and branched alkyl chains of varying end-groups (acidic-end or aliphatic-end) in the other, showed that several features of indigenous asphaltenes can be mimicked. In particular, the model compound C5Pe exhibited similar solubility in heptane-toluene mixtures and similar IFT curve compared to indigenous asphaltenes. Studies at the water-air interface using Brewster Angle Microscopy (BAM) suggest that the polar groups adopt a *head-on* conformation with a face-to-face packing of the core. That is, the polar head (acidic group) prefers the aqueous phase and the polyaromatic cores stack normal to the surface.

A better and thorough understanding of sorption and rheological aspects of asphaltenes is needed. Hence in this work, a study based on asphaltene model compounds at the liquid/liquid and liquid/air interface is proposed and their properties whether similar or different are compared to the behavior of indigenous asphaltenes described in the literature. A series of pendant drop and shear rheology experiments are performed not only to achieve this goal but also to serve as an example of the importance of distinguishing between processes driven by surface/interfacial tension (adsorption/ desorption) that give rise to an apparent elasticity and processes dominated by extra deviatoric stresses that provide true linear viscoelastic moduli, material functions and elasticity in the rigorous sense. Although the system chosen for this work is aimed to establish more realistic model systems that resemble indigenous asphaltenes, the results can be extended to other colloidal systems.

## **2. Experimental section**

*Solvents and chemicals.*



12-tricosanone (97%), used as the starter for model compound synthesis and n-heptane (for analysis Emsure Reag. PhEur) were purchased from VWR-Norway. Toluene (99.8% anhydrous) used to prepare all the model compound solutions and other chemicals necessary for synthesis were purchased from Sigma-Aldrich. All chemicals were used as received with no further purification.

#### *Asphaltene model compounds.*

Two asphaltene model compounds were used for this work. The first one, named C5PeC11, has an acidic functionality. The second one, named BisAC11 has little to no interfacial activity. C5PeC11 was synthesized by following the 4-step procedure described in Nordgård et al.<sup>40</sup> and Holman et al.<sup>41</sup> and by replacing 7-tridecanone with 12-tricosanone. 12-tricosanone is first treated with ammonium acetate and sodium cyanoborohydride in isopropyl alcohol to convert it into its corresponding amine. The amine is then reacted with perylene-3,4,9,10-tetracarboxylicdianhydride in the presence of imidazole. This step yields BisAC11 as an intermediate product. BisAC11 is further treated with potassium hydroxide in tert-butanol to obtain a monosubstituted intermediate. This compound is then reacted with 6-aminohexanoic acid in imidazole. Fig. S1 of the supporting information provides the chemical structure and the molar mass of the model compounds of this study.

Intermediate and final products were characterized by <sup>1</sup>H NMR spectroscopy in CDCl<sub>3</sub>. All the peaks are accounted for and yield a match with the expected chemical structure; hence the purity of these compounds is assumed to be very good. C5PeC11 was purified by flash chromatography on silica gel using a methanol-chloroform mixture (0-5% in CHCl<sub>3</sub>) as eluent. BisAC11 was purified by contact with silica particles (Aerosil 200) for 24h to remove any surface active impurities.

*Water phase.* The water phase for adsorption/desorption measurements and for dilatational rheological measurements was a buffer solution of pH 8 prepared with Mili-Q water (resistivity of 18.2 MΩ·cm) and 0.1M KH<sub>2</sub>PO<sub>4</sub> adjusted with 0.1M NaOH solution. The water phase for the compression-expansion curves and shear rheology experiments were buffer solutions of pH 5 (0.2M CH<sub>3</sub>COONa·3H<sub>2</sub>O adjusted with 0.2M CH<sub>3</sub>COOH), pH 6 (0.1M KH<sub>2</sub>PO<sub>4</sub> adjusted with 0.1M NaOH) and pH 8 (0.1M KH<sub>2</sub>PO<sub>4</sub> adjusted with 0.1M NaOH) prepared with Mili-Q water.

#### *Interfacial tension, dilatational rheology and desorption measurements.*

A commercially available sessile/pendant drop tensiometer (PAT 1m, SINTERFACE Technologies, Berlin, Germany) was used. This instrument determines the surface/interfacial tension of a surfactant-covered liquid droplet (or air bubble) by recording its silhouette onto a CCD camera. The digital images are then analyzed and fitted to the Young-Laplace equation with an accuracy of  $\pm 0.1 \text{ mN/m}$ . This equation relates the curvature of a liquid drop and the surface/interfacial tension. The built-in software produces a series of theoretical curves by changing the values of the surface/interfacial tension. The curve that yields the best fit to the experimental points is then used to report the measured surface/interfacial tension. For this procedure, only the densities of the oil and aqueous phase are needed. This technique is also known as axisymmetric drop shape analysis (ADSA). It is important to note that for systems dominated by surface/interfacial tension (adsorption/desorption) as, for instance, the present study, the contributions of extra mechanical stresses are negligible thus the Young-Laplace equation remains valid. However, for systems in which these deviatoric stresses are not negligible (for example asphaltenes that are known to form an elastic interfacial skin) the validity of the equation is questionable.

Desorption experiments were performed with a previously used<sup>42, 43</sup> accessory to the tensiometer that consists of two concentric capillary tubes (a schematic is shown in Fig. S2 of the supporting material). Material can be pumped or withdrawn independently by two automatic pumps. An oil droplet (i.e. C5PeC11 droplet in toluene) is formed at the tip of an outer capillary with one automatic pump and the droplet is allowed to equilibrate for a fixed period of time ( $t_0 = 30 \text{ min}$ ) inside a cuvette (25 mL) that contains the aqueous solution (pH 8 buffer). The volume of the droplet is  $V_D = 18 \mu\text{L}$ . This particular equilibration time was chosen for practical reasons and because the equilibrium interfacial tension did not change even after 6h. After the fixed equilibration time, the convection-driven subphase exchange inside the well-mixed droplet begins. The subject solution (toluene, HepTol or BisAC11) is injected through an inner capillary the second pump at a given volumetric flow rate ( $Q = 0.4 \mu\text{L/s}$ ). During this stage, the droplet volume is kept constant at  $V_D = 18 \mu\text{L}$  through simultaneous withdrawal from the outer capillary using the first pump and video feedback control. Once the total predetermined volume ( $V_E = 1000 \mu\text{L}$ ) has been exchanged, pumping/withdrawal stops. The IFT then reaches a plateau value. This process takes exactly  $V_E/Q = (1000 \mu\text{L})/(0.4 \mu\text{L/s}) = 2500 \text{ s}$ . The interfacial tension is continuously measured during all stages of the experiments. The plots regarding desorption experiments correspond to the average of two duplicates and only the IFT-time lapse of the desorption stage is shown

(2500s, that is from  $t_0$  until  $V_E$  has been exchanged) as a function of the characteristic time ( $Q(t' - t_0)/V_D$  or simply  $Qt/V_D$ ) where  $t'$  corresponds to the total time. . To avoid handling a large number of experimental points, a 2 s moving average was used. All experiments were performed by duplicate at 22°C and the experimental conditions were set up based on our previous studies<sup>42,43</sup>. Additional details on the technique can be found elsewhere<sup>44,45</sup>.

Interfacial dilatational rheology measurements were automatically started after the fixed equilibration time of 30min. Once again, the volume during the oscillations is controlled by the software via constant feedback. Five cycles at five different frequencies were performed using an amplitude of 7% ( $20 \pm 1.4 \mu\text{L}$ ). The five frequencies were 0.01, 0.013, 0.02, 0.04 and 0.1 Hz.

#### *Langmuir trough experiments*

Compression-expansion curves performed at a liquid-air interface and a liquid-liquid interface were also completed in Langmuir troughs (KSV Instruments Ltd, Finland) with dimensions of 75 x 330 mm and 65 x 260 mm, respectively. Experiments were performed at 22°C, and a platinum Wilhelmy plate with a perimeter of 39.44 mm attached to a Wilhelmy balance (KSV Instruments Ltd.) was used to measure surface tension. All compression-expansion experiments were performed at a constant rate of barrier movement of 3 mm/min.

#### *Interfacial shear rheology.*

Shear rheological measurements were performed with a double wall ring (DWR) geometry<sup>46</sup> attached to a Discovery HR-3 rheometer (TA Instruments). The ring is 7 cm in diameter with a thickness of 1mm and was produced with additive manufacturing (Layerwise, Leuven) from titanium (Ti6Al4V Grade 5). The cross section of the ring is square and rotated 45 degrees such that two corners sit in the interfacial plane and pin the interface to the geometry. There are 3 evenly spaced openings in the ring to facilitate a homogeneous distribution of interfacial material inside and outside the confines of the ring geometry<sup>47</sup>. The cup geometry is Teflon and can be placed within the Langmuir trough. The cup has two openings to allow the interfacial coverage to come to equilibrium inside and outside the cup perimeter, and it has a 0.5 mm deep step on the inside of the cup to pin a horizontal interface. The distance between the inner and outer walls at the point of pinning is 8 mm. Surface shear viscosities of approximately  $10^{-5}$  Pa.s.m can be resolved with this setup and this geometry. Since these experiments are performed at constant area and with well-defined kinematics, extra stresses

originate solely from the deformation of interfacial structure and can be related to proper material functions.

### 3. Theory

Theoretical considerations can be divided in three stages: (1) interfacial tension data (2) Apparent interfacial dilatational elasticity and apparent elastic modulus modeled using the approach proposed by Lucassen-van den Tempel<sup>23</sup> and (3) extra stresses probed by interfacial shear rheology and the soft glassy rheology model (SGR)<sup>48</sup>.

*Langmuir Isotherm.*

Equation (1), is a two parameter equation which assumes that there are no interactions between the adsorbed species and that the molecules are reversibly adsorbed as a monolayer. The analogous equation of state (2) is known as the Szyszkowski equation, as reported by Chang and Franses<sup>49</sup>.

$$\Gamma = \Gamma_{\infty} \left( \frac{K_L c}{1 + K_L c} \right) \quad (1)$$

$$\pi = nRT\Gamma_{\infty} \ln(1 + K_L c) \quad (2)$$

In these equations,  $\Gamma$  is the surface coverage,  $\Gamma_{\infty}$  is the surface excess at the saturation point,  $K_L$  is commonly known as the adsorption equilibrium constant,  $\pi$  is the difference in interfacial/surface tension between a freshly formed interface/surface and the value at a given concentration of surface active species,  $c$  is the bulk concentration and  $n$  is a parameter that accounts for the adsorption of counter-ions. In this case this parameter is equal to one<sup>49</sup>.

A desorption model based on equations (1) and (2) was established by Svitova et al.<sup>50</sup> for the convective-type of flow present in a coaxial capillary. They proposed equation (3) to be used in equation (2) and successfully described desorption of non-interacting and reversibly adsorbed species under convection flow. Pradilla et al.<sup>42</sup> used this model to successfully describe desorption of simple surfactants at the liquid-liquid and liquid-air interface.

$$C = C_0 \exp(-Qt/V_D) \quad (3)$$

In this equation,  $C$  is the evolution of the concentration inside the drop during desorption,  $C_0$  is the initial bulk concentration,  $Q$  is the volumetric flow rate,  $t$  is the time of the desorption stage and  $V_D$  the volume of the droplet.

*Interfacial dilatational rheology.*

Axisymmetrical drop shape analysis (ADSA) has been recognized as a reliable method for measuring adsorption/desorption dynamics and the compressibility of the interface<sup>51, 52</sup>, and provided that the contributions of extra mechanical stresses are negligible, it is an accurate method for interfacial tension experiments.

The principle behind the oscillating drop is that the interfacial tension varies when the area ( $A$ ) of a droplet is changed in an oscillatory manner at a given frequency ( $\omega$ ) from an initial ( $A_0$ ) to a value ( $A_a$ ) following equation (4)<sup>53</sup>.

$$\Delta A = A - A_0 = A_a \sin(\omega t) \quad (4)$$

The complex dynamic apparent dilatational modulus ( $E^*$ ) is then typically defined as the Fourier transform ( $\mathcal{F}$ ) of the change in interfacial tension ( $\gamma$ ) relative to the change in interfacial area via equation (5)<sup>54</sup>. The complex modulus can also be interpreted by a real and an imaginary part. The real part characterizes the elastic properties of the interfacial layer and the imaginary part characterizes the viscous properties. These parts are referred as to the apparent elastic dilatational modulus  $E'$  and the apparent viscous dilatational modulus  $E''$ .

$$E^*(\omega) = \frac{\mathcal{F}\{\Delta\gamma(t)\}}{\mathcal{F}\{\Delta\ln(A(t))\}} = E'(\omega) + iE''(\omega) \quad (5)$$

Lucassen and van den Tempel<sup>23</sup> proposed a model for the variation of the elastic and viscous dilatational moduli as a function of the concentration ( $c$ ) which is only valid for flat surfaces. The main underlying assumption of this model is that the adsorption is diffusion-controlled. In this model, the elastic and viscous components of the complex modulus depend on the independent contributions of the so called Gibbs elasticity ( $E_0 = \Gamma(dy/d\Gamma)$ ) which characterizes the compressibility and a parameter that accounts for diffusion defined as:  $\Omega = \sqrt{D/2\omega}(dc/d\Gamma)$  in which ( $D$ ) is the diffusion coefficient. The apparent elastic and viscous dilatational moduli are therefore calculated using equations (6) and (7).

$$E'(\omega) = E_0 \frac{1 + \Omega}{1 + 2\Omega + 2\Omega^2} \quad (6)$$

$$E''(\omega) = E_0 \frac{\Omega}{1 + 2\Omega + 2\Omega^2} \quad (7)$$

Equation (6) and Equation (7) provide apparent moduli and not true material functions. It has been recently shown<sup>54</sup> how the curvature of the droplets will influence the measured apparent moduli. This is due to its impact on mass transport: unlike a planar surface in which the bulk concentration can be regarded as constant, in the case of a droplet surfactant depletion becomes relevant. Hence changes in the area will alter the lengthscale over which diffusion occurs. The authors also propose that this transition from a planar transport timescale to the faster spherical timescale can be used to establish the dominant transport mechanism for the measurement being made. Additionally, for systems in which extra stresses are significant, these effects are unaccounted for in the classical analysis for pendant drop experiments and dilatational rheology measurements<sup>53</sup>.

#### *Interfacial shear rheology.*

A model which describes the rheology of crowded systems in which rearrangement of internal structure is difficult is the soft glassy rheology (SGR) model<sup>48</sup>. This empirical model predicts rheological behavior of soft materials with meta-stability and structural disorder at high concentrations. A soft glassy material has time and frequency dependent viscoelastic properties, and the SGR describes this dependence in terms of an effective noise temperature. This effective noise temperature is indicative of the ability of a disordered, metastable microstructure to rearrange, and depends on internal microstructure and flow history. Thus, small values of effective noise temperature would indicate a highly arrested system, while large values indicate a system that will readily flow. For an effective noise temperature with a value between one and three the SGR model predicts<sup>48</sup>:

$$G' \propto \omega^{x-1} \text{ for } 1 < x < 3 \quad (8)$$

$$G'' \propto \omega^{x-1} \text{ for } 1 < x < 2 \quad (9)$$

where  $x$  is the effective noise temperature,  $\omega$  is the frequency, and  $G'$  and  $G''$  are the storage and loss moduli respectively. For an effective noise temperature between one and two the

model predicts a viscoelastic response with shear-thinning behavior and the same scaling of  $G'$  and  $G''$  with  $\omega$ . An effective noise temperature less than one indicates a glassy system with arrested dynamics<sup>48</sup>. The SGR model has been used to describe interfacial rheological properties in polymers at an air/water interface<sup>55</sup>, rough carbon black particles at a water/n-octane interface<sup>56</sup>, and indigenous asphaltenes at a water/hexadecane interface<sup>12</sup>.

## 4. Results and discussion

### 4.1 Adsorption and desorption dynamics.

**Adsorption isotherm.** Before determining the adsorption isotherm of C5PeC11, the influence of the pH on the equilibrium (30 min) interfacial tension at a fixed concentration (0.05mM) was assessed. This was done not only to show the influence of the acidic functionality of the molecule, but also to choose a suitable pH for the rest of the experiments. Fig. 1 shows that lower pH values do not strongly influence the equilibrium IFT. There is a sharp transition at pH 6, and IFT values decrease rapidly with increasing pH. At pH values greater than 9 it was not possible to generate a stable droplet for measurement, which suggests very low IFT values (<1-2 mN/m). Based on these observations, pH 8 was chosen as the water phase for the rest of the experiments of this work. The interesting aspect of Fig. 1 is that this behavior is similar to C<sub>6</sub>-asphaltene solutions in xylene at 0.1 g/L reported by Nenningsland et al.<sup>22</sup> when compared to the neutral and basic media.

The interfacial tension after an equilibrium time (aging) of 30 min as a function of the bulk concentration of C5PeC11 solutions in toluene is presented in Fig. 2. After the aging time, the changes in IFT were less than 0.2 mN/m, thus equilibrium was attained. The solid line represents the fit to the Langmuir equation of state (EoS). The equilibrium parameters obtained via equations (1) and (2) are also shown. The surface excess for this molecule was found to be  $\Gamma_{\infty} = 2.26 \times 10^{-6} \text{ mol/m}^2$  which yields a mean molecular area at maximum coverage of  $Mma = 73.46 \text{ \AA}^2/\text{molecule}$ . Nordgård et al.<sup>39,57</sup> measured the mean molecular area after adsorption onto silica particles and the limiting area ( $A_0$ ) on a surface-pressure isotherm at the liquid-air interface of a similar model compound, namely C5Pe. They reported the values 120 and 46  $\text{\AA}^2/\text{molecule}$  which are consistent with a *head-on* arrangement of the molecule at the interface. Taking these values into account, this means that the asphaltene model compound C5PeC11 adsorbs most likely perpendicular to the interface with the acidic group into the water phase and the rest of the molecule into the oil

phase. The surface-pressure isotherms of the upcoming sections will go into further details about the conformations at the interface.

All the assumptions behind the Langmuir EoS are not necessarily met, especially since the system C5PeC11/Toluene does not exhibit complete reversibility of adsorption as it will be shown in later sections. However, from a semi-quantitatively point of view, the equilibrium parameters are of the same order of magnitude to those obtained by Pradilla et al.<sup>43</sup> for C<sub>6</sub>-asphaltene solutions in xylene ( $K_L = 228 \text{ m}^3/\text{mol}$  and  $\Gamma_\infty = 9.54 \times 10^{-7} \text{ mol}/\text{m}^2$ ) and a demulsifier of similar molecular weight ( $K_L = 834 \text{ m}^3/\text{mol}$  and  $\Gamma_\infty = 1.06 \times 10^{-6} \text{ mol}/\text{m}^2$ ). These values give a semi-quantitative notion of their surface activity and are only valid as long as the area is kept constant. When compression/expansion occurs, the equilibrium parameters evidently change.

**Interfacial dilatational rheology.** The influence of pH on the apparent elastic dilatational modulus measured after an equilibration time of 30min is also presented in Fig. 1 for two different frequencies. The apparent elastic modulus increases when the pH increases and tends to reach a plateau at high pH values. Similar results were obtained when the equilibration time was changed to ~6h (results not shown). This behavior was expected because of the acidic nature of the molecule. The important aspect of this trend is that it is very similar to that reported for C<sub>6</sub>-asphaltene solutions in xylene under similar conditions<sup>22</sup>. They obtained an increase of the apparent elastic dilatational modulus from ~10 to ~25 mN/m when the pH changed from 6 to 12 under similar experimental conditions. The values however are always higher for asphaltenes due to the known phenomenon of the formation of a mechanically robust film at the interface (skin). This could indicate that the acidic functional groups present in asphaltenes are largely responsible for the interfacial behavior at liquid-liquid interfaces<sup>58</sup>.

To test the system C5PeC11/Toluene for skin formation, a series of droplet contraction/expansion qualitative experiments similar to those performed by Jeribi et al.<sup>7</sup> were done on C5PeC11 droplets. First, a droplet of C5PeC11 in toluene is formed at the tip of a capillary. Second, the droplet is aged for a fixed amount of time; in this case, 30 min. And third, the droplet is contracted and expanded rapidly, changing the volume up to 60% of the original value. In the case of asphaltene solutions in toluene reported by Jeribi et al.<sup>7</sup>, the “skin” is clearly visible as well as droplet distortion after the given aging times (crumpling). Additionally, after the contraction/expansion cycles, the original shape of the droplet was



never recovered. These remarks were explained through asphaltene multilayer formation and the irreversibly adsorbed nature of the asphaltene rigid layer. Fig. S3 of the supporting material shows the contraction/expansion experiments for C5PeC11 solutions in toluene and there is no indication of skin formation, even after 5 consecutive cycles the shape after compression remained the same and the Young Laplace equation fitted it well. This does not mean extra stresses are absent, but it indicates that the response to dilatational deformations is dominated by interfacial tension and its variations.

Fig. 3a and 3b show the evolution of the apparent elastic and viscous dilatational moduli as a function of the concentration of C5PeC11 solutions in toluene after an equilibration time (aging) of 30 min. The apparent moduli were measured at five different frequencies ranging from 0.01 to 0.1 Hz. These frequencies were chosen to compare the results obtained with the model compound to those reported in the literature for asphaltenes of different sources<sup>18, 19, 21, 22</sup>. The general trend of the curves to shift towards areas of lower apparent elastic (and viscous) modulus as the frequency decreases. This behavior is expected because at low frequencies (0.01 Hz), the expanding interface is exposed to the bulk for longer times allowing diffusion mechanisms to restore the surface tension to its equilibrium value. At high frequencies the timescale of the deformation is fast compared to the diffusive time scale and changes in area lead to variations in surface tension that are picked up in the measurement as an apparent elasticity<sup>18</sup>. An important feature of Fig. 3 is that the apparent moduli increase as a function of concentration, congruent with the increase in Gibbs elasticity ( $E_0$ ). At high concentrations ( $>0.05$  mM), after a maximum, both contributions decrease and reach a plateau. This behavior is precisely what has been observed for asphaltenes<sup>21</sup> and crude oil solutions<sup>20</sup>. Care should be taken here when interpreting the data. Although the trends in the apparent elastic and viscous moduli are similar between asphaltenes and C5PeC11, adsorption features are different. Whereas asphaltenes are known to irreversibly adsorb at the liquid-liquid interface with subsequent multilayer stacking and “skin” formation, which influences the Young Laplace equation fit, C5PeC11 does not form such a skin. The results in the next section strongly suggest that the relaxation of C5PeC11 is almost purely diffusional, and that the observed effects can be attributed to changes in surface tension.

Fig. 3 shows the fits of the apparent elasticity using the LvdT model for C5PeC11 solutions in toluene at different frequencies and bulk concentrations. The fitting procedure is performed assuming that the Langmuir EoS remains valid which allows setting  $E_0 = \Gamma_\infty K_L c R T$  for each concentration taking the values from Fig. 2. In this way, the parameters  $\Omega$

and  $\omega$  present in equation (6) and equation (7) are fixed. This leaves the diffusion coefficient  $D$  as the only variable to be adjusted to the best match of the experimental data. Fig. 3a and 3b show the best fit to the elastic and viscous dilatational moduli respectively, with a diffusion coefficient (which is the material property underlying the phenomena) of  $4 \times 10^{-10} \text{ m}^2/\text{s}$ . This value for the diffusion coefficient is comparable to those reported by Chang et al.<sup>59</sup> for molecules of similar molecular weight. Although the predictions of the model are not perfect, they describe the evolution qualitatively, especially in the vicinities of the maxima, which are well predicted, and the decrease of the moduli at higher bulk concentrations. This suggests that C5PeC11 adsorption governs the phenomena, and that this is reversible, a fundamental assumption underpinning the LvdT model. It was also shown that there is no skin (or crumpling) preset at the interface even at long aging times and that thermodynamic equilibrium between interface and bulk was attained. The adsorption of C5PeC11 is almost completely reversible, meaning that after desorption experiments the interfacial tension of pure toluene/water is almost achieved. The small portion of C5PeC11 that remains at the interface could explain the prediction differences of the LvdT model.

Different attempts have been reported in the literature to improve the fit of the interfacial dilatational rheology data of indigenous asphaltenes<sup>17, 18, 19, 20, 22</sup> using the LvdT approach and assuming different mathematical variations of the asphaltene diffusion coefficient with concentration. The assumed diffusion coefficients are generally low ( $1 \times 10^{-11} \text{ m}^2/\text{s}$  -  $1 \times 10^{-10} \text{ m}^2/\text{s}$ <sup>21</sup> or  $1 \times 10^{-18} \text{ m}^2/\text{s}$  -  $2 \times 10^{-12} \text{ m}^2/\text{s}$ <sup>42</sup>). However, LvdT is not a general model describing the response to interface deformations, as it describes only the response to variations of the surface tension governed by the Gibbs elasticity and the time scale of transport to and from the interface. In the case of asphaltenes there are several other effects that may contribute. First, asphaltene adsorption is almost irreversible<sup>43</sup>. Secondly, extra stresses inherent to the interface are not accounted for in the LvdT model<sup>54</sup>. Also multilayer formation may occur which will influence the response to changes in area. In this sense, there is a fundamental difference between the behavior of indigenous asphaltenes and the asphaltene model compound C5PeC11. Even though several aspects of interfacial dilatational rheology, in particular those related to changes in surface tension, are similar and can be used to make predictions about the stability of the equivalent emulsions, some phenomena are not present in C5PeC11 adsorption, especially that of skin formation.

**Desorption from the liquid-liquid interface.** This section deals with the study of desorption of the asphaltene model compound C5PeC11 from the liquid-liquid interface by means of

three different substances: desorption of the model compound by pure solvent (in this case toluene) is first presented, followed by desorption by a mixture of heptane and toluene (HepTol) close to the precipitation onset, ending with desorption induced by the model compound BisAC11. This was achieved using a double-capillary system (Fig. S2 of the supporting material) accessory to the ADSA instrument. This system has been previously used to study desorption of asphaltenes and model demulsifiers, hence details on how it works can be found elsewhere<sup>42, 43</sup>.

Fig. 4 shows a plot of the interfacial tension as a function of the dimensionless characteristic time ( $Qt/V_D$ ) for desorption of C5PeC11 at three different concentrations induced by toluene. For comparison purposes, a desorption model based on the Langmuir isotherm is also included (equation (3)). This model has been shown to adequately describe desorption of non-interacting reversibly adsorbed species at the liquid/air<sup>50</sup> and liquid-liquid<sup>42</sup> interface. However, desorption of C5PeC11 is slower than the prediction which suggests the presence of interactions at the liquid/liquid interface among the model compound. These interactions, which are rather weak to be detected by dilatational experiments dominated by surface tension changes, are most likely due to intermolecular forces such as hydrogen bonding and  $\pi$ - $\pi$  stacking of the core as it will be shown in later sections. From the desorption experiments it could be possible, in principle, to calculate a convective mass transfer coefficient. However this goes beyond the scope of this article.

The data in Fig. 4 suggest that the adsorption is almost fully reversible. Comparing the final value of the interfacial tension after desorption,  $\gamma \sim 33 \text{ mN/m}$ , and the value for toluene/aqueous solution,  $\gamma \sim 36 \text{ mN/m}$ , it can be concluded that there is some material that remains irreversibly adsorbed at the interface (within the time scales of the experiment). Fig. 5 shows similar data, but desorption is now induced by a mixture of heptane-toluene or, "HepTol" at 30/70 (%v/v) and the model compound BisAC11 has an aliphatic end group. The filled symbols in Fig. 4 show that when using a HepTol mixture that is close to the precipitation onset of the asphaltene model compound, the degree of desorption is the same as that of toluene (open symbols). It is important to highlight that C5PeC11 was dissolved in the same HepTol mixture for this curve (filled symbols). From this it follows that the reversible nature of adsorption of C5PeC11 onto the liquid-liquid interface is not related to its solubility. Even in a poor solvent (HepTol), desorption was the same as in a good solvent (pure toluene). Extrapolating this idea to asphaltenes, which also precipitate in HepTol solutions at volume fractions  $\sim 30/70\%$  and  $\sim 40/60\%$ <sup>60</sup>, it could be hypothesized that the

irreversibility in their adsorption is not related to their poor solubility but instead to other mechanisms such as changes in conformations and  $\pi$ - $\pi$  interactions at the interface. Strong interactions might be responsible for the observed delay in desorption when comparing with a non-interacting model (Fig. 4) which was also previously observed for asphaltenes<sup>42</sup>.

Fig. 5 contains data on the desorption curves of C5PeC11 at a fixed concentration of 0.1mM induced by the asphaltene model compound BisAC11, which has an aliphatic end group. Two concentrations of BisAC11 were chosen: a lower concentration of 0.05mM and a higher concentration of 1.74 mM which is roughly 20 times greater than that of C5PeC11. The model compound BisAC11 has little to no influence on the desorption of C5PeC11 suggesting that there are little to no interactions between these two model compounds. More importantly, the delay in C5PeC11 desorption that occurs between  $Qt/V_D \sim 0-15$  and the final values of the interfacial tension  $\gamma \sim 33$  mN/m indicate that the portion of irreversibly adsorbed C5PeC11 does not interact with BisAC11 at the liquid-liquid interface. The small decrease in the interfacial tension that occurs at a high concentration of BisAC11 after  $Qt/V_D \sim 25$  is attributed to surface active impurities that accumulate at the interface and the low surface active nature of BisAC11 that could potentially displace small portions of C5PeC11 or fill empty pockets created by desorption of large aggregates. To emphasize this point, the equilibrium interfacial tension of BisAC11 in toluene was measured at pH 8 and found it to be  $\gamma \sim 34.5$  mN/m suggesting, once again, low to no interfacial activity of this compound. This type of minor interactions between C5PeC11 and BisAC11 at the liquid/liquid interface could be comparable to that of acidic and non-acidic components of crude oil that exhibit a similar behavior in terms of interfacial tension<sup>61</sup>.

#### **4.2 Extra stresses as probed by shear rheology.**

At an air/water interface C5PeC11 behaves as an insoluble Langmuir film. Although the behavior of an interfacially active material at an air/water interface is expected to be significantly different than at an oil/water interface, one can learn a great deal about certain aspects of interfacial behavior, such as the tendency to aggregate. Model molecules at an air/water interface may display certain features characteristic of skin-forming asphaltenes.

In Fig. 6a a series of compression-expansion curves for C5PeC11 at an air/water interface and a pH of 6 are shown. Cycles of compression-expansions were consecutive, the first of which began 30 minutes after spreading C5PeC11 from toluene. The first compression curve in Fig. 6a is different than all of the following compression curves, and has a local maximum

at a molecular area of approximately  $90 \text{ \AA}^2/\text{molecule}$ . This bump in the curve is a non-thermodynamic behavior that appears at a molecular area consistent with the molecules of C5PeC11 at monolayer coverage and with a strong tilt. The competing dynamics involved are the continuous compression of the interface and the slow dynamics associated with rearrangement of the molecules at the interface as they become increasingly confined. The local maximum in the curve is present only in the first compression, suggesting that the initial state of the interface is dependent on the initial solvent spreading and evaporation history. After the first compression-expansion, consecutive curves in Fig. 6a look similar but continue to shift to lower values of molecular area with each compression-expansion. In an insoluble system this behavior is indicative of irreversible aggregate formation at large surface pressures and the formation of multilayers. Evidence for the surface-pressure dependence of aggregate formation is seen in Fig. 6b, where consecutive compression-expansion curves are shown but the surface pressure never exceeds  $30 \text{ mN/m}$  (i.e. a surface pressure lower than the collapse value). At low surface pressures, after the first compression, consecutive compression-expansion curves are repeatable and indicate that aggregate formation is strongly surface-pressure dependent. Data in Fig. 6 suggest that C5PeC11 has a slow dynamic associated with molecular rearrangements at monolayer coverage, and at high surface coverage there is a driving force toward irreversible aggregation and the formation of multi-layer structures<sup>62</sup>.

Rheological behavior is coupled to material microstructure, and the rheological data shown in Fig. 7 is indicative of a material with elastic, fragile microstructure. In Fig. 7a storage and loss moduli are plotted as a function of strain at  $30 \text{ mN/m}$ . The deviation from a linear viscoelastic regime begins at relatively small strain values of 0.2 to 0.5%. The structures which dominate the transfer of stress through the interface are easily ruptured. Frequency sweep data obtained at 0.1% strain is shown in Fig. 7b and reveals that a broad range of relaxation times are present in C5PeC11 at the air/water interface. The values of the storage moduli show that significant elasticity is present at the interface, as expected for a strongly interacting insoluble system.

The behavior of C5PeC11 at the oil/water interface is more relevant for comparison to indigenous asphaltene behavior in crude oil emulsions and the data presented in the previous sections. Compression-expansion curves from C5PeC11 at a decane/water interface are shown in Fig. 8. Prominent in the compression curves is the non-thermodynamic local maximum that was also observed in the first compressions in Fig. 6. In Fig. 8 the molecular

area at which this peak is found is 65-70 Å<sup>2</sup>/molecule. This is a smaller value than that found for the air/water interface in Fig. 6, and it can be explained in terms of the tilt of the molecules at the interface. With an oil phase, it would be expected that the hydrocarbon tails and aromatic groups of C5PeC11 would preferentially immerse in the oil phase, resulting in less tilt and a smaller molecular area at monolayer coverage. Unlike the air/water interface, the peak is observed on all consecutive compressions at the decane/water interface. The presence of oil makes the dynamics of molecular rearrangement reversible, and indicates the nature of the rearrangement; indigenous asphaltenes have the ability to undergo  $\pi$ - $\pi$  stacking and one might expect to observe similar behavior in C5PeC11 because of the prominent aromatic groups at the core of the molecule. The local maximum observed may be the competition between compression of the interface and the dynamics associated with the formation of  $\pi$ - $\pi$  stacks and rearrangement of the resulting domains. The reversibility of this behavior at an oil/water interface may be attributed to the ability of decane molecules to reinsert between molecules at low surface pressure, reversibly destroying bonds associated with  $\pi$ - $\pi$  stacking upon expansion of the interface. Although all compression-expansion measurements were made at a barrier movement rate of 3 mm/min, it is worth noting that the soluble nature of these molecules in the oil phase is expected to result in a dependence on compression rate that might affect both the hysteresis behavior and the non-thermodynamic local maximum observed during compression. The results are consistent with the data obtained in the pendant drop experiments.

Shear flow at a constant area isolates the mechanical response of the interfacial structure in the absence of adsorption/desorption dynamics. In this way the material functions give rise to the extra stresses generated at the interface and can be measured. Results for C5PeC11 at the decane/water interface at 30 mN/m are shown in Fig. 9. The linear viscoelastic regime is small, similar to the behavior observed in Fig. 6a for the air/water interface and again indicative of fragile structures. Storage and loss moduli as a function of frequency were obtained at a strain of 0.1%, and are shown in Fig. 9b. The magnitudes of the moduli are smaller than those for the water-air interface, and rather small. The frequency dependence reveals a viscoelastic structure with a broad range of relaxation time. This rheological behavior is characteristic of a soft-glassy material, where rearrangement under flow of a densely packed internal structure takes place with a broad range of characteristic times. The straight lines plotted in Fig. 9 come from fitting the soft-glassy rheology (SGR) model to the linear viscoelastic data in Fig. 9b. An effective noise temperature of 1.34 was obtained from

the fit, and the prediction of the SGR model of the scaling of  $G''$  in the non-linear regime is plotted in Fig. 9a. A value of the effective noise temperature between one and two is indicative of a soft-glassy rheological response with storage and loss moduli that both vary with respect to  $\omega^{x-1}$ . This behavior is characteristic of what is found in indigenous asphaltenes at surface concentrations sufficient to stabilize oil and water emulsions<sup>12, 63</sup>. A comparison of effective noise temperature measured here and values measured in indigenous asphaltenes by Samaniuk et al.<sup>12</sup> reveals that indigenous asphaltenes form a more arrested interface. Values of effective noise temperature between 1.3 and 1.4 were obtained in indigenous asphaltenes at surface pressures between 13 mN/m and 14 mN/m, and continued to decrease (indicating an increasingly arrested system) at higher surface pressures. The 1.34 value found here in the model molecule system was obtained at a high surface pressure of 30 mN/m, indicating that higher surface pressures are required in order to obtain the same effective noise temperature values observed in indigenous asphaltenes. This results in smaller extra stresses developing in the interface when deformed, which is in agreement with the absence of significant elastic effects contributing in the dilatational measurements. Although indigenous asphaltenes are a complex mixture of many molecules that form hierarchic structures, we have found here that it is nevertheless possible to capture important characteristics of their rheological behavior with model molecules of a single chemistry and architecture.

The influence of pH on the stabilizing effect of indigenous asphaltenes is significant, and pH modification has been considered as a strategy for emulsion breaking<sup>64</sup>. Compression curves for C5PeC11 at a decane/water interface are shown in Fig. 10a for three different subphase pH values. With the subphase at a pH of 8 the carboxylate functional group of C5PeC11 is highly deprotonated and expected to be more surface active than at lower pH. In addition to increased surface activity, a decrease in the tilt of the molecule at the interface is expected. This is seen in Fig. 10a as a shift of the location of the local maximum in the compression curve to lower values of molecular area. The value of  $66 \text{ \AA}^2/\text{molecule}$  is at the low end of the range of values obtained from similar particles adsorbed onto silica<sup>57</sup>, and consistent with a very upright orientation of the molecule at the interface. An illustration of this arrangement is shown in Fig. 10b, where the tilt-state of the C5PeC11 is expected to depend on the state of the carboxylate functional group. As the pH is decreased the carboxylate group becomes more protonated, less charged, and less surface active. At a pH of 5 the surface activity decreased significantly and the local maximum in the compression curve shifted to a

molecular area of  $105 \text{ \AA}^2/\text{molecule}$ , consistent with a highly tilted orientation of the molecules of C5PeC11. The strong dependence of the interfacial activity of C5PeC11 on pH is consistent with behavior observed in C<sub>6</sub>-asphaltenes<sup>22</sup>. The carboxylate functional group on C5PeC11 captures important aspects of this behavior.

## Conclusions

Sorption dynamics of C5PeC11, an asphaltene model compound, showed that it is almost reversibly adsorbed at the toluene/water interface even under conditions near the precipitation onset (Fig. 4 and Fig. 5). Interactions between C5PeC11 and BisAC11 at the same interface are not relevant, suggesting that alkyl end groups have little to no influence in asphaltene adsorption whereas polar interactions (COOH groups) dominate this behavior. Unlike indigenous asphaltenes, C5PeC11 does not exhibit skin formation and significant extra stresses at the interface. However, equilibrium parameters based on the Langmuir EoS and interfacial dilatational rheological results are similar, suggesting that these model compounds can be systematically used to study separately the interfacial tension related effects of indigenous asphaltenes. Unlike for indigenous asphaltenes the responses observed in pendant drop experiments are dominated by surface/interfacial tension (diffusion).

At the air/water interface C5PeC11 shows a strong hysteresis between the first compression-expansion cycle and consecutive cycles that is indicative of an irreversible rearrangement of the molecules upon the first compression. Compression to large surface pressures results in a shift of the consecutive curves to smaller molecular areas, a sign of aggregation and the formation of multilayer structures. At a decane/water interface the rearrangement of molecules during compression is reversible upon expansion and is attributed to the ability of oil molecules to penetrate  $\pi$ - $\pi$  stacking arrangements between C5PeC11 molecules. Soft-glassy rheological behavior is observed in C5PeC11, consistent with behavior observed in indigenous asphaltenes at an oil/water interface, but the behavior is less pronounced, congruent with observations in the dilatational experiments. In addition to soft glassy rheology, C5PeC11 shows a strong pH dependence that is very similar to that observed in indigenous asphaltenes. Although indigenous asphaltenes are polydisperse structures that aggregate to form larger clusters, we have found that important characteristics of asphaltenes at an oil/water interface, such as rheological behavior and pH dependence, can be captured with a single model molecule of a defined chemistry and architecture.

## Acknowledgements



The authors thank the JIP-Asphaltene consortium “Improved Mechanism of Asphaltene Deposition, Precipitation and Fouling to Minimize Irregularities in Production and Transport (NFR PETROMAKS)”, consisting of Ugelstad Laboratory (NTNU, Norway), University of Alberta (Canada), University of Pau (France) and Universidade Federal do Parana (Brazil) funded by the Norwegian Research Council (234112) and the following industrial sponsors: AkzoNobel, BP, Canada Natural Resources, Nalco-Champion, Petrobras, Statoil and Total E&P Norge AS.

## References

1. Speight, J. G. Chapter 11: Asphaltene Constituents. In *The chemistry and technology of petroleum*, 4th Edition ed.; CRC Press. Taylor & Francis group. : Boca Ratón, FL. , 2007, pp 315-344.
2. Mullins, O. C. The Asphaltenes. *Annual Review of Analytical Chemistry* **2011**, *4* (1), 393-418.
3. Hammami, A., Ratulowski, John. Chapter 23. Precipitation and Deposition of Asphaltenes in Production Systems: A Flow Assurance Overview. In *Asphaltenes, Heavy Oils, and Petroleomics*, Mullins, O. C., Sheu, E., Hammani, A., Marshall, A., Ed.; Springer, LLC, 2007.
4. Buckley, J. S. Asphaltene Deposition. *Energy & Fuels* **2012**, *26* (7), 4086-4090.
5. Gonzalez, D. L.; Vargas, F. M.; Hirasaki, G. J.; Chapman, W. G. Modeling Study of CO<sub>2</sub>-Induced Asphaltene Precipitation. *Energy & Fuels* **2008**, *22* (2), 757-762.
6. Kilpatrick, P. K. Water-in-Crude Oil Emulsion Stabilization: Review and Unanswered Questions. *Energy & Fuels* **2012**, *26* (7), 4017-4026.
7. Jeribi, M.; Almir-Assad, B.; Langevin, D.; Hénaut, I.; Argillier, J. F. Adsorption kinetics of asphaltenes at liquid interfaces. *Journal of Colloid and Interface Science* **2002**, *256* (2), 268-272.
8. Hannisdal, A.; Orr, R.; Sjöblom, J. Viscoelastic properties of crude oil components at oil-water interfaces. 1. The effect of dilution. *Journal of Dispersion Science and Technology* **2007**, *28* (1), 81-93.
9. Pensini, E., Harbottle, D., Yang, F., Tchoukov, P., Li, Z., Kailey, I., Behles, J., Masliyah, J., Xu, Z. Demulsification Mechanism of Asphaltene-Stabilized Water-in-Oil Emulsions by a Polymeric Ethylene Oxide–Propylene Oxide Demulsifier. *Energy & Fuels* **2014**.
10. Zhang, L. Y.; Xu, Z.; Masliyah, J. H. Langmuir and Langmuir-Blodgett films of mixed asphaltene and a demulsifier. *Langmuir* **2003**, *19* (23), 9730-9741.
11. McLean, J. D.; Kilpatrick, P. K. Effects of Asphaltene Solvency on Stability of Water-in-Crude-Oil Emulsions. *Journal of Colloid and Interface Science* **1997**, *189* (2), 242-253.
12. Samaniuk, J. R.; Hermans, E.; Verwijlen, T.; Pauchard, V.; Vermant, J. Soft-Glassy Rheology of Asphaltenes at Liquid Interfaces. *Journal of Dispersion Science and Technology* **2015**, *36* (10), 1444-1451.
13. Verruto, V. J.; Le, R. K.; Kilpatrick, P. K. Adsorption and Molecular Rearrangement of Amphoteric Species at Oil–Water Interfaces. *The Journal of Physical Chemistry B* **2009**, *113* (42), 13788-13799.
14. Fan, Y.; Simon, S.; Sjöblom, J. Interfacial shear rheology of asphaltenes at oil–water interface and its relation to emulsion stability: Influence of concentration, solvent aromaticity

- and nonionic surfactant. *Colloids and Surfaces A: Physicochemical and Engineering Aspects* **2010**, *366* (1–3), 120-128.
15. Spiecker, P. M.; Kilpatrick, P. K. Interfacial rheology of petroleum asphaltenes at the oil-water interface. *Langmuir* **2004**, *20* (10), 4022-4032.
  16. Harbottle, D.; Chen, Q.; Moorthy, K.; Wang, L.; Xu, S.; Liu, Q.; Sjoblom, J.; Xu, Z. Problematic Stabilizing Films in Petroleum Emulsions: Shear Rheological Response of Viscoelastic Asphaltene Films and the Effect on Drop Coalescence. *Langmuir* **2014**, *30* (23), 6730-6738.
  17. Bouriat, P.; El Kerri, N.; Graciaa, A.; Lachaise, J. Properties of a Two-Dimensional Asphaltene Network at the Water–Cyclohexane Interface Deduced from Dynamic Tensiometry. *Langmuir* **2004**, *20* (18), 7459-7464.
  18. Yarranton, H. W.; Sztukowski, D. M.; Urrutia, P. Effect of interfacial rheology on model emulsion coalescence: I. Interfacial rheology. *Journal of Colloid and Interface Science* **2007**, *310* (1), 246-252.
  19. Yarranton, H. W.; Urrutia, P.; Sztukowski, D. M. Effect of interfacial rheology on model emulsion coalescence: II. Emulsion coalescence. *Journal of Colloid and Interface Science* **2007**, *310* (1), 253-259.
  20. Alvarez, G.; Poteau, S.; Argillier, J. F.; Langevin, D.; Salager, J. L. Heavy oil-water interfacial properties and emulsion stability: Influence of dilution. *Energy and Fuels* **2009**, *23* (1), 294-299.
  21. Sztukowski, D. M.; Yarranton, H. W. Rheology of asphaltene-toluene/water interfaces. *Langmuir* **2005**, *21* (25), 11651-11658.
  22. Nenningsland, A. L.; Simon, S.; Sjöblom, J. Influence of Interfacial Rheological Properties on Stability of Asphaltene-Stabilized Emulsions. *Journal of Dispersion Science and Technology* **2014**, *35* (2), 231-243.
  23. Lucassen, J.; Van Den Tempel, M. Dynamic measurements of dilational properties of a liquid interface. *Chemical Engineering Science* **1972**, *27* (6), 1283-1291.
  24. Sjöblom, J.; Simon, S.; Xu, Z. Model molecules mimicking asphaltenes. *Advances in Colloid and Interface Science* **2015**, *218*, 1-16.
  25. Nalwaya, V.; Tantayakom, V.; Piumsomboon, P.; Fogler, S. Studies on Asphaltenes through Analysis of Polar Fractions. *Industrial & Engineering Chemistry Research* **2004**, *43* (23), 7682-7682.
  26. Marques, J. M., I.; Baudot, A.; Barré, L.; Guillaume, D.; Espinat, D.; Brunet, S. Asphaltenes Size Polydispersity Reduction by Nano- and Ultrafiltration Separation Methods – Comparison with the Flocculation Method. *Oil & Gas Science and Technology* **2008**, *63* (1), 139-149.
  27. Akbarzadeh, K., Hammami, A., Kharrat, A., Zhang, D., Allenson, S., Creek, J., Kabir, S., Jamaluddin, A., Marshall, A., Rodgers, R., Mullins, O., Solbakken, T. Asphaltenes: Problematic but rich in potential. *Oilfield Review* **2007**, 22-43.
  28. Yen, T. F.; Erdman, J. G.; Pollack, S. S. Investigation of the Structure of Petroleum Asphaltenes by X-Ray Diffraction. *Analytical Chemistry* **1961**, *33* (11), 1587-1594.
  29. Espinat, D. Application of Light, X-ray and Neutron Diffusion Techniques to the study of colloidal systems. *Rev. Inst. Fr. Pet* **1991**, *45*, 775-820.
  30. Groenzin, H.; Mullins, O. C. Asphaltene Molecular Size and Structure. *The Journal of Physical Chemistry A* **1999**, *103* (50), 11237-11245.
  31. Groenzin, H.; Mullins, O. C.; Eser, S.; Mathews, J.; Yang, M.-G.; Jones, D. Molecular Size of Asphaltene Solubility Fractions. *Energy & Fuels* **2003**, *17* (2), 498-503.
  32. Mullins, O. C. The Modified Yen Model. *Energy & Fuels* **2010**, *24* (4), 2179-2207.

33. Akbarzadeh, K.; Bressler, D. C.; Wang, J.; Gawrys, K. L.; Gray, M. R.; Kilpatrick, P. K.; Yarranton, H. W. Association Behavior of Pyrene Compounds as Models for Asphaltenes. *Energy & Fuels* **2005**, *19* (4), 1268-1271.
34. Rakotondradany, F.; Fenniri, H.; Rahimi, P.; Gawrys, K. L.; Kilpatrick, P. K.; Gray, M. R. Hexabenzocoronene Model Compounds for Asphaltene Fractions: Synthesis & Characterization. *Energy & Fuels* **2006**, *20* (6), 2439-2447.
35. Tan, X.; Fenniri, H.; Gray, M. R. Pyrene Derivatives of 2,2'-Bipyridine as Models for Asphaltenes: Synthesis, Characterization, and Supramolecular Organization. *Energy & Fuels* **2008**, *22* (2), 715-720.
36. Alshareef, A. H.; Scherer, A.; Tan, X.; Azyat, K.; Stryker, J. M.; Tykwinski, R. R.; Gray, M. R. Effect of Chemical Structure on the Cracking and Coking of Archipelago Model Compounds Representative of Asphaltenes. *Energy & Fuels* **2012**, *26* (3), 1828-1843.
37. Kuznicki, T.; Masliyah, J. H.; Bhattacharjee, S. Aggregation and Partitioning of Model Asphaltenes at Toluene-Water Interfaces: Molecular Dynamics Simulations. *Energy & Fuels* **2009**, *23* (10), 5027-5035.
38. Kuznicki, T.; Masliyah, J. H.; Bhattacharjee, S. Molecular Dynamics Study of Model Molecules Resembling Asphaltene-Like Structures in Aqueous Organic Solvent Systems. *Energy & Fuels* **2008**, *22* (4), 2379-2389.
39. Nordgård, E. L.; Landsem, E.; Sjöblom, J. Langmuir Films of Asphaltene Model Compounds and Their Fluorescent Properties. *Langmuir* **2008**, *24* (16), 8742-8751.
40. Nordgård, E. L.; Sjöblom, J. Model compounds for asphaltenes and C80 isoprenoid tetraacids. Part I: Synthesis and interfacial activities. *Journal of Dispersion Science and Technology* **2008**, *29* (8), 1114-1122.
41. Holman, M. W.; Liu, R.; Adams, D. M. Single-Molecule Spectroscopy of Interfacial Electron Transfer. *Journal of the American Chemical Society* **2003**, *125* (41), 12649-12654.
42. Pradilla, D.; Simon, S.; Sjöblom, J. Mixed interfaces of asphaltenes and model demulsifiers part I: adsorption and desorption of single components. *Colloids and Surfaces A: Physicochemical and Engineering Aspects* **2015**, *466*, 45-56.
43. Pradilla, D.; Simon, S.; Sjöblom, J. Mixed Interfaces of Asphaltenes and Model Demulsifiers, Part II: Study of Desorption Mechanisms at Liquid/Liquid Interfaces. *Energy & Fuels* **2015**, *29* (9), 5507-5518.
44. Ferri, J. K.; Gorevski, N.; Kotsmar, C.; Leser, M. E.; Miller, R. Desorption kinetics of surfactants at fluid interfaces by novel coaxial capillary pendant drop experiments. *Colloids and Surfaces A: Physicochemical and Engineering Aspects* **2008**, *319* (1-3), 13-20.
45. Ferri, J. K.; Miller, R.; Makievski, A. V. Equilibrium and dynamics of PEO/PPO/PEO penetration into DPPC monolayers. *Colloids and Surfaces A: Physicochemical and Engineering Aspects* **2005**, *261* (1-3), 39-48.
46. Vandebril, S.; Franck, A.; Fuller, G. G.; Moldenaers, P.; Vermant, J. A double wall-ring geometry for interfacial shear rheometry. *Rheologica Acta* **2010**, *49* (2), 131-144.
47. Hermans, E.; Vermant, J. Interfacial shear rheology of DPPC under physiologically relevant conditions. *Soft Matter* **2014**, *10* (1), 175-186.
48. Sollich, P. Rheological constitutive equation for a model of soft glassy materials. *Phys. Rev. E* **1998**, *58* (1), 738-759.
49. Chang, C. H.; Franses, E. I. Adsorption dynamics of surfactants at the air/water interface: a critical review of mathematical models, data, and mechanisms. *Colloids and Surfaces A: Physicochemical and Engineering Aspects* **1995**, *100* (C), 1-45.
50. Svitova, T. F.; Wetherbee, M. J.; Radke, C. J. Dynamics of surfactant sorption at the air/water interface: Continuous-flow tensiometry. *Journal of Colloid and Interface Science* **2003**, *261* (1), 170-179.

51. Ravera, F.; Loglio, G.; Kovalchuk, V. I. Interfacial dilational rheology by oscillating bubble/drop methods. *Current Opinion in Colloid & Interface Science* **2010**, *15* (4), 217-228.
52. Yeung, A.; Dabros, T.; Masliyah, J.; Czarnecki, J. Micropipette: a new technique in emulsion research. *Colloids and Surfaces A: Physicochemical and Engineering Aspects* **2000**, *174* (1-2), 169-181.
53. Derkach, S. R.; Krägel, J.; Miller, R. Methods of measuring rheological properties of interfacial layers (Experimental methods of 2D rheology). *Colloid Journal* **2009**, *71* (1), 1-17.
54. Reichert, M. D.; Alvarez, N. J.; Brooks, C. F.; Grillet, A. M.; Mondy, L. A.; Anna, S. L.; Walker, L. M. The importance of experimental design on measurement of dynamic interfacial tension and interfacial rheology in diffusion-limited surfactant systems. *Colloids and Surfaces A: Physicochemical and Engineering Aspects* **2015**, *467*, 135-142.
55. Srivastava, S.; Leiske, D.; Basu, J. K.; Fuller, G. G. Interfacial shear rheology of highly confined glassy polymers. *Soft Matter* **2011**, *7* (5), 1994-2000.
56. Van Hooghten, R.; Imperiali, L.; Boeckx, V.; Sharma, R.; Vermant, J. Rough nanoparticles at the oil-water interfaces: their structure, rheology and applications. *Soft Matter* **2013**, *9* (45), 10791-10798.
57. Nordgård, E. L.; Sørland, G.; Sjöblom, J. Behavior of asphaltene model compounds at W/O interfaces. *Langmuir* **2010**, *26* (4), 2352-2360.
58. Nenningsland, A. L.; Simon, S.; Sjöblom, J. Surface properties of basic components extracted from petroleum crude oil. *Energy and Fuels* **2010**, *24* (12), 6501-6505.
59. Chang, H. C.; Tsen, C. H.; Chang, C. H. A model for simulating the dynamic surface tension behavior of aqueous surfactant dispersions. *Colloid and Polymer Science* **2006**, *285* (1), 57-63.
60. Spiecker, P. M.; Gawrys, K. L.; Kilpatrick, P. K. Aggregation and solubility behavior of asphaltenes and their subfractions. *Journal of Colloid and Interface Science* **2003**, *267* (1), 178-193.
61. Hemmingsen, P. V.; Kim, S.; Pettersen, H. E.; Rodgers, R. P.; Sjöblom, J.; Marshall, A. G. Structural Characterization and Interfacial Behavior of Acidic Compounds Extracted from a North Sea Oil. *Energy & Fuels* **2006**, *20* (5), 1980-1987.
62. Zhang, L. Y.; Lopetinsky, R.; Xu, Z.; Masliyah, J. H. Asphaltene Monolayers at a Toluene/Water Interface. *Energy & Fuels* **2005**, *19* (4), 1330-1336.
63. Pauchard, V.; Rane, J. P.; Banerjee, S. Asphaltene-Laden Interfaces Form Soft Glassy Layers in Contraction Experiments: A Mechanism for Coalescence Blocking. *Langmuir* **2014**, *30*, 12795-12803.
64. Strassne, J. Effect of pH on interfacial films and stability of crude oil-water emulsions. *Journal of Petroleum Technology* **1968**, *20*, 303-312.

**Figure 1.** Influence of pH on the equilibrium interfacial tension values and the apparent elastic dilatational modulus of C5PeC11 at 0.05mM in toluene after 30min of equilibration. The solid lines are visual aids.

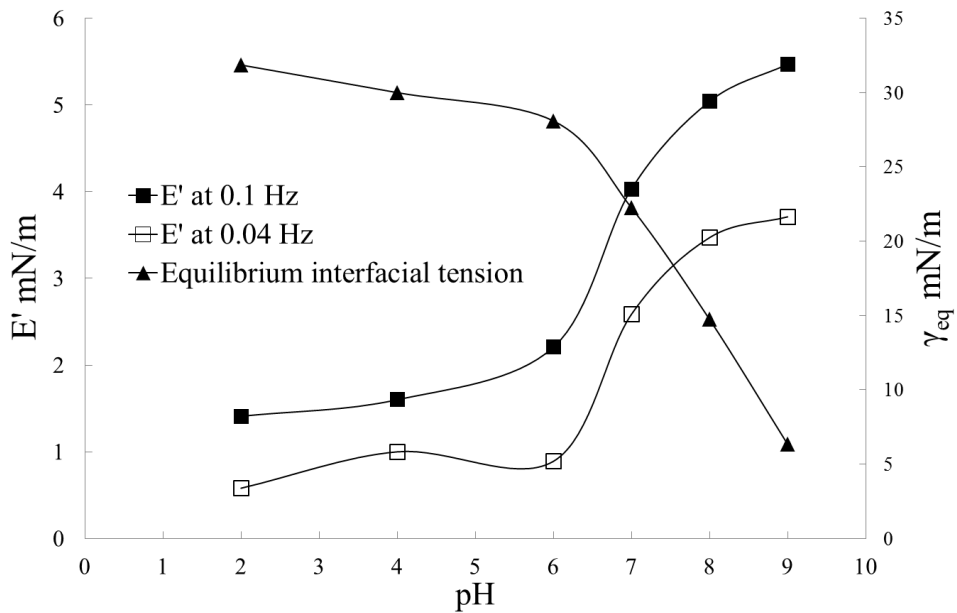


**Figure 2.** Equilibrium interfacial tension ( $\gamma_{eq}$ ) as a function of the bulk concentration for C5PeC11 solutions in toluene after 30 min of equilibration time. Experimental points measured using ADSA. The solid line represents the best fit to equations (1) and (2). Equilibrium parameters are also shown.

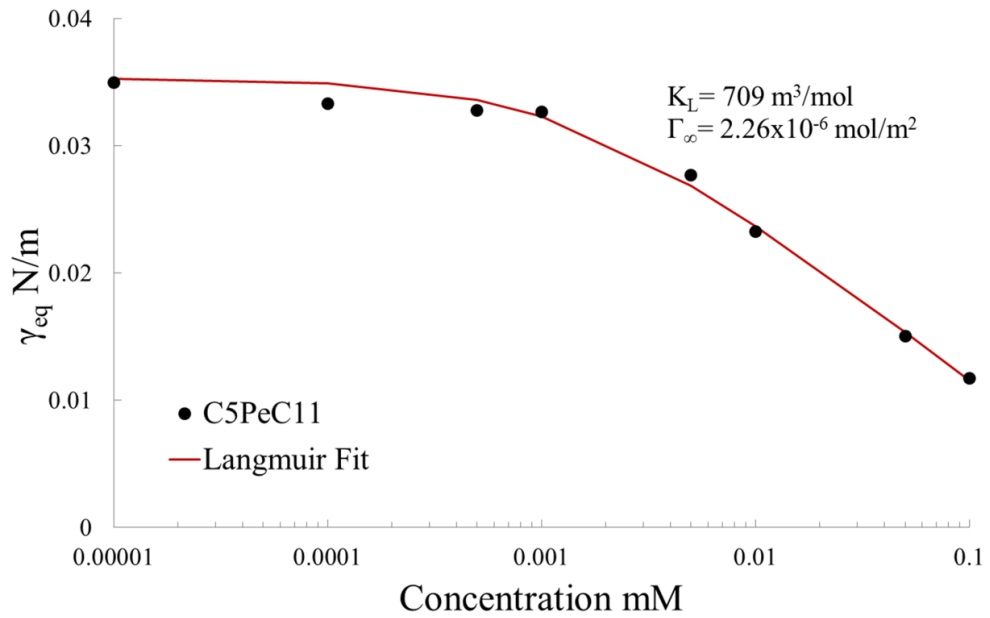


**Figure 3.** Measured (after 30 min of equilibration time) and modeled a) Apparent elastic modulus and b) Apparent viscous modulus of C5PeC11 solutions in toluene at different frequencies and bulk concentrations. The solid lines show the best fit with a diffusion coefficient of  $4 \times 10^{-10} \text{ m}^2/\text{s}$  using the Lucassen van den Tempel model (equations (6) and (7)).

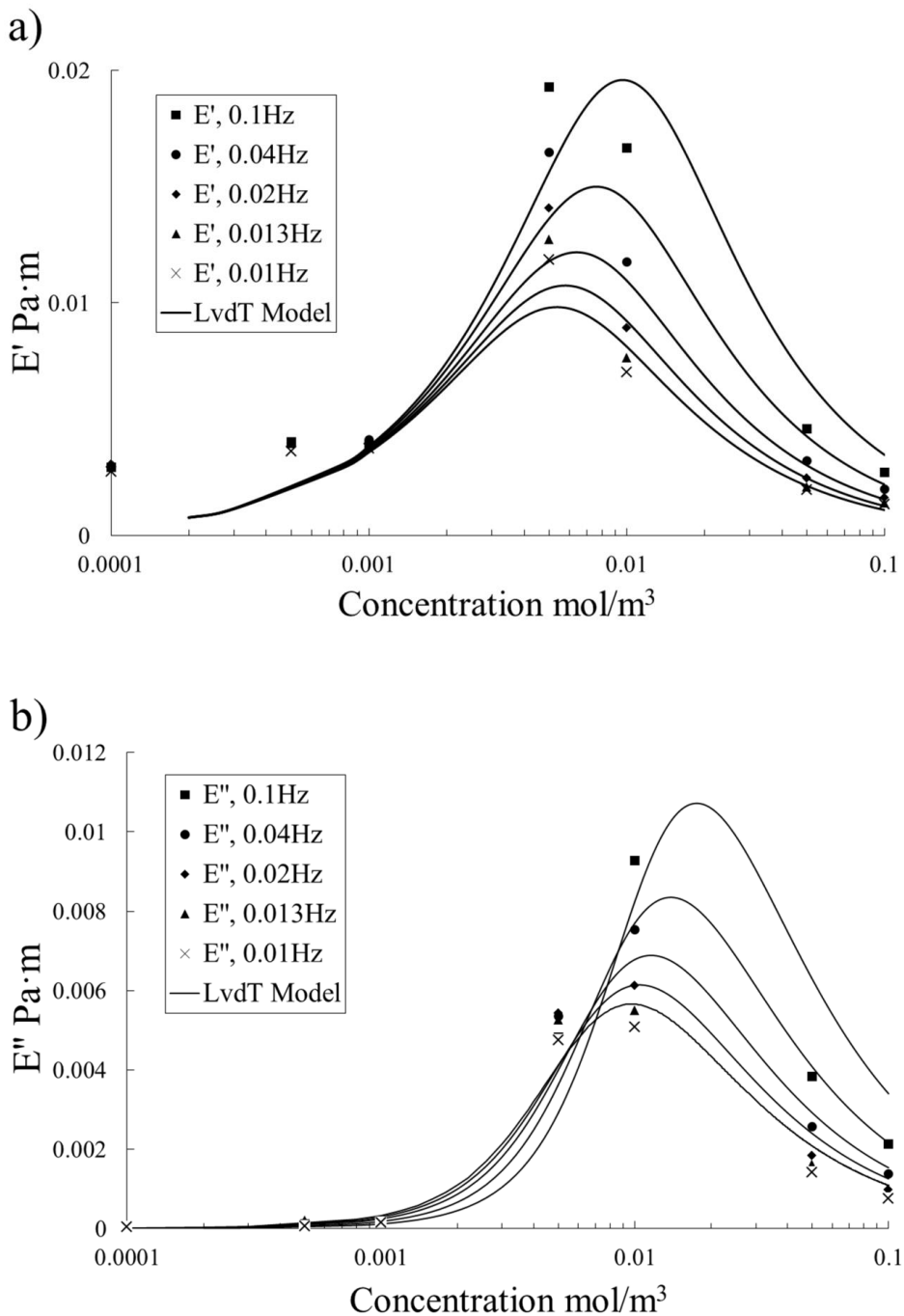


**Figure 4.** Interfacial tension as a function of the dimensionless characteristic time for desorption ( $Qt/V_D$ ) of C5PeC11 at three different concentrations by toluene. The experimental conditions for the experiments were: Exchange flow rate  $Q = 0.4 \mu\text{L/s}$ , total predetermined volume  $V_E = 1000 \mu\text{L}$  and volume of the droplet  $V_D = 18 \mu\text{L}$ . The solid red line represents the desorption model, or equation (3).

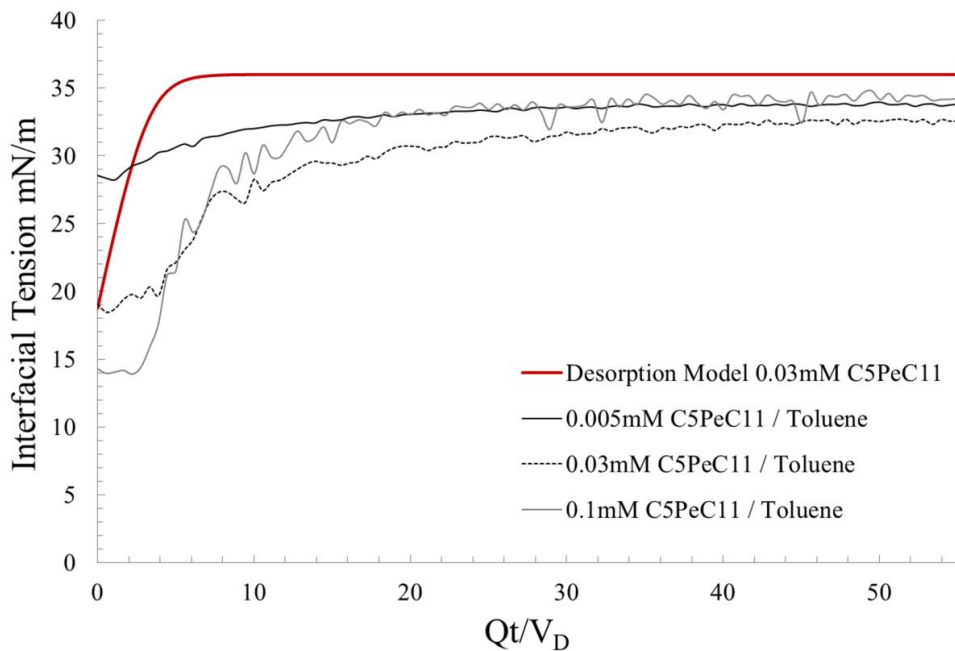




**Figure 5.** Interfacial tension as a function of the dimensionless characteristic time for desorption ( $Qt/V_D$ ) of C5PeC11 (0.1mM in toluene) by toluene (open symbols) and BisAC11 solutions in toluene at 0.05mM (solid line) and 1.74mM (dashed line). Filled symbols represent desorption of C5PeC11 (solutions in a mixture of heptane and toluene, HepTol at 30/70 %v/v) desorbed by the same HepTol mixture. The experimental conditions for the experiments were: Exchange flow rate  $Q = 0.4 \mu\text{L}/\text{s}$ , total predetermined volume  $V_E = 1000 \mu\text{L}$  and volume of the droplet  $V_D = 18 \mu\text{L}$

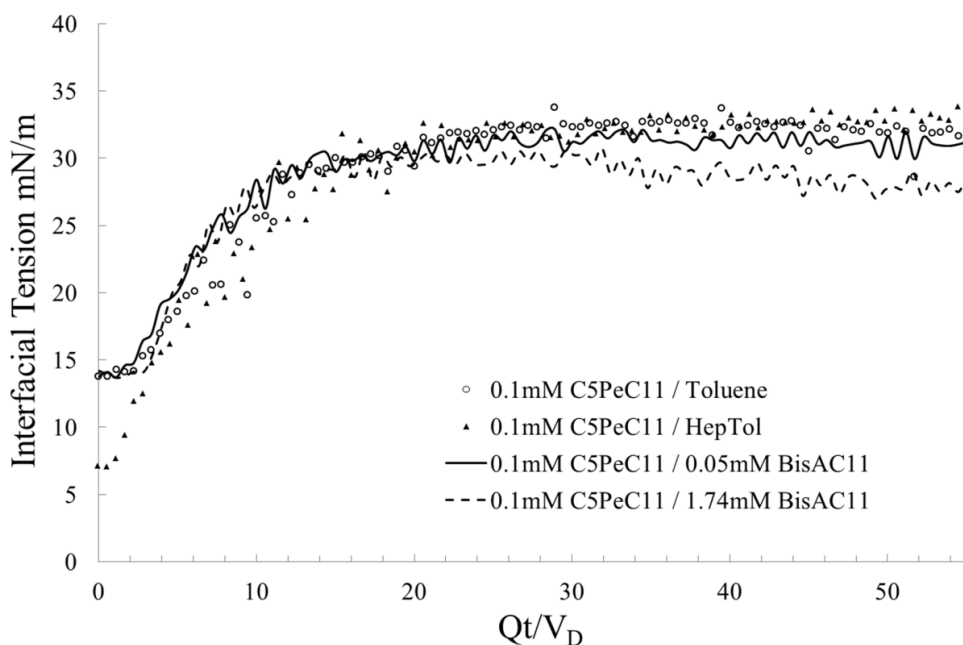


**Figure 6.** Compression-expansion curves for C5PeC11 at an air water interface of pH 6. Consecutive cycles of compression-expansions show (a) evidence of aggregation when large surface pressures are achieved, and (b) complete reversibility when surface pressure is kept below 30 mN/m.

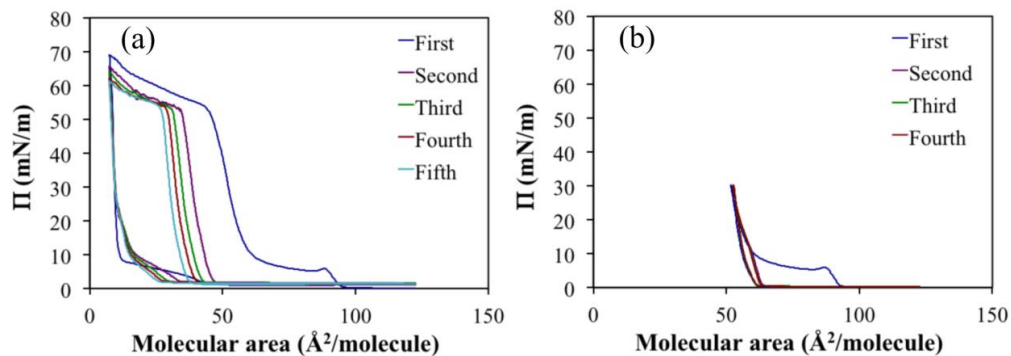


**Figure 7.** Dynamic moduli of C5PeC11 at an air/water interface (pH 6) at 30 mN/m as a function of (a) strain, and as a function of (b) frequency.

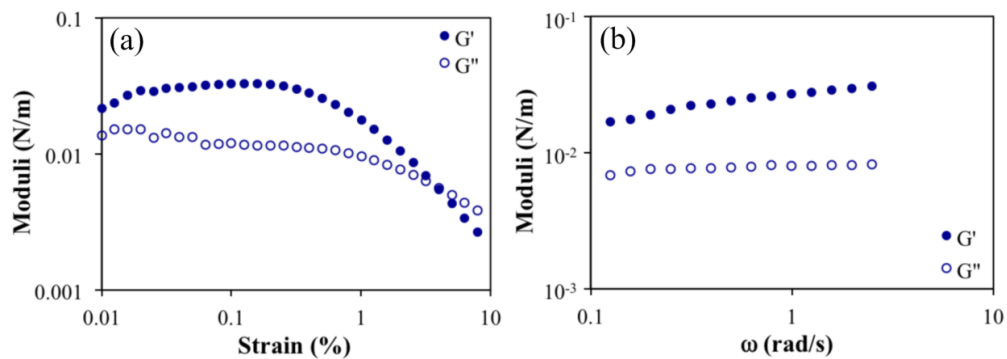


**Figure 8.** Compression-expansion curves from C5PeC11 at a decane/water interface. Two consecutive cycles are shown with a sub-phase pH of 6.

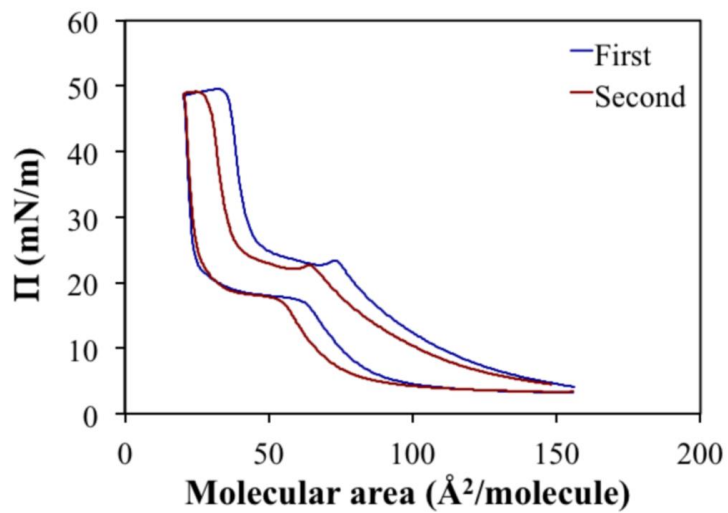


**Figure 9.** Dynamic moduli of C5PeC11 at an decane/water interface (pH 6) as a function of (a) strain, and as a function of (b) frequency. The surface pressure was 30 mN/m.

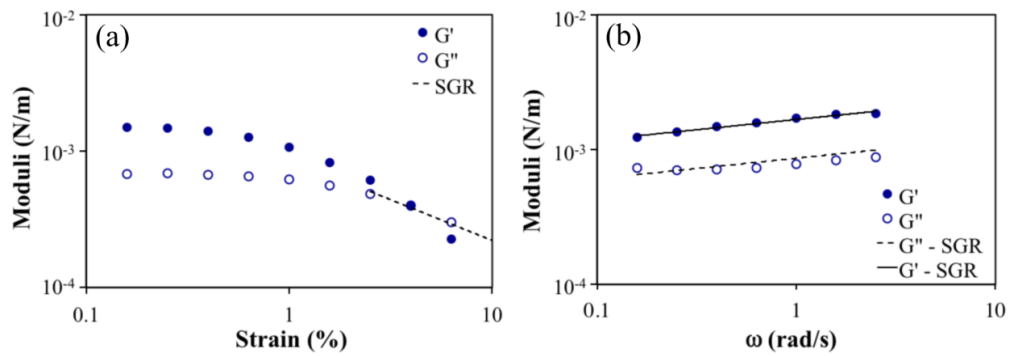


**Figure 10.** (a) Compression curves for C5PeC11 at a decane/water interface. The pH of the subphase was controlled with a buffer solution. Increasing pH deprotonates the carboxylate functional group of C5PeC11, increases surface activity and decreases molecular tilt at the interface. (b), (c) Conceptual drawing showing the effect of pH on molecular tilt.

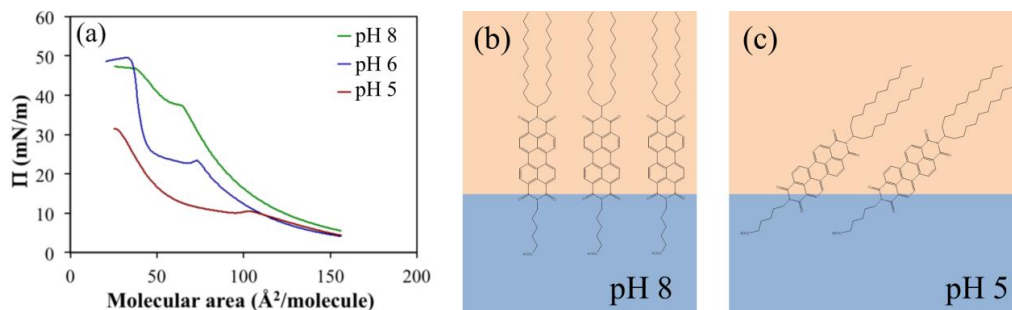
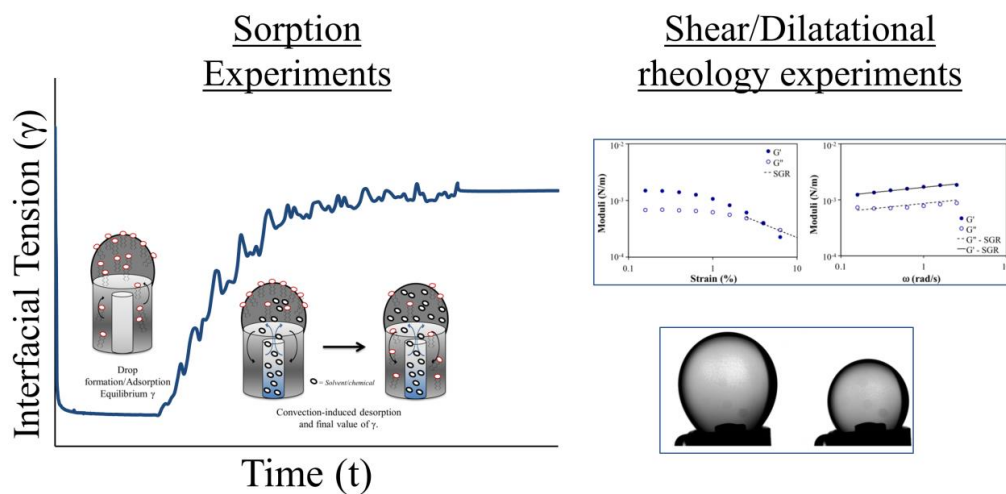


## Table of contents graphic

Coupled analysis between sorption experiments (adsorption and desorption from the liquid-liquid interface) and shear/dilatational rheology experiments (at the liquid-liquid and liquid-air interface) for asphaltene model compounds.



*A microcalorimetry study on the adsorption of asphaltenes and model asphaltene compounds at the liquid-solid surface.*



Is not included due to copyright

